



**Michigan
Technological
University**

Michigan Technological University
Digital Commons @ Michigan Tech

Dissertations, Master's Theses and Master's Reports

2016

THE EFFECT OF POSTTRANSLATIONAL MODIFICATIONS ON PROTEIN AGGREGATION, MORPHOLOGY, AND TOXICITY

Mu Yang


Michigan Technological University, muy@mtu.edu

Copyright 2016 Mu Yang

Recommended Citation

Yang, Mu, "THE EFFECT OF POSTTRANSLATIONAL MODIFICATIONS ON PROTEIN AGGREGATION, MORPHOLOGY, AND TOXICITY", Open Access Dissertation, Michigan Technological University, 2016.
<https://doi.org/10.37099/mtu.dc.etr/116>

Follow this and additional works at: <https://digitalcommons.mtu.edu/etr>

 Part of the [Biochemistry Commons](#), and the [Molecular Biology Commons](#)

THE EFFECT OF POSTTRANSLATIONAL
MODIFICATIONS ON PROTEIN AGGREGATION,
MORPHOLOGY, AND TOXICITY

By

Mu Yang

A DISSERTATION

Submitted in partial fulfillment of the requirements for the degree of

DOCTOR OF PHILOSOPHY

In Chemistry

MICHIGAN TECHNOLOGICAL UNIVERSITY

2016

© 2016 Mu Yang

This dissertation has been approved in partial fulfillment of the requirements for the Degree of DOCTOR OF PHILOSOPHY in Chemistry.

Department of Chemistry

Dissertation Advisor: *Dr. Ashutosh Tiwari*

Committee Member: *Dr. Qinghui Chen*

Committee Member: *Dr. Haiying Liu*

Committee Member: *Dr. Lynn R. Mazzoleni*

Department Chair: *Dr. Cary F. Chabalowski*

Table of Contents

Preface.....	vii
Acknowledgements.....	ix
Abstract.....	xi
Chapter 1 Background.....	1
1.1 History of protein folding studies.....	1
1.2 Physical forces in protein folding.....	4
1.2.1 Electrostatic interaction.....	5
1.2.2 Hydrogen bonding.....	6
1.2.3 Van der Waals interactions.....	7
1.2.4 Hydrophobic interaction.....	8
1.2.5 Intrinsic propensities.....	9
1.2.6 Chain entropy – principle opposing force.....	10
1.3 Energy landscape – A global overview of protein energy surfaces.....	11
1.4 Misfolded proteins.....	15
1.4.1 Amyloid fibrils.....	15
1.4.2 Amorphous/unstructured aggregates.....	20
1.5 <i>In vivo</i> factors of protein folding and aggregation.....	21
1.5.1 Disulfide bonds.....	23

1.5.2	Posttranslational modifications.....	25
1.6	Motivations and hypothesis	29
1.7	References.....	31
Chapter 2	Methods.....	45
2.1	UV-visible absorbance spectroscopy	46
2.2	Fluorescence spectroscopy.....	49
2.2.1	Protein intrinsic fluorescence	51
2.2.2	Extrinsic fluorescence.....	53
2.3	Non-reducing gel electrophoresis	56
2.4	Scanning electron microscopy (SEM)	59
2.5	Cell viability (MTS) assay	60
2.6	Live cell fluorescence imaging.....	62
2.7	References.....	65
Chapter 3	Disulfide-Bond Scrambling Promotes Amorphous Aggregates in Lysozyme and Bovine Serum Albumin†.....	68
3.1	Introduction.....	69
3.2	Materials and methods	72
3.3	Results.....	76
3.4	Discussion.....	89
3.5	Conclusion	101

3.6	References.....	102
Chapter 4	Acetylation of Amyloid β_{1-42} at Lysine 16 disrupts amyloid formation ...	111
4.1	Introduction.....	112
4.2	Materials and methods	114
4.3	Results.....	118
4.4	Discussion.....	126
4.5	Conclusion	131
4.6	References.....	131
Chapter 5	Toxicity of different protein aggregates	138
5.1	Introduction.....	139
5.2	Materials and methods	140
5.3	Results and discussion	144
5.4	Conclusion	160
5.5	References.....	161
Chapter 6	Live cell fluorescence imaging of fluorescent probes for sensitive detection of intracellular pH ¹ and lysosomal pH ²	167
6.1	Introduction.....	168
6.2	Materials and methods	170
6.3	Results and discussion	174
6.3.1	Intracellular pH probe.....	174

6.3.2	Lysosomal pH probe.....	180
6.4	Conclusion	188
6.5	Reference	188
Chapter 7	Summary and perspectives	191
Appendix A	Supporting Information for Chapter 4.....	194
Appendix B	Supporting Information for Chapter 5.....	201
	Copyright permissions	206

Preface

All the contents in chapters 1, 2, 4, 5, and 7 were written by the author of this dissertation. The contents in chapters 3 and 6 were edited and organized by the author of this dissertation based on previously published papers, which are described in detail as below.

Chapter 3 is based on the multi-author article that was previously published in “*J. Phys. Chem. B* **2015**, 119, 3969–3981”. The author of this dissertation was responsible for collection of all TCEP experiments, all seeding experiments, Non-reducing SDS-PAGE, and the ANS and bis-ANS fluorescence measurements for DTT experiments, data analysis and manuscript writing. The reported intrinsic and ThT fluorescence measurements and SEM images were collected by Ms. Colina Dutta. Dr. Ashutosh Tiwari revised the manuscript and is the corresponding author.

Chapter 4 is based on the multi-author article that is currently under preparation. The author of this dissertation was responsible for collection and analysis of all laboratory experiments, data analysis and manuscript writing. All molecular dynamic calculations were conducted by Mr. Ergun Kara. Mr. Ergun Kara also contribute to data analysis and manuscript writing of molecular dynamic calculation part. SEM images were collected by Ms. Colina Dutta. Dr. Michael Lee also participated in the computational data analysis. Dr. Ashutosh Tiwari revised the manuscript and is the corresponding author.

Chapter 5 is based on the multi-author article that is currently under preparation. The author of this dissertation was responsible for part of the cytotoxicity measurements, all the sample preparation, fluorescence measurements, data analysis, and manuscript

writing. The major cell culture and toxicity measurements were completed by Ms. Rashmi Adhikari. SEM images were collected by Ms. Colina Dutta. Dr. Ashutosh Tiwari revised the manuscript and is the corresponding author.

Chapter 6 is based on two multi-author articles that were previously published in “*ACS Sensors*. **2015**. DOI: 10.1021/acssensors.5b00065” and “*J. Mater. Chem. B*, 2015, 3, 2173-2184”. The author of this dissertation was responsible for all live cell fluorescence imaging, cellular uptake, and toxicity measurements. Dr. Jingtuo Zhang did all synthetic work, NMR study, and spectroscopic analysis. Mr. Cong Li helped to conduct spectroscopic data collection and Mr. Fei Xie helped to synthesize starting materials. Dr. Haiying Liu, Dr. Ashutosh Tiwari and Dr. Fen-Tair Luo revised the manuscript as the corresponding authors.

Acknowledgements

I would like to express my gratitude to numbers of amazing people who helped me along the path toward this dissertation. My Ph.D. journey would not have been possible without these supports in so many ways.

First, I would like to express my heartfelt thanks to my advisor, Dr. Ashutosh Tiwari, for his guidance and support throughout the time of my graduate study. Without his ongoing faith and encouragement of my efforts, I could not have complete my research over the years.

I am tremendously fortunate to have Dr. Haiying Liu, Dr. Lynn R. Mazzoleni, and Dr. Qinghui Chen as my defense committee. I would like to thank them for their valuable time and thoughtful feedback. I also appreciate former department chair Dr. Sarah A. Green and current department chair Dr. Cary F. Chabalowski for their support during my 5-year Ph.D. study.

I am very much grateful to my research collaborators Dr. Haiying Liu (Chemistry Department, MTU) and his group members, and Dr. Michael S. Lee (Army Research Laboratory, Adelphi). Their efforts made indispensable contributions to the projects in this dissertation.

Many thanks to my multi-talented labmates: Ms. Colina Dutta, Dr. Jagadeesh Janjanam, Mr. Nethaniah Dorh, Ms. Rashmi Adhikari, and Mr. Ergun Kara. I sincerely give my appreciation to their generosity and kindness help.

The deepest thank to my teaching supervisors: Ms. Kelley M. Smith, Ms. Lorri A. Reilly, Ms. Aparna Pandey, Dr. Sarah Hill, and Dr. Lynn R. Mazzoleni, without the

training and help from you, I could not have the precious teaching experience during my graduate study.

I would like to thank Department of Chemistry for five years financial support. I truly appreciate all the help from staffs of Department of Chemistry including Ms. Celine Grace, Ms. Denise Laux, Ms. Margaret Dunsten, Ms. Charlene Page, Mr. Jerry Lutz, Mr. Andrew Galerneau, Mr. Dean Seppala and Mr. Joel Smith. I also would like to thank my colleagues and friends Ni Fan, Yunzhu Zhao, Katrina Bugielski, Zichen Qian, Yuan Liu, Jie Zhou, and Weilue He for their great support and help.

Finally, I would like to express my sincere gratitude to my family for their always support, encouragements and understandings. Especially, the warmest thank to my beloved husband, Jingtuo Zhang, for his continued and unconditional love, his countless emotional support, and his thoughtful research advises. He is a collaborator, a senior colleague, who helped me grow from a student to a researcher. He is the dear husband, the best friend, who made me strong and fearless. Without him, my graduate career would be full of troubles and struggles. Thank you, my love, you are my destiny and the meaning of my life.

Abstract

Proteins are one of the most versatile macromolecules in the biological system. The function or activity of a protein highly depends on its 3D native structure. However, under stress, they are at risk of misfolding/aggregation, leading to formation of structures that can indicate loss of function or gain of toxicity. In severe cases, protein aggregation can result in many diseases, including neurodegenerative diseases, such as Alzheimer's, Parkinson's, Huntington's, and amyotrophic lateral sclerosis. Due to the heterogeneous nature of cellular environment and protein molecules, mechanism of *in vivo* folding and related toxicity still remains elusive. To have a better understanding of the cellular protein aggregations process and subsequent toxicity, we have performed aggregation studies of proteins with different types of posttranslational modifications, which is critical to protein's functional diversity.

In this dissertation, two common types of covalent modification of proteins, i.e. disulfide reduction and acetylation, were selected. In aggregation studies of two globular proteins, hen egg white lysozyme and bovine serum albumin (BSA), formation of amorphous aggregates were observed as a consequence of disulfide bond scrambling. The structural properties of the observed aggregates were distinct and depended on disulfide reduction level. In study of amyloid β ($A\beta$) peptide, the major pathological protein in Alzheimer's disease, effect of acetylation of the two lysine (K) positions, K16 and K28, on protein aggregation were investigated. We observed that acetylation on K16 can significantly increase hydrophobicity of $A\beta$ and disrupt amyloid fibril formation. Interestingly, the heterogeneous mixtures of wild type and acetylated peptides displayed

increased cytotoxicity compared to the homogeneous samples. To further understand the toxicity of protein aggregates, we then compared the cytotoxicity of eleven different aggregates from lysozyme and BSA, varying in morphology, size, flexibility, and hydrophobicity. The results suggest that the protein conformational changes in the early stage of aggregation process are essential for a gain in toxicity. They observed toxic species are structurally flexible, however, no clear correlation was found between cytotoxicity and hydrophobicity. Considering all the toxicity results of A β peptide, lysozyme, and BSA, we noticed that mixtures of native and modified proteins or aggregates are usually highly toxic. Therefore, the observed cytotoxicity of different structures may result from the heterogeneity of samples that are flexible rather than any defined structure. Further analysis of the toxic conformation would require high resolution structure determination of different aggregated protein species.

Chapter 1 Background

Proteins are the most versatile macromolecules that are involved in almost all of the biological processes. Formed from 20 basic building blocks (amino acids), a protein's biological function or activity is determined by its well-defined 3D native structure. In the cellular environment, there are risks for proteins to form wrong structures, which may result in loss of function, or in some cases, gain of toxicity. Even the proteins that successfully fold into correct native structures are only marginally stable (thermodynamically) in a very narrow range of physiological conditions. To understand the remarkable relationship between protein's structure and function, the folding process of protein has been studied for more than 50 years. Researchers tried to answer the questions: How can a protein fold from the 1D sequence code to 3D structure? How can cells control protein folding? What happens if a protein folds into the wrong structure? Can we predict folding? *Science* magazine framed protein folding problem as one of the 125 most important unsolved problems in science¹. While the information in this area is still growing rapidly, protein folding has already grown into a whole field of research. In the following sections, basics of the protein folding process will be reviewed, including history of protein folding, the driving forces and factors of protein folding, and problems caused by misfolded proteins.

1.1 History of protein folding

About a half-century ago, Max Perutz and John Kendrew won the 1962 Nobel Prize in Chemistry for determining the 3D structure of globular protein at the atomic level²⁻⁴.

Their work laid the foundation for molecular biological mechanisms of the relationship between protein function and structure, and became great support to studies on protein folding. But the story of protein folding actually started 60 years earlier, in 1902, when Emil Fischer and Franz Hofmeister discovered that proteins were formed from covalently linked amino acid chains⁵. By 1911, Henrietta Chick and C. J. Martin discovered the denaturation process of protein. It was the first time that protein denaturation was distinguished from aggregation⁵. In fact, the concept of “protein folding” was not put forward until 1929 by Hsien Wu. When the denaturation process was believed to be either dehydration (Robertson, 1925) or hydrolysis (Anson and Mirsky, 1925) of the protein⁵, Wu proposed it to be a purely conformational change: during denaturation, the 3D network of the protein chain changed from a “rigid, regular arrangement” to an “irregular, flexible open chain”⁶. However, Wu’s hypothesis was not accepted in the field immediately, because of the limited knowledge of protein structure. Until 1950s, reversible denaturation was investigated for serum albumin, hemoglobin⁷, ribonuclease A⁸ and many other proteins, which proved Wu’s hypothesis and also demonstrated that protein folding and denaturation are thermodynamic processes. The free energy change between the native and denatured states of a protein was discovered⁷. Shortly thereafter, Anfinsen established the “thermodynamic hypothesis”, suggesting that proteins exist in thermodynamic configurational equilibrium, with the folded state representing the global minimum of configuration energy⁸.

Even though in the early studies denatured proteins were successfully refolded to their native structure and restoring the biological activities in test tubes, the investigators realized that the folding in a test tube was too slow compared to those carried out in cells.

In the talk “How to fold Graciously” (1969), Cyrus Levinthal mentioned the astronomical number of possible configurations of protein, which was later called “Levinthal’s Paradox”⁹: for a polypeptide chain of 100 residues, if each amino acid has 3 stable conformations, there will be total 3^{100} possible conformations that the protein may fold into. On that basis, if a protein reached its native structure by sequentially sampling all the possible conformations, it would take time that is longer than the life span of any organism in this universe. Therefore Levinthal proposed that in a biological system, there must be pathways that guide and speed up protein folding to the correct configuration¹⁰.

Study of the role of the intracellular environment in protein folding started from renaturation of ribonuclease¹¹, influenza hemagglutinin¹², and bovine pancreatic trypsin inhibitor (BPTI)¹³ in isolated microsomal fractions. From the results, it was noticed that protein folding can be facilitated by certain proteins in the endoplasmic reticulum (ER) in eukaryotic cells. For example, the protein disulfide isomerase on ER was found to be involved in folding of proteins which have disulfide bonds^{13, 14}. However folding of large complex, multi-domain proteins was found much harder than the small single domain proteins, which can easily form the native fold by themselves. Large proteins can only fold efficiently in the presence of certain proteins called “molecular chaperones”. The term molecular chaperones was first used to introduce nucleoplasmin, a protein that promotes assembly of DNA and histone-histone interactions without itself being part of the nucleosome¹⁵. Later it was applied to represent families of proteins that facilitate protein folding, assembly and translocation in bacterial and eukaryotic systems¹⁶. To date, molecular chaperones define a variety of factors that assist generation of native structures of biomolecules including proteins and nucleic acids⁷.

It has been more than a century since the first exploration of Fischer and Hofmeister, but the study of protein folding never stopped. Even though there is no specific commercial target in this field, protein folding has drawn intense interest as one of the frontiers in science today. Knowledge of protein folding is building from research in bench-top experiments and computational simulations. Now there are over 100,000 protein structures at atomic detail available on databases like Protein Data Bank (PDB, www.rcsb.org/pdb)¹⁷, and the number keeps growing every year. With the advances in modern technologies, achievement of protein folding problems can be made not only through the professional supercomputers¹⁸, but also millions of normal home computer users through Folding@home (folding.stanford.edu)¹⁹, or even through a multiplayer online video game called Foldit (Fold.it/portal)²⁰. Moreover, studies of protein folding, and misfolding, sheds lights on a whole new class of disease, protein-misfolding diseases, including Alzheimer's, Parkinson's, and type II diabetes. However, to answer the questions arisen 100 years ago, there is still a long way to go. In the following parts, fundamentals of protein folding and aggregation process will be discussed in detail.

1.2 Physical forces in protein folding

One of the very first questions asked in protein folding studies is: how can protein form its 3D structure from its 1D amino acid sequence? Researchers used to propose the major folding force as electrostatic interactions⁵, hydrogen bonding²¹ or hydrophobic interactions. However since the stability difference between the native and denatured states of a protein is only 5-10 kcal/mol²², even minuscule interactions may contribute significantly. All the interactions are important. After years of studies, the common

physical forces involved in protein folding⁵ appear to be electrostatic interaction, hydrogen bonding, van de waals interaction, hydrophobic interaction, intrinsic propensities, and chain entropy.

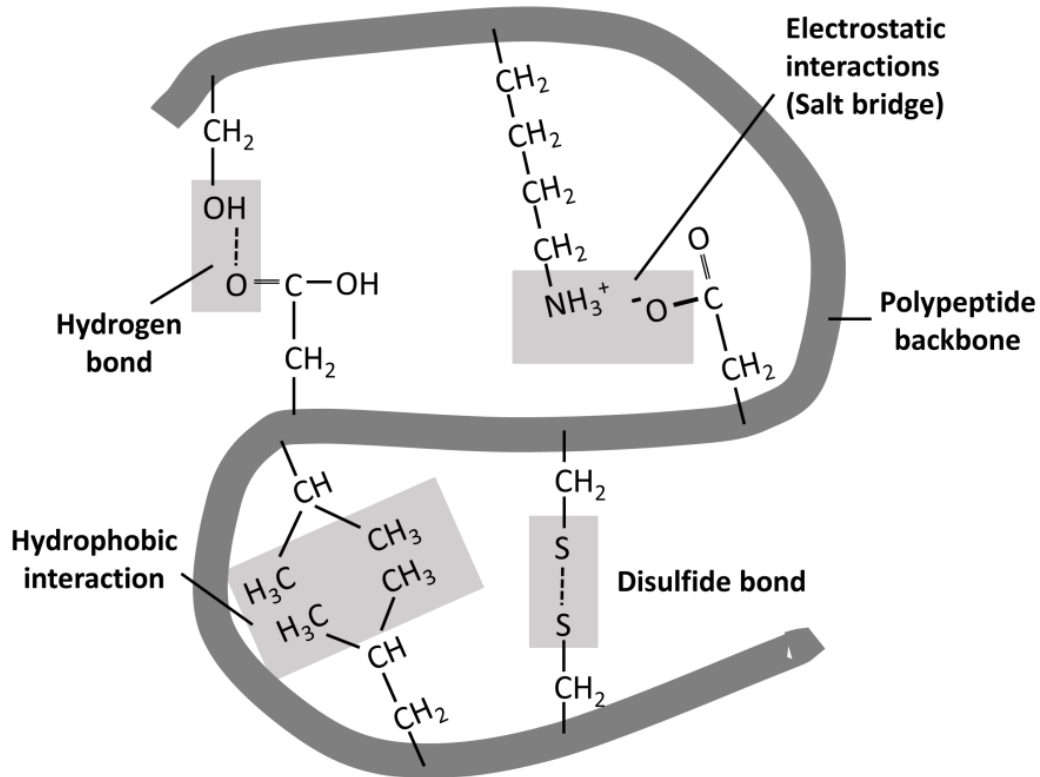


Figure 1.1. Examples of molecular interactions that stabilize protein structures.

1.2.1 Electrostatic interaction

As acids and bases were the earliest denaturants used in protein denaturation studies, electrostatic interactions were first hypothesized to be the folding force⁵. In 1924, Linderstrom-Lang came up with the first quantitative model of electrostatic interactions on native proteins. Electrostatic interaction, or in another word, ionic bonds, exist between oppositely charged residues (also called salt bridge) or between salts and

charged protein side chains (see example of electrostatic interactions in figure 1.1). The interactions between protein and ions in solution can destabilize protein by causing nonspecific repulsions. In detail, one can increase protein net charge by adding acid or base in the solution. As density of the same charge increases in a tightly-folded protein molecule, the charge repulsion will force the structure to loosen. This is known as classical electrostatic effect. However, in contrast, the specific charge interactions, or salt bridge, between oppositely charged side chains could stabilize the folded structure, because such interactions only occur in close spatial proximity. During the 1930s, ionic bonds between protein side chains were believed to be the major contributor to stability and driving force of folding²³⁻²⁵. More studies on protein structures showed that ionic bond indeed affect stability^{26, 27}, but since most charge residues are concentrated on the protein surface, it's not the dominant force of protein folding. Jacobsen and Linderstrom-Lang proved the first evidence that if driven by ion pairing, folding would result in a negative volume change, which is in contrast to experimental results²⁸. Investigation also showed that proteins have little dependence on pH (near neutral) or ionic strength (at low concentration) near their most stable pH²⁹. Actually, the free energy contribution of ionic bonds to total stability was later proved 5-10-fold smaller than hydrophobic interactions⁵. In average, there are only about 5 salt bridges per 150 residues in protein, involving less than 10% of the protein molecule³⁰, which is unlikely to be the dominant folding force.

1.2.2 Hydrogen bonding

The hydrogen bonds are defined as attractive interactions between a hydrogen atom (or a molecular fragment X-H in which X is more electronegative than H) and an electronegative atom/group of atoms (See example of hydrogen bond in Figure 1.1). In

the 1930s, Pauling proposed the importance of hydrogen bonds in molecules²⁴, and based on hydrogen bonding patterns, he successfully predicted the model of secondary structures, α -helix and β -sheets³¹. It was soon investigated that hydrogen bonds among amid and carbonyl groups on the backbone is the principle driving force for α -helix and β -sheets from random coil structure³²⁻³⁴, and the force increased with more polar groups in the protein. Since helices and sheets are common features in proteins, hydrogen bonding should naturally play an important role in folding. There are about 90% of C=O groups and NH groups in proteins form hydrogen bonds to either water molecules, protein backbone, or other side chains³⁵. Remarkably, all possible hydrogen bonds are generally satisfied in protein native fold³⁶. Studies on tyrosyl-tRNA synthetase³⁷ and phage-T4 lysozyme^{38, 39} found that hydrogen bonds stabilized protein structures. However, all proteins share the same peptide bond connections to form the backbone, but the native folded configurations are all different. Thus, the hydrogen bonding interactions that majorly from the backbone atoms are not specific for a protein to fold into a unique structure. Kauzmann⁴⁰ concluded that the intrachain hydrogen bonds have similar free energy in both folded and unfolded states, suggesting that folding is not favored for hydrogen bonds formation. In addition, hydrogen bond angles in protein share the same distribution with those in small molecular compounds³⁵. The hydrogen bond turns out to be a weak folding driving force, but contributes significantly to the internal organization in the folded protein⁵.

1.2.3 Van der Waals interactions

Van der Waals interactions represent the attractions among fixed or induced dipoles⁵. Since a folded protein molecule is tightly packed, attractive or repulsive forces between

closely arranged atoms are important. In general, for the large numbers of van der Waals interactions from protein backbone, folding is favored. However van der Waals interaction is naturally not selective, which cannot count for why there is only one specific native conformation of the polypeptide chain.

1.2.4 Hydrophobic interaction

Hydrophobic interaction was actually first discovered in the study of electrostatics forces in protein folding. In early studies, it was noticed that both the processes of folding and transferring nonpolar compounds from water into nonpolar solutions involved a significant decrease of heat capacity. In work of Jacobsen and Linderstron-Lang²⁸, protein folding was driven by the “aversion” from the nonpolar residues to water, the same force drives micelle formation. While in nonpolar solvent, proteins are easily denatured. This kind of interaction was first considered as van der Waals⁴¹; till 1960s, Kauzmann and other researchers brought the name hydrophobic bond (earlier called “antihydrogen bond”), which is now used to describe the relation between hydrophobes (low water soluble molecules) surrounded by water⁵. Thus, it is also called “water mediated hydrophobic interaction”. As more crystal structures of proteins become available, a core structure formed by nonpolar residues protected from water was found as a predominant feature of globular proteins⁴². The compact arrangement of hydrophobic core helps proteins to reduce the surface area and decrease undesirable interactions with water molecules. Compared to other types of interactions, the hydrophobic core residues are more strongly conserved and correlated with the structure⁴³⁻⁴⁶. In addition, substitution of nonpolar residues turned to be more disruptive to protein stability than other types of substitution^{47, 48}. Therefore, hydrophobic interactions among the nonpolar

sidechains from core residues are considered one of the major folding forces. However, without other interactions, hydrophobic interaction alone still cannot fold protein into unique native conformation.

1.2.5 Intrinsic propensities

Instead of describing a single type of force, intrinsic propensity represents certain types of configurations preferred by the peptide chains, depending on size or sequence, which could be results of the total local interactions among residues⁵. For example, the stability of the helix structure increased with length of the polypeptide chain^{49, 50}, in which the small free energy contribution from each residue summed to become a strong force what favors helix formation. Globular proteins have unique internal organizations as combination of helix, sheets, and turns, determined by amino acid sequence. Among all the attempts to predict protein structures using only intrinsic propensities, the success rate is ~ 60%, which will be higher within in a given family of proteins⁵¹⁻⁵³. Polymer chains, not only proteins, share a similar tendency to fold. When a chain molecule forms self-contact, it will prefer to form a loop as small as possible, which leaves more accessible conformations for the main chain⁵⁴. For the same reason, if the chain is to form a second self-contact, it will be as close as possible to the first structure in the sequence. As a consequence, when a chain becomes more and more compact, a considerable number of secondary structures will be developed⁵⁴. This is not to say that other forces are not important. This is only to say that intrinsic propensities of a protein chain also limits the possible conformations when it folds.

1.2.6 Chain entropy – principle opposing force

Entropy is the main force opposing folding, in another word, unfolding^{5,24}. As a long polymer, the polypeptide chain can gain entropy in many possible configurations, depending on the relevant degree of freedom. While changing conformation, the arrangement of connected residues would be affected, including changing specific ion pairs, or the bond ϕ , ψ , and χ angles. Entropies that arise from these local configuration changes are called local entropy. These local entropies resemble translational, vibrational, and rotational entropies of small molecules⁵⁵, being independent from the global properties of the protein, like size or distributions of polar/nonpolar residues⁵. Although local entropy is normally small, there are evidences that local entropy could affect protein stabilities⁵⁶. There is another type of entropy, nonlocal entropy, arises from “excluded volume”, which means one part of a long chain cannot occupy the space that was already occupied by the other part of the same chain. If there is no limitation of volume, a chain can occupy any large space with any configuration. However, the excluded volume reduces the ways the polypeptide chain can configure. Recent structure simulation achievement showed that as a compact polymer, the protein reaches its internal architecture more as a consequence of steric constraints^{54, 57}, which has presumably hydrophobic interaction as the driving force, and nonlocal entropy as the opposing force. The external thermodynamic conditions, such as pH, temperature, and ionic strength of the solution can affect the radius and conformations of the denatured proteins, and therefore the nonlocal entropies. In general, the excluded volume effect is proportional to the number of residues. Larger proteins have relatively smaller free volume. In this light, cross-links were introduced to increase protein stability. Evidences showed that after

adding cross-link residues, which reduces the number of accessible configurations, the unfolded state became less favored^{58, 59}. It appears that the most commonly used protein cross-link is disulfide bonds, which will be discussed in section 1.5.1.

1.3 Energy landscape – A global overview of protein energy surfaces

With a tremendous amount of experimentation achievements on the physical forces of protein folding, using statistical ideas, the theory of funnel-shaped protein folding energy landscape was emerged in the late 1980s⁶⁰⁻⁶². The energy landscape is the mathematical description of the relationship between folding forces and chain entropy (the major opposing force), as introduced in the last section. It has generally been based on the assumption that protein folding occurs by searching through an ensemble of accessible configurations, rather than directly through certain defined structure intermediates. Since the unstable denatured proteins are conformationally heterogeneous, in all different types of energy landscape models, proteins always have many high energy states and only a few low energy states, resulting in a funnel shape. Figure 1.2 shows the most realistic model, a rugged energy landscape with kinetic traps that proteins can transiently reside^{60, 62}. With no pathway but multiple folding routes at different conditions a protein starts folding from the unstable high energy states, crossing substantial kinetic barriers, toward the low energy native structure. As protein stability increases (lower energy), conformational entropy decreases⁶³. In this way, the funnel-shaped model describes protein's conformational heterogeneity.

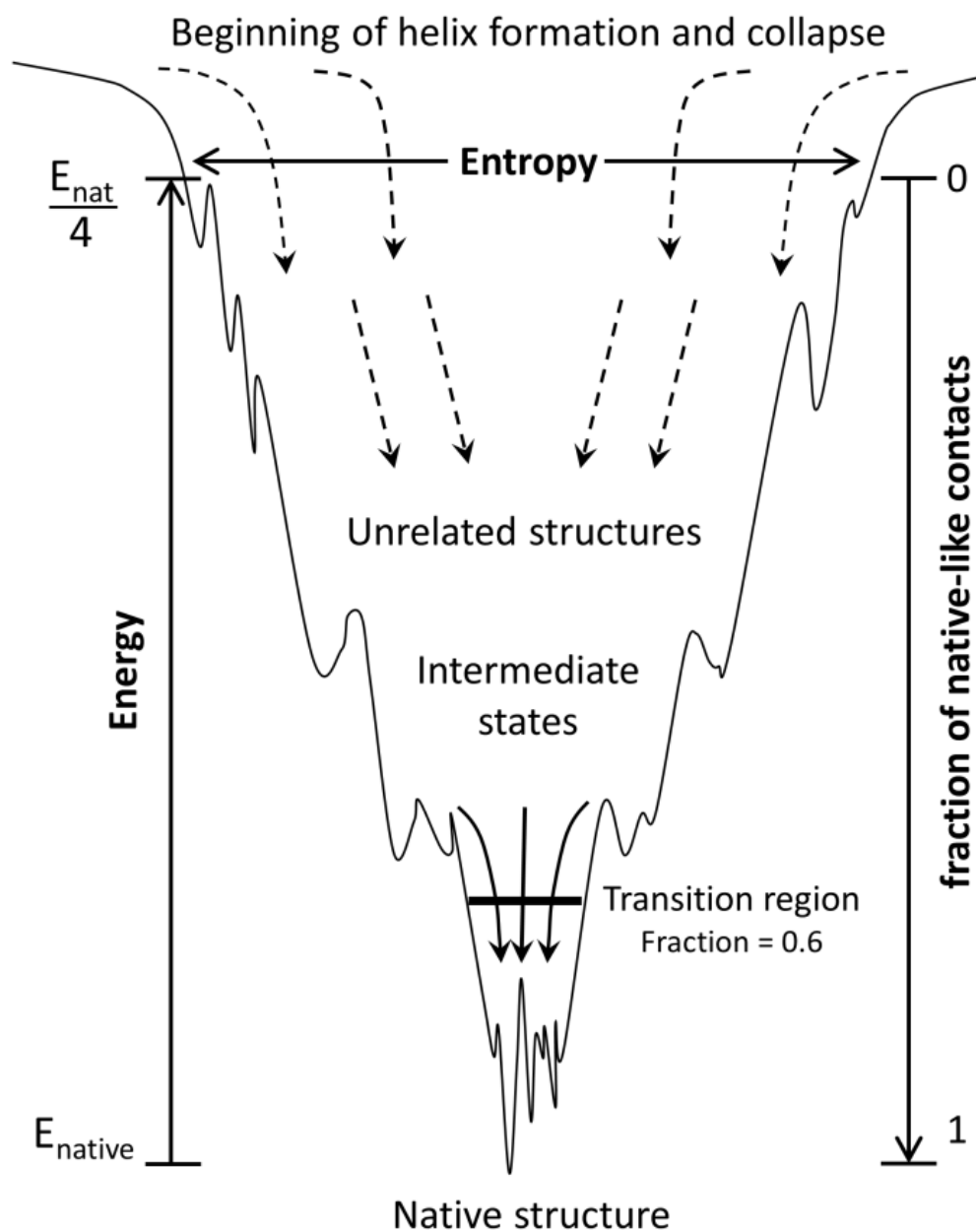


Figure 1.2. A classic rugged model of protein folding energy landscape (modified from Onuchic, *Annu. Rev. Phys. Chem.* 1997⁶⁰ Copyright © 2015 Annual Reviews). Energy represents the solvent-averaged energy, and the fraction of native-like contacts, is used to describe the position of a state during folding.

Usually, small single domain proteins, less than 100 amino acids, have relatively smooth folding funnels. However about 90% proteins in the cell are larger than 100

amino acids, which have a strong tendency to form compact structures in aqueous solvent via hydrophobic collapse⁶⁴. In those cases, the rapid folded states may not relate to the correct folding pathway, but there probably are substantial elements of native structures contained in such species (Figure 1.2, unrelated structures). Structure reorganization that may involve a high free-energy barrier is then required to convert the rapid folded structures to the correct fold, resulting in population of intermediate states (Figure 1.2), which may only have <50% structure similarity to native-like structures⁶⁵. By limiting the accessible configurations, intermediates could assist folding on the correct pathway⁶⁶. On the other hand, if the intermediates cannot reach native state through the structural reorganization process, the intermediates are then defined “off-pathway”⁶⁷. Abundant evidences had been found that off-pathway intermediates lead to formation of misfolded structures or aggregates⁶⁸. Figure 1.3 shows a schematic energy landscape of protein aggregation, with some common misfolded protein aggregate species, including oligomers, amorphous aggregates, and amyloid fibrils. Although the native fold and aggregates appear as very distinct structures, they share the same physical folding forces: hydrophobic interactions, hydrogen bonding, and many other interactions as introduced in section 1.2. Since native protein molecules need to keep certain conformation flexibility to fulfill their biological functions, the native states are only marginally stable compared to the denatured state. However, as intermolecular assemblies without biological activities, the protein aggregates are more thermodynamically stable than the native state of single molecules, showing much lower free energy and less structural entropy on energy landscape (Figure 1.3). Therefore, the off-pathway aggregation processes are more kinetically trapped through formation of misfolded proteins or

aggregation nucleus by local unfolding events. Next section will focus on different types of protein aggregates and the different mechanisms by which all manages/removes these aggregates.

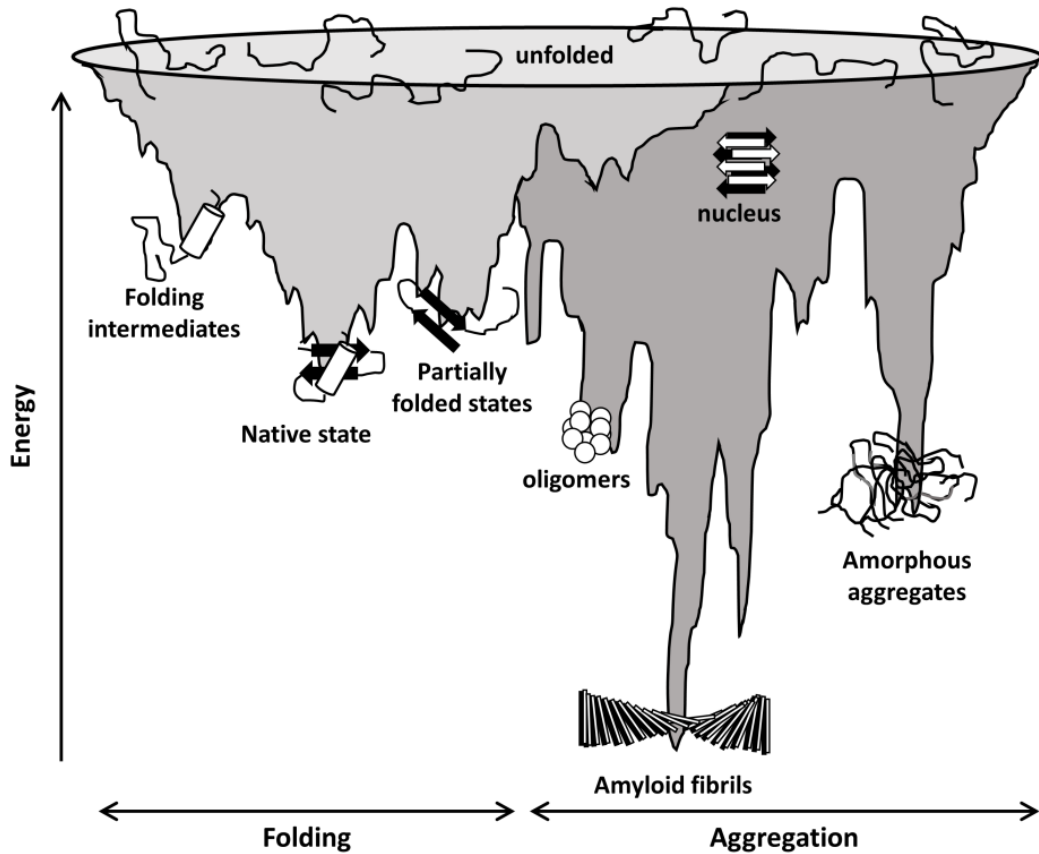


Figure 1.3. Schematic energy landscape for protein folding and aggregation (modified from Hartl and Hayer-Hartl. *Nat. Struct. Mol. Biol.* 2009⁶⁹). The light gray shaded folding part shows the typical on-pathway folding funnel that unfolded proteins funneling towards the native state via different intermediate states. While the dark gray shaded part describes the off-pathway aggregation process of unfolded proteins toward the thermodynamic global free energy minimum form, the amyloid fibrils, via conversion from kinetically stabilized globular structures, such as oligomers, or amorphous aggregates.

1.4 Misfolded proteins

Cells have a protein quality control system that is formed by a large machinery of proteins, to ensure correct folding and rapid degradation of any mutated or misfolded protein structures. Irreversibly misfolded and aggregated proteins are normally removed by ubiquitin-proteasome system (UPS) and autophagy system. However, even after escaping the cellular quality control machinery, the folded proteins may still form aggregation intermediates, which can be induced by random conformational fluctuations or environmental factors. When misfolded proteins cannot be degraded, they may accumulate inside cells or tissues in form of distinct aggregates. Some of them may form structures that are toxic and are known to be associated with diseases, such as amyloidosis, Prion disease, Parkinson's disease, Alzheimer's disease, amyotrophic lateral sclerosis, and Huntington's disease (Table 1.1). Even for proteins that do not cause amyloidosis, their aggregates can cause toxicity as well^{70, 71}. Especially in age-related amyloidosis, protein quality control machinery could be saturated by large numbers of partially folded or misfolded proteins, which keep accumulating in the crowded cellular environment and eventually form intracellular aggregates before being refolded or degraded⁷². In this section, the major pathologic protein aggregates, amyloid fibril, protofibrils, oligomers, and amorphous aggregates will be highlighted.

1.4.1 Amyloid fibrils

Amyloid fibrils are a specific class of abnormal extracellular protein assembly with long branchless fiber structures and are resistant to degradation (Figure 1.4). The amyloid fibril structures were first found about 100 years ago by Dr. Alois Alzheimer, in brains of

patients diagnosed with dementia. Now amyloid fibrils have been found in many diseases affecting almost all the organs in the human body, formed by more than 30 plasma proteins (Table 1.1). Diseases such as Alzheimer's, type II diabetes, spongiform encephalopathies, and amyotrophic lateral sclerosis that pathologically associate with amyloid fibrils are classified as amyloidosis diseases. Recently, the biological function, instead of pathologic effects, of the amyloid has also been identified⁷³.

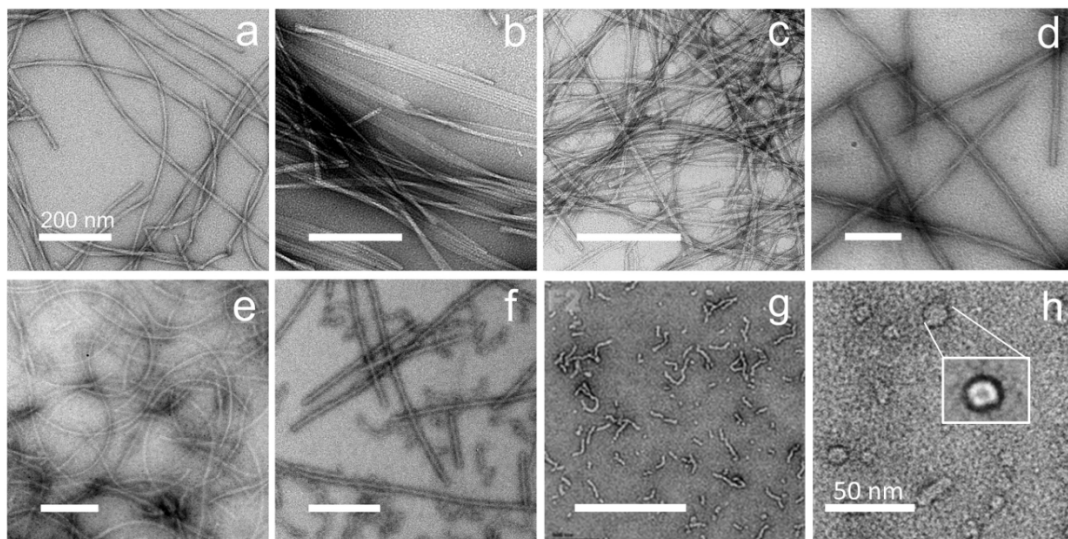


Figure 1.4. Different types of amyloid fibrils and pre-fibril intermediates imaged by transmitted electron microscope (TEM). (a, b) Amyloid β peptide 1-40 ($A\beta$ 1-40) fibrils with (a) "twisted" and (b) "striated" ribbon morphologies. (c) Islet amyloid polypeptide (amylin) fibrils. (d, e) PrP fibrils with (d) "R" and (e) "S" morphologies. (f) Pmel17 repeat domain fibrils (g) $A\beta$ 1-40 (E22G) protofibrils. (h) $A\beta$ 1-40 (E22G) amyloid pores. Scale bars in (a)-(g) are 200 nm, in (h) is 50 nm. Images are reprinted with permission from Tycko et al. 2013⁷⁴. Copyright © 2015 American Chemical Society.

Table 1.1. Some human amyloidogenesis proteins and the related diseases⁷⁵.

Protein name	Amyloid diseases	# of S-S	Structure
--------------	------------------	----------	-----------

Androgen receptor	Spinal and bulbar muscular atrophy	0	α -helical with unfolded N-terminal
Amyloid-β	Alzheimer's disease	0	Natively unfolded
α-synuclein	Parkinson's disease Alzheimer's disease	0	Natively unfolded
Huntingtin exon 1	Huntington Disease	0	Natively unfolded
Tau protein	Frontotemporal dementias	0	Probably natively unfolded
Ataxin-1	Spinocerebellar ataxia	0	Probably natively unfolded
Calcitonin	Medullary Carcinoma of the Thyroid	1	Natively unfolded
Islet amyloid polypeptide (IAPP)	Type 2 diabetes	1	Natively unfolded
Prion	Spongiform encephalopathies	1	unfolded (N-terminal) and α -helical (C-terminal)
Tansthyretin	Senile systemic amyloidosis	1	Predominantly β -sheet
Abri	Familial British dementia	1	Predominantly β -strand
Superoxide dismutase 1	Amyotrophic lateral sclerosis	1	Predominantly β -strand
β2-Microglobulin	Haemodialysis-related amyloidosis	1	β -sheet
Ig light chains	Primary systemic amyloidosis	1	β -sheet
Gelsolin	Finnish-type familial amyloidosis	1	Globular protein
Atrial natriuretic factor	Atrial amyloidosis	1	Globular protein
Cystatin C	Hereditary cystatin c	2	Globular protein

	amyloid angiopathy		
Insulin	Injection-localized amyloidosis	3	Globular protein
Lysozyme	Hereditary systemic amyloidosis	4	Globular protein
Fibrinogen	Hereditary renal amyloidosis	29	β -sheet

The insoluble amyloid fibrils are structurally dominated by antiparallel β -sheet structures. Remarkably, the precursor proteins of amyloid fibrils are structurally diverse and share nearly no sequence similarity, ranging from < 5 kDa small peptide (amyloid β -peptide) to >55 kDa large protein assemblies [transthyretin (TTR)]^{67, 74}. More intriguingly, there are many more proteins that do not associate with amyloidosis can aggregate into amyloid fibril structures under laboratory conditions⁷⁶, strongly suggesting that polypeptide chain forms cross- β structures as an inherent property⁷⁷. Therefore, study of fibrillization mechanism of one single protein may cast important insights on the fibril formation process of all proteins.

Amyloid fibrils are normally formed from soluble proteins. Taking non-amyloidogenic globular proteins as an example, fibrils typically form under extreme pH or temperature conditions, or with denaturant, which destabilize the protein's native structure into flexible unfolded or partially folded conformations⁷⁸. The typical amyloid formation for lysozyme is at pH 2.0, 65 °C, at high protein concentration^{79, 80}. Other factors such as mutations were shown to significantly destabilize structures, leading to increased tendency for fibril formation. The early onset familial Alzheimer's disease was found to be closely related to certain A β mutations, including Dutch (E22Q), Italian

(E22K), Tottori (D7N), Flemish (A21G), and Iowa (D23N)⁸¹⁻⁸³. For some proteins, increase in concentration of native proteins can also result in onset of amyloid disease. For example, high serum concentration (~60-fold higher than normal) of β_2 -microglobulin can decrease the stability of monomeric proteins and lead to renal impairment⁶⁷. While for the proteins that are intrinsically unstructured/disordered, such as amyloid β -peptides, α -synuclein, partial folding is the critical first step in assembly⁸⁴. However, the exact amyloid precursor structure of any protein has not yet been identified, leaving folding and aggregation disconnected.

Studies of amyloid fibrils started since amyloid deposition was found as a key character of amyloidosis diseases. However, the question now becomes when do amyloid fibrils form, before or after the disease occurred? According to the amyloid cascade hypothesis⁸⁵, the amyloid precursor protein (APP) initiates the pathogenesis of Alzheimer's disease when the protein's metabolism is altered. As a consequence of disease conditions, $A\beta$ aggregates into fibrils and form neuritic plaques, which may further cause neuronal cell loss and that may result in dementia. However, it is the concentration of soluble $A\beta$ monomers, but not the density of amyloid plaques that correlate with cognitive impairments⁸⁶⁻⁸⁸. Using electron microscopy and atomic force microscopy techniques, several pre-fibril intermediate structures, such as protofibrils, small oligomers, and membrane embedded pores (Figure 1.4) have been identified. These intermediates could be either on the fibril pathway or off-pathway, which may end up as amorphous aggregates. Remarkably, the pre-fibril intermediates, especially small oligomers, were found to be more toxic than mature fibrils, becoming the major pathologic structures in amyloidosis diseases. Thus, formation of mature fibrils may

serve a protective role by reducing the population of toxic intermediates⁸⁹. Therefore, the research of amyloid fibrils is trying to answer the two questions: (1) what is the atomic structure of the toxic intermediate species; (2) what is the toxic mechanism.

1.4.2 Amorphous/unstructured protein aggregates

There are many other structures of protein aggregates that are very different than amyloid fibril structures and all are called amorphous aggregates (Figure 1.5). Amorphous aggregates are frequently observed during protein expression and purification, coupled with protein denaturation, when more hydrophobic areas are exposed on the unfolded conformations. These aggregates are often in a granular appearance without ordered intermolecular interactions, formed from random assembly of monomers, or through intermediates like oligomers or protofibrils⁹⁰. Amyloidogenic proteins also form amorphous aggregates, when they failed to form amyloid fibrils. However, in contrast with amyloid fibrils, we know very little about amorphous aggregates. Due to the high structural flexibility and heterogeneity, it is extremely hard to measure structures of amorphous aggregates at the atomic level and classify them. Various amorphous aggregates have been identified recently with different structure properties and toxicity levels. In many studies, formation of amorphous aggregates was considered as a sign of successful inhibition of amyloid fibril formation⁹¹⁻⁹³. However, some amorphous aggregates also associate with diseases, for example, the amorphous aggregates formed from α -crystallin in cataracts⁹⁴. Moreover, some amyloid plaques in amyloidosis are mixtures of amyloid fibrils and amorphous aggregates^{95, 96}. Since amorphous aggregates share a lot of structural similarity with intermediate oligomers and protofibrils, which were recently found to be the most toxic species in human

amyloidosis, it will be crucial to increase our understanding of the aggregation and toxicity mechanism of amorphous aggregates. Considering that the normal function of proteins directly relate to structure, the toxicity of misfolded protein assembly may also be controlled by certain structure properties. In this light, studies of amorphous aggregates could benefit understanding of other species in protein folding and fibrillization as well.

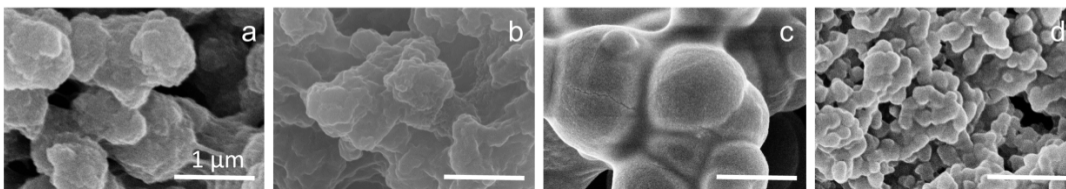


Figure 1.5. Four different amorphous aggregate structures formed from hen egg white lysozyme, imaged by scanning electron microscope (SEM). (a) Lysozyme (40 μM) with 10 mM DTT at pH 7.2, 37 $^{\circ}\text{C}$. (b) Lysozyme (40 μM) seeded by aggregates showed in (a) at pH 7.2, 37 $^{\circ}\text{C}$. (c) Lysozyme (700 μM) at pH 7.4, 65 $^{\circ}\text{C}$. (d) Lysozyme (120 μM) at pH 12.0, 25 $^{\circ}\text{C}$. All scale bars = 1 μm . Images (a) and (b) are reprinted with permission from Yang et al. 2015⁹⁷ Copyright © 2015 American Chemical Society.

1.5 *In vivo* factors of protein folding and aggregation

While a variety of conditions that direct correct folding have been successfully developed, there are still differences between folding processed in cell compared to those in a test tube. Taking hCG- β subunit¹⁴ and tail spike protein P22⁹⁸ as examples, the *in vitro* folding processes appeared to parallel their intracellular assembly, proceeding through the same folding intermediates to the same final native fold, but the *in vitro* folding rates and efficiency were much lower. On the other hand, small proteins can fold within microseconds into the native structures in diluted buffer solutions; however, the

same process may take minutes even hours to large, multidomain proteins. Knowing the highly crowded cellular environment normally contains 300-400 g/l⁹⁹ cytosolic proteins, efficient correct folding of large proteins in cells is more challenging. The entire folding process is, thus, assisted and controlled by molecular chaperones, which are also widely applied to *in vitro* conditions to assist folding⁷. Most chaperones that participate in protein folding are multicomponent molecular machines that typically recognize and bind to the hydrophobic regions of a polypeptide chain or non-native proteins. This protects the hydrophobic patches from random interactions and aggregation, and at the same time, may also lead to conformational rearrangements to remove kinetic barriers in folding¹⁰⁰. When released from chaperones, the hydrophobic residues can collapse rapidly (nano- to few microseconds) forming the core. Normally small proteins reach partially folded structures after fast folding and can then rapidly fold into the native states. Whereas the longer chains that require more time to fold will bind to the chaperone again and undergo another cycle⁹⁹. Proteins that are not able to accomplish folding through fast-folding trajectories will be transferred to the chaperonin cages, which are 800-900 kDa protein complexes that are specialized to assist folding of large proteins, such as actin and tubulins¹⁰¹.

In the cells, most eukaryotic membrane or secreted proteins follow a similar route: First, the nascent proteins are synthesized in rough ER. Then, they are translocated to the cisternae of ER, where (1) signal peptide is cleaved; (2) secondary structures and/or tertiary structure form as a result of co-translational folding; (3) posttranslational modifications takes place; and (4) disulfide bonds are formed. Finally, proteins are transferred to the Golgi apparatus or cell surface. This section will focus on disulfide

bonds and posttranslational modifications, which play important but distinct roles in protein folding and aggregation.

1.5.1 Disulfide bonds in proteins

A favorable redox potential is required in many folding systems to assist disulfide bond formation, which is important for proteins to maintain the ordered structures. Disulfide bonds, the reversible covalent linkages between the side-chain β -thiol groups of cysteine (C) residues, are by far the second most common covalent bond in proteins and peptides¹⁰². They are naturally formed in 65% of secreted proteins and more than half of amyloidogenic proteins (Table 1.1)⁷⁵. Moreover, disulfide bonds exist in folded proteins as well as the unfolded ones (see examples in Table 1.1). However, the link between disulfide bonds and aggregate/amyloid formation is still a matter of debate. Some native disulfide bonds help to prevent aggregation or fibrillization. In general, hydrophobic residues are mostly buried inside the core structure with native disulfide bonds¹⁰³. Therefore, disruption of native disulfide bonds can result in exposure of hydrophobic structures, which may lead to protein aggregation. For example, the only disulfide bond in human cellular prion protein (PrP), C179-C214, is buried in the hydrophobic core, contributing to stabilize the globular structure¹⁰⁴ and does not exist in the pathological scrapie PrP. Instead, the pathological scrapie PrP forms intermolecular disulfide bonds. Evidences showed that the scrapie PrP polymers can convert monomers of normal cellular PrP into scrapie-like conformation through disulfide exchange⁷⁵ (Figure 1.6). Reduction of disulfide bond increases the protein conformational flexibility, which can assist conversion of the native α -helix structure into β -sheets and then form amyloid fibrils¹⁰⁵. In addition, cleavage of the disulfide bond not only promotes conversion of

scrapie PrP, but also leads to dramatic conformational change and exposure of interior structures of the protein, which enhances in PrP-membrane interaction, alters cell physiology, and finally causes cell death. Furthermore, reduction of native intramolecular disulfide bonds leads to protein disulfide cross-linking or self-assembly, results in fibrillation. This has been shown for many amyloid proteins^{75, 105, 106}.

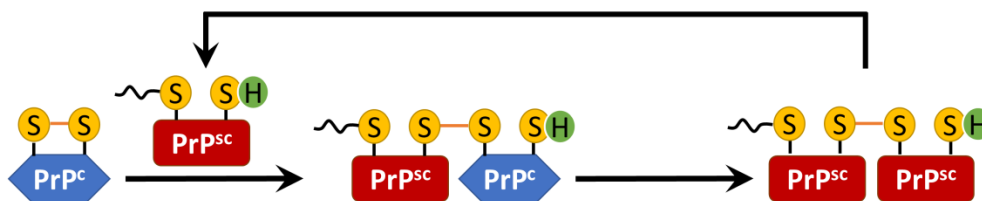


Figure 1.6. The transformation of cellular PrP (PrP^c) to the pathological scrapie PrP (PrP^{sc}) polymer.* The breakage of intramolecular disulfide bonds of PrP^c can be initiated by free thiol group on PrP^{sc} by forming intermolecular disulfide cross-linking and is followed by conformational change of PrP^c. When the conversion is completed, the newly formed polymer starts another cycle. *Adapted from Li et al. 2013⁷⁵

In some other proteins, the native disulfide bonds are essential to amyloid fibril formation. The β 2-microglobulin (β 2M) has one fully buried intra-chain disulfide bond, which significantly contributes to amyloid fibril formation rather than stabilizing the native fold^{107, 108}. Another example could be amyloidogenic peptide Abri, which predominantly has β -strands with one intramolecular disulfide bond (Table 1.1). In solution, the disulfide bond on Abri peptide promotes rapid formation of oligomers and the highly insoluble amyloid deposits in familial British dementia¹⁰⁹. According to Abkevich and Shakhnovich¹¹⁰, folding could be directly affected by the relative position of disulfide bonds, meaning that if the disulfides located in or near folding/aggregation

nucleus, they may guide the process, whereas those located far from the nucleus structures may slow down the progresses¹¹⁰.

Since natural protein/peptide with disulfide bonds have more constrained frameworks and higher stabilities than other biomolecules, intermolecular disulfide cross-linking have attracted the attention of protein engineering. Hundreds of peptide-based drugs design and valuable scaffolds in tissue engineering are based on the discovery of natural disulfide-rich architectures¹¹¹. Furthermore, some disulfide-rich peptides were also applied to solve the oral delivery and cell uptake issues in pharmacology. One such example is application of the cell-penetrating peptides (CPPs)¹¹² in drug delivery platforms. CPPs are short, water-soluble peptides that are capable of crossing cell membranes and even the blood-brain barrier. Since the intracellular glutathione concentration is ~ 1000-fold higher than those in the extracellular environment, disulfide moieties are widely used for building CPP-drug conjugates¹¹³. In this light, the CPP-conjugates are stable during transfer in the tissues, but once the conjugates crosses the cell membrane, the elevated thiol concentration breaks disulfide bonds and leads to release of the cargo drug¹¹⁴. This approach of CPP has been successfully applied in drug delivery field and may bring a large number of peptide drugs into the market, contributing to both academic and industrial worlds¹¹¹.

1.5.2 Posttranslational modifications in proteins

There are approximately 30,000 protein coding genes in human genome, but the actual number of cellular protein species in cells are more than one million. This diversification of protein first expands by mRNA splicing at the transcriptional level, which is a central topic of RNA metabolism¹¹⁵ and will not be discussed here. The second

proteome expansion route is the specific enzyme-catalyzed covalent posttranslational modification (PTM) on the side chain or backbones of nascent or folded proteins. Depending on the targeting amino acid side chains, the modifying enzyme, and the reversibility of the reaction, the major types of protein covalent modifications can be classified as phosphorylation, acetylation, methylation, ubiquitination, and glycosylation (Table 1.2). Other chemical events such as disulfide formation (discussed in section 1.2), backbone cleavage, proteasome autoactivation, and green fluorescent protein maturation are also considered as PTMs.

Table 1.2. Posttranslational modifications on protein side chains¹⁰².

Residue	Reaction
Arginine	N-methylation, N-ADP-ribosylation
Asparagine	N-glycosylation, N-ADP-ribosylation , protein splicing
Aspartic acid	Phosphorylation, Isomerization to isoAsp
Cysteine	S-hydroxylation (S-OH), Disulfide bond formation , Phosphorylation, S-acylation, S-prenylation, protein splicing
Glutamine	Transglutamination
Glutamic acid	Methylation, Carboxylation, Polyglycination, Polyglutamylation
Glycine	C-hydroxylation
Histidine	Aminocarboxypropylation, Phosphorylation, Regulatory systems, N-methylation
Lysine	N-methylation, N-acylation by acetyl, biotinyl, lipoyl, ubiquityl groups C-hydroxylation
Methionine	Oxidation to sulfoxide
Proline	C-hydroxylation
Serine	Phosphorylation, Phosphatases, O-glycosylation, Pphosphopantetheinylation

	Autocleavages
Threonine	Phosphorylation, O-glycosylation
Tryptophan	C-mannosylation
Tyrosine	Phosphorylation, Sulfation, <i>ortho</i> -Nitration, TOPA quinone

The major PTMs covalently add external chemical groups on the protein that alter the protein's structure, size, charge, or conformation, and result in changes of hydrophobicity, binding affinity, enzyme activity, or sometimes create architectural impetus for molecular signaling. As the most common PTM, phosphorylation introduces anionic phosphates to the neutral OH side chains of serine, tyrosine, and threonine. The local microenvironments around these residues are then altered, and as a consequence, protein conformation changes. Tau is a microtubule associated protein that contains 5 tyrosine and 80 serine/threonine as potential phosphorylation sites. When tau is abnormally hyper-phosphorylated, it aggregates into paired helical filaments and forms neurofibrillary tangles, which is identified as a histopathological hallmark in Alzheimer's disease¹¹⁶. Similarly, acetylation alters the charge distribution on proteins by blocking the positively charged lysine side chains with neutral acetyl groups. There are tens of thousands of glycoprotein variants that are added to at least one third of secretory proteins by glycosylation, which alters protein architecture during folding or quality-control processes¹⁰². A protein can be posttranslationally modified with the same group at many residues, as the tau protein introduced above, or a protein can also have several PTMs targeting on the same molecule. For example, histone has a total of 15 lysine residues on its four tails that organize how DNA is wrapped into nucleosomes. Two PTM types, acetylation and methylation, compete on the positively charged lysine and arginine

side chains on histone tails and result in opposite effects on gene transcription. Histone acetylation leads to loose packing of nucleosomes, which initiates binding of transcription factors and starts gene expression. Whereas blocking the lysine and arginine with methyl groups can result in tight packing of nucleosomes, and gene expression is turned off¹¹⁷. Another PTM, ubiquitination, also competes with acetylation and methylation on lysine side chains. Unlike the small single acetyl groups in acetylation, the ubiquityl acetyl moiety links to an 8-kDa protein ubiquitin and functions as a signaling scaffold that provides information with particular partner proteins during biological responses. Ubiquitination usually targets the proteins that need to be relocated and degraded in cells. The partner proteins that contain ubiquitin receptors can act as chaperones, importing the target protein into early endosomes and then lysosomes for hydrolytic degradation¹⁰².

To date there are more than 300 PTMs that have been discovered with the advancement of high-resolution mass spectrometry techniques, and the number is still increasing. It is not surprising that PTMs play an important role in protein folding and aggregation. The amyloidogenic proteins such as A β and tau in Alzheimer's patients' brains are recently detected to have various types of glycosylation on the side chains¹¹⁸,¹¹⁹. Extracellular phosphorylation and N-terminal truncation both result in acceleration of A β assembly, leading to neurotoxic aggregate species^{120, 121}. Therefore, studies of PTMs can not only give insight into how the bioactive structures have been tuned by nature for hundreds of thousands of years, they also help us to understand the pathology of diseases. Moreover, since many PTMs serve as parts of the signaling pathways, they have been also widely applied as biomarkers or potential therapeutic targets in many diseases^{122, 123}.

1.6 Motivations and hypothesis

As introduced in section 1.4, in addition to amyloid fibrils, the aggregation intermediates and amorphous aggregates now draw the biggest question marks in the field of amyloid diseases. Recent research strongly suggests that the non-fibril oligomers hold the key of toxicity. Even though several oligomeric structures have been characterized, there is still no common standard to define a “toxic structure”. In addition, there are many factors that can affect protein structure in a living cell in spite of great strides made in the field. The full picture of protein aggregation and its relationship to toxicity is not clear. Therefore, it is important to characterize and link many different structural forms of aggregates to toxicity to have a better understanding of the protein misfolding diseases.

One of the intracellular protein folding factors that can be possibly altered is the status of disulfide bonds. In the past, most studies on protein disulfide bonds were carried out at extreme pH or temperature^{79, 80, 124}, while the *in vivo* environment is relatively mild in terms of pH and temperature variations. Experiments under conditions close to physiological (pH 7.2 and 37 °C) may contribute to a better understanding of protein aggregation process in cells. Besides the high concentration of glutathione in cytosol, improper use of thiol based antioxidant supplements on a daily basis can also increase the levels of free thiol groups in the body, resulting in a highly reducing environment *in vivo*. The highly reducing environment has potential of breaking protein disulfide bonds. Therefore, in the first project (chapter 3) we selected a commonly used disulfide reducing agent, dithiothreitol (DTT), to treat two disulfide rich proteins, hen egg white lysozyme (Lysozyme) and bovine serum albumin (BSA), near physiological condition. Lysozyme

is the amyloidogenic protein that has the highest number of native disulfide bonds (4) and is globular in shape. While BSA is a globular protein with 17 native disulfide bonds but is not involved with any amyloid disorders. Investigating the effect of disulfide scrambling (i.e. non-native disulfide formation) on the aggregation process using these two different types of proteins could give insight into the aggregation pathways that may be relevant to several other proteins.

The other factor that we investigated was how a PTM, like acetylation on lysine side chains, can impact protein aggregation. As discussed in chapter 4, we blocked the positive charge on the two lysine residues of A β peptide, K16 and K28, by acetylation. The A β peptide has only 42 amino acids and is an intrinsically disordered structure. Aggregation of A β is simply driven by hydrophobic interactions. Residue K16 is located at an intermolecular binding region (K16-F20) and the K28 residue is known to form important intramolecular salt bridges that stabilize the β -sheets in amyloid fibrils. Therefore, we propose that acetylation on one or both of these two lysine residues could impact A β fibrillization process. How do these acetylation modulate A β aggregation may give insight into therapeutic strategies of Alzheimer's disease.

Finally, we wanted to focus on the central problem in protein aggregation field, the relationship between aggregate structure and its toxicity. Unlike the amyloid structure that is well defined, the structural characteristics of amorphous aggregates are still not clear. After generating many different types of amorphous aggregates using literature reported condition, we noticed that the amorphous structures are variable. In chapter 5, amorphous aggregates that were generated at ten different conditions were characterized and classified in terms of size, hydrophobicity, or structural flexibility. Then these

aggregates were used to measure cell cytotoxicity. By comparing the cytotoxicity of these amorphous aggregates, we want to identify the dominant structure that is toxic. Once we have a good understanding of the structures, the goal is to identify small molecules that can efficiently bind to these structures and hence can decrease their toxicity. This will have serious implication for many protein misfolding diseases for developing effective drug candidates.

1.7 References

1. So much more to know. *Science* **2005**, *309*, 78-102.
2. Kendrew, J. C.; Bodo, G.; Dintzis, H. M.; Parrish, R. G.; Wyckoff, H., et al., A three-dimensional model of the myoglobin molecule obtained by x-ray analysis. *Nature* **1958**, *181*, 662-6.
3. Kendrew, J. C.; Dickerson, R. E.; Strandberg, B. E.; Hart, R. G.; Davies, D. R., et al., Structure of myoglobin: A three-dimensional Fourier synthesis at 2 A. resolution. *Nature* **1960**, *185*, 422-7.
4. Perutz, M. F.; Rossmann, M. G.; Cullis, A. F.; Muirhead, H.; Will, G., et al., Structure of haemoglobin: a three-dimensional Fourier synthesis at 5.5-A. resolution, obtained by X-ray analysis. *Nature* **1960**, *185*, 416-22.
5. Dill, K. A., Dominant forces in protein folding. *Biochemistry* **1990**, *29*, 7133-55.
6. Wu, H., Studies on Denaturation of Proteins. XIII. A Theory of Denaturation. *Chinese Journal of Physiology* **1931**, 321-44.
7. Ruddon, R. W.; Bedows, E., Assisted protein folding. *Journal of Biological Chemistry* **1997**, *272*, 3125-8.

8. Anfinsen, C. B., Principles that govern folding of protein chains. *Science* **1973**, *181*, 223-30.
9. Levinthal, C., How to fold graciously. *Mossbauer Spectroscopy in Biological Systems: Proceedings of a meeting held at Allerton House, Monticello, Illinois*. **1969**, 22-4.
10. Levinthal, C., Are there pathways for protein folding? *Journal de Chimie Physique et de Physico-Chimie Biologique* **1968**, *65*, 44-5.
11. Goldberger, R. F.; Epstein, C. J.; Anfinsen, C. B., Acceleration of reactivation of reduced bovine pancreatic ribonuclease by a microsomal system from rat liver. *The Journal of biological chemistry* **1963**, *238*, 628-35.
12. Marquardt, T.; Hebert, D. N.; Helenius, A., Posttranslational folding of influenza hemagglutinin in isolated endoplasmic reticulum-derived microsomes. *Journal of Biological Chemistry* **1993**, *268*, 19618-25.
13. Zapun, A.; Creighton, T. E.; Rowling, P. J. E.; Freedman, R. B., Folding invitro of bovine pancreatic trypsin-inhibitor in the presence of proteins of the endoplasmic-reticulum. *Proteins-Structure Function and Genetics* **1992**, *14*, 10-5.
14. Huth, J. R.; Perini, F.; Lockridge, O.; Bedows, E.; Ruddon, R. W., Protein-folding and assembly in-vitro parallel intracellular folding and assembly - Catalysis of folding and assembly of the human chorionic-gonadotropin alpha-beta dimer by protein disulfide-isomerase. *Journal of Biological Chemistry* **1993**, *268*, 16472-82.
15. Laskey, R. A.; Honda, B. M.; Mills, A. D.; Finch, J. T., Nucleosomes are assembled by an acidic protein which binds histones and transfers them to DNA. *Nature* **1978**, *275*, 416-20.
16. Ellis, R. J.; Hemmingsen, S. M., Molecular chaperones - Proteins essential for the biogenesis of some macromolecular structures. *Trends in Biochemical Sciences* **1989**, *14*, 339-42.

17. Berman, H. M.; Kleywegt, G. J.; Nakamura, H.; Markley, J. L., The Protein Data Bank archive as an open data resource. *Journal of Computer-Aided Molecular Design* **2014**, *28*, 1009-14.
18. Allen, F.; Almasi, G.; Andreoni, W.; Beece, D.; Berne, B. J., et al., Blue Gene: A vision for protein science using a petaflop supercomputer. *Ibm Systems Journal* **2001**, *40*, 310-27.
19. Shirts, M.; Pande, V. S., Computing - Screen savers of the world unite! *Science* **2000**, *290*, 1903-4.
20. Cooper, S.; Khatib, F.; Treuille, A.; Barbero, J.; Lee, J., et al., Predicting protein structures with a multiplayer online game. *Nature* **2010**, *466*, 756-60.
21. Pauling, L., The nature of the chemical bond. Application of results obtained from the quantum mechanics and from a theory of paramagnetic susceptibility to the structure of molecules. *the Journal of American Chemical Society* **1931**, *53*, 1367-400.
22. Yang, J. S.; Chen, W. W.; Skolnick, J.; Shakhnovich, E. I., All-atom ab initio folding of a diverse set of proteins. *Structure* **2007**, *15*, 53-63.
23. Cohn, E.; McMeekin, T.; Edsall, J.; Blanchard, M., The electrical forces in systems containing biological components. II. The molal volumes of amino acids, proteins, and certain related substances. *the Journal of Biological Chemistry* **1933**, *100*, 28-31.
24. Mirsky, A. E.; Pauling, L., On the Structure of Native, Denatured, and Coagulated Proteins. *Proceedings of the National Academy of Sciences of the United States of America* **1936**, *22*, 439-47.
25. Eyring, H.; Stearn, A., The application of the theory of absolute reaction rates to proteins. *Chemical Reviews* **1939**, *24*, 253-70.

26. Fersht, A. R., Conformational equilibria in α - and β -chymotrypsin. The energetics and importance of the salt bridge. *Journal of molecular biology* **1972**, *64*, 497-509.
27. Perutz, M. F.; Raidt, H., Stereochemical basis of heat-stability in bacterial ferredoxins and in hemoglobin-A2. *Nature* **1975**, *255*, 256-9.
28. Jacobsen, C. F.; Linderstrom-Lang, K., Salt linkages in proteins. *Nature* **1949**, *164*, 411-.
29. Stigter, D.; Dill, K. A., Charge effects on folded and unfolded proteins. *Biochemistry* **1990**, *29*, 1262-71.
30. Barlow, D. J.; Thornton, J. M., Ion-pairs in proteins. *Journal of Molecular Biology* **1983**, *168*, 867-85.
31. Pauling, L.; Corey, R. B.; Branson, H. R., The structure of proteins; two hydrogen-bonded helical configurations of the polypeptide chain. *Proceedings of the National Academy of Sciences of the United States of America* **1951**, *37*, 205-11.
32. Lotan, N.; Bixon, M.; Berger, A., Alpha-helix formation by solvent-solvent interaction. *Biopolymers* **1967**, *5*, 69-77.
33. Mattice, W. L.; Scheraga, H. A., Matrix formulation of the transition from a statistical coil to an intramolecular antiparallel beta-sheet. *Biopolymers* **1984**, *23*, 1701-24.
34. Schellman, J., The factors affecting the stability of hydrogen-bonded polypeptide structures in solution. *the Journal of Physical Chemistry* **1958**, *62*, 1485-94.
35. Baker, E. N.; Hubbard, R. E., Hydrogen-bonding in globular-proteins. *Progress in Biophysics & Molecular Biology* **1984**, *44*, 97-179.
36. Dill, K. A.; Ozkan, S. B.; Shell, M. S.; Weikl, T. R., The protein folding problem. In *Annual Review of Biophysics*, 2008; Vol. 37, pp 289-316.

37. Fersht, A. R.; Shi, J. P.; Knilljones, J.; Lowe, D. M.; Wilkinson, A. J., et al., Hydrogen-bonding and biological specificity analyzed by protein engineering. *Nature* **1985**, *314*, 235-8.
38. Alber, T.; Sun, D. P.; Wilson, K.; Wozniak, J. A.; Cook, S. P., et al., Contributions of hydrogen-bonds of thr-157 to the thermodynamic stability of phage-T4 lysozyme. *Nature* **1987**, *330*, 41-6.
39. Grutter, M. G.; Gray, T. M.; Weaver, L. H.; Alber, T.; Wilson, K., et al., Structural studies of mytant of the lysozyme of bacteriophage-T4 - The temperature-sensitive mutant protein Thr157-IIE. *Journal of Molecular Biology* **1987**, *197*, 315-29.
40. Kauzmann, W., Some factors in the interpretation of protein denaturation. *Adv. Protein Chem.* **1959**, *14*, 1-63.
41. Debye, P., Light scattering in soap solutions. *The Journal of physical and colloid chemistry* **1949**, *53*, 1-8.
42. Chothia, C., Hydrophobic bonding and accessible surface-area in proteins. *Nature* **1974**, *248*, 338-9.
43. Lim, W. A.; Sauer, R. T., Alternative packing arrangements in the hydrophobic core of lambda-repressor. *Nature* **1989**, *339*, 31-6.
44. Bowie, J. U.; Reidhaarolson, J. F.; Lim, W. A.; Sauer, R. T., Dediphering the message in protein sequences - tolerance to amino-acid substitutions. *Science* **1990**, *247*, 1306-10.
45. Sweet, R. M.; Eisenberg, D., Correlation of sequence hydrophobicities measures similarity in 3-dimensional protein-structure. *Journal of Molecular Biology* **1983**, *171*, 479-88.

46. Bashford, D.; Chothia, C.; Lesk, A. M., Determinants of a protein fold - unique features of the flobin amino-acid-sequences. *Journal of Molecular Biology* **1987**, *196*, 199-216.
47. Yutani, K.; Ogasahara, K.; Tsujita, T.; Sugino, Y., Dependence of conformational stability on hydrophobicity of the amino-acid residue in a series of variant proteins substituted at a unique position of tryptophan synthase alpha-subunit. *Proceedings of the National Academy of Sciences of the United States of America* **1987**, *84*, 4441-4.
48. Matsumura, M.; Bechtel, W. J.; Matthews, B. W., Hydrophobic stabilization in T4 lysozyme determined directly by multiple substitutions of ILE-3. *Nature* **1988**, *334*, 406-10.
49. Goodman, M.; Verdini, A. S.; Toniolo, C.; Phillips, W. D.; Bovey, F. A., Sensitive criteria for the critical size for helix formation in oligopeptides. *Proceedings of the National Academy of Sciences of the United States of America* **1969**, *64*, 444-50.
50. Zimm, B.; Bragg, J., Theory of the phase transition between helix and random coil in polypeptide chains. *Journal of Chemical Physics* **1959**, *31*, 526-35.
51. Rooman, M. J.; Wodak, S. J., Identification of predictive sequence motifs limited by protein-structure data-base size. *Nature* **1988**, *335*, 45-9.
52. Qian, N.; Sejnowski, T. J., Prediction the secondary structure of globular-proteins using neural network models. *Journal of Molecular Biology* **1988**, *202*, 865-84.
53. Holley, L. H.; Karplus, M., Protein secondary structure prediction with a neural network. *Proceedings of the National Academy of Sciences of the United States of America* **1989**, *86*, 152-6.
54. Chan, H. S.; Dill, K. A., Compact polymers. *Macromolecules* **1989**, *22*, 4559-73.
55. Karplus, M.; Ichiye, T.; Pettitt, B. M., Configurational entropy of native proteins. *Biophysical Journal* **1987**, *52*, 1083-5.

56. Matthews, B. W.; Nicholson, H.; Becktel, W. J., Enhanced protein thermostability from site-directed mutations that decrease the entropy of unfolding. *Proceedings of the National Academy of Sciences of the United States of America* **1987**, *84*, 6663-7.
57. Chan, H. S.; Dill, K. A., Origins of structure in globular-proteins. *Proceedings of the National Academy of Sciences of the United States of America* **1990**, *87*, 6388-92.
58. Matsumura, M.; Becktel, W. J.; Levitt, M.; Matthews, B. W., Stabilization of phage-t4 lysozyme by engineered disulfide bonds. *Proceedings of the National Academy of Sciences of the United States of America* **1989**, *86*, 6562-6.
59. Yamaguchi, T.; Yagi, H.; Goto, Y.; Matsuzaki, K.; Hoshino, M., A Disulfide-Linked Amyloid-beta Peptide Dimer Forms a Protofibril-like Oligomer through a Distinct Pathway from Amyloid Fibril Formation. *Biochemistry* **2010**, *49*, 7100-7.
60. Onuchic, J. N.; LutheySchulten, Z.; Wolynes, P. G., Theory of protein folding: The energy landscape perspective. *Annu. Rev. Phys. Chem.* **1997**, *48*, 545-600.
61. Bryngelson, J. D.; Wolynes, P. G., Spin-glasses and the statistical-mechanics of protein folding. *Proceedings of the National Academy of Sciences of the United States of America* **1987**, *84*, 7524-8.
62. Bryngelson, J. D.; Onuchic, J. N.; Socci, N. D.; Wolynes, P. G., Funnels, pathways, and the energy landscape of protein-folding - a synthesis. *Proteins-Structure Function and Genetics* **1995**, *21*, 167-95.
63. Sridevi, K.; Lakshmikanth, G. S.; Krishnamoorthy, G.; Udgaonkar, J. B., Increasing stability reduces conformational heterogeneity in a protein folding intermediate ensemble. *Journal of Molecular Biology* **2004**, *337*, 699-711.
64. Bartlett, A. I.; Radford, S. E., An expanding arsenal of experimental methods yields an explosion of insights into protein folding mechanisms. *Nature Structural & Molecular Biology* **2009**, *16*, 582-8.

65. Vendruscolo, M.; Paci, E.; Karplus, M.; Dobson, C. M., Structures and relative free energies of partially folded states of proteins. *Proceedings of the National Academy of Sciences of the United States of America* **2003**, *100*, 14817-21.
66. Capaldi, A. P.; Shastry, M. C. R.; Kleanthous, C.; Roder, H.; Radford, S. E., Ultrarapid mixing experiments reveal that Im7 folds via an on-pathway intermediate. *Nature Structural Biology* **2001**, *8*, 68-72.
67. Jahn, T. R.; Radford, S. E., The Yin and Yang of protein folding. *Febs Journal* **2005**, *272*, 5962-70.
68. Bollen, Y. J. M.; Sanchez, I. E.; van Mierlo, C. P. M., Formation of on- and off-pathway intermediates in the folding kinetics of *Azotobacter vinelandii* apoflavodoxin. *Biochemistry* **2004**, *43*, 10475-89.
69. Hartl, F. U.; Hayer-Hartl, M., Converging concepts of protein folding in vitro and in vivo. *Nature Structural & Molecular Biology* **2009**, *16*, 574-81.
70. Dobson, C. M., Protein folding and misfolding. *Nature* **2003**, *426*, 884-90.
71. Stefani, M.; Dobson, C. M., Protein aggregation and aggregate toxicity: new insights into protein folding, misfolding diseases and biological evolution. *Journal of Molecular Medicine-Jmm* **2003**, *81*, 678-99.
72. Pickart, C. M.; Cohen, R. E., Proteasomes and their kin: Proteases in the machine age. *Nature Reviews Molecular Cell Biology* **2004**, *5*, 177-87.
73. Fowler, D. M.; Koulov, A. V.; Alory-Jost, C.; Marks, M. S.; Balch, W. E., et al., Functional amyloid formation within mammalian tissue. *Plos Biology* **2006**, *4*, 100-7.
74. Tycko, R.; Wickner, R. B., Molecular Structures of Amyloid and Prion Fibrils: Consensus versus Controversy. *Accounts of Chemical Research* **2013**, *46*, 1487-96.

75. Li, Y.; Yan, J.; Zhang, X.; Huang, K., Disulfide bonds in amyloidogenesis diseases related proteins. *Proteins-Structure Function and Bioinformatics* **2013**, *81*, 1862-73.
76. Stefani, M., Protein misfolding and aggregation: new examples in medicine and biology of the dark side of the protein world. *Biochimica Et Biophysica Acta-Molecular Basis of Disease* **2004**, *1739*, 5-25.
77. Guijarro, J. I.; Sunde, M.; Jones, J. A.; Campbell, I. D.; Dobson, C. M., Amyloid fibril formation by an SH3 domain. *Proceedings of the National Academy of Sciences of the United States of America* **1998**, *95*, 4224-8.
78. Uversky, V. N.; Fink, A. L., Conformational constraints for amyloid fibrillation: the importance of being unfolded. *Biochimica Et Biophysica Acta-Proteins and Proteomics* **2004**, *1698*, 131-53.
79. Krebs, M. R. H.; Wilkins, D. K.; Chung, E. W.; Pitkeathly, M. C.; Chamberlain, A. K., et al., Formation and seeding of amyloid fibrils from wild-type hen lysozyme and a peptide fragment from the beta-domain. *Journal of Molecular Biology* **2000**, *300*, 541-9.
80. Morozova-Roche, L. A.; Zurdo, J.; Spencer, A.; Noppe, W.; Receveur, V., et al., Amyloid fibril formation and seeding by wild-type human lysozyme and its disease-related mutational variants. *Journal of Structural Biology* **2000**, *130*, 339-51.
81. Levy, E.; Carman, M. D.; Fernandezmadrid, I. J.; Power, M. D.; Lieberburg, I., et al., Mutation of the alzheimer's disease amyloid gene in hereditary cerebral-hemorrhage, dutch type. *Science* **1990**, *248*, 1124-6.
82. Murakami, K.; Irie, K.; Morimoto, A.; Ohigashi, H.; Shindo, M., et al., Synthesis, aggregation, neurotoxicity, and secondary structure of various A beta 1-42 mutants of familial Alzheimer's disease at positions 21-23. *Biochemical and Biophysical Research Communications* **2002**, *294*, 5-10.

83. Wakutani, Y.; Watanabe, K.; Adachi, Y.; Wada-Isoe, K.; Urakami, K., et al., Novel amyloid precursor protein gene missense mutation (D678N) in probable familial Alzheimer's disease. *Journal of Neurology Neurosurgery and Psychiatry* **2004**, *75*, 1039-42.
84. Der-Sarkissian, A.; Jao, C. C.; Chen, J.; Langen, R., Structural organization of alpha-synuclein fibrils studied by site-directed spin labeling. *Journal of Biological Chemistry* **2003**, *278*, 37530-5.
85. Hardy, J.; Allsop, D., Amyloid deposition and the central event in the etiology of Alzheimer's disease. *Trends in Pharmacological Sciences* **1991**, *12*, 383-8.
86. Lue, L. F.; Kuo, Y. M.; Roher, A. E.; Brachova, L.; Shen, Y., et al., Soluble amyloid beta peptide concentration as a predictor of synaptic change in Alzheimer's disease. *American Journal of Pathology* **1999**, *155*, 853-62.
87. Naslund, J.; Haroutunian, V.; Mohs, R.; Davis, K. L.; Davies, P., et al., Correlation between elevated levels of amyloid beta-peptide in the brain and cognitive decline. *Jama-Journal of the American Medical Association* **2000**, *283*, 1571-7.
88. Wang, J.; Dickson, D. W.; Trojanowski, J. Q.; Lee, V. M. Y., The levels of soluble versus insoluble brain A beta distinguish Alzheimer's disease from normal and pathologic aging. *Experimental Neurology* **1999**, *158*, 328-37.
89. Bucciantini, M.; Giannoni, E.; Chiti, F.; Baroni, F.; Formigli, L., et al., Inherent toxicity of aggregates implies a common mechanism for protein misfolding diseases. *Nature* **2002**, *416*, 507-11.
90. Ross, C. A.; Poirier, M. A., What is the role of protein aggregation in neurodegeneration? *Nature Reviews Molecular Cell Biology* **2005**, *6*, 891-8.
91. Anand, R.; Gill, K. D.; Mahdi, A. A., Therapeutics of Alzheimer's disease: Past, present and future. *Neuropharmacology* **2014**, *76*, 27-50.

92. Mossuto, M. E.; Bolognesi, B.; Guixer, B.; Dhulesia, A.; Agostini, F., et al., Disulfide Bonds Reduce the Toxicity of the Amyloid Fibrils Formed by an Extracellular Protein. *Angewandte Chemie-International Edition* **2011**, *50*, 7048-51.
93. Bramanti, E.; Fulgentini, L.; Bizzarri, R.; Lenci, F.; Sgarbossa, A., beta-Amyloid Amorphous Aggregates Induced by the Small Natural Molecule Ferulic Acid. *Journal of Physical Chemistry B* **2013**, *117*, 13816-21.
94. Truscott, R. J. W., Age-related nuclear cataract - oxidation is the key. *Experimental Eye Research* **2005**, *80*, 709-25.
95. Wang, L.; Maji, S. K.; Sawaya, M. R.; Eisenberg, D.; Riek, R., Bacterial inclusion bodies contain amyloid-like structure. *Plos Biology* **2008**, *6*, 1791-801.
96. de Groot, N. S.; Sabate, R.; Ventura, S., Amyloids in bacterial inclusion bodies. *Trends in Biochemical Sciences* **2009**, *34*, 408-16.
97. Yang, M.; Dutta, C.; Tiwari, A., Disulfide-Bond Scrambling Promotes Amorphous Aggregates in Lysozyme and Bovine Serum Albumin. *Journal of Physical Chemistry B* **2015**, *119*, 3969-81.
98. Mitraki, A.; Fane, B.; Haasepettingell, C.; Sturtevant, J.; King, J., Global suppression of protein folding defects and inclusion body formation. *Science* **1991**, *253*, 54-8.
99. Hartl, F. U.; Bracher, A.; Hayer-Hartl, M., Molecular chaperones in protein folding and proteostasis. *Nature* **2011**, *475*, 324-32.
100. Sharma, S. K.; De Los Rios, P.; Christen, P.; Lustig, A.; Goloubinoff, P., The kinetic parameters and energy cost of the Hsp70 chaperone as a polypeptide unfoldase. *Nature Chemical Biology* **2010**, *6*, 914-20.
101. Frydman, J.; Hartl, F. U., Principles of chaperone-assisted protein folding: Differences between in vitro and in vivo mechanisms. *Science* **1996**, *272*, 1497-502.

102. Walsh, C. T.; Garneau-Tsodikova, S.; Gatto, G. J., Protein posttranslational modifications: The chemistry of proteome diversifications. *Angewandte Chemie-International Edition* **2005**, *44*, 7342-72.
103. Wedemeyer, W. J.; Welker, E.; Narayan, M.; Scheraga, H. A., Disulfide bonds and protein folding. *Biochemistry* **2000**, *39*, 4207-16.
104. Zahn, R.; Liu, A. Z.; Luhrs, T.; Riek, R.; von Schroetter, C., et al., NMR solution structure of the human prion protein. *Proceedings of the National Academy of Sciences of the United States of America* **2000**, *97*, 145-50.
105. Feughelman, M.; Willis, B. K., Thiol-disulfide interchange a potential key to conformational change associated with amyloid fibril formation. *Journal of Theoretical Biology* **2000**, *206*, 313-5.
106. Chattopadhyay, M.; Durazo, A.; Sohn, S. H.; Strong, C. D.; Gralla, E. B., et al., Initiation and elongation in fibrillation of ALS-linked superoxide dismutase. *Proceedings of the National Academy of Sciences of the United States of America* **2008**, *105*, 18663-8.
107. Ohhashi, Y.; Hagihara, Y.; Kozhukh, G.; Hoshino, M.; Hasegawa, K., et al., The intrachain disulfide bond of beta(2)-microglobulin is not essential for the immunoglobulin fold at neutral pH, but is essential for amyloid fibril formation at acidic pH. *Journal of Biochemistry* **2002**, *131*, 45-52.
108. Yamamoto, K.; Yagi, H.; Ozawa, D.; Sasahara, K.; Naiki, H., et al., Thiol compounds inhibit the formation of amyloid fibrils by beta(2)-microglobulin at neutral pH. *Journal of Molecular Biology* **2008**, *376*, 258-68.
109. El-Agnaf, O. M. A.; Sheridan, J. M.; Sidera, C.; Siligardi, G.; Hussain, R., et al., Effect of the disulfide bridge and the C-terminal extension on the oligomerization of the amyloid peptide ABri implicated in familial British dementia. *Biochemistry* **2001**, *40*, 3449-57.

110. Abkevich, V. I.; Shakhnovich, E. I., What can disulfide bonds tell us about protein energetics, function and folding: Simulations and bioinformatics analysis. *Journal of Molecular Biology* **2000**, *300*, 975-85.
111. Gongora-Benitez, M.; Tulla-Puche, J.; Albericio, F., Multifaceted Roles of Disulfide Bonds. Peptides as Therapeutics. *Chemical Reviews* **2014**, *114*, 901-26.
112. Lundberg, P.; Langel, U., A brief introduction to cell-penetrating peptides. *Journal of Molecular Recognition* **2003**, *16*, 227-33.
113. West, K. R.; Otto, S., Reversible covalent chemistry in drug delivery. *Current drug discovery technologies* **2005**, *2*, 123-60.
114. Hallbrink, M.; Floren, A.; Elmquist, A.; Pooga, M.; Bartfai, T., et al., Cargo delivery kinetics of cell-penetrating peptides. *Biochim. Biophys. Acta-Biomembr.* **2001**, *1515*, 101-9.
115. Black, D. L., Mechanisms of alternative pre-messenger RNA splicing. *Annual Review of Biochemistry* **2003**, *72*, 291-336.
116. Wang, J.-Z.; Xia, Y.-Y.; Grundke-Iqbal, I.; Iqbal, K., Abnormal Hyperphosphorylation of Tau: Sites, Regulation, and Molecular Mechanism of Neurofibrillary Degeneration. *Journal of Alzheimers Disease* **2013**, *33*, S123-S39.
117. Jenuwein, T.; Allis, C. D., Translating the histone code. *Science* **2001**, *293*, 1074-80.
118. Halim, A.; Brinkmalm, G.; Ruetschi, U.; Westman-Brinkmalm, A.; Portelius, E., et al., Site-specific characterization of threonine, serine, and tyrosine glycosylations of amyloid precursor protein/amyloid beta-peptides in human cerebrospinal fluid. *Proceedings of the National Academy of Sciences of the United States of America* **2011**, *108*, 11848-53.

119. Morris, M.; Knudsen, G. M.; Maeda, S.; Trinidad, J. C.; Ioanoviciu, A., et al., Tau post-translational modifications in wild-type and human amyloid precursor protein transgenic mice. *Nature neuroscience* **2015**, *18*, 1183-9.
120. Bouter, Y.; Dietrich, K.; Wittnam, J. L.; Rezaei-Ghaleh, N.; Pillot, T., et al., N-truncated amyloid beta (A beta) 4-42 forms stable aggregates and induces acute and long-lasting behavioral deficits. *Acta Neuropathologica* **2013**, *126*, 189-205.
121. Kumar, S.; Rezaei-Ghaleh, N.; Terwel, D.; Thal, D. R.; Richard, M., et al., Extracellular phosphorylation of the amyloid beta-peptide promotes formation of toxic aggregates during the pathogenesis of Alzheimer's disease. *Embo Journal* **2011**, *30*, 2255-65.
122. Krueger, K. E.; Srivastava, S., Posttranslational protein modifications - Current implications for cancer detection, prevention, and therapeutics. *Molecular & Cellular Proteomics* **2006**, *5*, 1799-810.
123. Clark, R. S. B.; Bayir, H.; Jenkins, L. W., Posttranslational protein modifications. *Critical Care Medicine* **2005**, *33*, S407-S9.
124. Bhattacharya, M.; Jain, N.; Mukhopadhyay, S., Insights into the mechanism of aggregation and fibril formation from bovine serum albumin. *Journal of Physical Chemistry B* **2011**, *115*, 4195-205.

Chapter 2 Methods

Several biochemical and biophysical techniques are employed to investigate protein folding, misfolding, and aggregation. Table 2.1 shows techniques most frequently used for protein folding/aggregation research. Each technique listed below has its own strength and limitations. This chapter will focus on introducing the techniques and experimental methods used to carry out protein aggregation studies reported in this dissertation. This includes UV-vis absorbance spectroscopy, fluorescence spectroscopy, non-reducing gel electrophoresis, scanning electron microscopy, cytotoxicity assays, and live cell fluorescence imaging. Details of specific experimental conditions are mentioned in each chapter.

Table 2.1. Some common biophysical methods used to investigate protein folding and aggregation processes^{1, 2}. **U**, unfolded or partially folded states; **N**, native states; **O**, Oligomers; **A**, (amorphous) aggregates; **F**, amyloid fibrils.

Property	Technique	species
Folding/Aggregation		
kinetics	Ultraviolet absorbance	U, N, O, A, F
	Intrinsic fluorescence	U, N, O, A, F
	ANS fluorescence	U, N, O, A, F
	Mass Spectrometry	U, N, O, A, F
	Fluorescence resonance energy transfer (FRET)	U, N
	Hydrogen-deuterium exchange	U, N, O, F
Structure	X-ray diffraction	N, F

	Far-UV circular dichroism (CD)	U, N, O, A, F
	Solution/Solid state NMR	U, N/O, F
	Atomic force microscopy (AFM)	O, A, F
	Electron microscopy (EM)	O, A, F
	Fourier transform infrared spectroscopy (FTIR)	U, N, O, A, F
	Fluorescence microscopy	A, F
Conformation	bis-ANS fluorescence	U, N, O
	Congo red or Thioflavin T fluorescence	A, F
	Analytical ultracentrifugation	U, N, O, F
	Calorimetry	U, N
	Gel chromatography	U, N, O

2.1 UV-visible absorbance spectroscopy

Spectroscopy technique measures the effect of electromagnetic radiation on molecules. Light in the near-ultraviolet and visible (UV-vis) range (150-800 nm) comprises photon energies of about 150–400 kJ/mol³, which are sufficient to excite electrons to a higher energy orbital. Among the six electronic excitations that may occur in an organic molecule (Figure 2. 1), the transitions of n or π electrons to the π^* state can be achieved by the energies from UV-vis lights. Therefore, the substances that applied in spectroscopy analysis normally have delocalized aromatic systems, such as proteins and nucleic acids. The absorption maxima of proteins is normally near 280 nm, contributed mainly by the two aromatic amino acids tryptophan (Trp) and tyrosine (Tyr) (Figure 2.

2). The absorptivity of phenylalanine (Phe) is 10-fold lower than Tyr and 30-fold lower than Trp³, thus, Phe normally does not account for protein UV absorbance. For a protein that contains Trp residues, such as lysozyme, the protein UV absorbance spectra is in the same shape with Trp UV absorbance spectra. The absorbance measurements of proteins are usually carried out in aqueous buffer solution, where the protein absorbance is proportional to its concentration, following the Lambert Beer's law:

$$A = \epsilon \cdot c \cdot l$$

where A is absorbance; ϵ is the molar extinction coefficient ($M^{-1} \cdot cm^{-1}$), describing the light absorption ability of a molecule at certain wavelength; c is molar concentration; and l is the path length in cm. The UV-vis spectroscopy method is very sensitive and nondestructive, therefore, it is widely applied in quantitative analysis. Since the changes in local environment around the chromophores can alter the wavelength of peak absorbance, absorbance spectroscopy technique is also suited for measurements of ligand-binding reaction, conformational changes of proteins or nucleic acids, and protein assembly.

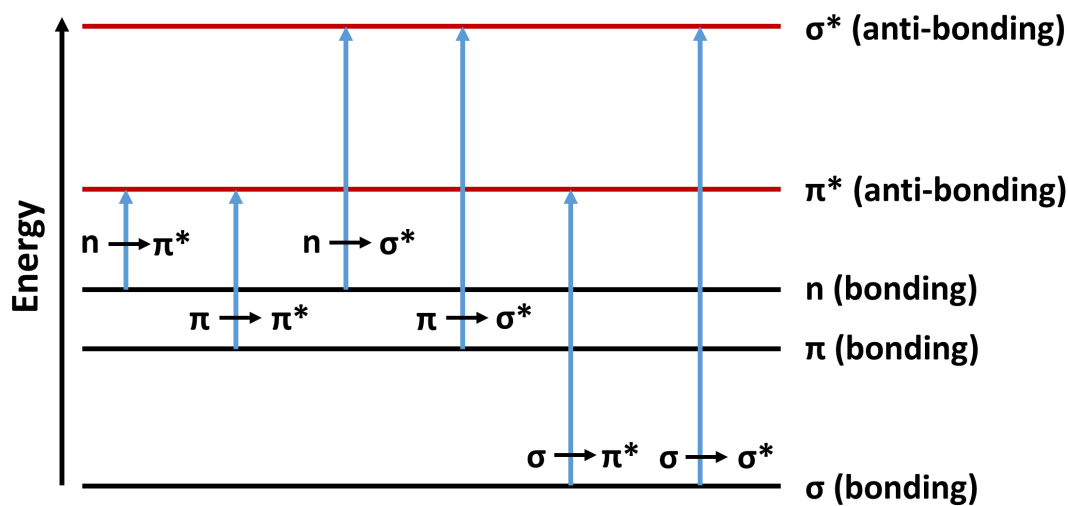


Figure 2.1. Molecular orbitals.

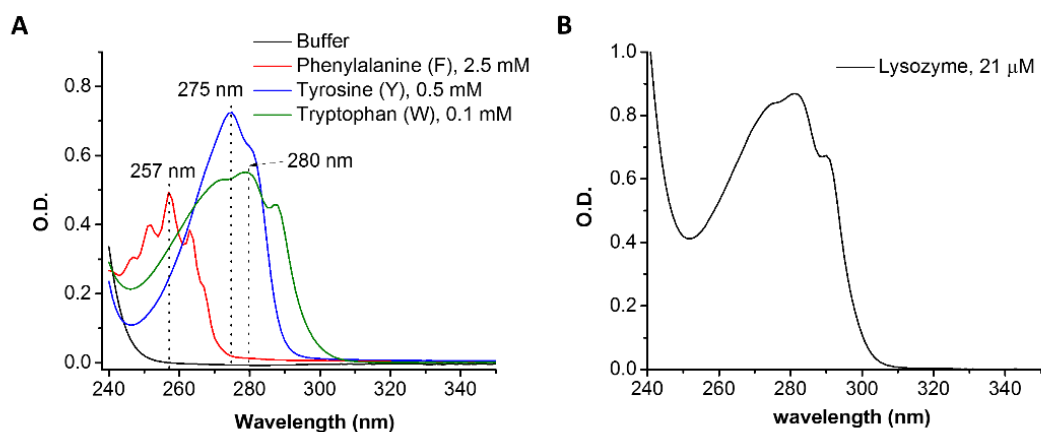
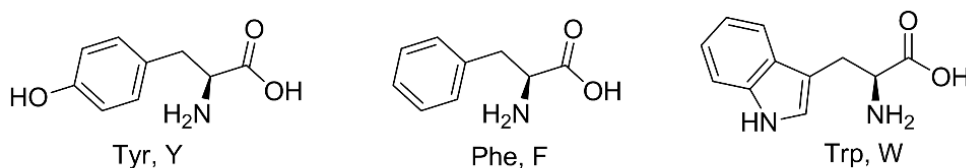


Figure 2.2. UV-vis absorbance spectrum of amino acids Phe, Tyr, and Trp (A) and lysozyme (B). (A) UV absorbance spectra of phenylalanine (2.5 mM), tyrosine (0.5 mM), and tryptophan (0.1 mM) in phosphate buffer (40 mM, pH 7.0). (B) UV absorbance spectra of lysozyme (D, 21 μ M).

All absorbance measurements in the following chapters were carried out on a Perkin Elmer Lambda 35 UV/VIS spectrometer. UV-vis absorbance was first used to measure the concentration of native proteins and fluorescence dyes in stock solutions. We also carried out UV-vis absorbance measurement to detect the soluble protein level in aggregation samples. Protein samples were incubated for the indicated time and then centrifuged at $20,000 \times g$ for 5 minute. The supernatant was collected and diluted to 50% with 20 mM pH 7.2 sodium phosphate buffer and then absorbance was measured from 240 to 600 nm. All measurements were done in triplicates. Controls were similarly prepared and incubated as the samples, had all the ingredients as in the sample except protein, and were used for background subtraction.

2.2 Fluorescence spectroscopy

Fluorescence describes the phenomenon that when electrons are excited from the ground state to S1 or S2 state, they emit energy in the form of light before returning to the ground state. Molecules with fluorescence properties are typically aromatic compounds, called fluorophores. As introduced in last section, electrons in delocalized aromatic systems can absorb energy from light and be excited to higher energy levels. However, these electrons are very unstable on the excited orbitals, thus, they rapidly return to the ground state by release energy as emitting photons. The Jablonski diagram can be used to illustrate the light absorption and fluorescence emission process (Figure 2.3). The energy levels S0, S1, and S2 represent the ground, first, and second electronic states, respectively, and each energy level has many vibrational levels. Depending on the light irradiation energy, the electrons could be excited to different vibrational levels of

excited states S1 or S2. Soon after that, when the electrons relax to the lowest vibrational level of S1 via vibrational relaxation from the higher vibrational levels of S1, or through internal conversion from S2 to S1. These rapid relaxation processes complete within ~10 picoseconds, which usually occur prior to the fluorescence emission and do not involve photons. The lowest vibrational state of S1 is a thermally equilibrated state. When electrons return to various vibrational levels of ground states (S0) from S1, energies are released through emission of photons, which is known as fluorescence. The electrons on S1 state can also be converted to the triplet states, T1, through intersystem crossing. If electrons return to S0 from T1, another type of luminescence could be observed, called phosphorescence. Since T1 is a lower energy level than S1, phosphorescence generally has longer emission wavelengths and lower emission rates compared to fluorescence.

The chemical structure and local environment of a fluorophore significantly affect the shape and intensity of its emission spectra, therefore, fluorescence spectroscopy has been employed as a sensitive analysis method in protein folding studies. In our studies, two fluorescence methods, protein intrinsic fluorescence and extrinsic fluorescence, were used to monitor protein structure change during aggregation.

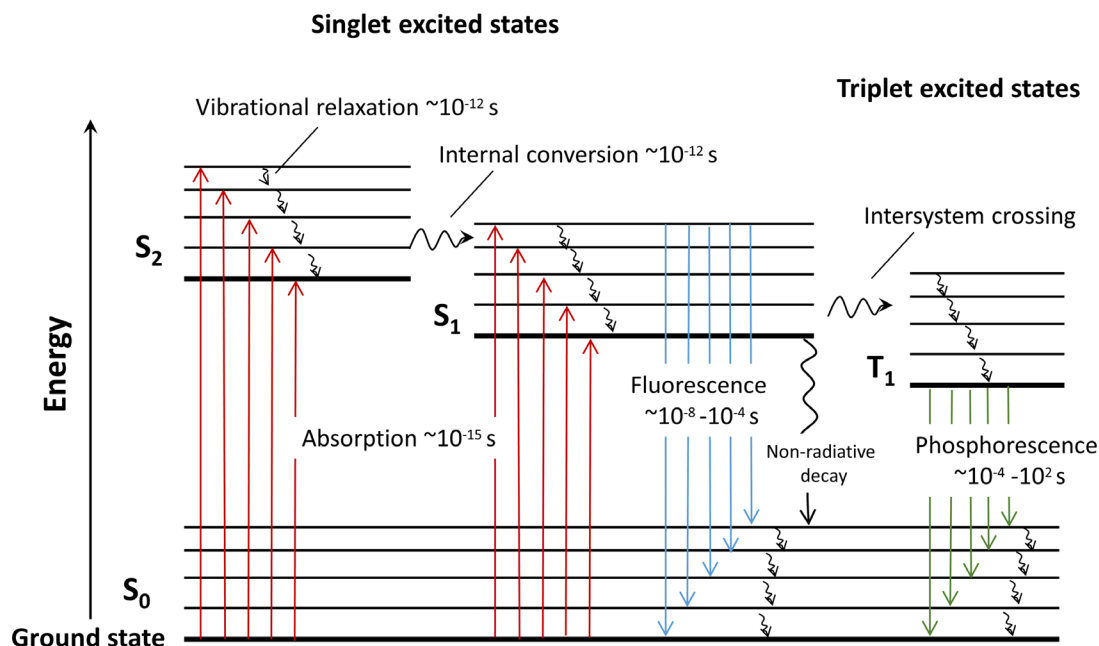


Figure 2.3. A typical Jablonski diagram. S₀, S₁, S₂, and T₁ represent the ground, first and second electronic states and triplet state. The colored straight arrows represent the processes that involve photons, including absorption (red), fluorescence (blue), and phosphorescence (green). The curved arrows represent the radiationless transitions.

2.2.1 Protein intrinsic fluorescence

The protein intrinsic fluorescence is derived majorly from the amino acid Trp and Tyr. Fluorescence intensities of Trp and Tyr are quite sensitive to the local environment, roughly correlating with the degree of solvent exposure of these residues. When transferred from a polar solvent to a non-polar environment, the fluorescence intensities of Tyr increased while Trp decreased (Figure 2.4 A). The peak wavelength (λ_{max}) of Trp also shifted from 360 nm to 345 nm from polar to non-polar. This is because that upon excitation, the electron density at the pyrrole ring will be shifted to the benzene ring⁴. On the proteins, same blue shift of tryptophan fluorescence can be observed during folding when the electron density near pyrrole end is higher than the benzene end due to the

electric field imposed by other charge residues or the solvent, while the opposite results in a red shift (to longer wavelengths) of λ_{\max} . Therefore, protein intrinsic fluorescence can provide information of protein conformational changes. Figure 2.4 C shows intrinsic fluorescence spectrum of lysozyme during chemical denaturation. When the concentration of denaturant guanidine HCl (GdmHCl), increases, the protein lysozyme unfolded and lost the compact native structure. As a consequence, the Trp residues which are normally buried in the hydrophobic core are exposed to the aqueous buffer environment during unfolding, resulting in increase of fluorescence intensity and red shift of λ_{\max} .

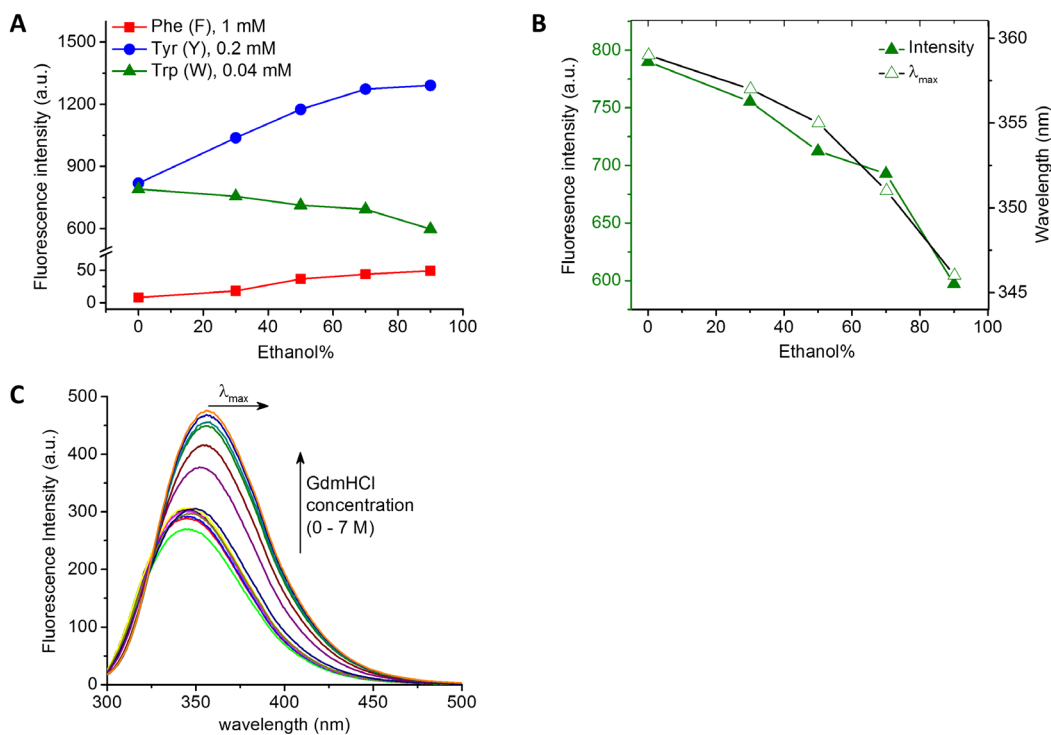


Figure 2.4. Intrinsic fluorescence of amino acids and protein. (A) Fluorescence intensity change of Phe, Tyr, and Trp in 0-90% ethanol solutions. Emission peak intensities at 324 nm of Phe, at 306 nm of Tyr, and at 346-359 nm of Trp were plotted as function of percentage of ethanol in the solution. (B) Change of fluorescence intensity

and peak wavelength of Trp in 0-90% ethanol solutions. (C) Intrinsic fluorescence emission spectra of lysozyme during denaturation by 0 -7 M guanidine HCl (GdnHCl).

Therefore, by monitoring the position change of Trp residues on proteins, intrinsic fluorescence can sensitively detect protein conformational changes during aggregation. Fluorescent measurements in the following chapters were all performed on a Horiba Jobin Yvon spectrofluorometer (Fluoromax-4) at room temperature. For protein intrinsic fluorescence analysis, samples were diluted with phosphate buffer (20 mM, pH 7.2) or with HEPES buffer (20 mM, pH 7.2) to a final protein concentration of 10 or 5 μ M. Intrinsic fluorescence spectra were collected from 300-450 nm with excitation at 280 nm. All measurements were done in triplicates. Bandwidths for excitation and emission were set at 2 nm. Controls were similarly prepared and incubated as the samples, had all the ingredients as in the sample except protein, and were used for background subtraction.

2.2.2 Extrinsic fluorescence

In addition of intrinsic fluorescence, the use of various extrinsic fluorescent probes provides additional possibilities for protein characterization. The extrinsic probes are normally synthetic chemical fluorophores that usually attach to protein via non-covalent interactions, including hydrophobic and electrostatic interactions. As introduced in Table 2.1, fluorescence analysis with extrinsic probes can be applied to almost all protein species generated during aggregation, to detect changes of kinetics, structure, size, and conformation.

The fluorescent dye 1-anilinonaphthalene-8-sulfonate (ANS, Figure 2.5) is the most frequently used hydrophobic probe in protein characterization. ANS is very sensitive to local solvent environments and is very weakly fluorescent in polar (aqueous)

environment, but shows blue shift of the emission maximum and an increase of fluorescence in non-polar environment e.g. organic solvents or hydrophobic pockets on proteins⁵⁻⁷. Therefore, ANS fluorescence can be used to measure protein's hydrophobicity. Hydrophobic and electrostatic interactions are believed to be the major binding mechanisms of ANS to proteins⁷⁻⁹, where electrostatic interactions between the negatively charged sulfonate group of ANS and the positively charged residues on proteins play a predominant role⁷. Complementary interactions like van der Waals also stabilize the ANS-protein binding⁵.

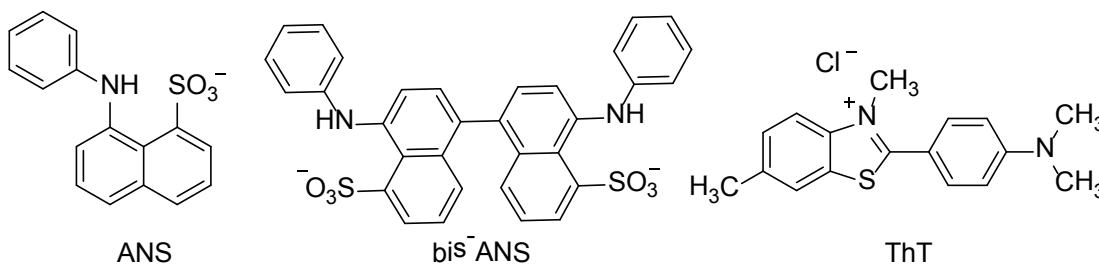


Figure 2.5. Molecular structures of the extrinsic fluorescent dyes used in our protein aggregation studies.

Interestingly, the dimeric analog of ANS, bis-ANS, does not bind tightly to organized structures, even though the binding of bis-ANS to protein is dominated by hydrophobic interactions¹⁰. The different sizes of ANS and bis-ANS result in differences in their binding affinities and the number of binding sites on a protein. Bis-ANS requires a flexible molten globule like structures for tight binding^{11, 12}, and reacts weakly to amyloid fibrils¹³. Therefore, ANS and bis-ANS provide different information in protein aggregation measurements. ANS fluorescence measures the aggregation by monitoring the extent of protein hydrophobicity, which is the major driving force during aggregation.

Whereas, bis-ANS fluorescence detects how flexible the misfolded hydrophobic structures is giving insight about the nature of aggregate (i.e. is it loose or compact).

Thioflavin T (ThT, figure 2.5) is a probe that is widely used to characterize and quantify amyloid fibril structures. With the hydrophobic ring structures, ThT absorption λ_{\max} can be affected by solvent polarity¹⁴. However, ThT fluorescence intensity depends more on viscosity and the rigidity of the microenvironment rather than polarity⁵. It has been proposed that when ThT interacts with amyloid fibrils, the steric constraints of amyloid structures require flat conformation of the dye molecule, which changes the twisted angle ϕ of the single bond between benzothiazole and the benzene ring from $\sim 90^\circ$ to $\sim 30^\circ$, resulting in increase of fluorescent signal at 480 nm¹⁵. The binding of ThT to amyloid fibrils was proposed to occur at the grooves that parallel to the long axis of fibrils, driven by the hydrophobic interactions with amino acid side chains¹⁶. However, many recent studies found that ThT also binds to non-fibrils structures and generates high fluorescence^{17,18}. It was then suggested that hydrophobic structures with cavity of 8-9 Å in diameter that are capable to bind ThT and generate the character fluorescence peak at 480 nm^{5, 19}. Therefore, we used ThT fluorescence in the experiments to analyze the structural detail of aggregates/fibrils.

Fluorescence measurements in the following chapters were all performed on a Horiba Jobin Yvon spectrofluorometer (Fluoromax-4) at room temperature. Stock solutions of extrinsic fluorescent dyes were prepared in ethanol, and then freshly diluted with phosphate buffer (or HEPES buffer for TCEP treated samples) as working stocks at concentration of 350 μM (ANS), 70 μM (bis-ANS), and 700 μM (ThT) for incubation with the protein samples. Concentrations of stock solutions were determined by UV-vis

absorbance using extinction coefficients: ANS $\epsilon_{350 \text{ nm}} = 5,000 \text{ M}^{-1}\text{cm}^{-1}$, bis-ANS $\epsilon_{385 \text{ nm}} = 16,790 \text{ M}^{-1}\text{cm}^{-1}$, and ThT $\epsilon_{416 \text{ nm}} = 26,620 \text{ M}^{-1}\text{cm}^{-1}$. ANS and bis-ANS were used at a final concentration of 5 μM and 1 μM , respectively, with 15 minute equilibration with 10 μM of proteins in samples on ice. Fluorescence spectra (400-700 nm range) were collected with excitation at 380 nm for ANS and 360 nm for bis-ANS. For ThT fluorescence, 10 μM dye was incubated with 5 μM proteins on ice for 30 minutes and emission spectra (460-700 nm range) were collected with excitation at 450 nm. All samples containing fluorescent dyes were incubated in dark for the time indicated before the emission spectra were acquired. All measurements were done in triplicates. Bandwidths for excitation and emission were set at 2 nm. Controls were similarly prepared and incubated as the samples, had all the ingredients as in the sample except proteins, and were used for background subtraction.

2.3 Non-reducing gel electrophoresis

Gel electrophoresis is a technique frequently applied for the separation and characterization of nucleic acids and proteins in biochemistry and molecular biology analysis. Based on the principle that the charged particles migrate in solution under the influence of an electrical field, gel electrophoresis methods can separate molecules by size, charge, or shape. The polyacrylamide gel electrophoresis (PAGE) is most suitable to separate proteins ranging in size from 5 to 2,000 kDa, depending on the uniform pore size of the gel, which can be modulated by the ratio of acrylamide and bis-acrylamide when casting the gel. In general, smaller protein molecules migrate faster and further than the large ones, resulting in separated bands on the gel (Figure 2.6). To make sure all the

proteins that have different net charges move in the same direction on the gel, a negatively charged detergent, sodium dodecyl sulfate (SDS), is usually added to protein samples to unfold their 3D structures and add negative net charges on the molecules. Therefore, on a SDS-PAGE, the migration of proteins is mainly affected by their molecular weight.

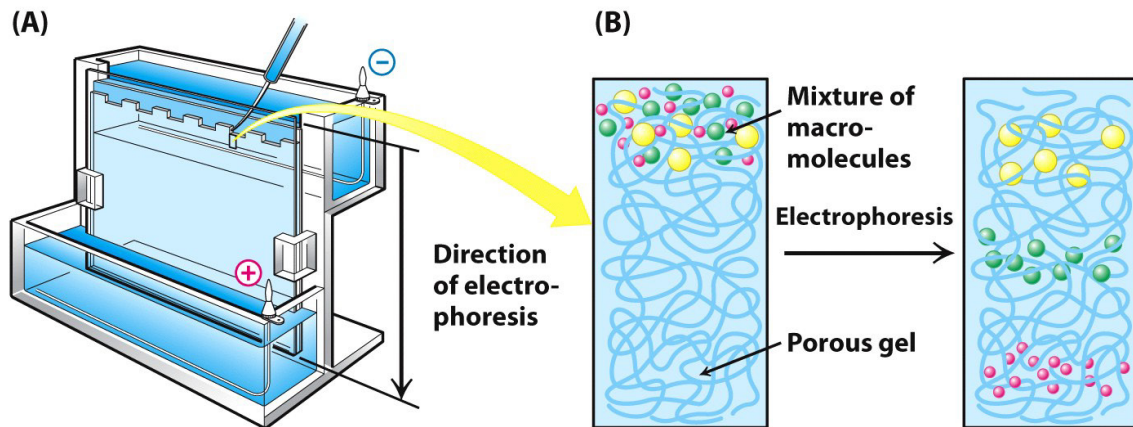


Figure 2.6. Principle of SDS-PAGE. From: BIOCHEMISTRY 8E, by Jeremy M. Berg, John L. Tymoczko, Gregory, J. Gatto, Lubert Stryer, Copyright © 2015 by W.H. Freeman and Company. Used by permission of the publisher.

Depending on their stability and structure, proteins may or may not be able to maintain disulfide bonds intact through boiling with SDS sample buffer. The regular denaturing SDS-PAGEs usually contain reducing agent DTT or β -mercaptoethanol in the sample buffer to reduce any disulfide bonds, so electrophoretic mobility of proteins in SDS-PAGE depends only on size. Whereas in non-reducing SDS-PAGE (Figure 2.7), sample buffer contains no disulfide reducing agent, that is, proteins could maintain their intact disulfide bridges during migration through the gel. Since disulfide bridges can significantly change the tertiary structure of a protein, migration of proteins on non-reducing SDS-PAGE depends on hydrodynamic volume, which is a combination of size

and shape²⁰. Generally, with disulfide bridges, proteins should have more compact shape and run faster on a gel. Therefore, when studying the effect of disulfide bonds on protein aggregation, we decided to use the non-reducing SDS-PAGE, which allows us to analyze the aggregates formed through intermolecular disulfide linkages.

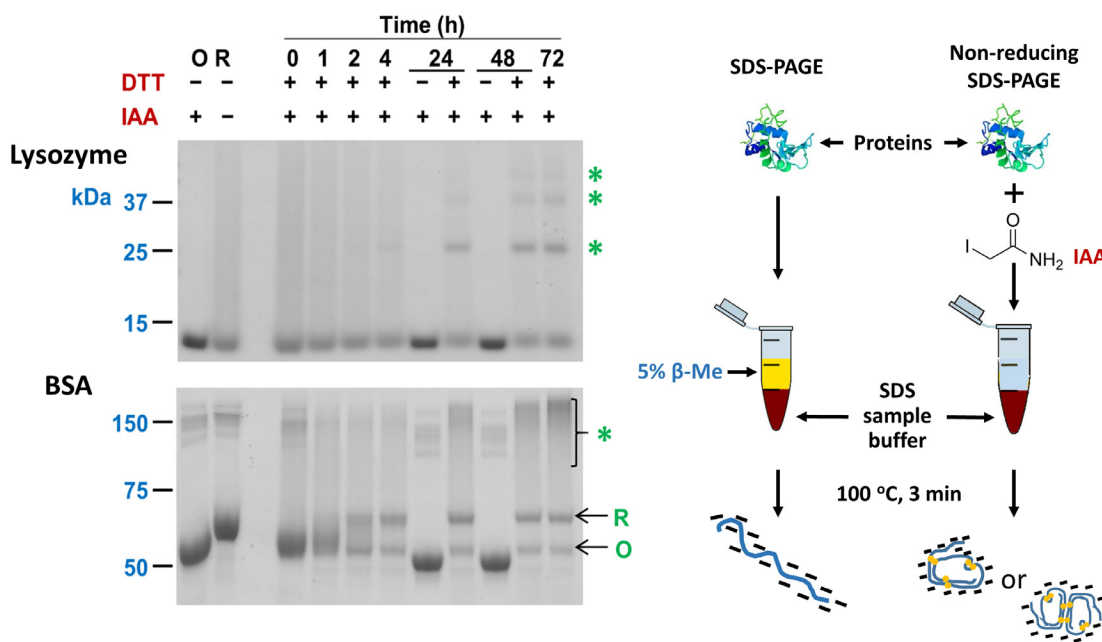


Figure 2.7. Non-reducing SDS-PAGE. Gel images are reprinted with permission from Yang et al. 2015. Copyright © 2015 American Chemical Society.

In the non-reducing SDS-PAGE experiment, incubated protein samples were first mixed with 5 mM iodoacetamide and incubated for 2 h at room temperature to block any free thiol groups. To terminate the reaction with iodoacetamide, protein samples were boiled with SDS sample buffer (lacking reducing agent) for 3 minutes. For the fully reduced samples, freshly prepared 40 μ M protein solutions at pH 7.2 (20 mM phosphate buffer having 150 mM NaCl) were boiled with SDS sample buffer containing 10, 40, or 100 mM DTT or 5% 2-mercaptoethanol for 3 minute. Lysozyme (10 μ g/lane) and BSA (5

µg/lane) samples were loaded on 15% and 10% Criterion Tris-HCl polyacrylamide precast gels (Bio-Rad), respectively. Tris-glycine-SDS buffer (25 mM Tris, 192 mM glycine, 0.1% SDS, pH 8.3; Bio-Rad) was used as running buffer and proteins were separated by SDS-PAGE. The gels were stained with Coomassie blue stain and images were acquired using an Epson scanner.

2.4 Scanning electron microscopy (SEM)

Instead of light, the electron microscopes use a beam of accelerated electrons as an illumination source. Since the wavelength of an electron is 10^5 fold shorter than a photon, the magnifications of electron microscope can be up to about 10,000,000x, which is 5,000 higher than most light microscopes. The SEM produces images by scanning the specimen with a focused electron beam. When interacting with the specimen, the electron beam loses energy in form of secondary electrons, backscattered electrons, characteristic x-rays, and heat or photons, which provide signals of the surface properties of the specimen. SEM can provide very high resolution images that show details ~ 1 nm, but the resolution of SEM images is still generally at least an order of magnitude poorer than those from transmitted electron microscope (TEM)²¹. However, due to the contrast of secondary and backscattered electron signals and the large depth of field, SEM permits the observation of the 3D shape of samples, while TEM can only obtain 2D images²². Thus, SEM is a great tool to observe surface morphology of small structures.

The major limitation of applying the electron microscopy in molecular biology is that most organic materials are not solid and electrically conductive. To solve this problem, the biological samples are usually first dried on the spaceman holder and then

coated with an ultrathin layer of electrically conducting material, such as gold or platinum. Although material is coated with thin layer of metal, there are still chances for the soft biological sample to be burned by the high energy electron beam. SEM, uses lower energy electron beams, is more suitable for small oligomers and amorphous aggregates. To keep experiment consistency, all the aggregate structures in the following chapters were observed using SEM.

In chapters 3, 4, and 5, samples of amyloid fibrils and amorphous aggregates were analyzed on a Hitachi S-4700 FESEM, a cold field emission high resolution scanning electron microscope. Incubated samples were aliquoted in a Millipore Amicon® Ultra centrifugal filters (3 kDa cut off) and the samples were diluted with MilliQ water. The diluted samples were centrifuged and concentrated at $7,000 \times g$ at $4\text{ }^{\circ}\text{C}$ (3 repeats after dilution with MilliQ water) to wash off salts and buffer. The washed samples were aliquoted on scanning electron microscope (SEM) stubs and allowed to dry at room temperature. The samples were coated with 10 nm platinum using a sputter coater. Acceleration voltage of 10 kV and emission current of $5\text{ }\mu\text{A}$ were used to image the samples.

2.5 Cell viability (MTS) assay

Cell viability assays are often performed in laboratories to determine if a test molecule affects cell proliferation or shows direct cytotoxicity. Most cell-based assays measure the toxicity by quantifying the number of viable cells at the end of the experiment. The MTS (3-(4,5-dimethylthiazol-2-yl)-5-(3-carboxymethoxyphenyl)-2-(4-sulfophenyl)-2H-tetrazolium)²³ assay is a colorimetric method based on the tetrazolium

reduction to measure redox metabolism of viable cells. The tetrazolium reagent MTS is used in combination with an intermediate electron acceptor, phenazine methyl sulfate (PMS), which can enter viable cells and become reduced in the cytoplasm or at the cell surface by intracellular reductants, mostly NADH²⁴. Once it exits the cells, PMS transfers the electrons to MTS, converting this yellow color tetrazolium to a purple color formazan product (Figure 2.7)²⁴. The formazan production could be quantified by absorbance at 490 nm, which is proportional to the number of viable cells. While dead cells does not have the ability to reduce tetrazolium into formazan. This difference permits quantification of viable cells after incubation with substrates.

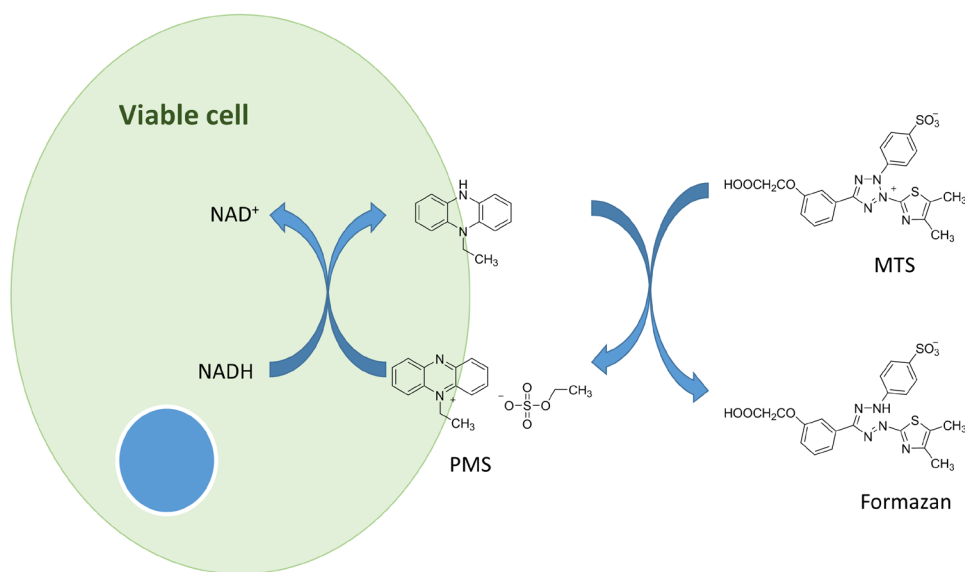


Figure 2.8. The intermediate electron acceptor PMS transfers an electron from NADH in the cytoplasm to reduce MTS into MTS formazan.

In the following chapters, MTS assay was performed to measure the cytotoxicity of protein amyloid fibrils, amorphous aggregates, and some intracellular fluorescent probes. Human breast cancer cells MDA-MB-231 and SH-SY5Y human neuroblastoma cells (from ATCC) were cultured in DMEM/F-12 medium with 10% FBS and 100 U/ml

penicillin-streptomycin at 37 °C in 5% CO₂ humidified environment and used for MTS assays within the first 10 passages. The MDA-MB-231 cells were plated at 1 x 10⁴ cells/well and SH-SY5Y cells were plated at 2 x 10⁴ cells/well on 96-well plates and allowed to grow overnight. The next day, the culture media were removed and cells were washed with 1X PBS buffer (pH 7.4) twice. Then 100 µl fresh media containing test samples at indicated concentrations were added to each well, and 6 replicates were prepared for each sample. The cells were incubated with the samples for 48 h. Media without any peptide were used as controls. To measure cell viability, 20 µl of CellTiter 96® Aqueous One Solution Cell Proliferation (MTS) Assay kit (Promega) were added to each well and incubated with cells at 37 °C for 4 h. Then absorbance at 490 nm were collected using an ELISA plate reader (BioTek Instruments, Inc.). Blanks that contains media and protein samples but no cells were similarly prepared and used for background subtraction.

2.6 Live cell fluorescence imaging

Recently live cell fluorescence microscopy is used to observe biological molecules, organelles, and many dynamic events in cells and tissues. The normal optical or electron microscopy cannot efficiently distinguish different cellular organelles, while fluorescence microscopy, can identify proteins and organelles are labeled with fluorescent probes (Figure 2.9). Fluorescent probes can also be used to identify cellular changes in pH, or its redox level. However, toxicity and photodamage effects from the chemical fluorescent probes limit the observation of cell dynamics over extended periods of time.

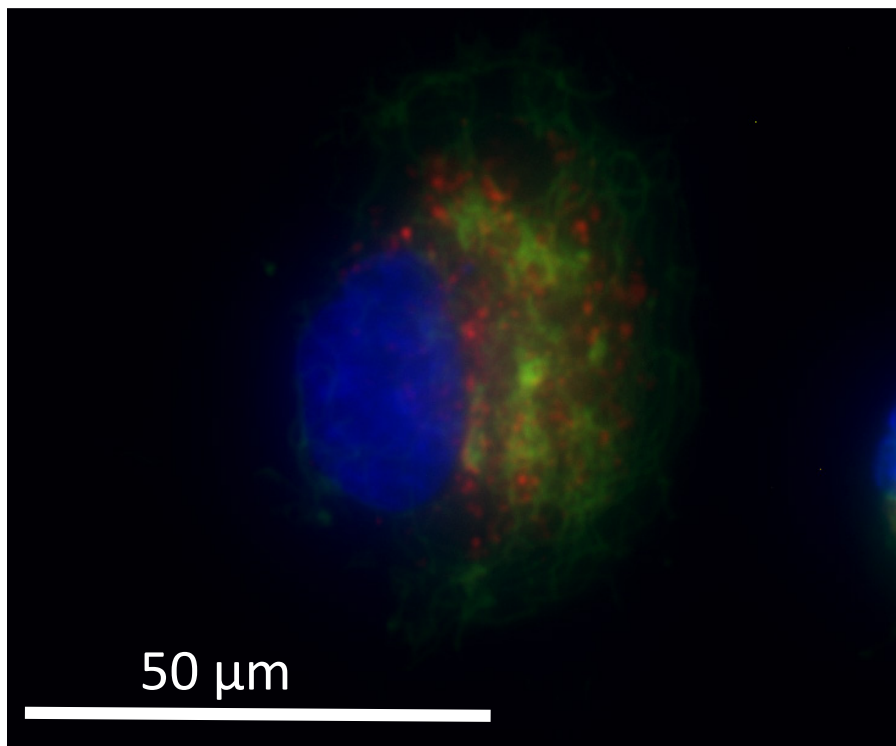


Figure 2.9. Fluorescence microscope image shows a human normal endothelial cell. The nuclei is stained in blue. The mitochondria and lysosomes are stained in green and red, respectively. Image is adapted from Zhang et al.²⁵ with permission from The Royal Society of Chemistry.

In chapter 6, two live cell fluorescent probes for sensitive detection of lysosomal and intracellular pH are tested on different mammalian cell lines. Breast cancer cells MDA-MB-231 and normal endothelial cells HUVEC-C (from ATCC) were cultured in DMEM/F-12 medium (MDA-MB-231) and Medium 199 (HUVEC-C) with 10% FBS and 100 U/ml penicillin-streptomycin at 37 °C in 5% CO₂ humidified environment and used for experiment within the first 10 passages. Cells were plated on 12-well culture plates at 1×10^5 cells/well and incubated at 37 °C in 5% CO₂ incubator overnight. The next day, the media was removed and cells were rinsed twice with 1 X PBS after which fresh serum-free media was added and cells were incubated for 2 h at 37 °C in CO₂

incubator. Following 2 h serum starvation, fresh serum free media with/without fluorescent probes (at indicated concentration) were added and incubated further with cells for 2 h. Live cell images were acquired using an inverted fluorescence microscope (AMF-4306, EVOSfl, AMG) with DAPI filter for Hoechst 33342 (Sigma-Aldich), GFP filter for LysoSensor Green DND-189 (Invitrogen), and RFP or CY5 filters for test fluorescent probes. The fluorescence images were obtained at 40x and 60x magnification for HUVEC-C and at 60x magnification for MDA-MB-231 cells. The exposure times for each filter were kept constant. Co-localization analysis based on Pearson's coefficient was done using JACoP plugin from ImageJ²⁶.

To alter the intracellular pH during live cell imaging, normal endothelial cells HUVEC-C (from ATCC) were cultured as previously described. After overnight incubation in 12-well culture plates, cells were rinsed twice with 1 X PBS (pH 7.4). The fresh serum free media with the test fluorescent probes were added to the cells and incubated for 2 h. After incubation, the media were removed and cells were gently rinsed with 1 X PBS (pH 7.4) three times. Cells were then treated with nigericin (5 µg/mL) in 2 mL potassium rich PBS (at pH 5.0, 5.5, 6.5, 7.5, and 8.5) and incubated for 15 min. Live cell images were acquired using an inverted fluorescence microscope (AMF-4306, EVOSfl, AMG) with DAPI filter for Hoechst 33342 (Sigma-Aldich), GFP filter for LysoSensor Green DND-189 (Invitrogen), and CY5 filter for test probes. The fluorescence images were obtained at 40x magnification. The exposure times for each filter were kept constant.

2.7 References

1. Dobson, C. M., Experimental investigation of protein folding and misfolding. *Methods* **2004**, *34*, 4-14.
2. Jahn, T. R.; Radford, S. E., The Yin and Yang of protein folding. *Febs Journal* **2005**, *272*, 5962-70.
3. Schmid, F.-X., Biological Macromolecules: UV-visible Spectrophotometry. In *eLS*, John Wiley & Sons, Ltd: 2001.
4. Vivian, J. T.; Callis, P. R., Mechanisms of tryptophan fluorescence shifts in proteins. *Biophysical Journal* **2001**, *80*, 2093-109.
5. Hawe, A.; Sutter, M.; Jiskoot, W., Extrinsic fluorescent dyes as tools for protein characterization. *Pharmaceutical Research* **2008**, *25*, 1487-99.
6. Lindgren, M.; Sorgjerd, K.; Hammarstrom, P., Detection and characterization of aggregates, prefibrillar amyloidogenic oligomers, and protofibrils using fluorescence spectroscopy. *Biophysical Journal* **2005**, *88*, 4200-12.
7. Matulis, D.; Baumann, C. G.; Bloomfield, V. A.; Lovrien, R. E., 1-anilino-8-naphthalene sulfonate as a protein conformational tightening agent. *Biopolymers* **1999**, *49*, 451-8.
8. Laurence, D. J. R., A study of the adsorption of dyes on bovine serum albumin by the method of polarization of fluorescence. *The Biochemical journal* **1952**, *51*, 168-80.
9. Stryer, L., The interaction of a naphthalene dye with apomyoglobin and apohemoglobin. A fluorescent probe of non-polar binding sites. *Journal of molecular biology* **1965**, *13*, 482-95.
10. Bothra, A.; Bhattacharyya, A.; Mukhopadhyay, C.; Bhattacharyya, K.; Roy, S., A fluorescence spectroscopic and molecular dynamics study of bis-ANS/protein interaction. *Journal of Biomolecular Structure & Dynamics* **1998**, *15*, 959-66.

11. Shi, L.; Palleros, D. R.; Fink, A. L., Protein conformational-changes induced by 1,1'-bis(4-Anilino-5-Naphthalenesulfonic Acid) - Preferential binding to the molten globule of DNAK. *Biochemistry* **1994**, *33*, 7536-46.
12. Celej, M. S.; Montich, C. G.; Fidelio, G. D., Protein stability induced by ligand binding correlates with changes in protein flexibility. *Protein Science* **2003**, *12*, 1496-506.
13. LeVine, H., 4,4'-Dianilino-1,1'-binaphthyl-5,5'-disulfonate: report on non-beta-sheet conformers of Alzheimer's peptide beta(1-40). *Archives of Biochemistry and Biophysics* **2002**, *404*, 106-15.
14. Maskevich, A. A.; Stsiapura, V. I.; Kuzmitsky, V. A.; Kuznetsova, I. M.; Povarova, O. I., et al., Spectral properties of thioflavin T in solvents with different dielectric properties and in a fibril-incorporated form. *Journal of Proteome Research* **2007**, *6*, 1392-401.
15. Wolfe, L. S.; Calabrese, M. F.; Nath, A.; Blaho, D. V.; Miranker, A. D., et al., Protein-induced photophysical changes to the amyloid indicator dye thioflavin T. *Proceedings of the National Academy of Sciences of the United States of America* **2010**, *107*, 16863-8.
16. Biancalana, M.; Koide, S., Molecular mechanism of Thioflavin-T binding to amyloid fibrils. *Biochimica Et Biophysica Acta-Proteins and Proteomics* **2010**, *1804*, 1405-12.
17. Yang, M.; Dutta, C.; Tiwari, A., Disulfide-Bond Scrambling Promotes Amorphous Aggregates in Lysozyme and Bovine Serum Albumin. *Journal of Physical Chemistry B* **2015**, *119*, 3969-81.
18. Yamaguchi, T.; Yagi, H.; Goto, Y.; Matsuzaki, K.; Hoshino, M., A Disulfide-Linked Amyloid-beta Peptide Dimer Forms a Protofibril-like Oligomer through a Distinct Pathway from Amyloid Fibril Formation. *Biochemistry* **2010**, *49*, 7100-7.

19. Groenning, M.; Olsen, L.; van de Weert, M.; Flink, J. M.; Frokjaer, S., et al., Study on the binding of Thioflavin T to beta-sheet-rich and non-beta-sheet cavities. *Journal of Structural Biology* **2007**, *158*, 358-69.
20. Rath, A.; Glibowicka, M.; Nadeau, V. G.; Chen, G.; Deber, C. M., Detergent binding explains anomalous SDS-PAGE migration of membrane proteins. *Proceedings of the National Academy of Sciences of the United States of America* **2009**, *106*, 1760-5.
21. Egerton, R. F., *Physical principles of electron microscopy: an introduction to TEM, SEM, and AEM*. Springer: 2005; p 202.
22. Goldstein, J., *Scanning electron microscopy and x-ray microanalysis*. third ed.; Springer: 2003.
23. Cory, A. H.; Owen, T. C.; Barltrop, J. A.; Cory, J. G., Use of an aqueous soluble tetrazolium formazan assay for cell-growth assays in culture. *Cancer Communications* **1991**, *3*, 207-12.
24. Berridge, M. V.; Herst, P. M.; Tan, A. S., Tetrazolium dyes as tools in cell biology: new insights into their cellular reduction. *Biotechnology annual review* **2005**, *11*, 127-52.
25. Zhang, J.; Yang, M.; Li, C.; Dorh, N.; Xie, F., et al., Near-infrared fluorescent probes based on piperazine-functionalized BODIPY dyes for sensitive detection of lysosomal pH. *Journal of Materials Chemistry B* **2015**, *3*, 2173-84.
26. Bolte, S.; Cordelieres, F. P., A guided tour into subcellular colocalization analysis in light microscopy. *Journal of Microscopy-Oxford* **2006**, *224*, 213-32.

Chapter 3 Disulfide-Bond Scrambling Promotes Amorphous Aggregates in Lysozyme and Bovine Serum Albumin[†]

Mu Yang, Colina Dutta, and Ashutosh Tiwari*

Department of Chemistry, Michigan Technological University, Houghton, Michigan
49931, United States

[†]The material included in this chapter was previously published in the *J. Phys. Chem. B* **2015**, 119, 3969–3981. DOI: 10.1021/acs.jpcc.5b00144

Publication date: Feb. 17, 2015 Copyright © 2015 American Chemical Society

<http://pubs.acs.org/doi/abs/10.1021/acs.jpcc.5b00144>

3.1 Introduction

Most proteins are functional in a narrow range of conditions where they are stable and which can be altered by changes in pH, temperature, and/or ionic strength. Once destabilized, proteins can misfold and aggregate resulting in loss of function or a novel gain of toxic function that can lead to cellular or neuronal toxicity¹⁻⁵. While, several studies have reported on the formation of amorphous or β -sheet rich amyloid-like fibrils due to denaturants and extreme pH, temperature, and/or ionic strength⁶⁻¹⁰, only a few studies have been carried out at or near physiological pH¹¹⁻¹⁴. It has been suggested that most proteins can form β -sheet rich fibrils under properly designed laboratory conditions that impact inter- and intra-molecular weak forces^{1, 2}. Interestingly, in most of the reported studies, proteins that form amyloid fibrils have intact disulfide bonds^{3, 4, 7, 15}. Disulfide bonds are critical to stabilizing protein structure and can either promote or inhibit molecular interactions affecting fibrillation^{12, 16-18}; leaving the relationship between disulfide bonds and protein aggregation still unclear¹⁹. Furthermore, previously reported studies on disulfide-reduced proteins were performed at extreme pH or temperature^{16, 17, 20, 21} in order to trigger aggregation/fibrillation. In addition, mutated or fully denatured proteins lacking disulfide bonds were found to form amyloid fibrils⁹, but these proteins are rare under physiological conditions. The cytosolic environment is highly reducing and under certain conditions may have reduced glutathione levels as high as 10 mM²². The cytosolic reducing agents like glutathione can break the disulfide bonds²³ resulting in protein misfolding leading to intracellular protein aggregates or inclusions formation. On the other hand, reducing stress could also be created in extracellular environment due to excessive or improper use of antioxidants²⁴⁻²⁶.

In this study, we used dithiothreitol (DTT), a well-known thiol-based protein disulfide reducing agent, to investigate disulfide-bond cleavage and protein aggregation in two model proteins, hen egg white lysozyme (lysozyme) and bovine serum albumin (BSA) at pH 7.2 and 37 °C^{21,27-29}. We also used a non-thiol based reducing agent, tris(2-carboxyethyl)phosphine (TCEP), at pH 7.2 and 37°C to verify the findings from DTT experiments. We chose lysozyme and BSA as both are globular, α -helical rich proteins containing multiple disulfide linkages^{30,31}. Lysozyme is a small protein (129 amino acid residues; 14.3 kDa) containing 4 disulfide bridges (C6-C127, C30-C115, C64-C80, and C76-C94) and has mostly α -helices, a β -sheet, and a long loop (Figure 3.1). The bond C6-C127 connects N- and C-terminals of the protein, and is partially exposed to solvent; the other three disulfide-bonds are buried and are not solvent accessible³². Lysozyme under disulfide-reducing conditions unfolds, loses its globular structure, and becomes a random coiled polypeptide^{9, 33}. Fibrillar, amyloid-like structures have been reported predominantly at non-physiological pH or in presence of denaturant such as guanidine hydrochloride^{6, 9, 14, 34}. Two other studies show that at high temperature and neutral/near-neutral pH, lysozyme can unfold and aggregate through hydrophobic interactions forming particulates or non-fibrillar large aggregates^{35, 36}. Earlier studies on lysozyme showed that at acidic pH and high temperature the aggregation of protein resulted in fibril formation and was dependent on disulfide-bond integrity. Fully reduced or oxidized lysozyme formed fibrils^{6, 9} but the partially reduced lysozyme (50% of free -SH) did not form amyloid fibrils even after 10 days of incubation²¹. These findings are very interesting but require further study to understand the role of disulfide bonds in lysozyme aggregation.

BSA is a large protein (583 amino acid residues; ~66 kDa) containing 17 disulfide bridges and one free cysteine and is pre-dominantly α -helical with three homologous domains (I, II, and III) that provide a variety of binding sites on the protein (Figure 3.1)³¹. BSA shares 76% sequence homology with human serum albumin (HSA)^{8, 31}. Serum albumin is an abundant transport protein that binds to acidic or lipophilic ligands, such as fatty acids, bilirubin, hemein, and thyroxine, and transports it across the circulatory system³⁷. At pH that is between acidic to neutral (pH 5 to 7), almost all the disulfide bonds are protected on BSA. However, when pH is increased from neutral to basic (pH 7 to 10), approximately 5 disulfide bonds out of 17 become solvent accessible and can be cleaved by a reducing agent^{38, 39}. In addition, raising the temperature from 35 °C to 55 °C also increases the number of solvent accessible disulfide bonds on BSA⁴⁰. Fully disulfide reduced BSA protein was found to lose its native structure and binding abilities⁴¹. Although, BSA is not related to any amyloidogenic disease, it is able to form aggregates that are either amorphous in nature or show amyloid fibrillar structures under certain laboratory conditions^{8, 13, 42, 43}.

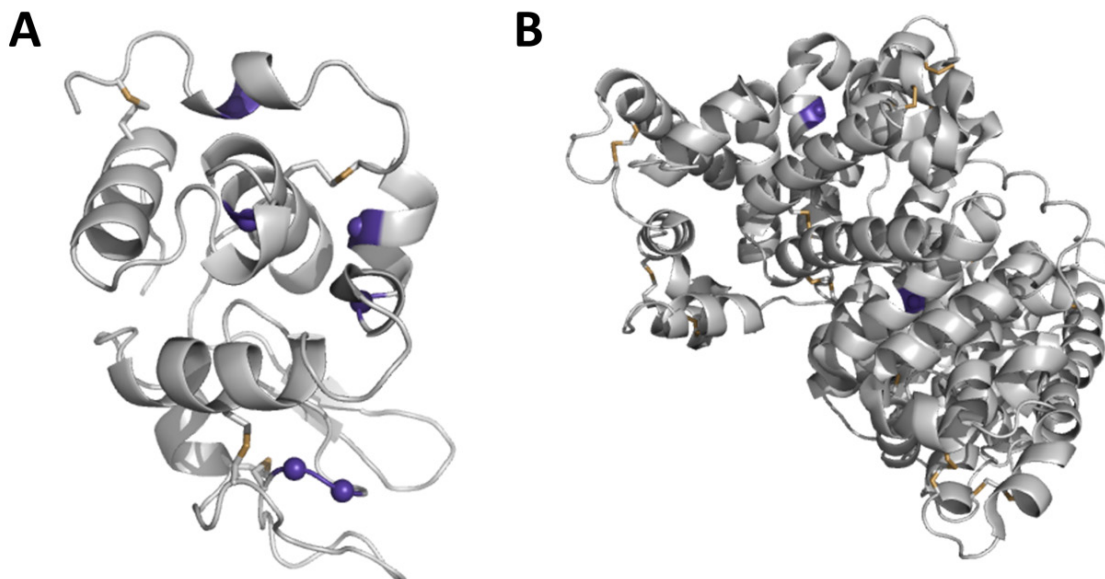


Figure 3.1. Structures of lysozyme (A) and BSA (B), showing the disulfide bonds (S-S, *sand-yellow*). The tryptophan residues are shown as *purple-blue spheres*. The backbone is shown in *grey* color. The structures were generated using PyMOL 1.3 and PDB files (1UCO)³⁰ for lysozyme and (4F5S)³¹ for BSA.

Comparing and contrasting aggregation of lysozyme with BSA under identical disulfide-reducing conditions can provide insights into how disulfide bonds affect protein aggregation. Under the experimental conditions, both lysozyme and BSA formed amorphous aggregates that are significantly different from the amyloid fibrils reported in earlier studies. Interestingly, both lysozyme and BSA form amorphous aggregates that show different properties; lysozyme forms highly flexible aggregates whereas BSA aggregates are rigid and compact.

3.2 Materials and methods

Unless otherwise indicated, all materials were used as supplied by the manufacturer without any further purification. Tris(2-carboxyethyl)phosphine (TCEP) was from

Thermo Scientific Pierce; Lysozyme, BSA, DTT, Thioflavin T (ThT), 8-anilino-1-naphthalenesulfonic acid (ANS) dye, 4,4'-Dianilino-1,1'-binaphthyl-5,5'-disulfonic acid (bis-ANS) dye were purchased from Sigma.

Preparation of protein samples- Stocks of lysozyme and BSA were prepared by dissolving lyophilized protein powder in 20 mM pH 7.2 sodium phosphate buffer having 150 mM NaCl. The protein samples reduced with TCEP were prepared in 20 mM pH 7.2 HEPES buffer having 150 mM NaCl instead of phosphate buffer. NaOH was added to 20 and 40 mM TCEP samples to neutralize the acidic TCEP HCl and maintain the final pH at 7.2. The protein concentrations were determined by UV-visible spectroscopy using extinction coefficient $\epsilon_{280\text{nm}} = 38,940 \text{ M}^{-1}\text{cm}^{-1}$ and $\epsilon_{280\text{nm}} = 43,824 \text{ M}^{-1}\text{cm}^{-1}$ for lysozyme and BSA, respectively. The working protein solutions (protein samples) had 40 μM protein in 20 mM pH 7.2 phosphates buffer having 150 mM NaCl and 0 or 10 mM DTT. All samples were prepared on ice and then incubated at 37 °C for the indicated time periods (see figures for details). Lysozyme fibrils were prepared using the method from Krebs et al. 2000⁶. Briefly, 1 mM of lysozyme at pH 2.0 (in 20 mM glycine-HCl buffer) was incubated at 65 °C for 7 days to generate the fibrils.

Seeding activity of disulfide-reduced protein aggregates- After 72 h incubation of both lysozyme and BSA proteins with 10 mM DTT in 20 mM phosphate buffer (pH 7.2), aggregates of both proteins were washed with water and then added to 40 μM of respective protein solutions at physiological pH (20 mM phosphate buffer, pH 7.2, having 150 mM NaCl) and acidic pH (20 mM glycine-HCl buffer, pH 2.0, having 150 mM NaCl). Aggregated protein seeds were added at a final concentration of 5%, 15%, and 50% v/v concentrations, respectively. Negative controls were prepared under

identical conditions but without adding seeds. All samples were prepared on ice and then incubated at 37 °C for the indicated time periods (see Figure 3.7 for details).

Non-reducing gel electrophoresis- Non-reducing SDS-PAGEs were performed as previously introduced in chapter 2. In brief, protein samples were first reacted with 5 mM iodoacetamide, and then boiled with sodium dodecyl sulfate (SDS) sample buffer (lacking reducing agent) for 3 minute. Fully reduced samples were freshly prepared and boiled with SDS sample buffer containing 10, 40, or 100 mM DTT or 5% 2-mercaptoethanol for 3 minute. Lysozyme (10 µg/lane) and BSA (5 µg/lane) samples were loaded on 15% and 10% Criterion Tris-HCl polyacrylamide precast gels (Bio-Rad), respectively. Tris-glycine-SDS buffer (25 mM Tris, 192 mM glycine, 0.1% SDS, pH 8.3; Bio-Rad) was used as running buffer and proteins were separated by sodium dodecyl sulfate polyacrylamide gel electrophoresis (SDS-PAGE). The gels were stained with Coomassie blue stain and image was acquired using a scanner.

UV-visible absorbance spectroscopy- All absorbance measurements were carried out on Perkin Elmer Lambda 35 UV/VIS spectrometer as previous described in chapter 2. In brief, protein samples were centrifuged at $20,000 \times g$ for 5 minute after incubation. The supernatant was collected and diluted to 50% with 20 mM pH 7.2 sodium phosphate buffer and then absorbance was measured from 240 to 600 nm. All measurements were done in triplicates. Controls were similarly prepared and incubated as the samples, had all the ingredients as in the sample except protein, and were used for background subtraction.

Intrinsic and extrinsic fluorescence- Fluorescence measurements were performed on Horiba Jobin Yvon spectrofluorometer (Fluoromax-4) at room temperature as previously described in chapter 2. The samples were diluted with phosphate buffer (20 mM, pH 7.2;

for DTT treated samples) or with HEPES buffer (20 mM, pH 7.2; for TCEP treated samples) to a final protein concentration of 10 or 5 μM for fluorescence experiments. Intrinsic fluorescence spectra for lysozyme and BSA (5 μM) were collected in 300-450 nm range with excitation at 280 nm. Extrinsic fluorescent dyes were dissolved in ethanol and then freshly diluted with phosphate buffer (or HEPES buffer for TCEP treated samples) as working stocks at concentration of 350 μM (ANS), 70 μM (bis-ANS), and 700 μM (ThT) for incubation with the protein samples. ANS and bis-ANS were used at a final concentration of 5 μM and 1 μM , respectively, with 15 minute equilibration with 10 μM of proteins in samples on ice. Fluorescence spectra (400-700 nm range) were collected with excitation at 380 nm for ANS and 360 nm for bis-ANS. For ThT fluorescence, 10 μM dye was incubated with 5 μM proteins on ice for 30 minute and emission spectra (460-700 nm range) was collected with excitation at 450 nm. All samples containing fluorescent dyes were incubated in dark for the time indicated before the emission spectra were acquired. All measurements were done in triplicates. Bandwidths for excitation and emission were set at 2 nm. Controls were similarly prepared and incubated as the samples, had all the ingredients as in the sample except protein, and were used for background subtraction.

Field Emission Scanning Electron Microscopy (FESEM)- FESEM images were acquired on a Hitachi S-4700 FESEM microscope as previously described in chapter 2. In brief, samples were washed using a Millipore Amicon[®] Ultra centrifugal filters (3 kDa cut off) with double-distilled water to remove salts and buffer. The washed samples were aliquoted on scanning electron microscope (SEM) stubs and allowed to dry at room temperature. The samples were coated with 10 nm platinum using a sputter coater.

Acceleration voltage of 10 kV and emission current of 5 μ A were used to image the samples.

3.3 Results

In this study, lysozyme and BSA proteins were incubated with 0-100 mM of DTT at pH 7.2 and 37 °C for the indicated time periods and aggregation was monitored by different techniques. Changing the concentration of DTT altered the aggregation kinetics slightly but did not affect the nature of aggregates observed (Figure 3.2). Therefore, we chose 10 mM DTT for all our subsequent studies with proteins as it showed optimum response. We incubated the proteins in the presence or absence of 10 mM DTT at pH 7.2 and 37 °C for the indicated time periods and aggregation was monitored by different techniques. The protein samples were centrifuged and the concentration of protein in the supernatant (soluble fraction) was measured by UV-visible spectroscopy and morphology of aggregates was characterized by scanning electron microscope (Figure 3.3). The amount of soluble protein did not change over time in the protein samples incubated in the absence of DTT (Figure 3.3A, B, open symbols). In addition, no aggregates were observed in the SEM images (Figure 3.3C, H). However, for protein samples incubated in the presence of 10 mM DTT, the fraction of soluble protein decreased significantly in 4 h (Figure 3.3A, B, closed symbols). After 12 h, < 20% of soluble proteins were detected in the sample solution (Figure 3.3A, B). Insoluble protein aggregates, as visualized by SEM, increased in amount and size as the incubation time increased for samples in the presence of 10 mM DTT (Figure 2E-F, I-J). For both proteins, the aggregates were amorphous with an average subunit diameter of 400 ± 200 nm. Even when the DTT-treated lysozyme

was incubated for a longer time (48-day sample, Figure S6), the aggregates were still amorphous in nature.

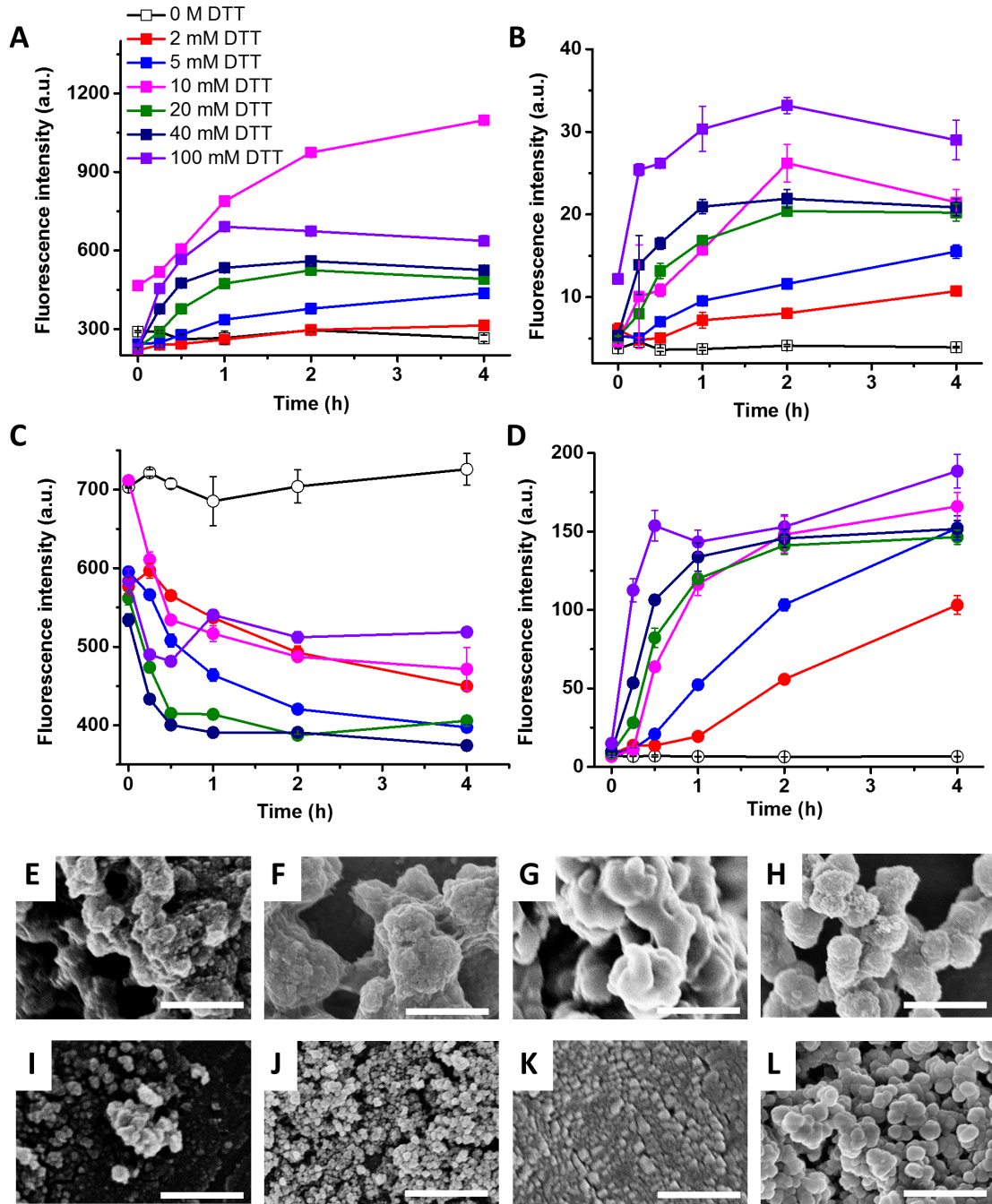


Figure 3.2. The effect of increasing concentrations of DTT on lysozyme and BSA aggregation are monitored by intrinsic fluorescence (A, C) and ThT assay (B, D) and

SEM (E-L). Intrinsic and ThT fluorescence results showed the protein aggregation of lysozyme (A, B) and BSA (C, D) in 0-24 h. Error bars indicate \pm S.D. Aggregates formed in presence of 5 mM (E, I), 10 mM (F, J), 40 mM (G, K), and 100 mM (H,L) DTT from lysozyme (E-H) and BSA (I-L) were images using SEM. Scale bars = 1 μ m.

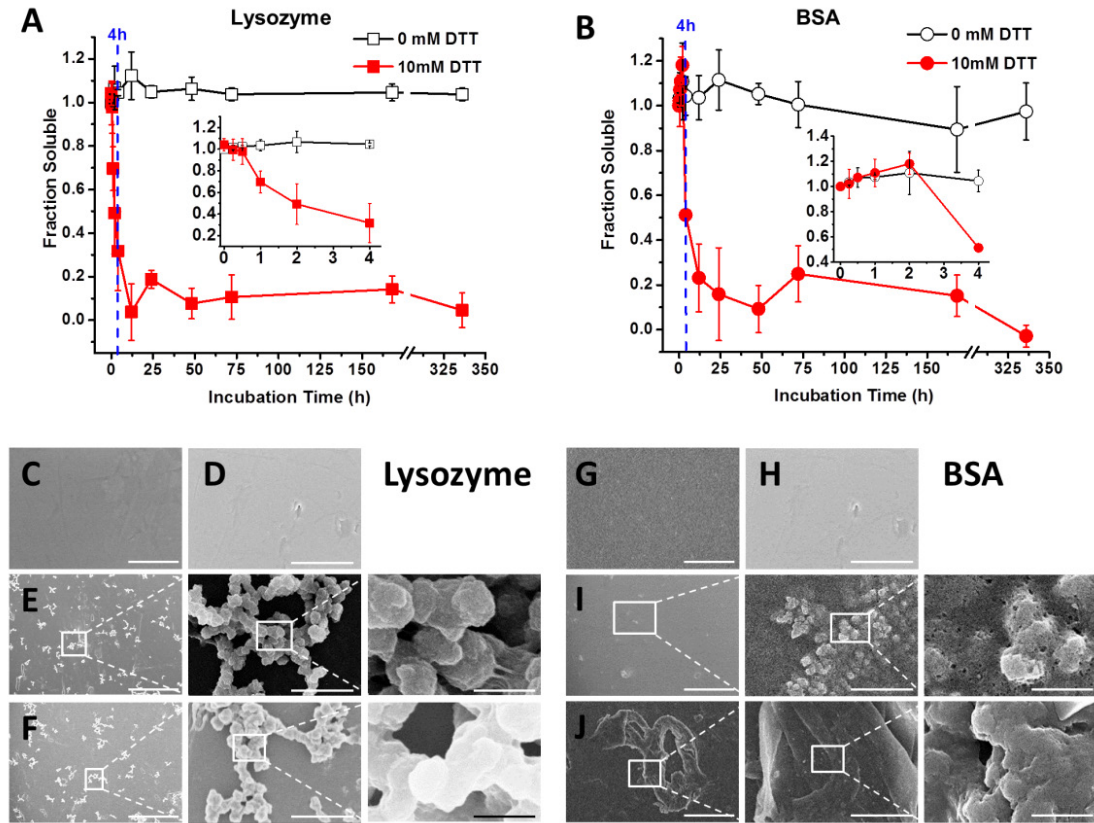


Figure 3.3. UV absorbance showing the fraction soluble protein and SEM images of the insoluble aggregates. Protein samples were incubated at 37 °C for the indicated periods of time and then centrifuged. Fraction soluble proteins in supernatant were determined by UV absorbance at 280 nm for lysozyme (A) and BSA (B). Error bars indicate \pm S.D. Insoluble aggregates were imaged using SEM. The samples for lysozyme and BSA respectively are: proteins incubated without DTT (C, G; scale bars = 10 μ m); with 10 mM DTT for 0 h (D, H; scale bars = 10 μ m), 4 h (E, I; scale bars are 50, 5, and 1 μ m from left to right), and 7 days (168 h) (F, J; scale bars are 50, 5, and 1 μ m from left to right).

Non-reducing gel electrophoresis was used to check if proteins under the experimental conditions were fully disulfide reduced or formed higher molecular weight protein species as the incubation time increased (Figure 3.4). For samples incubated in the absence of DTT, no new high molecular weight protein species were observed even after 48 h and was comparable to freshly prepared fully oxidized protein samples (Figure 3.4; lane **O** in panels A, B, and C). Freshly prepared proteins that were fully reduced by 2-mercaptoethanol (Figure 3.4; lane **R** in panels A, B and C) showed a slight decrease in electrophoretic mobility compared to the fully oxidized protein samples (Figure 3.4; lane **O** in panels A, B and C) but did not show any additional higher molecular weight protein bands. While 10 mM DTT in sample buffer is not sufficient to completely reduce BSA, 40 mM and 100 mM DTT resulted in complete reduction of BSA (Figure 3.4; compare lanes R and R'). However, for samples incubated in the presence of 10 mM DTT, appearance of higher molecular weight protein species were observed for lysozyme as early as 4 h (Figure 3A). Higher molecular weight protein bands increased with increasing incubation time. In the case of BSA, the major protein band is at ~66 kDa that faded with time and a smear of protein in the higher molecular weight region was observed for protein incubated for 24 h or more (Figure 3.4B, C). The DTT-treated BSA proteins incubated for 2 h or longer also showed a mixture of reduced (R) and oxidized (O) proteins (Figure 3.4B). Even BSA proteins treated with high concentrations of DTT (40 or 100 mM DTT) showed mixture of reduced (R) and oxidized (O) proteins at 48 h (Figure 3.4C). To check if the high molecular weight protein species are present in soluble fraction or not, samples from different timed incubation (1, 2, 4, 24, 48, and 72 h) were centrifuged at high speed and pellets and supernatant were analyzed by non-

reducing SDS-PAGE (Figure 3.4D). All high molecular weight protein species were observed in the pellet fraction only.

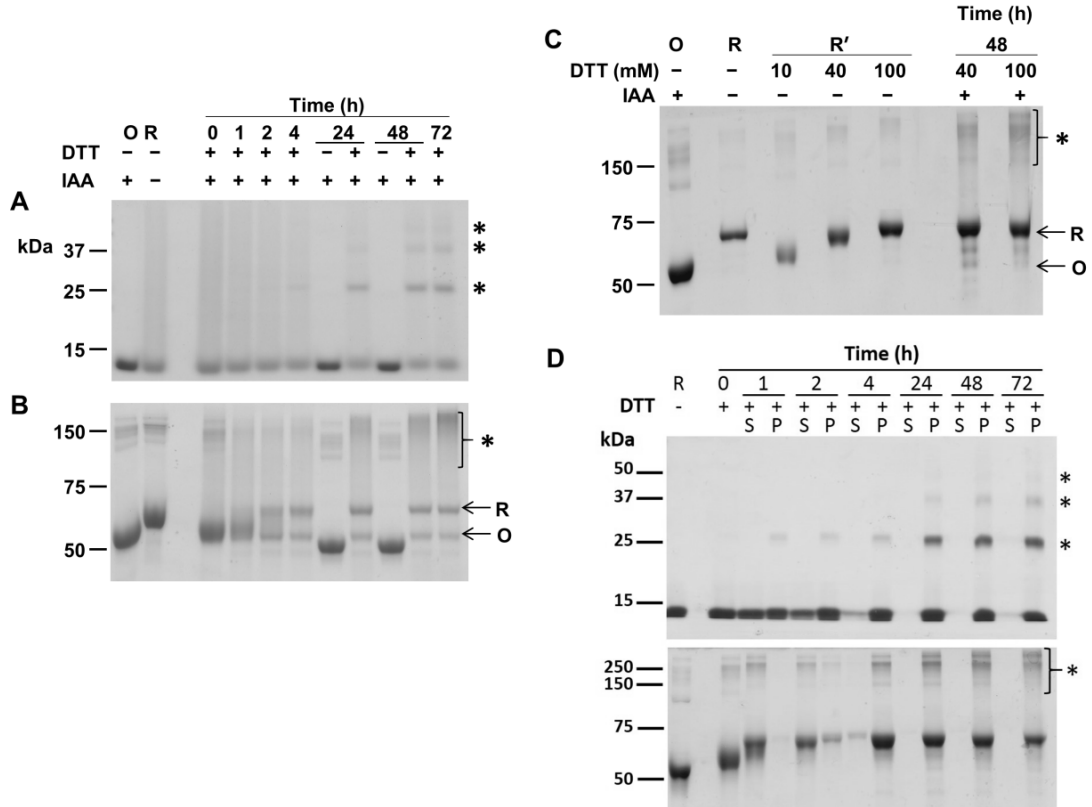


Figure 3.4. Non-reducing SDS-PAGE indicated the presence of high molecular weight species. Lysozyme (10 $\mu\text{g}/\text{lane}$) and BSA samples (5 $\mu\text{g}/\text{lane}$) were loaded on 15% gel (A) and 10% gel (B, C), respectively. The gels were run at 80 V for 3.5 and 4 h (lysozyme and BSA, respectively) followed by staining with Coomassie blue. Lanes “O” were fully oxidized proteins that reacted with iodoacetamide in the absence of DTT. Lanes “R” in panel A, B, and C were proteins that were fully reduced by 2-mercaptoethanol. Loading orders are same for gels A and B. Lanes “R” in panel C were BSA samples boiled in sample buffer containing 10, 40 or 100 mM DTT instead of 5% 2-mercaptoethanol. The last two lanes on panel C were BSA samples treated with 40 and 100 mM DTT for 48 h. In panel D lanes “S” and “P” were soluble fractions

and insoluble pellets in samples, respectively. * signifies the presence of high molecular weight protein species.

Conformational changes, hydrophobic exposure, and aggregation in lysozyme and BSA were monitored by intrinsic fluorescence and by extrinsic fluorophores such as 8-anilino-1-naphthalene sulfonate (ANS), 4,4'-dianilino-1,1'-binaphthyl-5,5'-disulfonic acid (bis-ANS), and Thioflavin T (ThT). Intrinsic fluorescence intensity for disulfide-reduced lysozyme increased rapidly in the first 4 h followed by a fast and significant decrease in fluorescence up to 72 h (Figure 3.5A). After 72 h the decrease in fluorescence intensity was slow. On the other hand, the intrinsic fluorescence for disulfide reduced-BSA showed a very rapid drop in fluorescence up to 24 h (Figure 3.5B). After 24 h, the decrease in fluorescence slowed down considerably. Both lysozyme and BSA that had intact disulfide bands (samples with no DTT) showed negligible fluorescence changes over time (Figure 4).

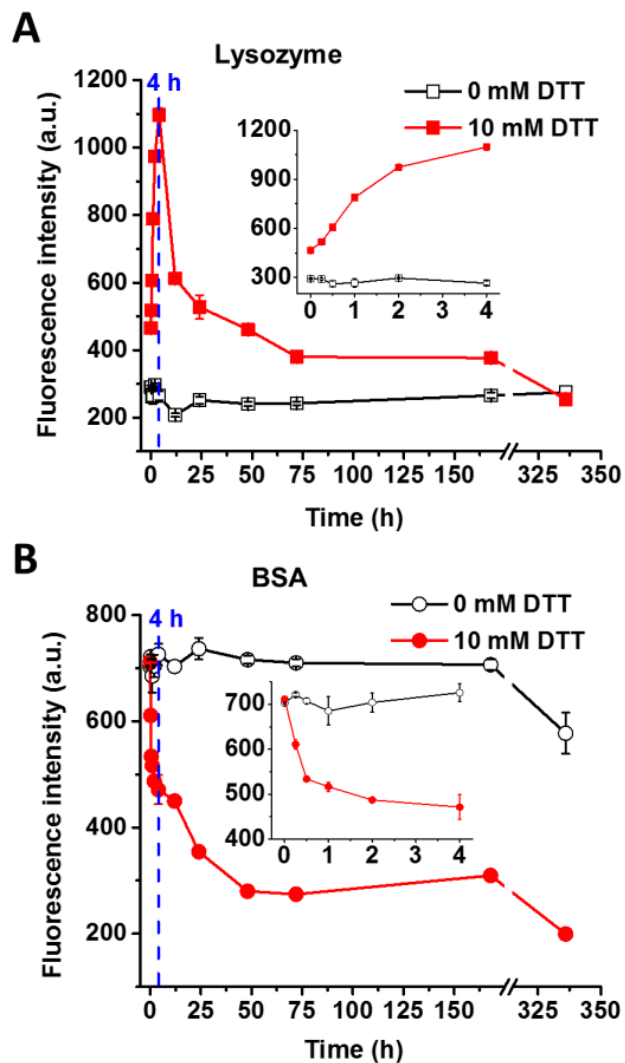


Figure 3.5. Intrinsic fluorescence peak intensities over time for both lysozyme and BSA proteins. Fluorescence spectra for 5 μ M each of lysozyme and BSA were collected from 300-450 nm with excitation at 280 nm. Peak emission wavelength of 346 nm and 336 nm were selected for lysozyme (A) and BSA (B), respectively. Peak fluorescence intensities are shown using open symbols (without DTT) and closed symbols (with 10 mM DTT) as a function of time. Inset shows a plot for the first 4 h of incubation. Error bars indicate \pm S.D.

The disulfide-reduced lysozyme and BSA showed opposite trends for ANS and bis-ANS fluorescence (Figure 3.6). In the case of DTT-treated lysozyme samples, ANS

(Figure 3.6A) and bis-ANS (Figure 3.6C) probes showed increased fluorescence with fluorescence increasing rapidly for the first 4 h (Figure 3.6A, C). After 4 h, the fluorescence plateaued and no significant change in fluorescence was observed as a function of time (Figure 3.6A, C). However, DTT-treated BSA showed a rapid decrease in ANS fluorescence for the first 4 h followed by a slower decrease in fluorescence over time (Figure 3.6B). Interestingly, bis-ANS showed a similar decrease in fluorescence for BSA proteins treated with or without DTT (Figure 3.6D). The aggregation of proteins monitored by ThT showed increased fluorescence intensity for DTT-treated lysozyme and BSA in the first 4 h (Figure 3.7A, B; closed symbols) whereas, protein samples in the absence of DTT showed no change in ThT fluorescence (Figure 3.7A, B; open symbols).

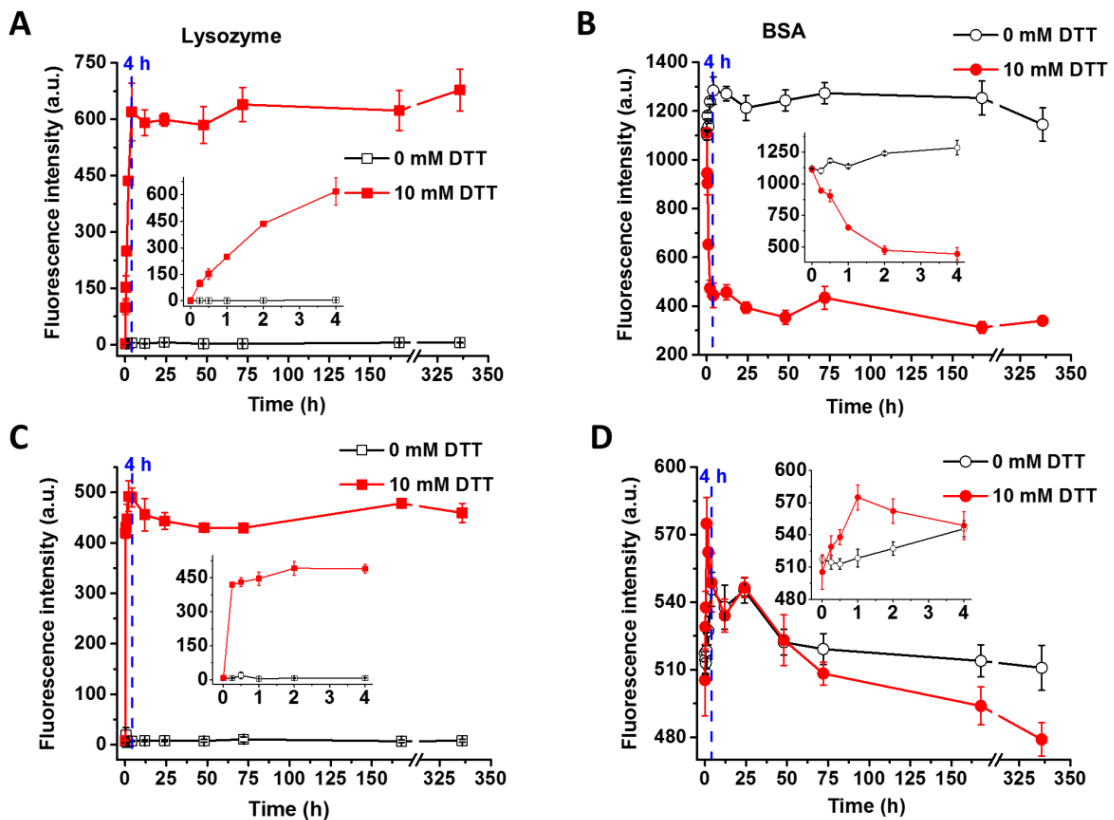


Figure 3.6. Changes in protein hydrophobicity and aggregation were monitored by ANS and bis-ANS fluorescence. 10 μM of protein samples were incubated with 5 μM ANS or 1 μM bis-ANS for 15 minute, before acquiring spectra. Emission spectra for lysozyme (A, C) and BSA (B, D) were collected from 400-700 nm with excitation at 380 nm for ANS and 360 nm for bis-ANS. Average emission peak wavelength of 471 nm and 484 nm were selected for ANS (A, B) and bis-ANS (C, D), respectively. Peak fluorescence intensities are shown using open symbols (without DTT) and closed symbols (with 10 mM DTT). Inset shows plot for first 4 h of incubation. Error bars indicate \pm S.D.

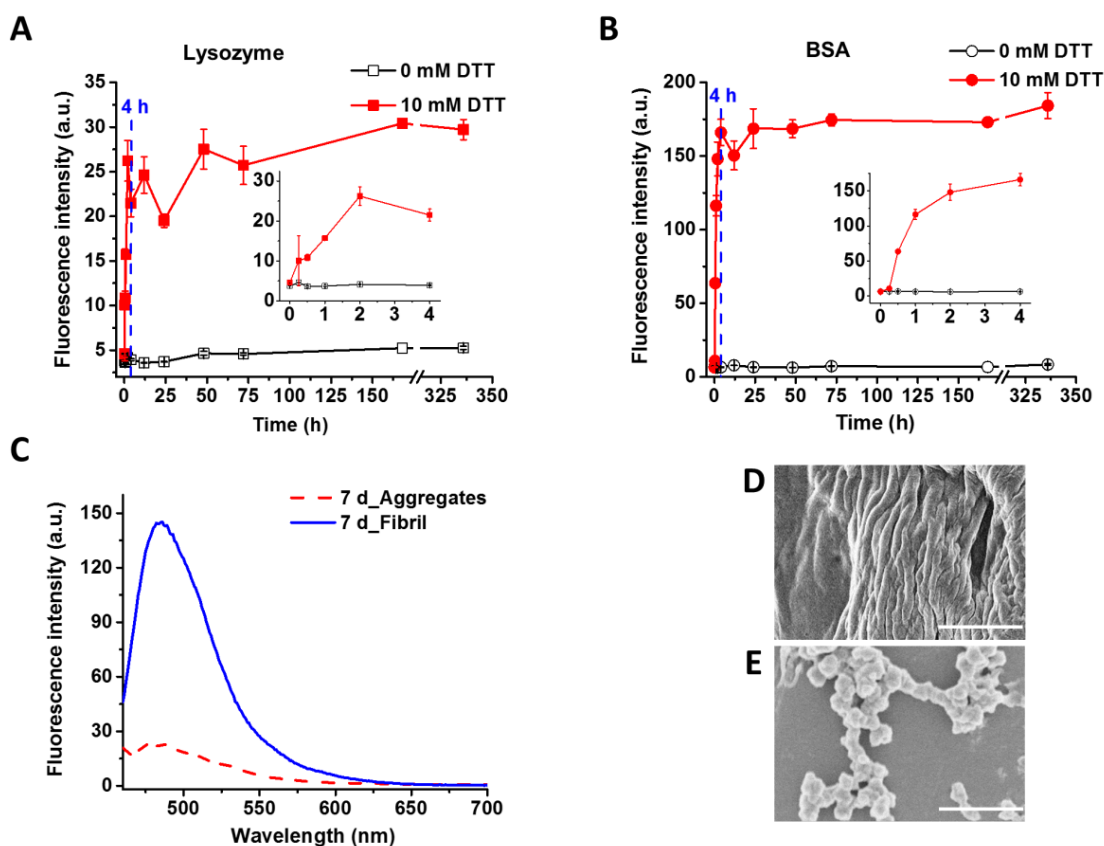


Figure 3.7. ThT fluorescence of protein aggregates and lysozyme fibrils. Emission spectra for 5 μM of lysozyme and BSA in presence of 10 μM ThT were acquired from 460-700 nm with excitation at 450 nm. Average emission peak wavelength of 486 nm and 484 nm were selected for lysozyme (A) and BSA (B), respectively. Peak fluorescence intensities are shown as open symbols (without DTT) and closed symbols

(with 10 mM DTT). Inset shows a plot for first 4 h of incubation. Error bars indicate \pm S.D. Fluorescence spectrum showing signal for 5 μ M lysozyme fibril and amorphous aggregates from 7-day old samples incubated with 10 μ M of ThT dye (C). SEM images shows structures of lysozyme fibril (D) and lysozyme aggregates (E) from 7 day old samples (scale bars = 5 μ m).

SEM analysis (Figure 2) of disulfide reduced lysozyme and BSA proteins showed that aggregates are amorphous in nature that stays amorphous even upon longer incubation. To further investigate if formation of these aggregates are seed-dependent or whether seeding can lead to fibril formation or not, we carried out cross-seeding assays at two different pHs (pH 7.2 and pH 2.0; Figure 3.8). The aggregates formed from 72 h incubated disulfide-reduced proteins (lysozyme and BSA) were washed and added as seeds (5%, 15%, and 50% v/v) into respective lysozyme and BSA protein solutions having intact disulfide bonds (native proteins). Proteins even with small amount of seeds (5% v/v aggregated proteins) initiated aggregation of native proteins at pH 7.2 that share similar morphology with the seeds and showed increased binding to ThT (Figure 3.8, A, B, E, G). In contrast, at pH 2.0, no increase of ThT fluorescence was observed except for lysozyme and BSA that showed increase in ThT fluorescence with 50% seeds (Figure 3.8C, D). And after 72 h, no structured species could be found by SEM, indicating aggregates were destabilized at acidic pH.

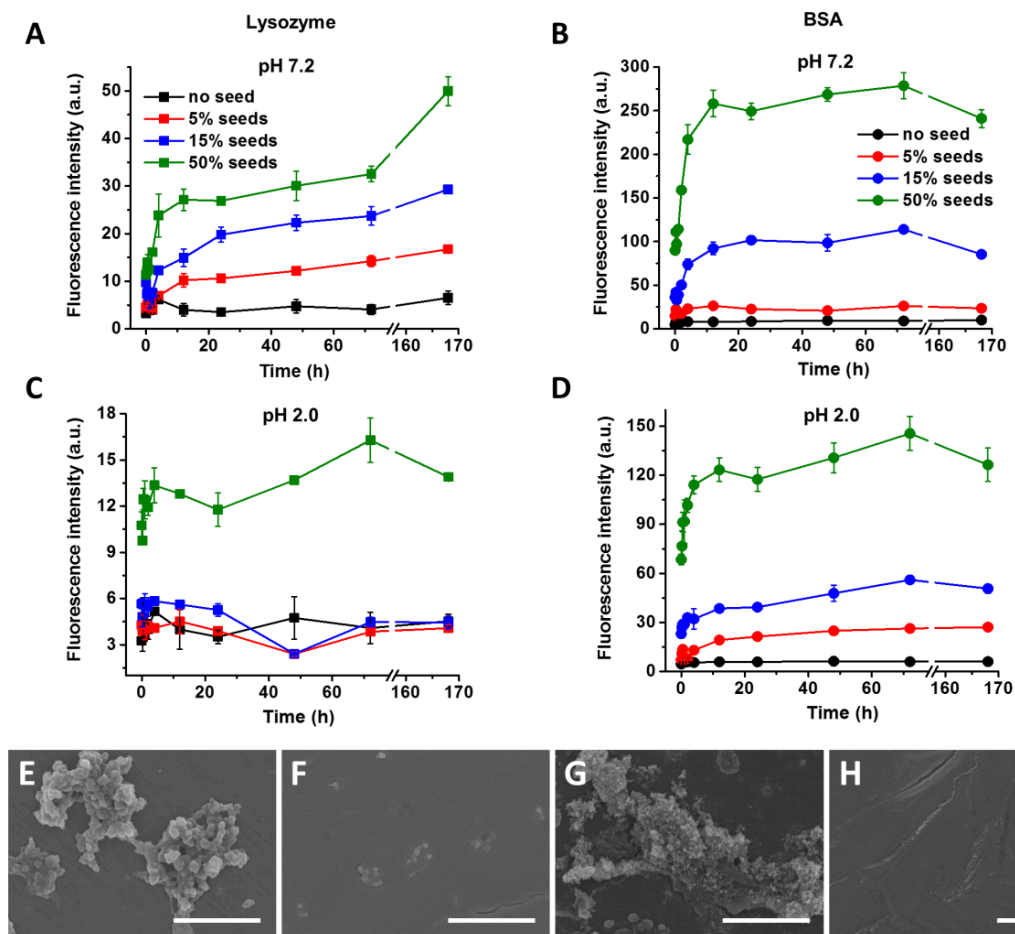


Figure 3.8. Effect of seeding of lysozyme and BSA aggregates on native protein monitored by ThT fluorescence. 5%, 15% and 50% (v/v) of aggregates generated by incubating lysozyme and BSA protein at pH 7.2 and in presence of 10 mM DTT were added as seeds to 40 μM native protein solutions and incubated at 37°C: lysozyme pH 7.2 (A, E), lysozyme pH 2.0 (C, F), BSA pH 7.2 (B, G), and BSA pH 2.0 (D, H). ThT fluorescence experiments were performed as detailed in Figure 6. Error bars indicate ± S.D. SEM images (E-H) show morphology of aggregates formed with 15% seeds after 72 h of incubation (scale bars = 10 μm).

To further confirm the role of disulfide bonds in aggregation, we incubated protein samples with TCEP, a non-thiol based reducing agent, and monitored protein aggregation by intrinsic and ThT fluorescence (Figure 3.9, A-D). As TCEP is not stable in phosphate

buffer, especially around neutral pH, we changed buffer to HEPES (20 mM, pH 7.2). Without adding TCEP, both proteins remained stable, and no aggregates was observed up to 24 hours. The intrinsic fluorescence data for lysozyme samples showed an increase in fluorescence in first 4 h a trend similar to DTT treated samples but upon longer incubation remained steady instead of decreasing in intensity (Figure 3.5A, 3.9A). However, intrinsic fluorescence for TCEP treated BSA, and ThT fluorescence for lysozyme and BSA showed trends similar to that observed for DTT treated protein samples (Figure 3.5B, 3.7A, 3.7B, 3.9B-D). SEM images showed amorphous aggregates for proteins incubated with 2 mM TCEP (Figure 3.9 E, F) that share morphology similar to aggregates seen for proteins incubated with 10 mM DTT (Figure 3.3 E, F, I, J). Interestingly, we did not observe aggregates of either lysozyme or BSA incubated with 5 mM or more TCEP in 24 h.

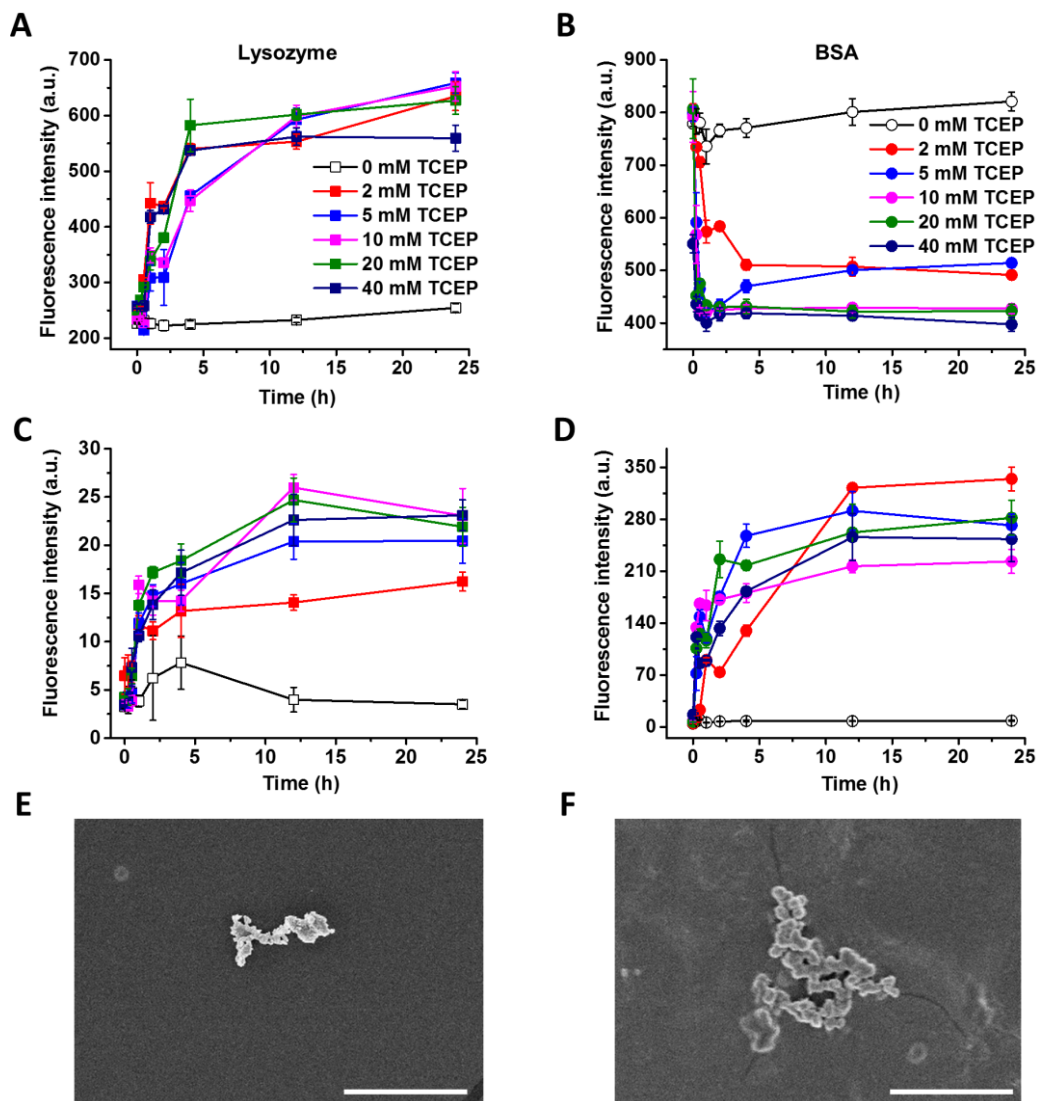


Figure 3.9. Concentration dependence of TCEP on protein aggregation. Protein aggregation rates were monitored using intrinsic fluorescence (A, B) and ThT fluorescence (C, D) for lysozyme (A, C) and BSA (B, D). Error bars indicate \pm S.D. Intrinsic fluorescence experiments were performed as detailed in Figure 4 and ThT fluorescence experiments were performed as detailed in Figure 6. SEM images for aggregates of lysozyme and BSA in presence of 2 mM TCEP are shown in panels (E) and (F), respectively. Scale bars = 10 μ m.

3.4 Discussion

Disulfide bonds are formed naturally in 65% of secreted proteins, 15% of human proteome, and in more than 50% of amyloidogenic proteins¹⁹. The native disulfide bonds are critical for correct folding and normal function of proteins, and the disruption of disulfide bonds were shown to alter protein structures and even result in protein aggregation^{9, 23, 44}. Although cellular redox status can be tuned by certain reducing agents²⁶, cells have great coping mechanism to resist changes. In this study we chose DTT, a disulfide reducing agent to mimic the excessive or improper use of thiol-based antioxidants at physiological pH and temperature. The role of disulfide bonds have been previously studied using strong reducing agents⁴⁵, single site mutations⁹, artificial disulfide linkages¹⁸, and/or at extreme pH conditions¹⁶. Therefore, we wanted to study how disulfide-reduced proteins misfold and form aggregates at physiological pH in absence of any other destabilizing influences. The two proteins (lysozyme and BSA) used in this study could form amorphous aggregates but with unique structural properties.

UV absorbance and fluorescence spectroscopy data showed that both lysozyme and BSA protein samples that lack DTT were stable at 37 °C up to 4 weeks with no measurable changes in their spectral properties (Figure 3.3 and Figures 3.5-3.7). In addition, no visible aggregates were observed for the proteins by SEM (Figure 3.3C, G). This suggests that these two proteins are stable at pH 7.2 and 37 °C for long term in the absence of any destabilizing influence. But for proteins incubated at 37 °C in the presence of reducing agent (10 mM DTT), we observed amorphous aggregates appearing as early as 2 h, signifying the importance of disulfide-bond integrity in providing protein stability (Figure 3.3E). This is in contrast to the fibrils found in several previous studies

performed at extremes of pH or temperature in combination with other solvent additives^{9, 20, 23, 34}. The amorphous aggregates in this study are ~400 nm in diameter with a maximum length of 30 μm (Figure 3.3) that shares some physicochemical characteristics with protofibril, such as size (lysozyme aggregates) and ThT binding capacity. An earlier study shows that ThT positive amorphous aggregates were able to convert into protofibrils after long term incubation, and eventually formed long, unbranched fibril structure⁴⁶. However, under our experimental conditions, the DTT-treated aggregates were not able to convert into fibrils with increased incubation time (Figure 3.10). Although DTT-treated lysozyme and BSA aggregates show rapid increase in ThT fluorescence (Figure 3.7A,B), the ThT signal from aggregates is low and about 1/5th compared to a mature fibril under identical experimental conditions (Figure 3.7C). ThT is a well-known dye for characterizing amyloid-like structures⁴⁷; however, recent studies have shown that some non-fibril/amorphous aggregates were able to bind ThT and show ThT characteristic fluorescence at ~485 nm⁴⁸. The different fluorescence intensities of mature fibril and the aggregates could be caused by difference binding modes of ThT on these structures. It is widely studied and believed that ThT binds to the grooves parallel to the long axis of amyloid fibrils and is stabilized by the hydrophobic and aromatic amino acid side chains⁴⁹. The DTT treated aggregates have very distinct structure from amyloid fibrils (Figure 3.7D, E) but ANS fluorescence results (Figure 3.6A, B) shows the aggregates are very hydrophobic, indicating the ThT molecules could bind to the hydrophobic pockets on the aggregates⁴⁹. In other cases, Groenning and colleagues⁵⁰ showed that β -sheet rich proteins, β -cyclodextrin and transthyretin, could tightly bind ThT molecule without inducing the characteristic fluorescence as the binding site on

proteins was smaller than 8 Å. However, non- β -sheet proteins, γ -cyclodextrin and acetylcholinesterase could induce high ThT fluorescence signal similar to amyloid fibrils as these two proteins had structures with cavity diameters of 8-9 Å, allowing binding of ThT molecules⁵⁰. This is in line with another study showing ThT fluorescence can be induced by non-fibril, protofibril-like aggregates⁴⁸. Another key factor of ThT fluorescence is the rotation of the single bond connecting the benzothiazole ring and the dimethylaminobenzene ring. Wolfe et al.⁵¹ compared the co-crystal structures of ThT with monomeric and amyloid-like oligomer of β -2 microglobulin (β 2m) and found that the twisted angle ϕ of the ThT single bond is $\sim 60^\circ$ in presence of amyloid-like oligomers while $\phi = \sim 30^\circ$ when ThT binds to β 2m monomers. Therefore, the weak ThT fluorescence of DTT treated aggregates could be result of the binding mode of ThT, or the twisted angle ϕ . However, before taking enough atomic level information about the binding of ThT with amorphous aggregate, we are not able to make any clear conclusion of the mechanism of modest ThT fluorescence of DTT treated aggregates. Even though the lysozyme aggregates in this study are more “structured”, there is no direct evidence demonstrating that these aggregates could be classified as protofibrils or protofibril-like aggregates.

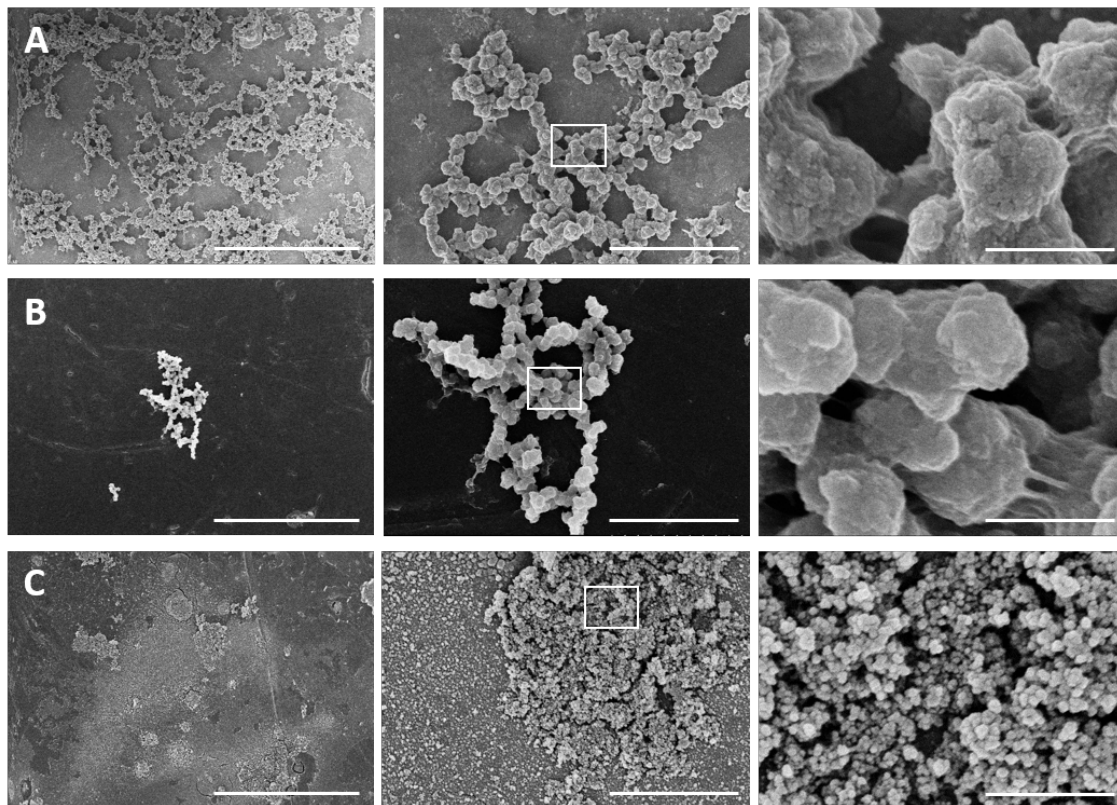


Figure 3.10. Lysozyme and BSA samples which were incubated for long time at 37 °C show amorphous aggregates only. Lysozyme (A, B) and BSA (C) aggregates were imaged after 14 days (A, C) and 48 days (B) of incubation at 37 oC in presence of 10 mM DTT. Scale bars are 50, 5, and 1 μm from left to right in each panel.

Non-reducing SDS-PAGE was used to visualize higher molecular weight cross-linked protein species that can arise due to the scrambling of disulfide bonds (Figure 3.4). The non-reducing gel electrophoresis for lysozyme shows appearance of distinct high molecular weight bands as early as 4 h that can result from disulfide-bond scrambling (Figure 3.4A). This is in line with an earlier study that reported formation of scrambled disulfide-bonds for lysozyme in the presence of 2-mercaptoethanol, a disulfide reducing agent¹⁸. Based on an earlier study the 17 disulfide-bonds in BSA can be grouped in three classes centered on their location and susceptibility to disulfide reducing agent: fully

exposed (reactive with 0.5 mM DTT), partially buried (reactive with 10 mM DTT), and buried (nonreactive in native solution without any denaturants)⁵². For a full reduction of disulfide bonds of the BSA polypeptide chain, 110-218-fold molar excess of DTT is required²⁸. In this study, the use of 10 mM DTT is only a 14-fold molar excess for BSA disulfide bonds. Therefore, we do not expect complete reduction of all the disulfide bridges in the BSA polypeptide chain (Figure 3.4C; see lane R'). Partial disulfide reduction can promote scrambling of disulfide bonds resulting in higher molecular weight species (Figure 3.4B). "R" and "O" bands indicate the presence of a mixture of reduced (R) and oxidized (O) proteins in the DTT-treated BSA samples after 4 h of incubation (Figure 3.4B). Presence of high molecular weight protein species in BSA samples treated with 40 mM or 100 mM DTT at 48 h suggests that proteins are not fully reduced even at high concentrations of DTT under the incubation conditions (Figure 3.4C). The atypical electrophoretic mobility of DTT-treated BSA samples is due to mixture of partially oxidized and reduced proteins affecting the overall hydrodynamic volume of proteins (apparent size) and hence its migration on SDS-PAGE^{53, 54}. In the gel "R" and "O" bands started to be clearly visible from 2 h and their intensities did not change after 4 h which is in line with trend of fluorescence results (Figure 3.5B, 3.6B, and 3.7B). This suggests that presence of scrambled (inter-/intra-molecular) disulfide bonds may be critical in driving and further stabilizing the amorphous aggregate formation (Figure 3.3, 3.11).

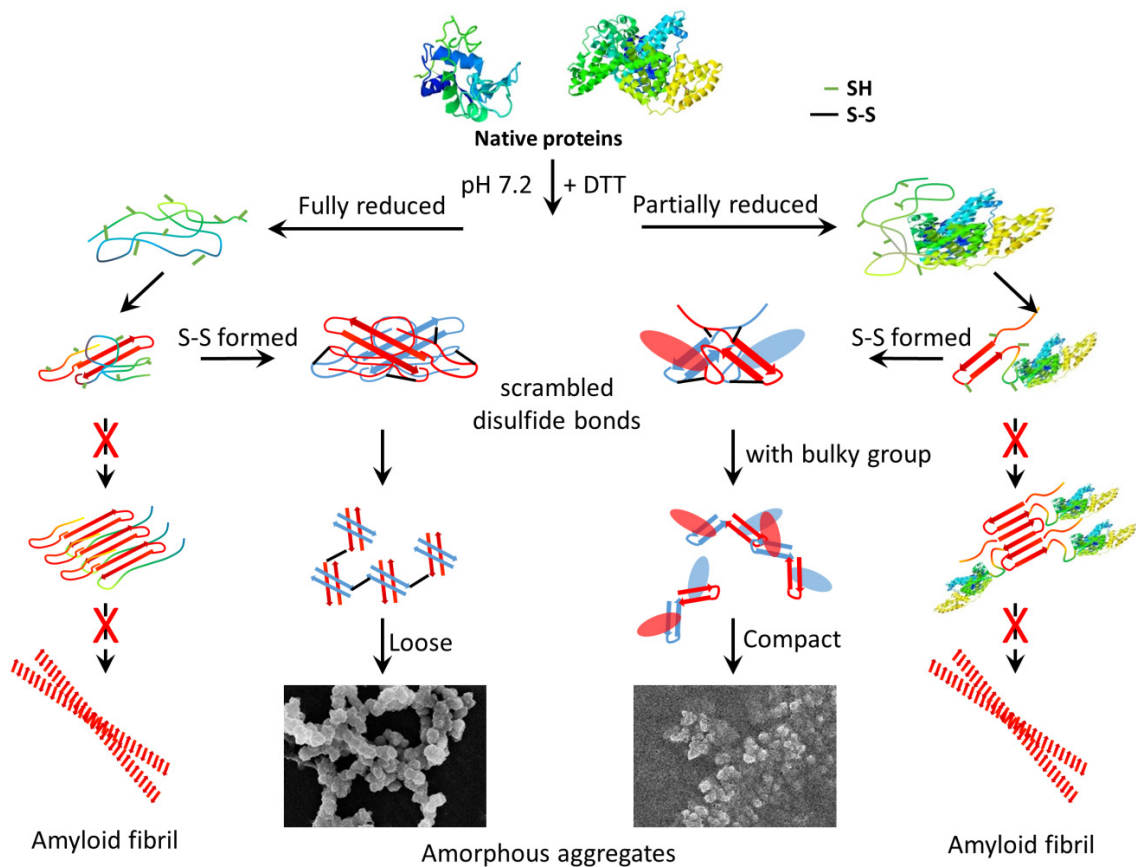


Figure 3.11. A generic aggregation model based on the results of both lysozyme and BSA proteins treated with 10 mM DTT at pH 7.2 and 37 °C. Incomplete reduction of disulfide-bonds in proteins can affect misfolding and can result in formation of scrambled disulfide bonds (both inter- and intra-molecular) affecting the aggregation process. This can favor formation of amorphous aggregates over amyloid like structure.

Intrinsic fluorescence can provide information on protein conformational changes by measuring tryptophan fluorescence that is very sensitive to its local microenvironment. Although both lysozyme and BSA showed similar aggregation kinetics with major structural changes observed within first 4 h, they gave different fluorescence responses. Lysozyme showed an increase in intrinsic fluorescence for first 4 h followed by a rapid decrease in fluorescence signal (Figure 3.5A). The major contributors of intrinsic

fluorescence in native lysozyme are Trp 62 and Trp 108⁵⁵, which are exposed to the solvent⁵⁶. The other Trp residues are either tightly packed inside the structure (Trp 111 and Trp 123), or are located near disulfide bonds (Trp 28, Trp 63, Trp 111, Trp 123), which have Cys-linked sulfurs that can act as fluorescence quenchers⁵⁵. Therefore, the increase of lysozyme intrinsic fluorescence in the first 4 hours could be a result of disulfide bonds breaking with and exposing Trp residues decreasing the quenching effects of reduced sulfur groups in the unfolded structure. Free thiols upon longer incubation can form scrambled disulfide bonds and quench intrinsic fluorescence as the aggregated proteins may have a more packed structure that may also bring the Trp residues closer to Cys residues. DTT-treated BSA showed a very different fluorescence response compared to that of lysozyme (Figure 3.5B). The major difference may be due to the size of the protein (66 kDa), number of disulfide bonds (17 S-S bonds) per molecule of protein, and location of aromatic residues in the protein structure³¹. BSA is a big protein with only two tryptophan residues (W-134 and W-213), and neither of them is located on the protein's surface. A blue shift in the emission peak that is associated with a decrease in fluorescence intensity is consistent with aggregation leading to shielding of Trp residues and its fluorescence being quenched by close proximity of other groups such as free Cys or peptide bond^{57, 58} (Figure 3.12A).

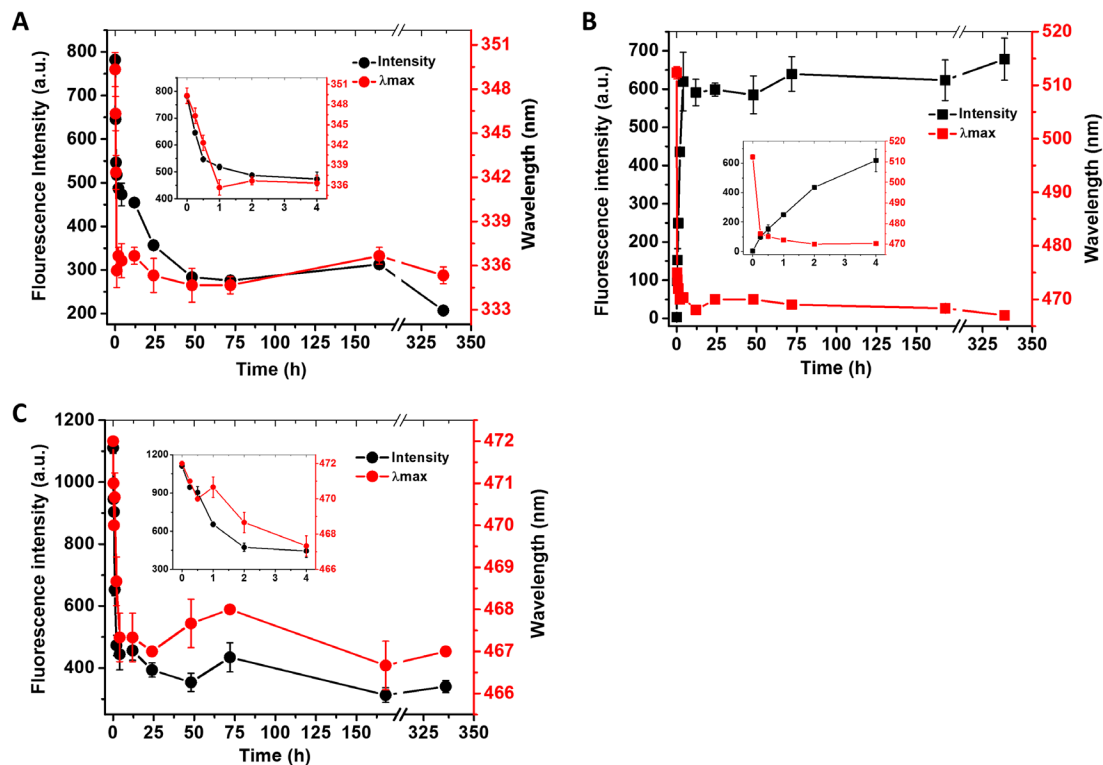


Figure 3.12. Intrinsic fluorescence peak intensity and wavelength shifts over time for BSA protein. Peak fluorescence intensities are shown in black and wavelength for peak maxima are plotted in red. The results from first 4 hour were zoomed as inset figures. Error bars indicate \pm S.D.

As all of the Trp residues in lysozyme and BSA are located near hydrophobic clusters^{17, 31, 59}, we used hydrophobic probe ANS to detect change in protein hydrophobicity. ANS is very sensitive to local solvent environments, shows high fluorescence and is blue shifted when buried in hydrophobic pockets, or shows decreased fluorescence that is red shifted when exposed to more polar environment^{47, 60, 61}. In presence of ANS, lysozyme showed a rapid increase in fluorescence for the first 4 h with subsequent fluorescence plateau (Figure 3.6A). This was mirrored by a shift in wavelength for peak cps from \sim 510 nm (considerable exposure to polar solvent) to \sim 470 nm (indicative of buried in hydrophobic core) and was stable around 470 nm after that

(Figure 3.12B). The high fluorescence signal and blue shift suggests that lysozyme aggregates may be flexible permitting tight binding of ANS molecules to the protein^{47, 62, 63}. To further study the flexibility of protein aggregates, we used the dimeric analog of ANS, bis-ANS, that has larger ring structure and does not bind tightly to organized structures, even if hydrophobic. Bis-ANS requires a flexible molten globule like structures for tight binding^{64, 65}, and reacts weakly to amyloid fibrils⁶⁶. Bis-ANS fluorescence of lysozyme aggregates suggests DTT reduced lysozyme aggregates have a highly flexible structure (Figure 3.6C). The continued high bis-ANS fluorescence of reduced lysozyme after 4 h indicates that aggregates of lysozyme even after long-term incubation were still flexible and had not converted into more organized and rigid structures. As ANS and bis-ANS have net negative charge we investigated the effect of ionic strength on fluorescence of lysozyme aggregates (Figure 3.13). Although it has been reported that high ionic strength can affect lysozyme structure⁶⁷, the removal of NaCl in this study did not affect lysozyme aggregation, suggesting that electrostatic interaction is not a major force driving the interaction at pH 7.2.

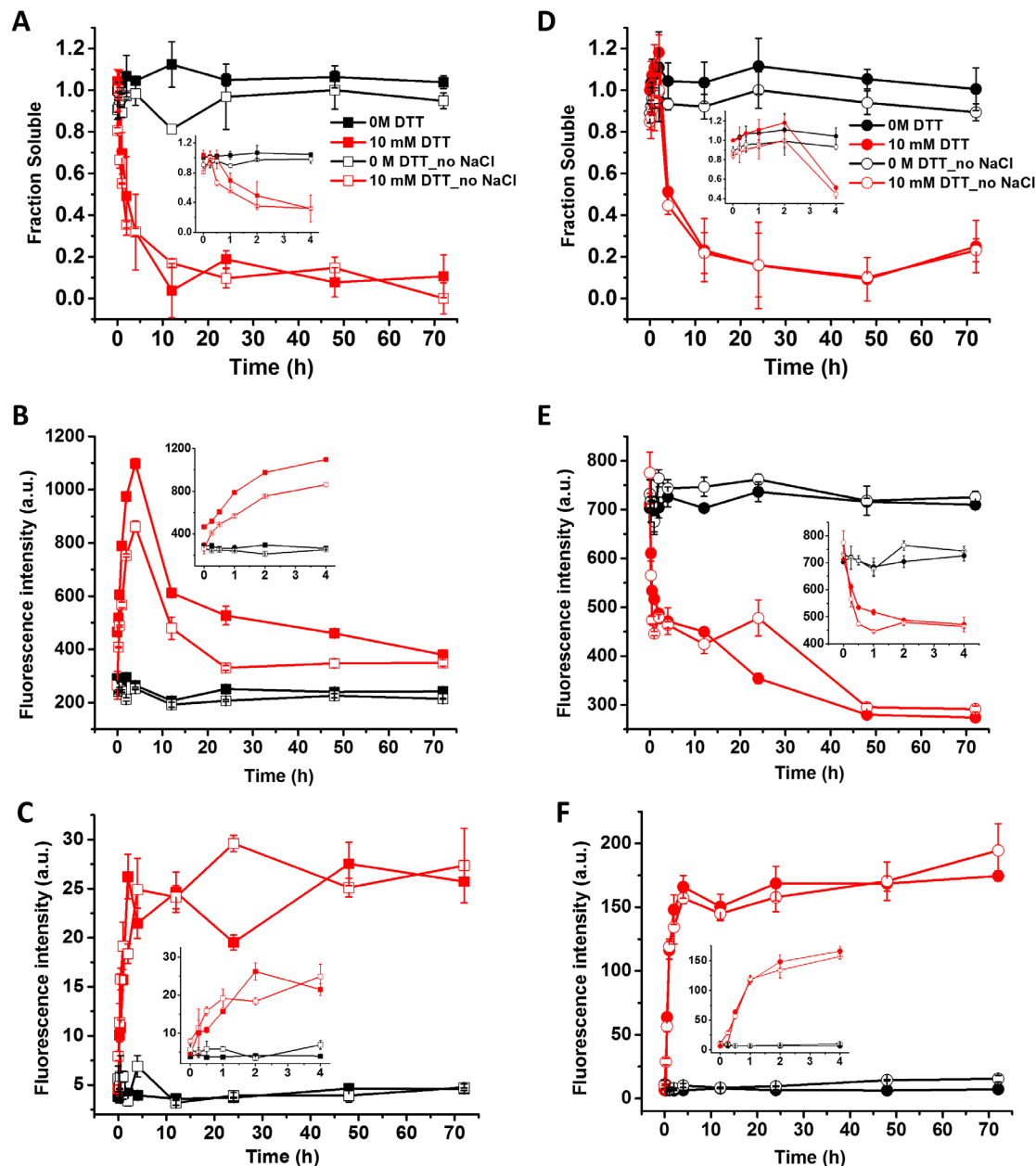


Figure 3.13. Effect of ionic strength (NaCl) monitored by UV absorbance, intrinsic and ThT fluorescence. Both lysozyme (A-C) and BSA (D-F) protein samples were prepared in presence (closed symbols) or absence (open symbols) of 150 mM NaCl having 0 (black) or 10 mM (red) DTT. Fraction soluble proteins at 280 nm (A, D) were estimated by UV absorbance. The peak intensities of intrinsic fluorescence (B, E) at 346 nm (for lysozyme) and 336 nm (for BSA) were plotted. For ThT assay (C, F): protein samples (5 μ M) were incubated with 10 μ M ThT, and peak fluorescence intensities at 486

nm (for lysozyme) and 484 nm (for BSA) were plotted. The results from first 4 hour were zoomed as inset figures. Error bars indicate \pm S.D.

Different from lysozyme, the reduced BSA showed a dramatic decrease in ANS fluorescence in first 4 h and then was stable at low signal level for long term (Figure 3.6B). The BSA samples with intact disulfide bonds (lacking DTT) showed high ANS fluorescence (Figure 3.6B). This could be because ANS can bind to the hydrophobic pockets on BSA and its fluorescence intensity and quantum yield depend upon the degree of exposure to solvent^{61,68}. In addition, serum albumin is a transport protein with highly flexible native structure and has many binding sites for lipids or drugs that can also bind ANS³⁷. The decrease in ANS fluorescence of DTT-treated BSA could be due to exposure of hydrophobic regions to the solvent phase, or collapsing and aggregating of hydrophobic regions that can be a result of scrambling of disulfide bonds, as BSA is only partially reduced under the experimental conditions. Peak emission wavelength for fluorescence in the 470 nm range suggests poor but hydrophobic binding of the dye, that maybe a result of rigid amorphous structure (Figure 3.12B). Bis-ANS was used to further investigate protein flexibility changes in oxidized and reduced BSA. Interestingly, we found that both DTT-treated and DTT lacking BSA samples had weak interactions with bis-ANS (Figure 3.6D). Bis-ANS was found to have dual effect on protein structure through binding: high concentration of bis-ANS induces more disordered protein structures, while at low concentration, binding with bis-ANS results in tighter conformers⁶⁵. Thus, in the case of the DTT lacking BSA samples, the equilibrium could shift from native conformation to a tighter conformer after binding bis-ANS. Native BSA has high affinity binding sites for ANS and bis-ANS, but on non-native conformations,

only low affinity binding sites were found⁶⁵. Plus the structure of DTT treated BSA aggregates are relatively rigid (Figure 3.3 I, J), indicating weak binding with bis-ANS. Therefore, we only observed weak bis-ANS fluorescence with both native and aggregated BSA samples.

In the cross-seeding experiments, the amorphous aggregates were able to act as seed and lead to rapid aggregation of native proteins at pH 7.2 (Figure 3.8), suggesting a low energy barrier between the native conformation and the aggregates^{69, 70}. In addition, the association of native proteins to seeds could also be driven by hydrophobic interactions, knowing that the aggregates have high ANS binding capacity (Figure 3.6). Whereas, the cross-seeded proteins at pH 2.0 (Figure 3.8) did not induce aggregation of native proteins. This may be due to difference in molecular organization of native proteins that favor fibril formation at pH 2.0⁴⁸. In addition, the scrambling of disulfide bonds increased the tendency for molecular self-assembling and collisions that results in lack of large homogeneous structures. Similar findings have been reported in previous studies of amyloid- β peptide⁴⁸ and β 2-microglobulin⁷¹. Therefore, the amorphous aggregates of disulfide-reduced proteins at pH 7.2 are probably formed through a kinetically trapped pathway, due to strong inter-/intra-molecular association caused by disulfide scrambling.

To further confirm the formation of amorphous aggregates observed in this study is a result of disulfide scrambling and not thiolated side product of DTT oxidation, we treated the proteins with 0 to 40 mM TCEP (Figure 3.9). It's noticeable that in presence of 2 mM TCEP, both lysozyme and BSA, show strong measurable fluorescence signals. Knowing that TCEP has stronger reducing activity⁷² and longer half-life than DTT⁷³, high concentration of TCEP could inhibit disulfide scrambling, which is the driving force for

the formation of amorphous aggregates observed in this study. SEM images of protein samples incubated with 2 mM TCEP formed amorphous aggregates (figure 3.9 E, F) that share morphology very similar to 10 mM DTT treated protein samples. However, we did not observe aggregates of either lysozyme or BSA up to 24 h with TCEP concentration higher than 5 mM. The high concentration of TCEP could possibly inhibit the scrambling of disulfide bonds and hence can affect the formation of amorphous aggregates. Since the result with 10 mM DTT could be reproduced with low concentration of TCEP (2 mM), we believe that the formation of amorphous aggregates in presence of 10 mM DTT is a result of disulfide scrambling.

3.5 Conclusion

In summary, under the experimental conditions reported in this work, both disulfide reduced lysozyme and BSA showed increased susceptibility to form amorphous aggregates that have very distinct structures. Both proteins show increased ThT binding but the fluorescence signal is still low compared to amyloid fibril. The lysozyme aggregates show higher structural flexibility in comparison to BSA aggregates. Formation of amorphous aggregates for these two proteins is a result of the interplay of disulfide bond scrambling and hydrophobic interactions that could kinetically affect the overall aggregation pathway (Figure 3.11). Cross-seeding experiments into native proteins for both proteins could only promote aggregation at pH 7.2 but not for proteins at acidic pH. This may be due to surface charge differences on proteins resulting in unique molecular organization at different pHs.

3.6 References

1. Fink, A. L., Protein aggregation: folding aggregates, inclusion bodies and amyloid. *Folding & Design* **1998**, *3*, R9-R23.
2. Ross, C. A.; Poirier, M. A., Protein aggregation and neurodegenerative disease. *Nat. Med.* **2004**, *10*, S10-S7.
3. Glabe, C. G., Structural classification of toxic amyloid oligomers. *Journal of Biological Chemistry* **2008**, *283*, 29639-43.
4. DeToma, A. S.; Salamekh, S.; Ramamoorthy, A.; Lim, M. H., Misfolded proteins in Alzheimer's disease and type II diabetes. *Chemical Society Reviews* **2012**, *41*, 608-21.
5. Bernstein, S. L.; Dupuis, N. F.; Lazo, N. D.; Wytttenbach, T.; Condrón, M. M., et al., Amyloid-beta protein oligomerization and the importance of tetramers and dodecamers in the aetiology of Alzheimer's disease. *Nature Chemistry* **2009**, *1*, 326-31.
6. Krebs, M. R. H.; Wilkins, D. K.; Chung, E. W.; Pitkeathly, M. C.; Chamberlain, A. K., et al., Formation and seeding of amyloid fibrils from wild-type hen lysozyme and a peptide fragment from the beta-domain. *Journal of Molecular Biology* **2000**, *300*, 541-9.
7. Morozova-Roche, L. A.; Zurdo, J.; Spencer, A.; Noppe, W.; Receveur, V., et al., Amyloid fibril formation and seeding by wild-type human lysozyme and its disease-related mutational variants. *Journal of Structural Biology* **2000**, *130*, 339-51.
8. Bhattacharya, M.; Jain, N.; Mukhopadhyay, S., Insights into the mechanism of aggregation and fibril formation from bovine serum albumin. *Journal of Physical Chemistry B* **2011**, *115*, 4195-205.
9. Cao, A. E.; Hu, D. Y.; Lai, L. H., Formation of amyloid fibrils from fully reduced hen egg white lysozyme. *Protein Science* **2004**, *13*, 319-24.

10. Qin, Z.; Hu, D.; Zhu, M.; Fink, A. L., Structural characterization of the partially folded intermediates of an immunoglobulin light chain leading to amyloid fibrillation and amorphous aggregation. *Biochemistry* **2007**, *46*, 3521-31.
11. Juarez, J.; Taboada, P.; Mosquera, V., Existence of Different Structural Intermediates on the Fibrillation Pathway of Human Serum Albumin. *Biophysical Journal* **2009**, *96*, 2353-70.
12. Maeda, R.; Ado, K.; Takeda, N.; Taniguchi, Y., Promotion of insulin aggregation by protein disulfide isomerase. *Biochimica Et Biophysica Acta-Proteins and Proteomics* **2007**, *1774*, 1619-27.
13. Holm, N. K.; Jespersen, S. K.; Thomassen, L. V.; Wolff, T. Y.; Sehgal, P., et al., Aggregation and fibrillation of bovine serum albumin. *Biochimica Et Biophysica Acta-Proteins and Proteomics* **2007**, *1774*, 1128-38.
14. Mossuto, M. F.; Dhulesia, A.; Devlin, G.; Frare, E.; Kumita, J. R., et al., The non-core regions of human lysozyme amyloid fibrils influence cytotoxicity. *Journal of Molecular Biology* **2010**, *402*, 783-96.
15. Dobson, C. M., Protein folding and misfolding. *Nature* **2003**, *426*, 884-90.
16. Sarkar, N.; Kumar, M.; Dubey, V. K., Effect of sodium tetrathionate on amyloid fibril: Insight into the role of disulfide bond in amyloid progression. *Biochimie* **2011**, *93*, 962-8.
17. Silvers, R.; Sziegat, F.; Tachibana, H.; Segawa, S.-i.; Whittaker, S., et al., Modulation of structure and dynamics by disulfide bond formation in unfolded states. *Journal of the American Chemical Society* **2012**, *134*, 6846-54.
18. Chang, J. Y.; Li, L., The unfolding mechanism and the disulfide structures of denatured lysozyme. *Febs Letters* **2002**, *511*, 73-8.

19. Li, Y.; Yan, J.; Zhang, X.; Huang, K., Disulfide bonds in amyloidogenesis diseases related proteins. *Proteins-Structure Function and Bioinformatics* **2013**, *81*, 1862-73.
20. Li, Y.; Gong, H.; Sun, Y.; Yan, J.; Cheng, B., et al., Dissecting the role of disulfide bonds on the amyloid formation of insulin. *Biochemical and Biophysical Research Communications* **2012**, *423*, 373-8.
21. Wang, S. S. S.; Liu, K.-N.; Wang, B.-W., Effects of dithiothreitol on the amyloid fibrillogenesis of hen egg-white lysozyme. *European Biophysics Journal with Biophysics Letters* **2010**, *39*, 1229-42.
22. Wu, G. Y.; Fang, Y. Z.; Yang, S.; Lupton, J. R.; Turner, N. D., Glutathione metabolism and its implications for health. *Journal of Nutrition* **2004**, *134*, 489-92.
23. Wang, G. Z.; Dong, X. Y.; Sun, Y., The role of disulfide bond formation in the conformational folding kinetics of denatured/reduced lysozyme. *Biochem. Eng. J.* **2009**, *46*, 7-11.
24. Michailidis, Y.; Karagounis, L. G.; Terzis, G.; Jamurtas, A. Z.; Spengos, K., et al., Thiol-based antioxidant supplementation alters human skeletal muscle signaling and attenuates its inflammatory response and recovery after intense eccentric exercise. *American Journal of Clinical Nutrition* **2013**, *98*, 233-45.
25. Sen, C. K., Redox signaling and the emerging therapeutic potential of thiol antioxidants. *Biochemical Pharmacology* **1998**, *55*, 1747-58.
26. Rushworth, G. F.; Megson, I. L., Existing and potential therapeutic uses for N-acetylcysteine: The need for conversion to intracellular glutathione for antioxidant benefits. *Pharmacology & Therapeutics* **2014**, *141*, 150-9.
27. Touch, V.; Hayakawa, S.; Saitoh, K., Relationships between conformational changes and antimicrobial activity of lysozyme upon reduction of its disulfide bonds. *Food Chemistry* **2004**, *84*, 421-8.

28. Ueki, T.; Hiragi, Y.; kataoka, M.; Inoko, Y.; Amemiya, Y., et al., Aggregation of bovine serum albumin upon cleavage of its disulfide bonds, studied by the time-resolved small-angle X-ray scattering technique with synchrotron radiation. *Biophysical Chemistry* **1985**, *23*, 115-24.
29. Tiwari, A.; Hayward, L. J., Familial amyotrophic lateral sclerosis mutants of copper/zinc superoxide dismutase are susceptible to disulfide reduction. *Journal of Biological Chemistry* **2003**, *278*, 5984-92.
30. Nagendra, H. G.; Sudarsanakumar, C.; Vijayan, M., An X-ray analysis of native monoclinic lysozyme. A case study on the reliability of refined protein structures and a comparison with the low-humidity form in relation to mobility and enzyme action. *Acta Crystallographica Section D-Biological Crystallography* **1996**, *52*, 1067-74.
31. Bujacz, A., Structures of bovine, equine and leporine serum albumin. *Acta Crystallographica Section D-Biological Crystallography* **2012**, *68*, 1278-89.
32. Guez, V.; Roux, P.; Navon, A.; Goldberg, M. E., Role of individual disulfide bonds in hen lysozyme early folding steps. *Protein Science* **2002**, *11*, 1136-51.
33. White, F. H., Studies on the relationship of disulfide bonds to the formation and maintenance of secondary structure in chicken egg-white lysozyme. *Biochemistry* **1982**, *21*, 967-77.
34. Vernaglia, B. A.; Huang, J.; Clark, E. D., Guanidine hydrochloride can induce amyloid fibril formation from hen egg-white lysozyme. *Biomacromolecules* **2004**, *5*, 1362-70.
35. Raccosta, S.; Manno, M.; Bulone, D.; Giacomazza, D.; Militello, V., et al., Irreversible gelation of thermally unfolded proteins: structural and mechanical properties of lysozyme aggregates. *European Biophysics Journal with Biophysics Letters* **2010**, *39*, 1007-17.

36. Navarra, G.; Troia, F.; Militello, V.; Leone, M., Characterization of the nucleation process of lysozyme at physiological pH: Primary but not sole process. *Biophysical chemistry* **2013**, *177-178*, 24-33.
37. He, X. M.; Carter, D. C., Atomic structure and chemistry of human serum albumin. *Nature* **1992**, *358*.
38. E. Katchalski, G. S. B., V. Gross, The availability of the disulfide bonds of human and bovine serum albumin and of bovine gamma-globulin to reduction by thioglycolic acid. *J Am Chem Soc* **1957**, *79*, 4096-9.
39. Borzova, V. A.; Markossian, K. A.; Kurganov, B. I., Relationship between the initial rate of protein aggregation and the lag period for amorphous aggregation. *International Journal of Biological Macromolecules* **2014**, *68*, 144-50.
40. Davidson, B. E.; Hird, F. J., The reactivity of the disulphide bonds of purified proteins in relationship to primary structure. *The Biochemical journal* **1967**, *104*, 473-9.
41. Johanson, K. O.; Wetlaufer, D. B.; Reed, R. G.; Peters, T., Refolding of bovine serum-albumin and its proteolytic fragments - regain of disulfide bonds, secondary structure, and ligand-binding ability. *Journal of Biological Chemistry* **1981**, *256*, 445-50.
42. Vetri, V.; D'Amico, M.; Fodera, V.; Leone, M.; Ponzoni, A., et al., Bovine Serum Albumin protofibril-like aggregates formation: Solo but not simple mechanism. *Archives of Biochemistry and Biophysics* **2011**, *508*, 13-24.
43. Arasteh, A.; Habibi-Rezaei, M.; Ebrahim-Habibi, A.; Moosavi-Movahedi, A. A., Response surface methodology for optimizing the bovine serum albumin fibrillation. *Protein Journal* **2012**, *31*, 457-65.
44. Kumar, S.; Ravi, V. K.; Swaminathan, R., How do surfactants and DTT affect the size, dynamics, activity and growth of soluble lysozyme aggregates? *Biochem. J.* **2008**, *415*, 275-88.

45. Mossuto, M. E.; Bolognesi, B.; Guixer, B.; Dhulesia, A.; Agostini, F., et al., Disulfide Bonds Reduce the Toxicity of the Amyloid Fibrils Formed by an Extracellular Protein. *Angewandte Chemie-International Edition* **2011**, *50*, 7048-51.
46. Bucciantini, M.; Giannoni, E.; Chiti, F.; Baroni, F.; Formigli, L., et al., Inherent toxicity of aggregates implies a common mechanism for protein misfolding diseases. *Nature* **2002**, *416*, 507-11.
47. Hawe, A.; Sutter, M.; Jiskoot, W., Extrinsic fluorescent dyes as tools for protein characterization. *Pharmaceutical Research* **2008**, *25*, 1487-99.
48. Yamaguchi, T.; Yagi, H.; Goto, Y.; Matsuzaki, K.; Hoshino, M., A Disulfide-Linked Amyloid-beta Peptide Dimer Forms a Protofibril-like Oligomer through a Distinct Pathway from Amyloid Fibril Formation. *Biochemistry* **2010**, *49*, 7100-7.
49. Biancalana, M.; Koide, S., Molecular mechanism of Thioflavin-T binding to amyloid fibrils. *Biochimica Et Biophysica Acta-Proteins and Proteomics* **2010**, *1804*, 1405-12.
50. Groenning, M.; Olsen, L.; van de Weert, M.; Flink, J. M.; Frokjaer, S., et al., Study on the binding of Thioflavin T to beta-sheet-rich and non-beta-sheet cavities. *Journal of Structural Biology* **2007**, *158*, 358-69.
51. Wolfe, L. S.; Calabrese, M. F.; Nath, A.; Blaho, D. V.; Miranker, A. D., et al., Protein-induced photophysical changes to the amyloid indicator dye thioflavin T. *Proceedings of the National Academy of Sciences of the United States of America* **2010**, *107*, 16863-8.
52. Malhotra, M.; Sahal, D., Anomalous mobility of sulfitolysed proteins in SDS-PAGE - Analysis and applications. *International Journal of Peptide and Protein Research* **1996**, *48*, 240-8.
53. Tiwari, A.; Liba, A.; Sohn, S. H.; Seetharaman, S. V.; Bilsel, O., et al., Metal Deficiency Increases Aberrant Hydrophobicity of Mutant Superoxide Dismutases That

Cause Amyotrophic Lateral Sclerosis. *Journal of Biological Chemistry* **2009**, *284*, 27746-58.

54. Light, D. L. S. a. A., Comparative Studies on the Modification of Specific Disulfide Bonds of Trypsinogen and Chymotrypsinogen. *Journal of Biological Chemistry* **1971**, *246*, 1630-7.

55. Laurents, D. V.; Baldwin, R. L., Characterization of the unfolding pathway of hen egg white lysozyme. *Biochemistry* **1997**, *36*, 1496-504.

56. Baldwin, R. L., Protein folding - Making a network of hydrophobic clusters. *Science* **2002**, *295*, 1657-8.

57. Babcock, J. J.; Brancaleon, L., Bovine serum albumin oligomers in the E- and B-forms at low protein concentration and ionic strength. *International Journal of Biological Macromolecules* **2013**, *53*, 42-53.

58. Adams, P. D.; Chen, Y.; Ma, K.; Zagorski, M. G.; Sonnichsen, F. D., et al., Intramolecular quenching of tryptophan fluorescence by the peptide bond in cyclic hexapeptides. *Journal of the American Chemical Society* **2002**, *124*, 9278-86.

59. Klein-Seetharaman, J.; Oikawa, M.; Grimshaw, S. B.; Wirmer, J.; Duchardt, E., et al., Long-range interactions within a nonnative protein. *Science* **2002**, *295*, 1719-22.

60. Lindgren, M.; Sorgjerd, K.; Hammarstrom, P., Detection and characterization of aggregates, prefibrillar amyloidogenic oligomers, and protofibrils using fluorescence spectroscopy. *Biophysical Journal* **2005**, *88*, 4200-12.

61. Matulis, D.; Baumann, C. G.; Bloomfield, V. A.; Lovrien, R. E., 1-anilino-8-naphthalene sulfonate as a protein conformational tightening agent. *Biopolymers* **1999**, *49*, 451-8.

62. Cunningham, E. L.; Agard, D. A., Interdependent folding of the N- and C-terminal domains defines the cooperative folding of alpha-lytic protease. *Biochemistry* **2003**, *42*, 13212-9.
63. Semisotnov, G. V.; Rodionova, N. A.; Razgulyaev, O. I.; Uversky, V. N.; Gripas, A. F., et al., Study of the molten globule intermediate state in protein folding by a hydrophobic fluorescent-probe. *Biopolymers* **1991**, *31*, 119-28.
64. Shi, L.; Palleros, D. R.; Fink, A. L., Protein conformational-changes induced by 1,1'-bis(4-Anilino-5-Naphthalenesulfonic Acid) - Preferential binding to the molten globule of DNAK. *Biochemistry* **1994**, *33*, 7536-46.
65. Celej, M. S.; Montich, C. G.; Fidelio, G. D., Protein stability induced by ligand binding correlates with changes in protein flexibility. *Protein Science* **2003**, *12*, 1496-506.
66. LeVine, H., 4,4'-Dianilino-1,1'-binaphthyl-5,5'-disulfonate: report on non-beta-sheet conformers of Alzheimer's peptide beta(1-40). *Archives of Biochemistry and Biophysics* **2002**, *404*, 106-15.
67. Takekiyo, T.; Yamazaki, K.; Yamaguchi, E.; Abe, H.; Yoshimura, Y., High Ionic Liquid Concentration-Induced Structural Change of Protein in Aqueous Solution: A Case Study of Lysozyme. *Journal of Physical Chemistry B* **2012**, *116*, 11092-7.
68. Togashi, D. M.; Ryder, A. G., Time-resolved fluorescence studies on Bovine Serum Albumin denaturation process. *Journal of Fluorescence* **2006**, *16*, 153-60.
69. Dobson, C. M., Principles of protein folding, misfolding and aggregation. *Semin. Cell Dev. Biol.* **2004**, *15*, 3-16.
70. Sanchez-Ruiz, J. M., Protein kinetic stability. *Biophysical Chemistry* **2010**, *148*, 1-15.

71. Hong, D. P.; Gozu, M.; Hasegawa, K.; Naiki, H.; Goto, Y., Conformation of beta(2)-microglobulin amyloid fibrils analyzed by reduction of the disulfide bond. *Journal of Biological Chemistry* **2002**, *277*, 21554-60.
72. Han, J. C.; Han, G. Y., A Procedure for Quantitative-Determination of Tris(2-carboxyethyl)phosphine, an Odorless Reducing Agent More Stable and Effective than Dithiothreitol. *Analytical Biochemistry* **1994**, *220*, 5-10.
73. Getz, E. B.; Xiao, M.; Chakrabarty, T.; Cooke, R.; Selvin, P. R., A comparison between the sulfhydryl reductants tris(2-carboxyethyl)phosphine and dithiothreitol for use in protein biochemistry. *Analytical Biochemistry* **1999**, *273*, 73-80.

Chapter 4 Acetylation of Amyloid β_{1-42} at Lysine 16 disrupts amyloid formation[†]

Mu Yang^a, Ergun Kara^a, Colina Dutta^a, Michael S. Lee^b, and Ashutosh Tiwari^{a*}

^a Department of Chemistry, Michigan Technological University, Houghton, Michigan 49931, United States

^b Adelphi Laboratory Center, United States Army research laboratory, Adelphi, Maryland 20783, United States

[†]This chapter contains the material from a manuscript which will be submitted to an international peer-reviewed journal.

4.1 Introduction

Protein misfolding/aggregation was long believed to hold the key to neurodegenerative diseases, among which Alzheimer's disease (AD) is most known and now affects 5.3 million Americans, with a total cost of \$217.7 billion in 2014^{1,2}. Without preventative treatments or effective therapeutic methods, the number of people suffering from AD in the US is expected to be 10 million by 2050^{1,2}. The extracellular amyloid plaques formed from amyloid β ($A\beta$) peptide was identified as one of the major hallmarks of this disease³. $A\beta$ peptides vary in length from 39 to 43 amino acids⁴. In a normal human brain, about 76-90% of $A\beta$ peptides are $A\beta$ 40, whereas only <10% are the more aggregation-prone one, $A\beta$ 42⁵⁻⁷. Since the discovery of $A\beta$ 30 years ago, great efforts have been done on understanding $A\beta$ fibrils⁸ and the associated toxicities^{9,10}. However, the toxic structure of $A\beta$ is still not defined. Many drugs or therapies have been developed in the past decades, but none to date shows clinical efficacy. In the past 5 years, over 5,000 projects and \$3 billion of funds contributing to researches of AD and related dementias². However, development of AD treatment is limited by the large variety of the highly transient dynamics of $A\beta$ species that is naturally formed in the brain^{8,10}.

The in vivo "pool" of $A\beta$ contains not only the $A\beta$ peptides in different length, but also the post-translated modified forms¹⁰. It has been well established that the posttranslational modifications (PTMs) play an important role in protein folding and aggregation. Extracellular phosphorylation on $A\beta$ accelerates the self-assembling of this peptide into neurotoxic aggregate species¹¹⁻¹³. Other modifications, such as phosphorylation¹¹⁻¹³, truncation¹⁴⁻¹⁶, isomerization^{17,18}, and pyroglutamate formation^{16,19}, were also found to influence $A\beta$ aggregation propensity and cytotoxicity. Glycosylation

was detected on A β 42 in human cerebrospinal fluid, but the functional effects are still not clear²⁰. Acetylation was recently found to be caused by the highly electrophilic diacetyl radicals that are related to many diseases²¹⁻²⁴. In the case of AD, acetylation on tau was recently identified and was proposed as a new therapeutic target^{25, 26}. Interestingly, acetylation on A β peptide was not as well studied as other modifications. A β acetylation on residue K28 has been previously demonstrated on A β ₂₅₋₃₅ fragment, showing negligible effect on the overall fibril morphology²⁷, but little is known about the effect of acetylation on full length A β ₄₂ peptide.

The A β 42 peptide has two lysine residues, K16 and K28 (Figure 1A). K16 contributes to amyloid fibril formation by serving as part of an intermolecular binding sequence (K16-F20)²⁸. While K28 forms a salt bridge with A42 in A β 42 fibrils (Figure 1B)²⁹, or with D23 in A β 40 fibrils³⁰, to stabilize the β -sheet structures of amyloid fibrils. Both lysine residues link to familial (K16N) and nonfamilial (K16A, K28A) mutations that cause early onset dementia in Alzheimer's disease^{31, 32}. Replacing lysine with alanine could affect the α -helical structure (K16A)³³ or the intrapeptide hydrophobic interaction (K28A)³⁴. However, K16R and K28R mutations on A β 40 peptide did not affect the formation of amyloid fibrils³⁵.

A $A\beta_{1-42}$: DAEFR HDSGY EVHHQ **K**LVFF AEDVG SN**K**GA IIGLM VGGVV IA

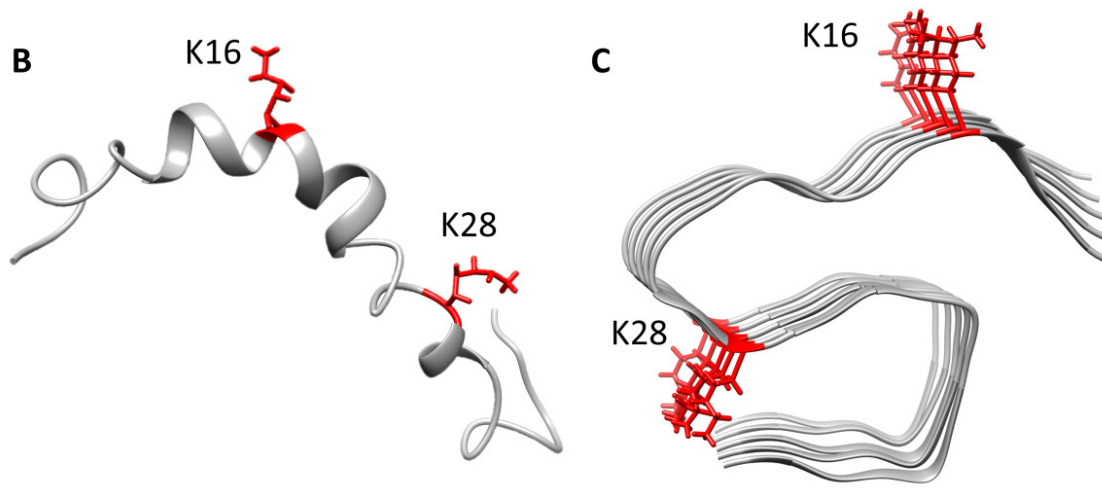


Figure 4.1. Sequence $A\beta_{1-42}$ (A) and atomic structure model of $A\beta_{42}$ monomer (B, in aqueous solution, PDB code: 1Z0Q³⁶) and mature fibril (C, PDB code: 2MXU²⁹). The two lysine residues K16 and K28 are shown in red stick structures. In fibril model, the first 10 N-terminal residues are omitted, because they are structurally disordered and exposed along the fibril surface. The structures were generated using UCSF Chimera³⁷.

In this study, three different acetylation modified $A\beta_{42}$ peptides were synthesized: single acetylation on K16 (K16Ac) or K28 (K28Ac), or double acetylation on both Lysine residues (KKAc). We found that the acetylation on K28 slows down the fibrillization process of $A\beta_{42}$, but still promotes a fibril-like structure. However side-chain acetylation on K16 can profoundly impair the fibrillization property and significantly affect toxicity of $A\beta_{42}$ peptide, which could account for the modulation of $A\beta_{42}$ related pathogenic.

4.2 Materials and methods

Prepare amyloid β peptide assembly samples – Synthetic wild-type (WT), K16Ac, K28Ac, and KKAc $A\beta_{42}$ peptides were purchased from Biomatik (Canada). The identity

and purity (>95%) of all four peptides were confirmed by mass spectrometry and RP-HPLC. Preparation of aggregate-free monomers followed the method from Teplow et al. 2013³⁸. In brief, the peptide lyophilizate was first dissolved in 10% (v/v) of 60 mM NaOH, followed by 45% (v/v) MilliQ water. The the pH was adjusted by adding 45% (v/v) of 10 mM sodium phosphate buffer (pH 7.4). After 10 min centrifuge at $16,000 \times g$ at 4 °C, the supernatant fluid was filtered through 0.22 μm membrane. Concentration of peptide stock was determined using $\epsilon_{214} = 75,887 \text{ M}^{-1}\text{cm}^{-1}$. All the solutions and MilliQ water were filtered through 0.22 μm membrane before use. Peptide stocks were stored at -80 °C until use.

Thioflavin T (ThT) fluorescence – Fluorescence measurements were performed on Horiba Jobin Yvon spectrofluorometer (Fluoromax-4) at room temperature as previously described in chapter 2. In brief, Samples (50 μM peptide in 50 mM phosphate buffer, 300 mM NaCl, pH 7.4) were incubated at 37 °C with agitation for indicated time. After incubation, samples were diluted by phosphate buffer (10 mM, pH 7.4) to a final concentration of 10 μM , followed by addition of ThT solutions (final concentration at 10 μM). Emission spectra were collected at room temperature from 460 – 700 nm, with excitation at 450 nm.

8-anilino-1-naphthalenesulfoni acid (ANS) fluorescence – Freshly prepared samples and 7-day fibril/aggregates samples that contain 10 μM peptides were mixed with ANS solution (final concentration at 10 μM). Emission spectra were collected at room temperature from 400 – 700 nm, with excitation at 380 nm.

Field emission scanning electron microscopy (FESEM) – FESEM images were acquired on a Hitachi S-4700 FESEM microscope as previous described in chapter 2. In

brief, samples were pelleted by centrifuging at $9,000 \times g$ for 45 min at room temperature. To wash off salts, the pellets were separated and suspended in MilliQ water (0.22 μm membrane filtered) and centrifuged at $9,000 \times g$ for 45 min at room temperature. Washed fibrils or aggregates were applied on SEM stubs and air dried at room temperature. The SEM samples were then coated with 10 nm platinum. For FESEM imaging, 10 kV of acceleration voltage and 5 μA of emission current were used.

Molecular dynamics (MD) calculations – Docking calculations were carried out using AutoDock Vina (Vina)³⁹ and DrugScore eXtended (DSX)⁴⁰. The 3D configuration of ANS is downloaded from PubChem database and saved as PDB file. The energetically most stable A β 42 configuration proposed by 1Z0Q³⁶ PDB file is used as WT template. Mutator Plugin of the VMD⁴¹ was applied to perform in silico acetylation of Lysine residues. PDB files for WT, K16Ac, K28Ac and KKAc A β 42 were created. The ANS-A β 42 complexes are refined VMD 1.9.2⁴¹. The initial topology and parameter files for Acetylated Lysine (ALY) and ANS are created by SwissParam Web Server⁴². The atomic charges on the topology files are refined by B3LYP level QM calculations using Gaussian 09 Revision D.01⁴³. The molecular simulations to minimize the energy of the ligand-protein complexes were performed in the canonical (NVT) ensemble with periodic boundary conditions in all three directions. The iteration was stopped after 10,000 time steps and the resultant geometries were recorded. ANS was re-docked on the resultant A β 42 PDB file and the Vina scores were recorded. The docking output by Vina and the backbone proteins were then used as input files for DSX. The z scores (standard scores) were calculated using the equation:

$$z = \frac{x - \mu}{\sigma}$$

Where x is the raw score, μ is the population mean and σ is the standard deviation of the population.

The resultant PDB files for different ANS-A β 42 complexes are submitted to the PLIP (Protein Ligand Interaction Profiler)⁴⁴ Web Server based on a Python command line application and an empirical database of non-covalent interactions⁴⁴. The interactions are visualized by JSMol applet embedded in the Web Server. Whole molecule is encapsulated by AutoDock Grid Box since no binding region is proposed prior to the calculations. The docking results are listed with respect to the scoring function and visualized by UCSF Chimera³⁷.

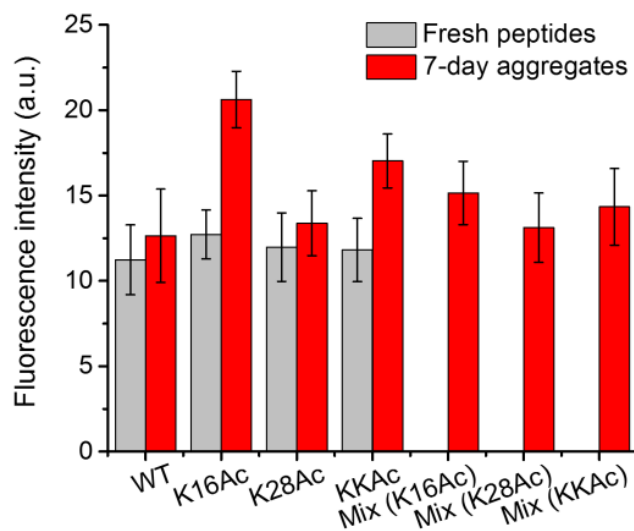
Cell viability (MTS) assay – SH-SY5Y human neuroblastoma cells (from ATCC) were cultured in DMEM/F-12 medium with 10% FBS and 100 U/ml penicillin-streptomycin at 37 °C in 5% CO₂ humidified environment and used within the first 10 passages. Cells were plated at 2×10^4 cells/well on 96-well plates and allowed to grow overnight. The next day, the culture media were removed and cells were washed with 1X PBS buffer (pH 7.4) twice. Then 100 μ l fresh media containing 1, 2, or 5 μ M of peptide samples were added to each well. Six replicates were prepared for each sample. Media without any peptide were used as controls. After 48 h incubation, 20 μ l of CellTiter 96® AQueous One Solution Cell Proliferation (MTS) Assay kit (Promega) were added to each well and incubated for 4 h. Then absorbance at 490 nm were collected using an ELISA plate reader (BioTek Instruments, Inc.). Blanks containing media and peptide samples but no cells were similarly prepared and used for background subtraction.

4.3 Results

Surface hydrophobicity of wild type (WT) A β 42 peptide and the three acetylation-modified peptides were measured by ANS fluorescence (Figure 4.2A). Even though freshly prepared peptides displayed very similar ANS fluorescence, all three acetylated peptides showed slightly higher fluorescence than WT. For better understanding of the results, the resultant geometries by NAMD calculations were optimized and ANS docking was remodeled. The final Binding Affinities and ligand-protein interactions are used to interpret the experimental findings. The top-ranked poses of ANS at all four A β 42 forms have one common major binding site: hydrophobic rings of ANS interact with the aromatic rings of Y10 and H14; the negative charge from ANS is paired with the positive charge on H14 (Figure 4.3). Two more potential binding sites were observed (Figure 4.3): the hydrophobic pocket which is known to play an important role in the aggregation (16-21) and also the region near C terminus (30-35). Table 4.1 and 4.2 show the docking scores of ANS on the four peptides, calculated using DSX and AutoDock Vina. Although the docking scores of Y10 & H14 site are very close in all four peptides (Table 4.1), the ANS binding in the central hydrophobic core (17-20) was strongly affected by acetylation on K16 (Table 4.1, Figure 4.3). With K16Ac, ANS docking scores are -39.132 kcal/mol and -5.0 kcal/mol by DSX and AutoDock Vina, respectively, which are significantly lower than other peptides (Table 4.1). That indicates a significant increase in the hydrophobicity of the 16-21 core, which is related to ANS fluorescence (Figure 4.2A). After 7 days of incubation, differences of hydrophobicity among the four peptides were amplified, especially in K16Ac and KKAc (Figure 4.2A). It is noticeable that fluorescence intensity of K16Ac is almost doubled after incubation for 7 days.

K28Ac showed results similar to WT peptide. Since the A β peptides normally appear in the brain in the heterozygous state, 1:1 ratio mixtures of WT A β 42 with each acetylated peptide were prepared. The hydrophobicity of aggregates generated from the mixtures showed a slight increase in fluorescence compared to WT peptides, except for K28Ac and WT mixture (Figure 4.2A).

A



B

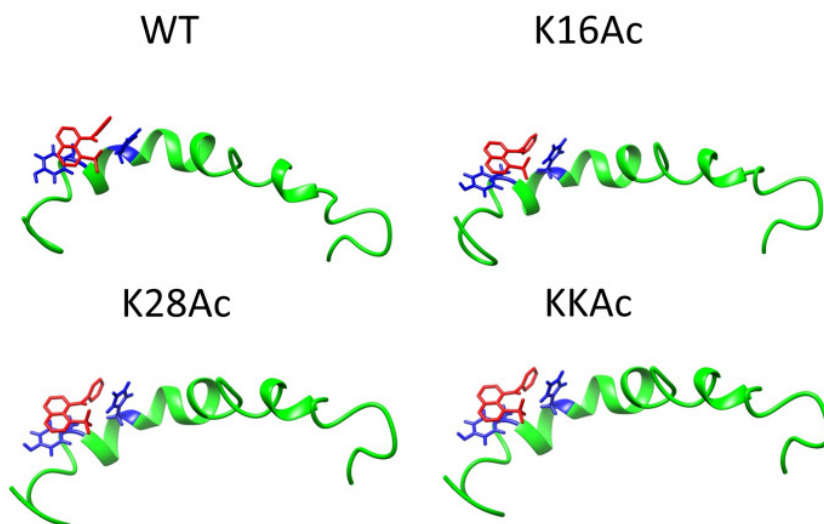
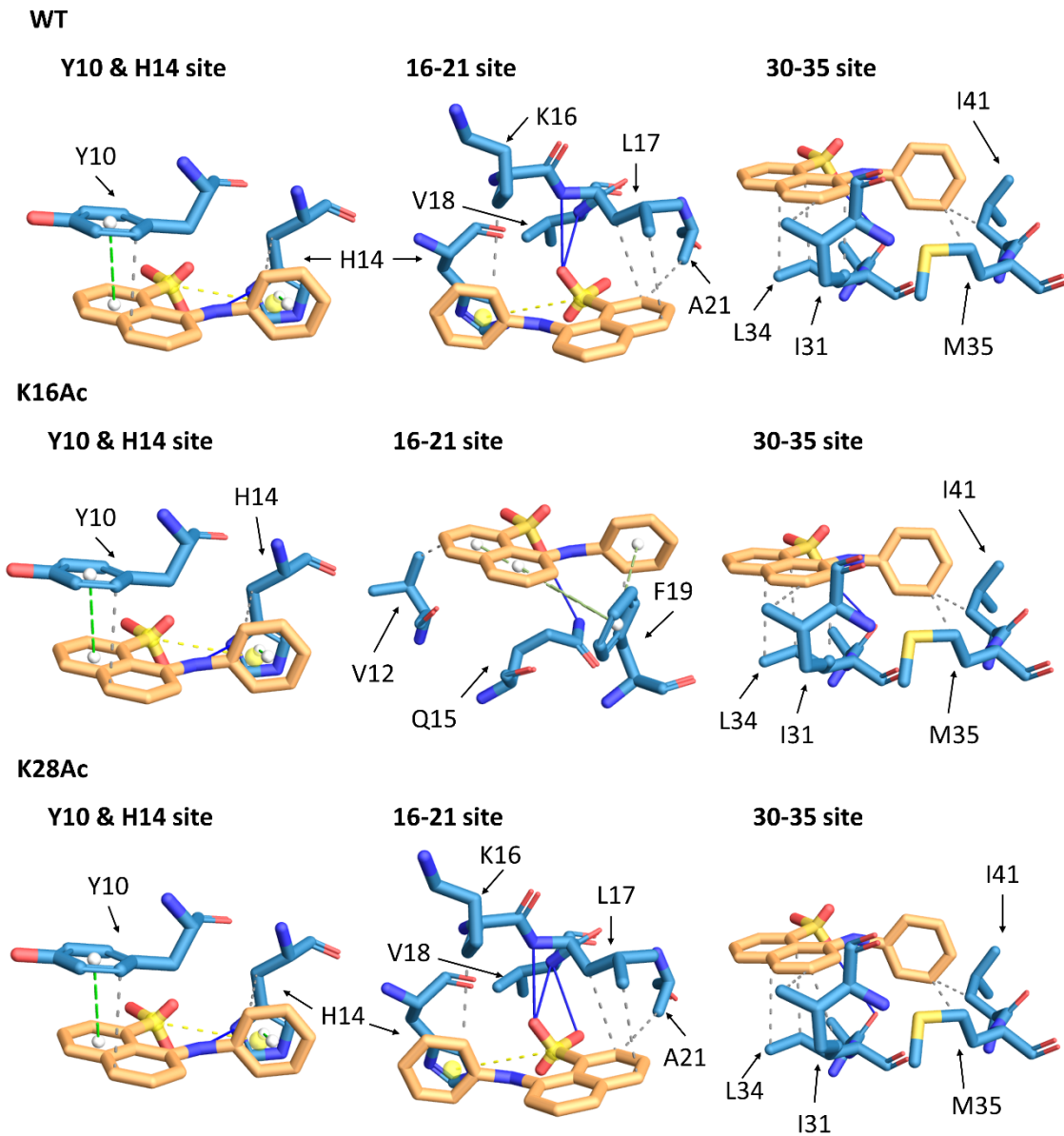


Figure 4.2. (A) Hydrophobicity of the fresh $A\beta_{42}$ peptides and the 7-day fibril/aggregates were measured by ANS fluorescence. Ten μM of peptide samples were incubated with 10 μM of ANS. Mix represents the 1:1 mixture of the acetylated peptide with WT as shown on the right side of the panel. Error bars = \pm S.D. (B) The most stable binding conformer of ANS and $A\beta_{42}$ peptide analyzed by PLIP⁴⁴. Peptide backbones are in green, ANS molecule is in red, and the major binding sites Y10&H14 are labeled in blue.



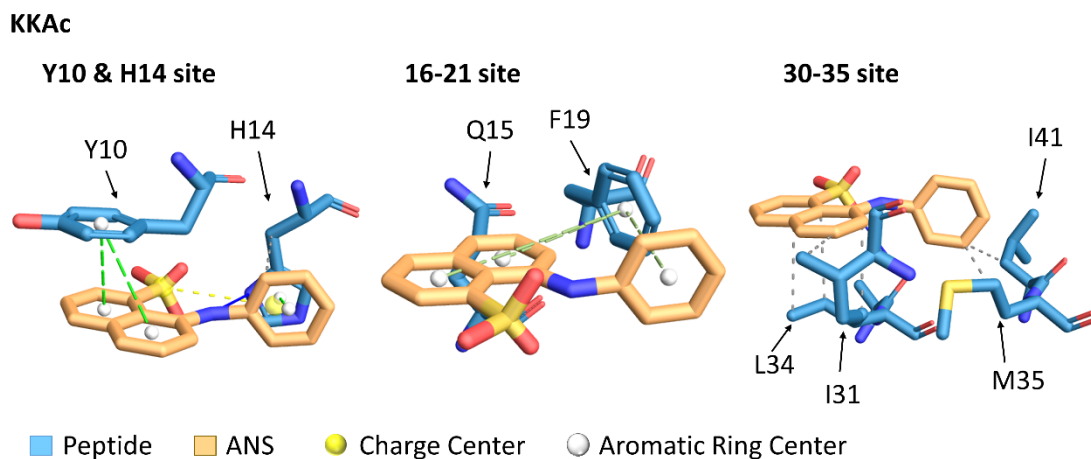


Figure 4.3. The three potential binding sites, Y10&H14, 16-21 region, and 30-35 region, on WT, K16Ac, K28Ac, and KKAc A β 42.

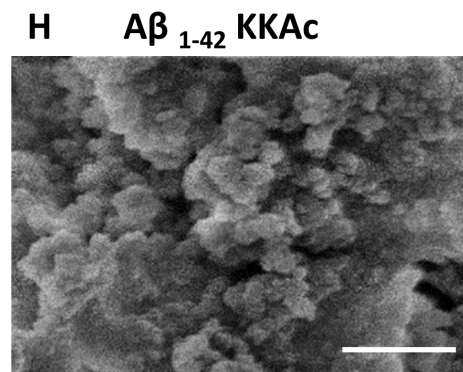
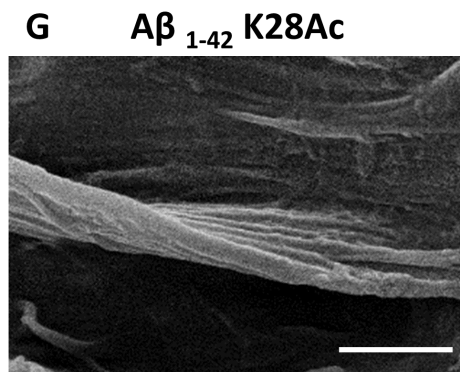
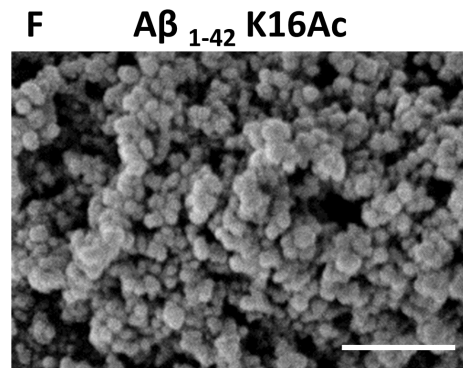
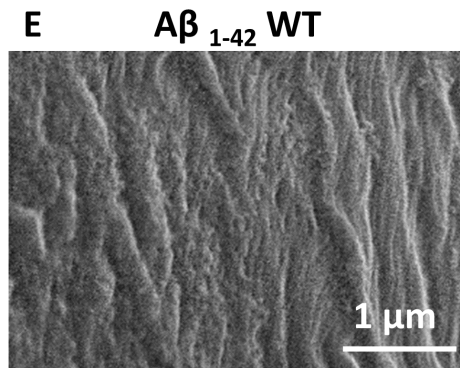
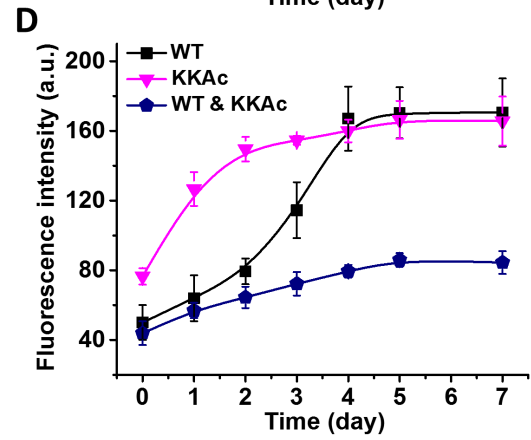
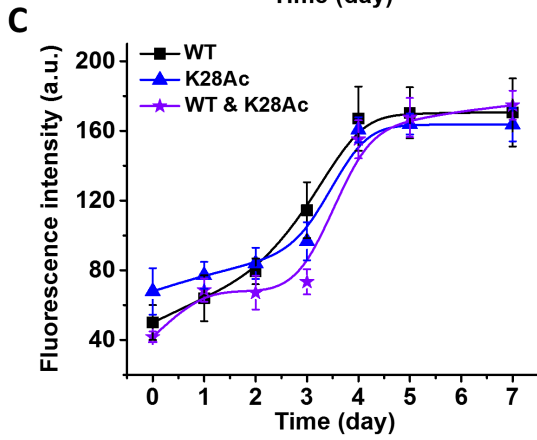
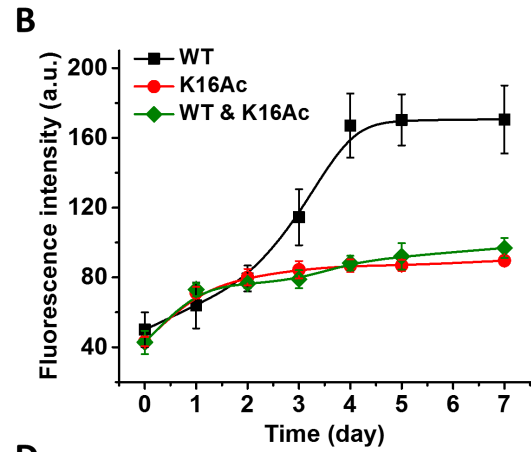
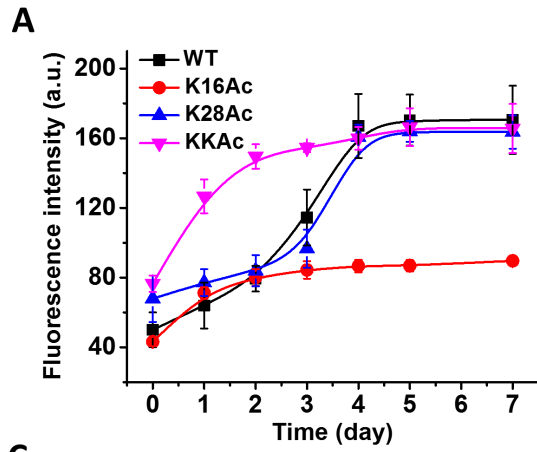
Table 4.1 Docking scores (in kcal/mol) of ANS on the sites Y10 & H14

	Y10 & H14			
	DSX Score	Z_{DSX}	AutoDock Vina Score	Z_{vina}
WT	-12.386	-1.12	-6.1	-2.48
K16Ac	-12.311	-1.74	-6.1	-1.96
K28Ac	-12.312	-1.39	-6.1	-2.04
KKAc	-12.339	-1.47	-6.1	-2.18

Table 4.2 Docking scores (in kcal/mol) of ANS on region 16-21

	region 16-21			
	DSX Score	Z_{DSX}	AutoDock Vina Score	Z_{vina}
WT	-14.250	0.44	-4.7	0.1
K16Ac	-39.132	-1.50	-5.0	-1.1
K28Ac	-12.975	-0.54	-4.4	1.3
KKAc	-13.284	0.52	-4.8	-0.3

Fibrillization/aggregation of the four peptides were monitored by ThT fluorescence (Figure 4.4 A-D). The K28Ac peptide showed very similar sigmoidal fluorescence trend with WT A β 42 and was able to form fibril-like structures in both homogenous K28Ac sample (Figure 4.4 A, G) and the equimolar mixture with WT (Figure 3C, J). In sharp contrast, the two peptides that have acetylation on K16 (K16Ac and KKAc) both showed non-sigmoidal ThT fluorescence trend (Figure 3A) and formed amorphous aggregates after 7 days (Figure 4.4 F, H) and even 14 days (Figure 4.5). Noticeably, even though KKAc did not form amyloid fibrils (Figure 3 H), it showed high ThT fluorescence intensity (Figure 4.4A). The aggregation processes of the 1:1 mixtures with WT showed that K16Ac and KKAc maintained their aggregation properties in presence of WT A β 42, and only amorphous aggregates were observed after incubation (Figure 4.4 B, D, J, L). These results suggest that acetylation on K16 position can significantly affect the fibrillization process of A β 42 peptide. Interestingly, even though the aggregates formed from the mixtures of K16Ac and KKAc were still amorphous, their morphologies were different from pure K16Ac or KKAc aggregates, also showing reduced bis-ANS fluorescence (Figure 4.4 I).



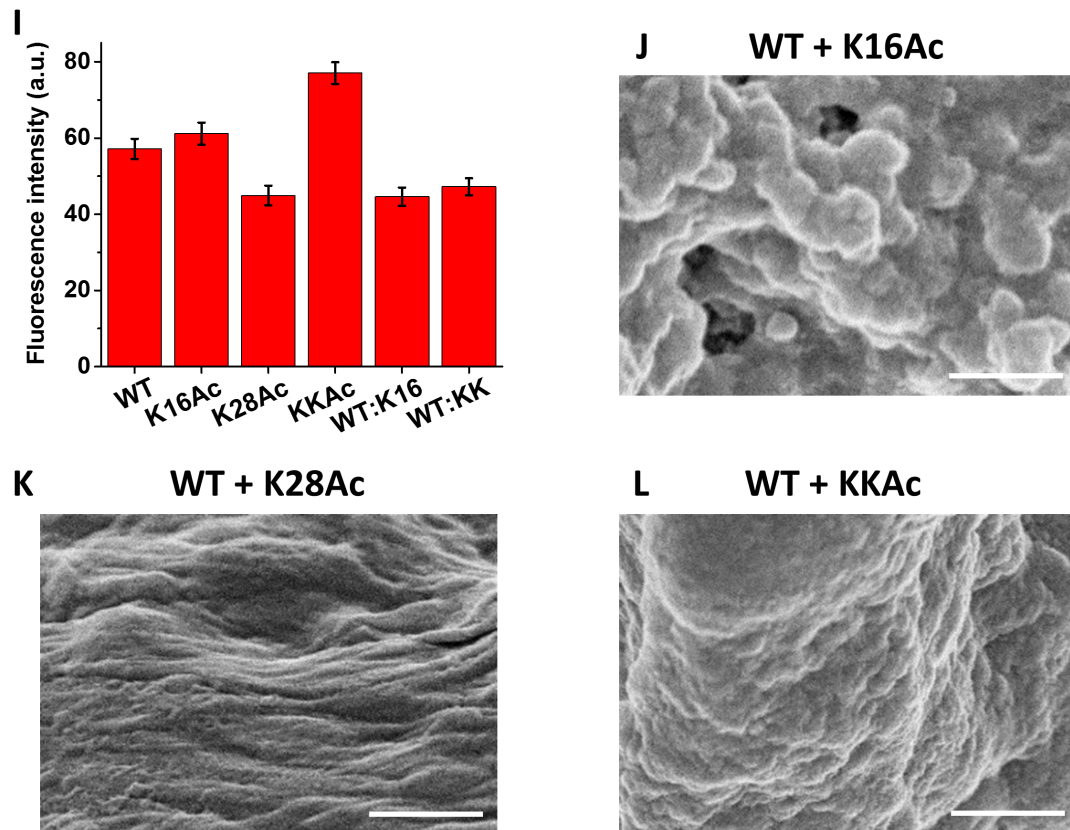


Figure 4.4. Fibrillization/aggregation of WT and acetylated peptides was monitored using ThT fluorescence, bis-ANS fluorescence, and SEM. For ThT fluorescence analysis (A-D), 10 μ M of peptide samples were incubated with 10 μ M of ThT. Peak intensities at 487 nm were plotted in function of time. After 7 days incubation, the structures of fibrils or aggregates were visualized using SEM (E-K). Scale bars are 1 μ m for all. Structure flexibility of the fibrils or aggregates were measured by bis-ANS fluorescence (I). Error bars = \pm S.D.

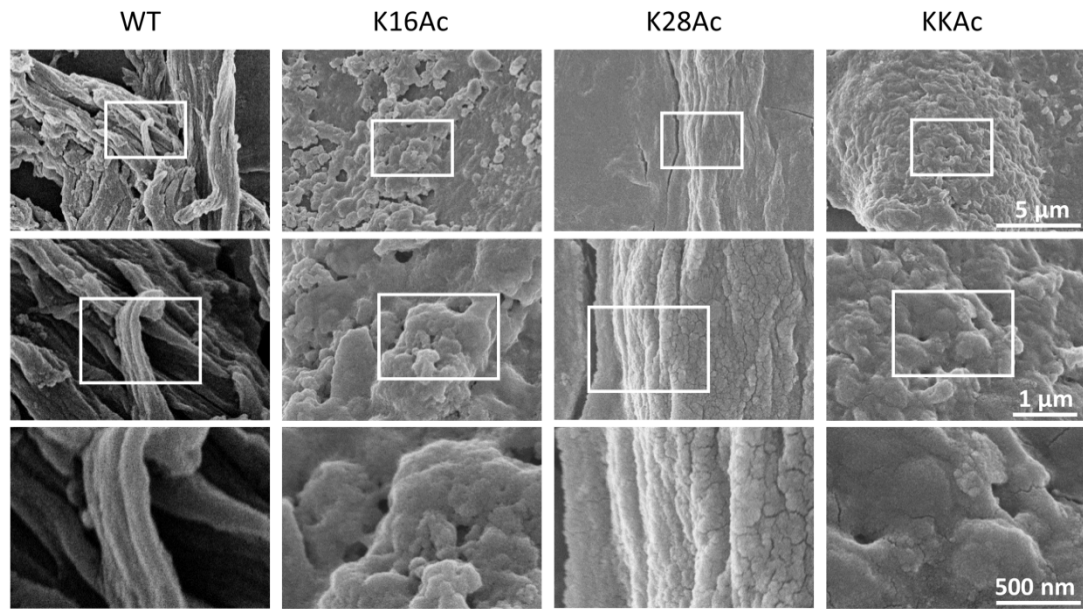


Figure 4.5. SEM images of samples after 14 days incubation. Scale bars are 5 μm , 1 μm and 500 nm for top panel to bottom panels, respectively.

Cell viability of $A\beta_{42}$ fibrils and aggregates were determined using using human HUVEC-C endothelial cells and SH-SY5Y neuroblastoma cells (Figure 4.6). At 2 μM , the WT fibrils and K16Ac aggregates were found harmful to normal cells (HUVEC-C) after 72 h (Figure 4.6). The rigid amorphous aggregates formed from the equal molar mixture of WT and K16Ac showed severe cytotoxicity (Figure 4.6). However, for SH-SY5Y cells, the fresh K16Ac showed the highest cytotoxicity, whereas its 7-day aggregates resulted in $>80\%$ cell viability. All the 72 h samples of WT and single acetylated peptides were found to be more harmful to neuroblastoma cells than the 7-day aggregates. Interestingly, for KKAc, the fresh peptide was protective but 7-day aggregate showed severe toxicity. Interestingly, the cell viability decreased in all three mixtures, especially the K16Ac mixture, showing 20% decrease in 7-day samples.

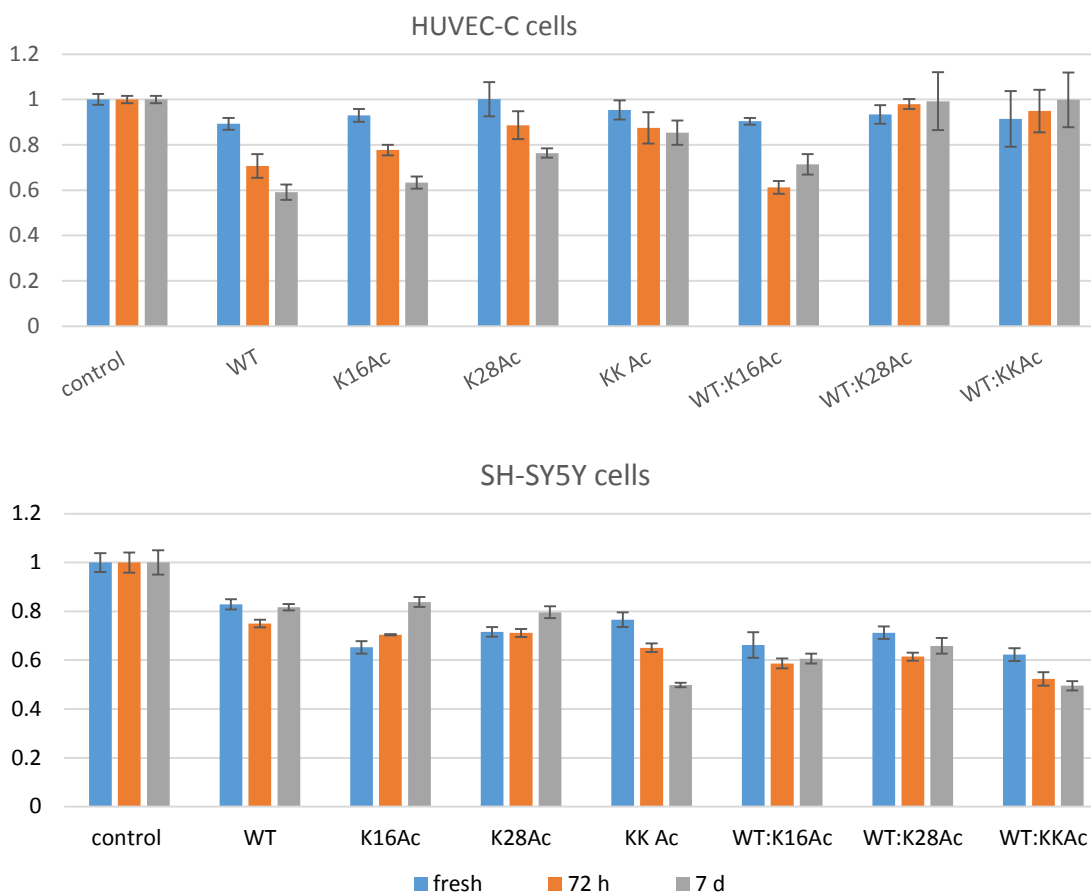


Figure 4.6. Cell viability of HUVEC-C cells and SH-SY5Y cells with A β 42 fibrils or aggregates. The WT or acetylated A β 42 peptides were incubated at pH 7.4 and 37 oC for 0 h, 72 h, or 7 d, and then added to cells to a final concentration of 2 μ M. The mixtures represent samples containing equimolar WT and acetylated peptides. Error bars = \pm S.D.

4.4 Discussion

Amyloid fibril dynamics could be affected by the chemical nature of the A β peptide through side-chain interactions⁴⁵. Here we demonstrated that acetylation on lysine 16 and 28 have distinct effects on A β 42 fibril formation. Acetylation on K16 is more essential to

the early stage inter-peptide interactions, which disrupted fibril formation and altered the related cytotoxicity.

In this study, acetylation on both K16 and K28 residues was expected to affect the hydrophobicity of A β 42, since these are located near hydrophobic patches. While negligible differences of ANS fluorescence was observed between WT and the acetylated peptides. PLIP analysis showed that the major binding site of hydrophobic probe ANS is Y10 & H14 and not the central hydrophobic core, L17-F20 (Figure 4.2, Table 4.1 and 4.2). However, K16 acetylation increased the binding affinity of ANS in the 16-20 region of both K16Ac and KKAc peptides, which later formed amorphous aggregates with higher hydrophobicity than amyloid fibrils (Figure 4.2).

The aggregation rate of K16Ac peptide was faster than K28Ac and WT peptide, showing a slightly greater slope in the first 2 days (Figure 4.4A, 4.5). Moreover, aggregation of K16Ac peptides completed in 2 days, which is almost the same as the lag time of WT and K28Ac peptides (Figure 4.4A). Similar rapid aggregation without lag time was previously observed in computational simulation of A β 16-22 fragment, in which the A β 16-22 peptide oligomers were found to be in a disordered molten globular structure as a result of strong hydrophobic interactions⁴⁶. As the oligomers undergo conformational reorganization, anti-parallel β -sheet structure form and was stabilized by inter-chain salt bridges between K16 and E22⁴⁷, which follows the “dock-lock” mechanism of fibril growth. During fibril formation, the addition of A β monomers to fibril template is a sequential process of two distinct kinetic steps. In the first step, dock, A β monomers bind to fibril (or fibril template) rapidly and fully reversibly. In the second step, lock, the deposited monomer undergoes conformational reorganization, which

significantly increased its association affinity to fibril, resulting in irreversible binding. It was also proposed that the formation of ordered amyloid fibril or oligomer structures could be affected by the competition of hydrophobic interactions and hydrogen bonding, as the higher ordered structures, protofibrils and mature fibrils, are stabilized by high density of direct inter-chain hydrogen bonds and steric zipper interactions^{46, 48}. According to the dock-lock mechanism, although the formation of amyloid fibrils is thermodynamically favored, the transition from monomers to amyloid conformations is kinetically limited⁴⁷. Considering that the 16-20 residues (KLVFF) was previously detected as a intermolecular binding sequence of A β 40 fibrillization²⁸, in case of K16Ac aggregation, it is possible that the inter-chain hydrophobic interactions of the residues 16-20 increased after removing the positive charge on K16, resulting in the initial rapid docking process becoming irreversible, which kinetically inhibited the conformational reorganization in the locking phase (Figure 4.7). As a consequence, K16Ac was able to inhibit amyloid fibril formation of WT A β 42 in their equimolar mixture (Figure 4.4C).

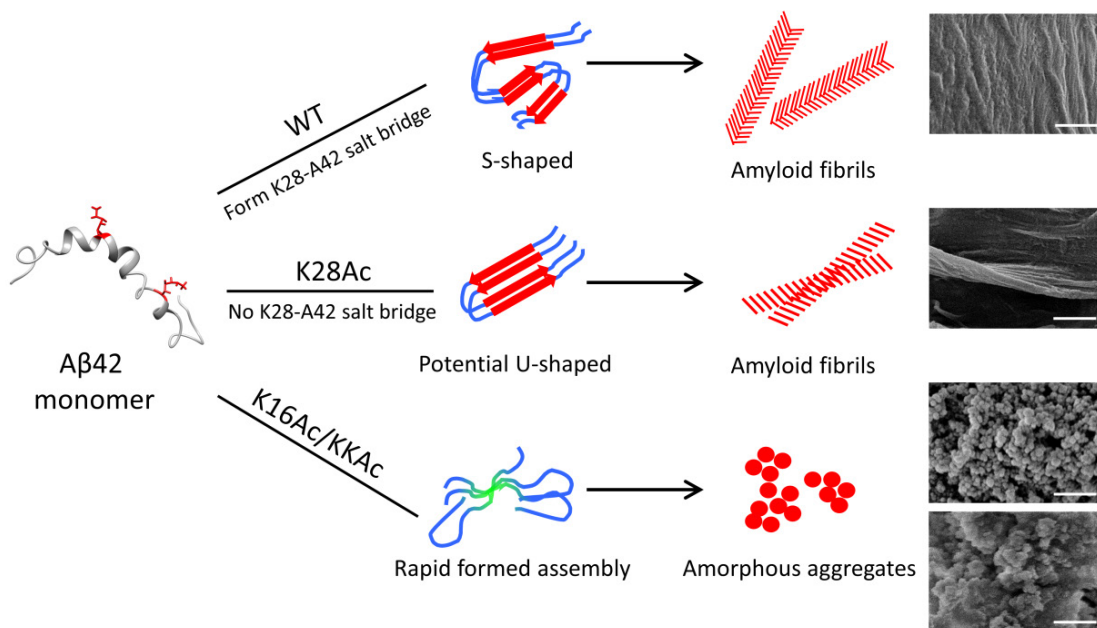


Figure 4.7. Suggested schematic model based on the aggregation results of WT and acetylation modified A β 42 peptides. Both WT and K28Ac A β 42 peptide formed amyloid fibril structures. Acetylation on K28 may cause formation of a different type of fibril, probably due to loss of the K28-A42 salt bridge, but does not show any critical effects on morphology. Acetylation on K16 possibly increased the binding affinity of the K16-F20 region (green), which serves as intermolecular binding sequence during A β 42 fibrillization. In consequence, aggregation was kinetically driven to form amorphous aggregates.

The A β 42 mature fibrils were recently found to form an S-shape “triple- β -motif”²⁹ (Figure 4.1), which is different from the U-shape conformation of A β 40 fibrils (Figure A3). The D23-K28 salt bridge, which was previously found to be essential in A β 40 fibrils^{30, 49, 50}, was missing in the A β 42 fibril structure; instead, a unique salt bridge was observed between K28 and A42²⁹. After removing the positive charge on K28 by acetylation, the K28Ac peptide has a longer lag time than WT A β 42 peptide during aggregation. This confirms the stabilizing role of K28-A42 during the early-stage conformational changes for nucleation⁵¹. However, the K28Ac peptides were capable of forming amyloid fibril structures eventually, no matter in homogeneous K28Ac peptide sample, or in a heterogeneous equimolar mixture with WT A β 42 (Figure 4.4A, C, G, J). This suggests that the salt bridge may not be essential to fibril morphology. N- ϵ -amino acetylation on K28 was previously done on A β ₂₅₋₃₅ fragment, and the gross structure of A β ₂₅₋₃₅-K28Ac fibril was very similar with WT A β ₂₅₋₃₅ fibrils²⁷. The K28Ac fibrils observed here may probably have a U-shape structure, which is different with the S-shape fibril of WT A β 42. Acetylation on K28 may alter the triple- β conformation by interrupting the K28-A42 salt bridge, and slowdown the early-stage misfolding and nucleation. However, it did not show significant effect on morphology or cytotoxicity of

A β 42 fibrils. The amorphous aggregates formed from KKAc (Figure 4.4H, K) suggest that the K16 is probably more critical to A β 42 fibrillization than K28.

Compared to other posttranslational modified A β ^{12, 15, 16}, the K16Ac and K28Ac peptides were not deleterious to the SH-SY5Y cells, exhibiting similar or less cell loss than WT A β 42 fibrils of 72 h oligomers and 7-day aggregates, respectively (Figure 4.6). Interestingly, the K16Ac peptide that added to cells as fresh monomers showed much less increased toxicity compared to other forms after 48 h incubation. It was recently noticed that the early species in aggregation are more toxic than the final aggregates or fibrils⁵². However, toxicity of KKAc peptide increased with longer incubation (7 d) and fresh peptide shows very mild damage to cells. Although both K16Ac and KKAc aggregates are amorphous, the K16Ac aggregates are defined bead-like structures compared to KKAc. The different toxicities of these two peptides may be related to their structural variations. Another hypothesis suggests that the cytotoxicity is due to the dynamic aggregation process, rather than any single structure species^{10, 52}. Minor shifts in the A β 40:A β 42 ratio was demonstrated to be enough to modulate neurotoxicity⁵. In addition, the K16N mutation of A β 42 is not harmful in isolation, but exhibits severe toxicity when mixed with WT peptides³². Whereas the mixture of WT A β 42 and its toxic mutation A2V was protective to the cells, both in vitro and in vivo⁵³. Here in this study, the aggregates formed from heterogeneous mixtures of WT and acetylate peptides all showed increased toxicity compared to homogeneous samples. Therefore, in addition to the structural characteristics, the dynamic interactions of different species contribute significantly to aggregation related toxicity.

4.5 Conclusion

In the present study, the A β 42 peptide was modified with lysine side-chain acetylation on residues K16 and K28. Acetylation on K16 position can significantly affect the hydrophobicity of residues K16-A21 and alter the A β 42 self-assembly resulting in formation of amorphous aggregates instead of amyloid fibril. This switch is probably kinetically driven by the increased inter-peptide hydrophobic interactions in the K16-A21 region. The peptides with single acetylation on K28 can still assemble into typical amyloid fibrils, confirmed by ThT fluorescence and SEM images. However, the amorphous aggregates formed from heterogeneous mixtures of WT and acetylated peptides exhibit severe cytotoxicity to SH-SY5Y cells, indicating the dynamics of A β 42 aggregation needs to be explored further in future studies.

4.6 References

1. *Alzheimer's Association Report 2015 Alzheimer's disease facts and figures*; 1552-5260; Alzheimer's Association: Mar, 2015; pp 332-84.
2. *National Plan to Address Alzheimer's Disease: 2015 Update*; U.S. Department of Health and Human Services: 2015.
3. Ballard, C.; Gauthier, S.; Corbett, A.; Brayne, C.; Aarsland, D., et al., Alzheimer's disease. *Lancet* **2011**, *377*, 1019-31.
4. Gravina, S. A.; Ho, L. B.; Eckman, C. B.; Long, K. E.; Otvos, L., et al., Amyloid-Beta Protein (A-Beta) in Alzheimer's disease brain - Biochemical and Immunocytochemical Analysis with Antibodies specific for forms ending at A-Beta-40 or A-Beta-42(43). *Journal of Biological Chemistry* **1995**, *270*, 7013-6.

5. Pauwels, K.; Williams, T. L.; Morris, K. L.; Jonckheere, W.; Vandersteen, A., et al., Structural Basis for Increased Toxicity of Pathological A beta(42):A beta(40) Ratios in Alzheimer Disease. *Journal of Biological Chemistry* **2012**, *287*, 5650-60.
6. Naslund, J.; Schierhorn, A.; Hellman, U.; Lannfelt, L.; Roses, A. D., et al., Relative Abundance of Alzheimer A-Beta Amyloid Peptide Variants in Alzheimer-Disease and Normal Aging. *Proceedings of the National Academy of Sciences of the United States of America* **1994**, *91*, 8378-82.
7. Lee, S.; Liu, Y.; Lim, M. H., Untangling Amyloid-beta, Tau, and Metals in Alzheimer's Disease. *Acs Chemical Biology* **2013**, *8*, 856-65.
8. Kodali, R.; Williams, A. D.; Chemuru, S.; Wetzel, R., A beta(1-40) Forms Five Distinct Amyloid Structures whose beta-Sheet Contents and Fibril Stabilities Are Correlated. *Journal of Molecular Biology* **2010**, *401*, 503-17.
9. Glabe, C. G., Structural classification of toxic amyloid oligomers. *Journal of Biological Chemistry* **2008**, *283*, 29639-43.
10. Hubin, E.; van Nuland, N. A. J.; Broersen, K.; Pauwels, K., Transient dynamics of A beta contribute to toxicity in Alzheimer's disease. *Cellular and Molecular Life Sciences* **2014**, *71*, 3507-21.
11. Kumar, S.; Singh, S.; Hinze, D.; Josten, M.; Sahl, H.-G., et al., Phosphorylation of Amyloid-beta Peptide at Serine 8 Attenuates Its Clearance via Insulin-degrading and Angiotensin-converting Enzymes. *Journal of Biological Chemistry* **2012**, *287*, 8641-51.
12. Kumar, S.; Rezaei-Ghaleh, N.; Terwel, D.; Thal, D. R.; Richard, M., et al., Extracellular phosphorylation of the amyloid beta-peptide promotes formation of toxic aggregates during the pathogenesis of Alzheimer's disease. *Embo Journal* **2011**, *30*, 2255-65.

13. Kumar, S.; Wirths, O.; Theil, S.; Gerth, J.; Bayer, T. A., et al., Early intraneuronal accumulation and increased aggregation of phosphorylated Abeta in a mouse model of Alzheimer's disease. *Acta Neuropathologica* **2013**, *125*, 699-709.
14. Jarrett, J. T.; Berger, E. P.; Lansbury, P. T., The Carboxy Terminus of the Beta-Amyloid Protein is Critical for the Seeding of Amyloid Formation - Implications for the Pathogenesis of Alzheimer's Disease. *Biochemistry* **1993**, *32*, 4693-7.
15. Sullivan, C. P.; Berg, E. A.; Elliott-Bryant, R.; Fishman, J. B.; McKee, A. C., et al., Pyroglutamate-A beta 3 and 11 colocalize in amyloid plaques in Alzheimer's disease cerebral cortex with pyroglutamate-A beta 11 forming the central core. *Neuroscience Letters* **2011**, *505*, 109-12.
16. Bouter, Y.; Dietrich, K.; Wittnam, J. L.; Rezaei-Ghaleh, N.; Pillot, T., et al., N-truncated amyloid beta (A beta) 4-42 forms stable aggregates and induces acute and long-lasting behavioral deficits. *Acta Neuropathologica* **2013**, *126*, 189-205.
17. Murakami, K.; Uno, M.; Masuda, Y.; Shimizu, T.; Shirasawa, T., et al., Isomerization and/or racemization at Asp23 of A beta 42 do not increase its aggregative ability, neurotoxicity, and radical productivity in vitro. *Biochemical and Biophysical Research Communications* **2008**, *366*, 745-51.
18. Shimizu, T.; Watanabe, A.; Ogawara, M.; Mori, H.; Shirasawa, T., Isoaspartate formation and neurodegeneration in Alzheimer's disease. *Archives of Biochemistry and Biophysics* **2000**, *381*, 225-34.
19. Jawhar, S.; Wirths, O.; Bayer, T. A., Pyroglutamate Amyloid-beta (A beta): A Hatchet Man in Alzheimer Disease. *Journal of Biological Chemistry* **2011**, *286*, 38825-32.
20. Halim, A.; Brinkmalm, G.; Ruetschi, U.; Westman-Brinkmalm, A.; Portelius, E., et al., Site-specific characterization of threonine, serine, and tyrosine glycosylations of amyloid precursor protein/amyloid beta-peptides in human cerebrospinal fluid.

Proceedings of the National Academy of Sciences of the United States of America **2011**, *108*, 11848-53.

21. Massari, J.; Tokikawa, R.; Zanolli, L.; Maggi Tavares, M. F.; Assuncao, N. A., et al., Acetyl Radical Production by the Methylglyoxal-Peroxynitrite System: A Possible Route for L-Lysine Acetylation. *Chemical Research in Toxicology* **2010**, *23*, 1762-70.

22. Tokikawa, R.; Loffredo, C.; Uemi, M.; Machini, M. T.; Bechara, E. J. H., Radical acylation of L-lysine derivatives and L-lysine-containing peptides by peroxynitrite-treated diacetyl and methylglyoxal. *Free Radic. Res.* **2014**, *48*, 357-70.

23. Alves, A. N. L.; Jedlicka, L. D. L.; Massari, J.; Juliano, M. A.; Bechara, E. J. H., et al., Electrospray Ionization Mass Spectrometry Applied to Study the Radical Acetylation of Amino Acids, Peptides and Proteins. *Journal of the Brazilian Chemical Society* **2013**, *24*, 1983-+.

24. Venkateshappa, C.; Harish, G.; Mahadevan, A.; Bharath, M. M. S.; Shankar, S. K., Elevated Oxidative Stress and Decreased Antioxidant Function in the Human Hippocampus and Frontal Cortex with Increasing Age: Implications for Neurodegeneration in Alzheimer's Disease. *Neurochemical Research* **2012**, *37*, 1601-14.

25. Morris, M.; Knudsen, G. M.; Maeda, S.; Trinidad, J. C.; Ioanoviciu, A., et al., Tau post-translational modifications in wild-type and human amyloid precursor protein transgenic mice. *Nature neuroscience* **2015**, *18*, 1183-9.

26. Cook, C.; Stankowski, J. N.; Carlomagno, Y.; Stetler, C.; Petrucelli, L., Acetylation: a new key to unlock tau's role in neurodegeneration. *Alzheimers Res. Ther.* **2014**, *6*, 8.

27. Karsai, A.; Nagy, A.; Kengyel, A.; Martonfalvi, Z.; Grama, L., et al., Effect of lysine-28 side-chain acetylation on the nanomechanical behavior of Alzheimer amyloid beta 25-35 fibrils. *Journal of Chemical Information and Modeling* **2005**, *45*, 1641-6.

28. Tjernberg, L. O.; Naslund, J.; Lindqvist, F.; Johansson, J.; Karlstrom, A. R., et al., Arrest of beta-amyloid fibril formation by a pentapeptide ligand. *Journal of Biological Chemistry* **1996**, *271*, 8545-8.
29. Xiao, Y.; Ma, B.; McElheny, D.; Parthasarathy, S.; Long, F., et al., A beta(1-42) fibril structure illuminates self-recognition and replication of amyloid in Alzheimer's disease. *Nature Structural & Molecular Biology* **2015**, *22*, 499-U97.
30. Kajava, A. V.; Baxa, U.; Steven, A. C., beta arcades: recurring motifs in naturally occurring and disease-related amyloid fibrils. *Faseb Journal* **2010**, *24*, 1311-9.
31. Kirkitadze, M. D.; Condron, M. M.; Teplow, D. B., Identification and characterization of key kinetic intermediates in amyloid beta-protein fibrillogenesis. *Journal of Molecular Biology* **2001**, *312*, 1103-19.
32. Kaden, D.; Harmeier, A.; Weise, C.; Munter, L. M.; Althoff, V., et al., Novel APP/Abeta mutation K16N produces highly toxic heteromeric Abeta oligomers. *Embo Molecular Medicine* **2012**, *4*, 647-59.
33. Nordling, E.; Kallberg, Y.; Johansson, J.; Persson, B., Molecular dynamics studies of alpha-helix stability in fibril-forming peptides. *Journal of Computer-Aided Molecular Design* **2008**, *22*, 53-8.
34. Tarus, B.; Straub, J. E.; Thirumalai, D., Structures and free-energy landscapes of the wild type and mutants of the A beta(21-30) peptide are determined by an interplay between intrapeptide electrostatic and hydrophobic interactions. *Journal of Molecular Biology* **2008**, *379*, 815-29.
35. Palhano, F. L.; Lee, J.; Grimster, N. P.; Kelly, J. W., Toward the Molecular Mechanism(s) by Which EGCG Treatment Remodels Mature Amyloid Fibrils. *Journal of the American Chemical Society* **2013**, *135*, 7503-10.
36. Tomaselli, S.; Esposito, V.; Vangone, P.; van Nuland, N. A. J.; Bonvin, A., et al., The alpha-to-beta conformational transition of Alzheimer's A beta-(1-42) peptide in

aqueous media is reversible: A step by step conformational analysis suggests the location of beta conformation seeding. *Chembiochem* **2006**, *7*, 257-67.

37. Pettersen, E. F.; Goddard, T. D.; Huang, C. C.; Couch, G. S.; Greenblatt, D. M., et al., UCSF chimera - A visualization system for exploratory research and analysis. *Journal of Computational Chemistry* **2004**, *25*, 1605-12.

38. Roychaudhuri, R.; Yang, M.; Deshpande, A.; Cole, G. M.; Frautschy, S., et al., C-Terminal Turn Stability Determines Assembly Differences between A beta 40 and A beta 42. *Journal of Molecular Biology* **2013**, *425*, 292-308.

39. Trott, O.; Olson, A. J., Software News and Update AutoDock Vina: Improving the Speed and Accuracy of Docking with a New Scoring Function, Efficient Optimization, and Multithreading. *Journal of Computational Chemistry* **2010**, *31*, 455-61.

40. Neudert, G.; Klebe, G., DSX: A Knowledge-Based Scoring Function for the Assessment of Protein-Ligand Complexes. *Journal of Chemical Information and Modeling* **2011**, *51*, 2731-45.

41. Humphrey, W.; Dalke, A.; Schulten, K., VMD: Visual molecular dynamics. *Journal of Molecular Graphics & Modelling* **1996**, *14*, 33-8.

42. Zoete, V.; Cuendet, M. A.; Grosdidier, A.; Michielin, O., SwissParam: A Fast Force Field Generation Tool for Small Organic Molecules. *Journal of Computational Chemistry* **2011**, *32*, 2359-68.

43. Frisch, M. J.; Trucks, G. W.; Schlegel, H. B.; Scuseria, G. E.; Robb, M. A., et al. *Gaussian 09, Revision D.01*, Gaussian, Inc., Wallingford CT: 2009.

44. Salentin, S.; Schreiber, S.; Haupt, V. J.; Adasme, M. F.; Schroeder, M., PLIP: fully automated protein-ligand interaction profiler. *Nucleic Acids Research* **2015**, *43*, W443-W7.

45. Kellermayer, M. S. Z.; Grama, L.; Karsai, A.; Nagy, A.; Kahn, A., et al., Reversible mechanical unzipping of amyloid beta-fibrils. *Journal of Biological Chemistry* **2005**, *280*, 8464-70.
46. Cheon, M.; Chang, I.; Mohanty, S.; Luheshi, L. M.; Dobson, C. M., et al., Structural reorganisation and potential toxicity of oligomeric species formed during the assembly of amyloid fibrils. *Plos Computational Biology* **2007**, *3*, 1727-38.
47. Nguyen, P. H.; Li, M. S.; Stock, G.; Straub, J. E.; Thirumalai, D., Monomer adds to preformed structured oligomers of A beta-peptides by a two-stage dock-lock mechanism. *Proceedings of the National Academy of Sciences of the United States of America* **2007**, *104*, 111-6.
48. Hartl, F. U.; Hayer-Hartl, M., Converging concepts of protein folding in vitro and in vivo. *Nature Structural & Molecular Biology* **2009**, *16*, 574-81.
49. Williams, A. D.; Shivaprasad, S.; Wetzel, R., Alanine scanning mutagenesis of A beta(1-40) amyloid fibril stability. *Journal of Molecular Biology* **2006**, *357*, 1283-94.
50. Kassler, K.; Horn, A. H. C.; Sticht, H., Effect of pathogenic mutations on the structure and dynamics of Alzheimer's A beta(42)-amyloid oligomers. *Journal of Molecular Modeling* **2010**, *16*, 1011-20.
51. Bernstein, S. L.; Dupuis, N. F.; Lazo, N. D.; Wytttenbach, T.; Condrón, M. M., et al., Amyloid-beta protein oligomerization and the importance of tetramers and dodecamers in the aetiology of Alzheimer's disease. *Nature Chemistry* **2009**, *1*, 326-31.
52. Ross, C. A.; Poirier, M. A., What is the role of protein aggregation in neurodegeneration? *Nature Reviews Molecular Cell Biology* **2005**, *6*, 891-8.
53. Di Fede, G.; Catania, M.; Morbin, M.; Rossi, G.; Suardi, S., et al., A Recessive Mutation in the APP Gene with Dominant-Negative Effect on Amyloidogenesis. *Science* **2009**, *323*, 1473-7.

Chapter 5 Toxicity of structurally diverse protein aggregates[†]

Mu Yang, Rashmi Adhikari, Colina Dutta, and Ashutosh Tiwari

Department of Chemistry, Michigan Technological University, Houghton, MI-49931

[†]This chapter contains the material from a manuscript which will be submitted to an international peer-reviewed journal.

5.1 Introduction

Abnormal protein folding and aggregations are constantly observed in neurodegenerative diseases and are believed to be pathogenic¹⁻⁴. In these diseases, the intracellular or extracellular accumulation of protein aggregates could be amyloid fibrils or amorphous structures, resulting from mutations or post-translational modifications of the disease-related proteins, or triggered by environmental stress⁵. Moreover, proteins that do not cause amyloid diseases are also able to form toxic aggregates^{3,6}. Although the literature has many reported studies that focus on amyloid fibrils, which are commonly observed in human diseases; recently, there has been a surge in numbers of pre-fibril oligomers and amorphous aggregates studies reported in the literature⁷⁻¹¹. Unlike amyloid fibrils, the non-fibril structures (amorphous) have very low stability, which limits high resolution structure determination using NMR or X-ray crystallography technique.

The toxicity of protein aggregates could be a consequence of losing the normal functions, sequestration, mislocalizations, or gain of toxic function¹². However, after decades of searching, the predominant toxic species in amyloid diseases is still remains unclear. Amyloids were found to disrupt cellular structure and function because of their large sizes¹³. However, only weak correlations were observed between the clinical severity of the diseases and the density of amyloid plaques or inclusion bodies formed from protein fibrils¹⁴⁻¹⁶. Increasing evidences indicated that the amyloid formation could be a consequence of cellular protective response¹. Some amyloids have no toxicity but biological functions, such as binding of peptide hormones, formation of biofilms, or launch of innate immune responses^{4, 17-19}. On the other hand, small non-fibril oligomers and many other amorphous aggregates were recently proposed to be the major toxic

species in human diseases^{7, 8, 20}. Many soluble oligomers of amyloid β peptide were isolated from Alzheimer's disease brain, causing severe synaptic toxicity both *in vitro* and *in vivo*^{21, 22}. In addition, *in vitro* cell culture models of Parkinson's disease also showed that co-transfection of α -synuclein and its interacting protein in cells could enhance the formation of inclusion bodies and cell viability^{23, 24}. Therefore, the early events of aggregation might cause toxicity, while the formation of mature fibril structures only represent the end-stage manifestation¹. To better understand the cellular toxic mechanism in the amyloidosis diseases, more information of the biochemistry and biophysics of the non-fibril structures, such as oligomers, protofibrils, and amorphous aggregates, will be critical. Many non-fibril oligomer or amorphous structures in previous studies have similar properties. Unfortunately, different laboratories in the field normally do not share or compare their protein aggregates.

In this study, different protein aggregates structures selected from previous reports were prepared and compared for their size, flexibility, hydrophobicity, and cytotoxicity. The goal is to characterize the differences of amorphous aggregates and correlate it to cytotoxicity. This will help to understand the relationship between different morphological structures and their toxicity.

5.2 Materials and methods

Unless otherwise indicated, all materials were used as supplied by the manufacturer without any further purification. Hen egg white lysozyme (lysozyme), bovine serum albumin (BSA), dithiothreitol (DTT), Thioflavin T (ThT), 8-anilino-1-naphthalenesulfonic acid (ANS) dye, 4,4'-Dianilino-1,1'-binaphthyl-5,5'-disulfonic acid

(bis-ANS) dye, 2',7'-dichlorofluorescein diacetate (DCFH-DA) were purchased from Sigma. The CellTiter 96[®] AQueous One Solution Cell Proliferation (MTS) Assay kit was from Promega.

Preparing protein fibrils/aggregates – Fibrils/aggregates were prepared using method from the following studies listed in Table 5.1 and 5.2.

Table 5.1. Sample preparation conditions of lysozyme aggregates

Sample #	structure	condition
I	Amyloid	Samples contain 1 mM lysozyme in HCl solution (pH 2.0) were incubated at 65 °C for 7 days ²⁵
II	Amorphous aggregates	Samples contain 140 uM lysozyme in HCl solution (pH 2.0, with 136.7 mM NaCl, 2.68 mM KCl, and 4 mM DTT). Samples were first mixed via vortex and then incubated were incubated at 55 °C for 30 days ²⁶
III	Amorphous aggregates	Samples contain 40 μM lysozyme in phosphate buffer (pH 7.2, 20 mM, with 150 mM NaCl) were incubated at 37 °C for 7 days ¹¹
IV & V	Amorphous aggregates	Samples contain 699 μM lysozyme in Phosphate buffer (pH 7.4, 100 mM) were incubated at 56 °C (IV) and 25 °C (V) ²⁷
VI	Amorphous aggregates	Samples contain 120 μM lysozyme in Phosphate buffer (pH 7.0, 50 mM) were incubated at 25 °C ²⁸
VII	Amorphous aggregates	Samples contain 120 μM lysozyme in Phosphate-NaOH buffer (pH 12.0, 50 mM) were incubated at 25 °C ²⁸

Table 5.2. Sample preparation conditions of BSA aggregates

Sample #	structure	condition
I	Amorphous	Samples contain 100 μ M BSA in glycine-HCl buffer (pH 3.0, 50 mM , with 50 mM NaCl) were incubated at 65 $^{\circ}$ C for 4 h then followed by 30 days room temperature incubation ²⁹
II	Amorphous aggregates	Samples contain 40 μ M BSA in phosphate buffer (pH 7.2, 20 mM, with 150 mM NaCl) were incubated at 37 $^{\circ}$ C for 7 days ¹¹
III	protofibrils	Samples contain 37.6 μ M BSA in Tris-HCl buffer (pH 7.4, 20 mM) were incubated at 70 $^{\circ}$ C for 4 days ³⁰
IV	Amorphous aggregates	Samples contain 7.5 μ M BSA in phosphate buffer (pH 8.9, 0.1 M) were incubated at 62 $^{\circ}$ C over 10 h ³¹

Fluorescence measurements – Fluorescence measurements were performed as previously described in chapter 2. In brief, samples were diluted by phosphate buffer (10 mM, pH 7.4) to a final concentration of 10 μ M. Fluorescent probes Thioflavin T (ThT), 8-anilino-1-naphthalenesulfoni acid (ANS), and 4,4'-dianilino-1,1'-binaphthyl-5,5'-disulfonic acid (bis-ANS) were prepared in ethonal and then added to samples to final concentrations of 10 μ M (ThT), 5 μ M (ANS), and 1 μ M (bis-ANS). Emission spectra were collected using a Horiba Hobin Yvon spectrofluorometer (Fluoromax-4) at room temperature. ThT spectra were collected from 460 – 700 nm, with excitation at 450 nm. ANS and bis-ANS spectra were acquired from 400 – 700 nm, with excitation at 380 nm and 360 nm, respectively.

Field emission scanning electron microscopy (FESEM) – Protein samples were analyzed using a cold field emission high-resolution scanning electron microscope,

Hitachi S-4700 FESEM as previously described in chapter 2. In brief, protein samples were washed in MilliQ water using a Millipore Amicon® Ultra centrifugal filters (3 kDa cut off) by centrifuging three times at $7,000 \times g$ for 30 min at 4 °C. Washed fibrils or aggregates were applied on SEM stubs and air dried at room temperature. The SEM samples were then coated with 10 nm platinum. For FESEM imaging, 10 kV of acceleration voltage and 5 μ A of emission current were used.

Cell viability (MTS) assay – SH-SY5Y human neuroblastoma cells (from ATCC) were cultured in DMEM/F-12 medium with 10% FBS and 100 U/ml penicillin-streptomycin at 37 °C in 5% CO₂ humidified environment and used within the first 10 passages. Cells were plated at 2×10^4 cells/well on 96-well plates and allowed to grow overnight. The next day, cells were washed with 1X PBS buffer (pH 7.4) twice. Then 100 μ l fresh media containing peptide samples were added. Six replicates were prepared per sample. Media without any peptide were used as controls. After 48 h incubation, 20 μ l of CellTiter 96® AQueous One Solution Cell Proliferation (MTS) Assay kit (Promega) were added and incubated for 4 h. Then absorbance at 490 nm were collected using an ELISA plate reader (BioTek Instruments, Inc.). Blanks containing media and peptide samples but no cells were similarly prepared and used for background subtraction.

Cytotoxicity (LDH) assay – SH-SY5Y cells were plated at 2×10^4 cells/well on 96-well plates and incubated with protein aggregate samples for 48 h. After incubation, 50 μ l of aliquots from each test and control well was transferred to a fresh 96-well plate. To prepare positive control that has maximum lactate dehydrogenase (LDH) release, 10 μ l of 10X lysis solution were added into each well and incubated for 45 min. Then 50 μ l of reagent from the CytoTox 96® Non-Radioactive Cytotoxicity Assay kit (Promega) were

added and incubated for 30 min, followed by addition of 50 μ l stop solution. The absorbance at 490 nm were collected using an ELISA plate reader (BioTek Instruments, Inc.). Blanks containing media and peptide samples but no cells were similarly prepared and used for background subtraction.

2',7'-dichlorofluorescein diacetate (DCFH-DA) fluorescence assay – Intracellular reactive oxidative species (ROS) can oxidize DCFH-DA to the highly fluorescent compound dichlorofluorescein (DCF). Therefore, respiratory burst activity in cells was detected by using the fluorescent probe DCFH-DA^{32, 33}. DCFH-DA was dissolved in ethanol at 25 mM as stock solution. SH-SY5Y cells were seeded in 96-well plates at 1×10^5 cells/well and were incubated with protein aggregate samples for 24 h. After incubation, cells were washed using 1X PBS and then incubated with 10 μ M DCFH-DA at 37 °C for 30 min, then washed with 1X PBS. The fluorescence intensity of DCF was measured in a Multiskan™ GO Microplate Spectrophotometer (Thermo Scientific) at excitation wavelength 485 nm and emission wavelength 538 nm.

5.3 Results and discussion

In this study, three fluorescent probes were used to characterize the protein aggregates. As introduced in chapter 2, ANS dye detects hydrophobic structures or nonpolar cavities in proteins with high fluorescence signals. The dimeric analogue of ANS, bis-ANS, is an important probe to determine structure flexibility. ThT was used to detect the structural property of the aggregates. From the previous publications^{11, 25-29, 31, 34}, a total of 17 samples at different conditions were selected (Table S1). However, we found that at the same pH and temperature, changes in concentration with 100 μ M did not

have significant effects on protein structure and related fluorescence analysis (Figure 5.1).

Therefore, only one concentration at each set of condition was selected as the most representative samples for toxicity measurements.

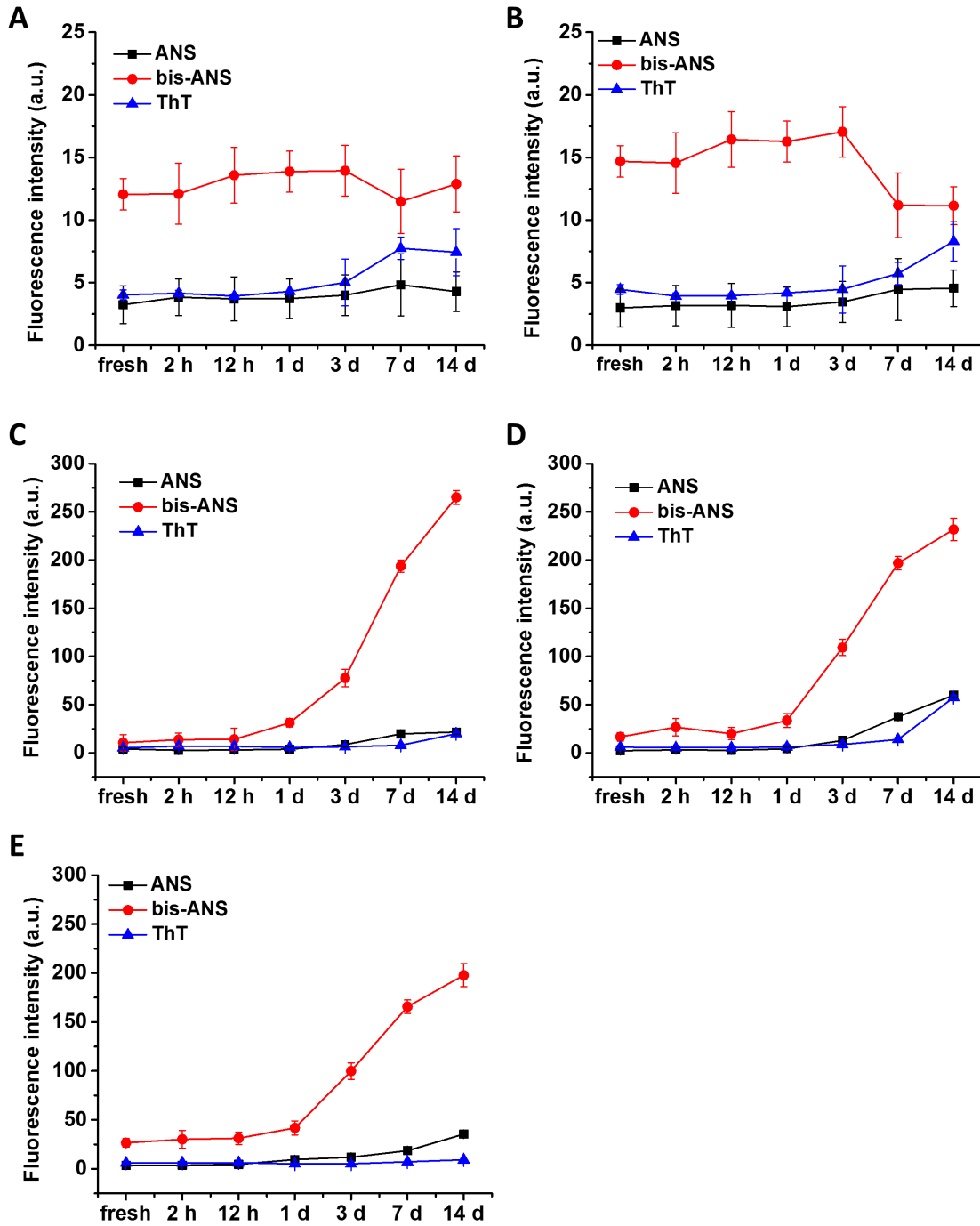
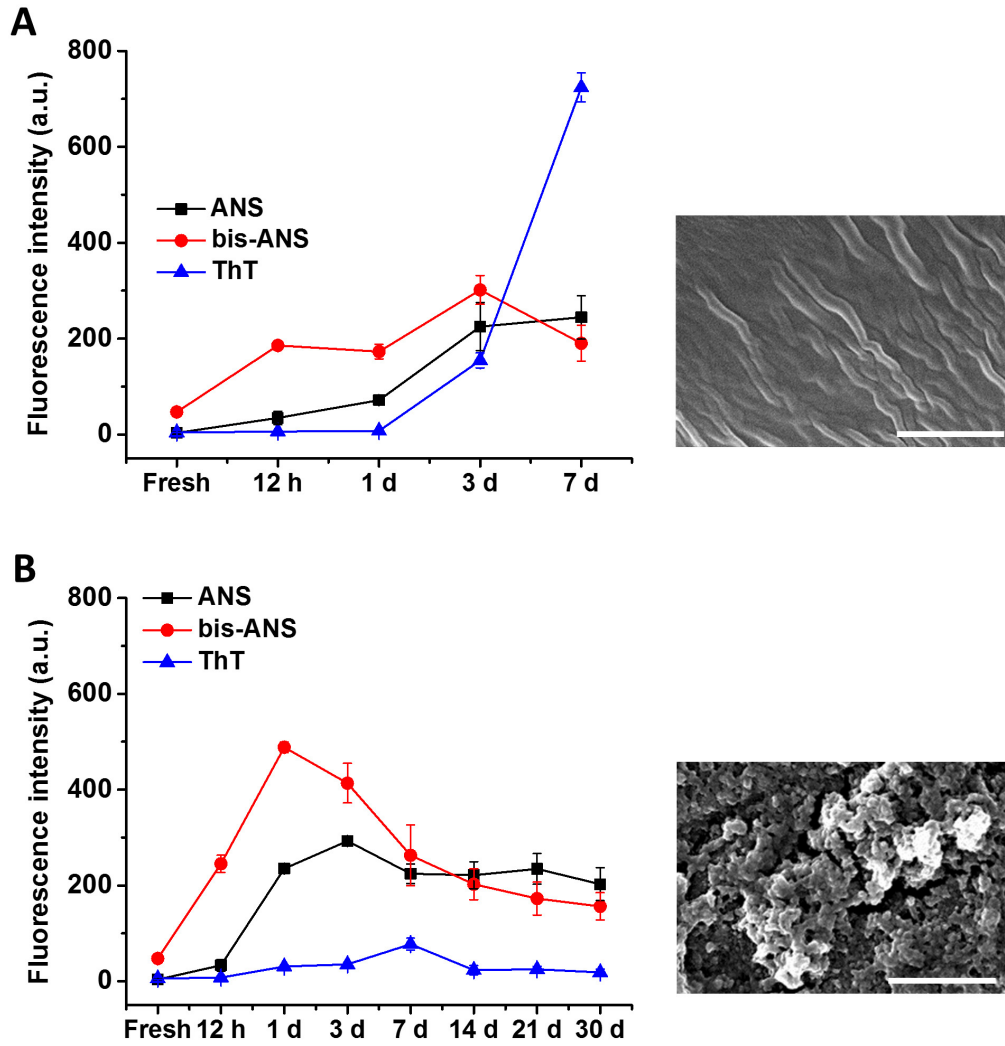


Figure 5.1. Samples at same pH and temperature but different concentrations showed similar ANS, bis-ANS, and ThT fluorescence results. (A, B) Samples that contain 80 μM (A) or 120 μM (B) of lysozyme at pH 7.0 were incubated at 25 °C up to 14 days. (C, D, E) Samples that contain 40 μM (C), 80 μM (D) or 120 μM (E) of lysozyme at pH 12.0 were incubated at 25 °C up to 14 days.

First, we compared different types of aggregates, amyloid and granular structures, from the same proteins (Figure 5.2 and 5.3). Figure 5.2 shows three different aggregate structures generated from lysozyme. The fibril structure showed increased ANS and ThT fluorescence and decreased cell viability upon incubation (Figure 5.2 A, D). This is in line with a previous hypothesis that the extracellular amyloid deposits can physically disrupt the cellular structure and function by a bulk process¹. While the other two amorphous aggregates had more hydrophobic and flexible structures than the fibrils, but did not bind to ThT (Figure 5.2 B, C). Even though both amorphous aggregates had a granular appearance when observed under SEM, aggregate II (Figure 5.2 B) had a smaller subunit size, which results in a more rigid structure. Unlike fibrils, both granular aggregates were most harmful to the cell after 12h incubation, suggesting that under these two conditions, the aggregation intermediates were more toxic. Interestingly, both 12 h and 7 d samples of aggregate III (Figure 5.2 C) resulted in < 40% cell viability, but the 3 d sample showed decreased toxic. Except ThT fluorescence, the aggregate III showed negligible changes in hydrophobicity, flexibility, and overall morphology after 12 h. According to a previous study¹¹, the amount of high molecular species increased from 12 h to 7 d, suggesting that although negligible changes were observed for fluorescence and morphology (Figure 5.2 and B1), the aggregation was still continuing, to form larger protein assemblies. Therefore, the 7d sample had most mature aggregates, while the 12 h

sample contains both intermediates and mature aggregates, the toxicity of 12 h samples is likely due to the heterogeneity of sample.



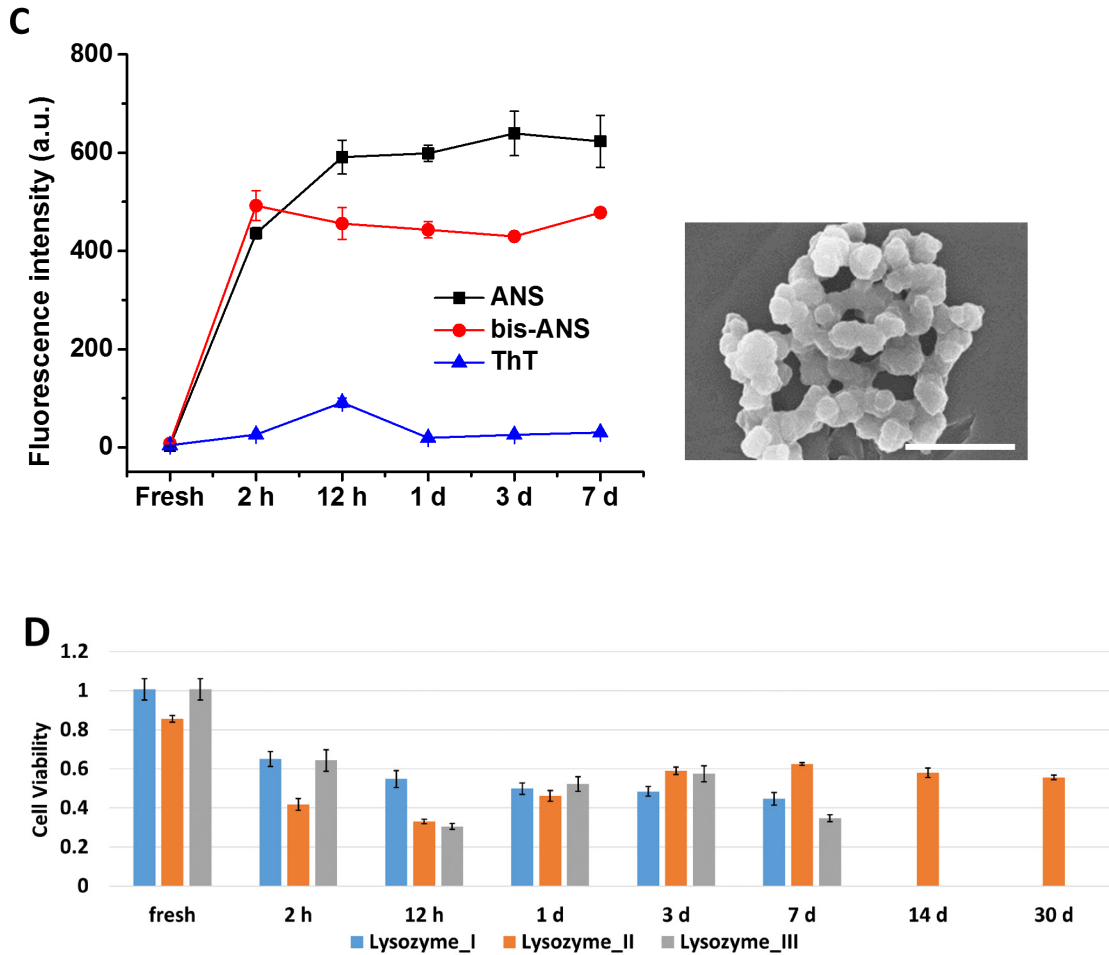
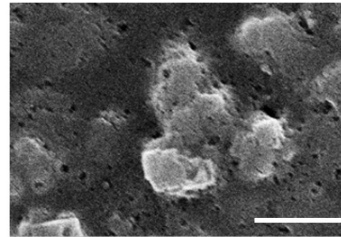
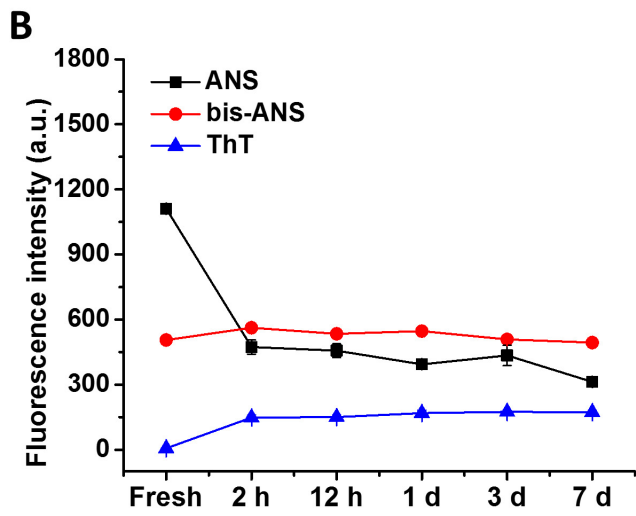
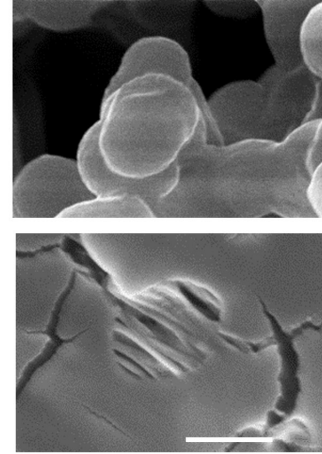
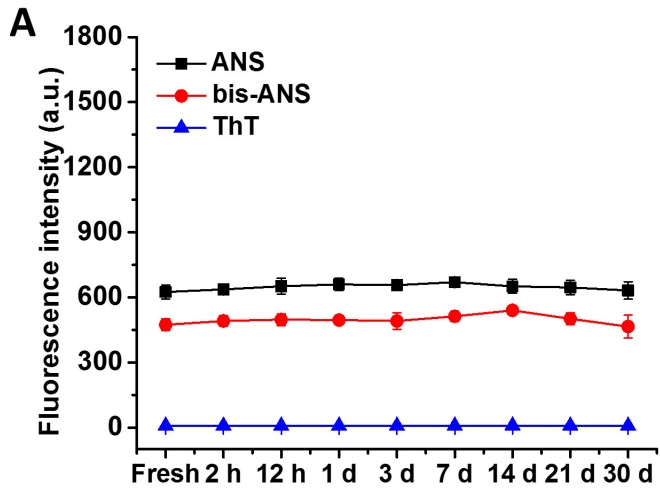


Figure 5.2. Three different structures generated from lysozyme were characterized using fluorescent probes, SEM, and MTS assay. (A) Fluorescence results and SEM image of lysozyme aggregate I: amyloid fibril generated from 1 mM lysozyme at pH 2.0, 65 °C. (B) Fluorescence results and SEM image of lysozyme aggregate II: amorphous aggregate generated from 140 μ M lysozyme at pH 2.0, 55 °C. (C) Fluorescence results and SEM image of lysozyme aggregate III: amorphous aggregate generated from 40 μ M lysozyme with 10 mM DTT at pH 7.2, 37 °C. (D) MTS assay of SH-SY5Y cells incubated with 15 μ M lysozyme aggregates I-III. Error bars = \pm S.D. Scale bars in SEM images = 5 μ m.

For BSA, all four aggregates tested here did not show any detectable changes of bis-ANS fluorescence. This may be due to the bulky nature of the BSA protein. The BSA_I (Figure 5.3A) showed negligible changes for up to 30 days of incubation, but two types

of structures, granular and fibril-like, were observed under SEM. However, these aggregates from BSA_I samples appear to be essentially harmless to the SH-SY5Y cell (Figure 5.3 E). During aggregation, BSA_II, III, and IV showed different levels of impairments of ANS fluorescence and increases in ThT fluorescence. Even though BSA_IV aggregates appeared in straight fibril-like morphology, we found that the structure could not bind ThT, and was very unstable under SEM, suggesting that this structure might not be classified as amyloid fibrils. Cytotoxicity of the two non-fibril aggregates, BSA_II and IV followed similar trends as their ANS fluorescence, where toxicity of BSA_II aggregates stayed stable after 12 h, but the number of live cell treated by BSA_IV samples kept decreasing till 7 d (Figure 5.3 B, D, E). Since a decrease of ANS fluorescence indicates conformational change and assembly of BSA molecules, the matched trends of the toxicity and ANS results suggests that the final aggregates are the major toxic species in these two cases. For BSA_III, the high ThT fluorescence signals and the short fibrillar structures (Figure 5.3 C) identified this structure as protofibrils. Both the 2 h intermediates and the 7d protofibrils of BSA_III caused impairment of cell viability (Figure 5.3E). Since the 12 h intermediates were more hydrophobic and less stable than the 7 d protofibrils (Figure S5.2), they might cause cell dysfunction or death through different mechanisms.



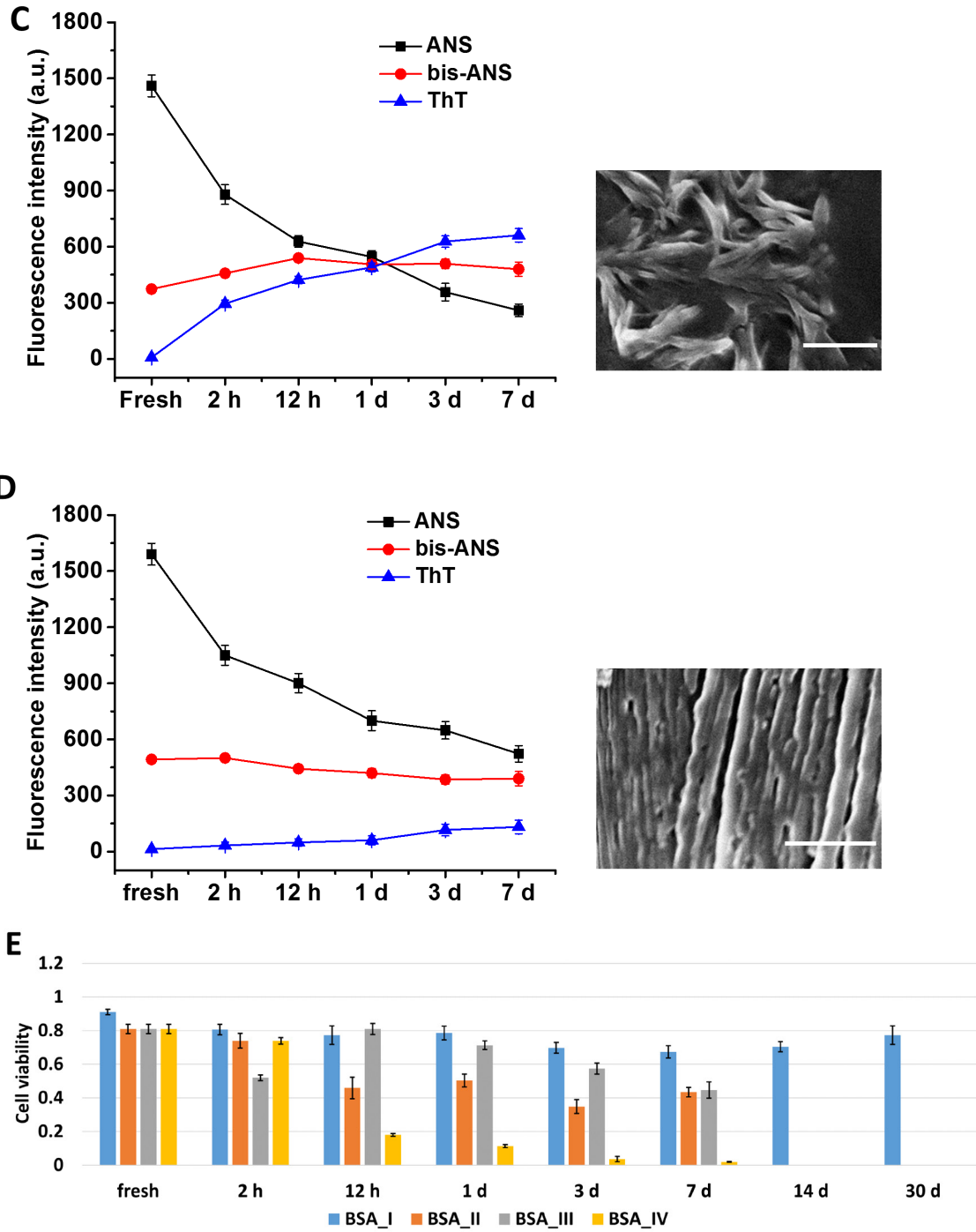


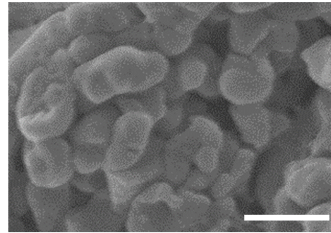
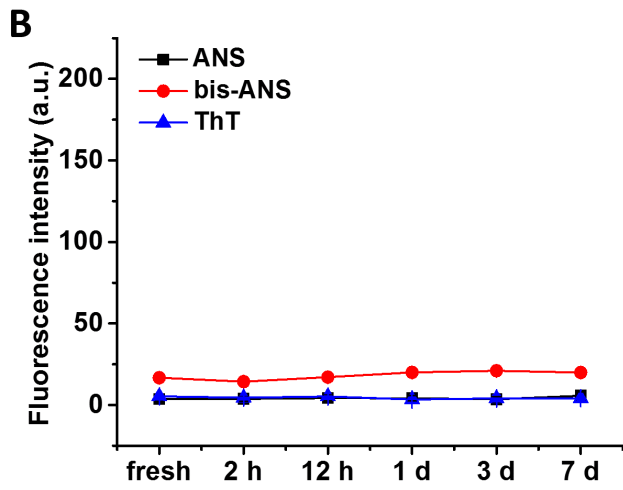
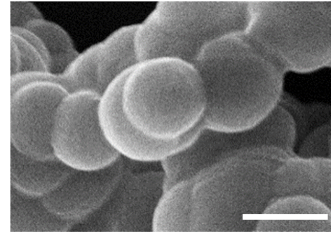
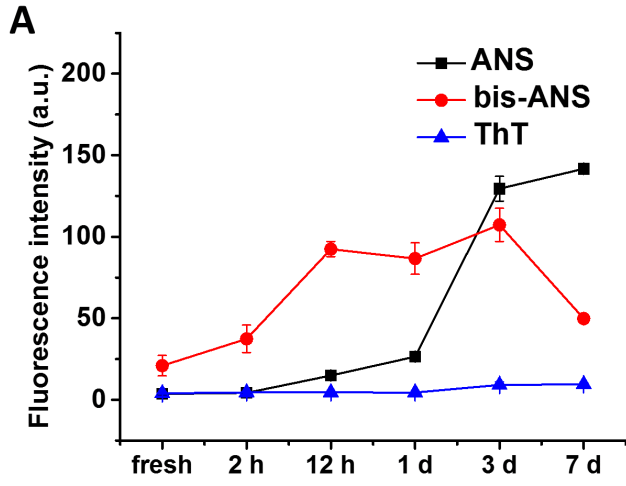
Figure 5.3. Four different structures generated from BSA were characterized using fluorescent probes, SEM, and MTS assay. (A) Fluorescence results and SEM image of BSA_I aggregate: amorphous aggregate mixed with fibril-like structures generated from 100 μM BSA at pH 3.0, 25 $^{\circ}\text{C}$. (B) Fluorescence results and SEM image of BSA aggregate II: amorphous aggregate generated from 40 μM BSA with 10 mM DTT at pH

7.2, 37 °C. (C) Fluorescence results and SEM image of BSA aggregate III: protofibril generated from 37.6 μM BSA at pH 7.4, 70 °C. (D) Fluorescence results and SEM image of BSA aggregate IV: amorphous aggregate generated from 7.5 μM of BSA at pH 8.9, 65 °C. (E) MTS assay of SH-SY5Y cells incubated with 15 μM BSA aggregates I-IV. Error bars = ± S.D. Scale bars in SEM images = 1 μm (A-C) or 10 μm (D).

There is an ongoing debate in the field, as to what is the primary toxic species responsible for diseases^{5, 7, 35, 36}. Many protein aggregate toxicity studies have shown that the rapidly formed non-fibril oligomers are more toxic than the highly organized fibrillar structures, which may be due to the exposure of hydrophobic side chains^{7, 35, 36}. Interestingly, we observed that the granular BSA_II aggregates showed a similar trend in the toxicity as lysozyme_I fibrils, where all aggregates from 12 h to 7 d had a similar level of cytotoxicity (Figure 5.3E and 5.2D). In addition, the protofibrils from BSA_III and the granular lysozyme_III aggregates both have toxic intermediates as well as toxic mature aggregates (Figure 5.3 C and 5.2 A). According to our observations of different protein aggregates from lysozyme and BSA, the toxic species may not be conclude as general fibrillar or granular structures. While the only sample that did not exhibit any toxicity, was BSA_I, which showed two different structures but no measurable changes in fluorescence. This suggest that the aggregate toxicity may not depend on the overall appearance of the structure, but depend on the molecular organization of the aggregates³⁵.

Next, we prepared four different non-fibrillar aggregate structures that are all in granular appearance from the same protein, lysozyme (Figure 5.4). Although generated under very different conditions (see Table 5.1), similar morphology and subunit size of the aggregates were observed. The four aggregates could be grouped as two pairs that lysozyme_IV and VI forms larger bead-like structures, while lysozyme_V and VII forms

smaller and more compact structures. Does size matter? In general, although size measurements may lack structural/conformational details, size could matter for the activity of small structures in 10-100 kDa, or the insoluble ones⁸. Smaller size would be expected to assist diffusion, and could provide larger surface to mass ratio for potential interactions. However, here among the four granular aggregates, structures that have the largest (Lysozyme_IV) and the smallest (Lysozyme_VII) unit size caused impairment of cell viability (Figure 5.4 E), indicating that size does not play a primary role to affect cytotoxicity. It is noticeable that the non-toxic structures did not show any measurable changes in ANS, bis-ANS, or ThT fluorescence (Figure 5.4 B, C), which is very similar with BSA_I (Figure 5.3A). These results again support the idea that toxicity is closely related to the conformational organization of protein aggregates. Interestingly, proteins formed non-toxic aggregates without significant conformational changes. Although these aggregates were stable and large, they stayed as harmless as the native monomers. Therefore, conformational rearrangement is probably the first step to gain toxicity. However, the toxic aggregates observed so far present a mixed picture: in general, the results support that the toxicity may likely be a consequence of the loss of protein's native fold, but whether the observed cytotoxicity is specifically associated with one certain structure/conformation or it is a consequence of general heterogeneous dynamics of the aggregation process still remains to be clarified.



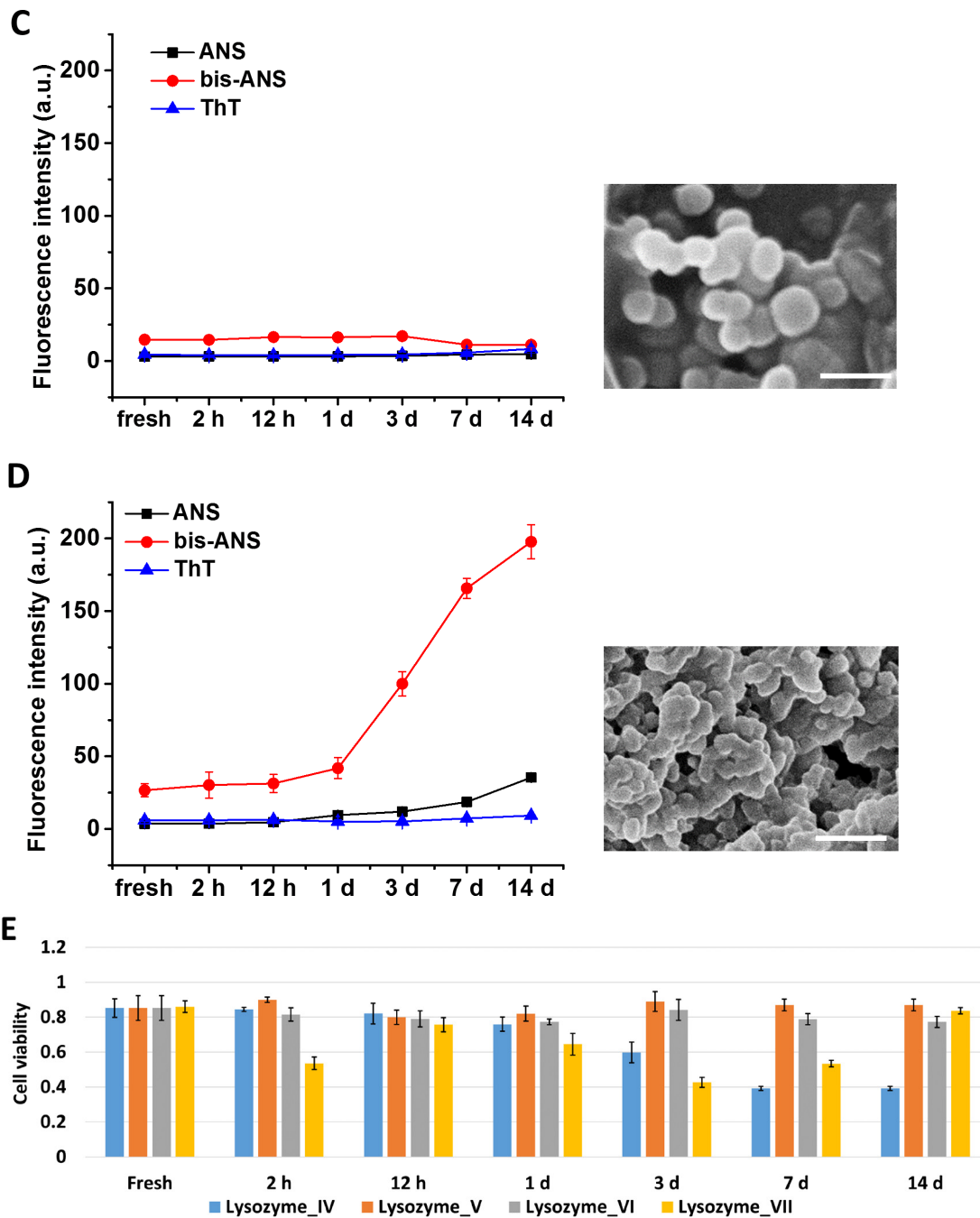


Figure 5.4. Four different bead-like amorphous aggregate structures generated from lysozyme were characterized using fluorescent probes, SEM, and MTS assay. (A, B) Fluorescence results and SEM image of lysozyme aggregate IV (A) and V (B): generated from 699 μ M lysozyme at pH 7.4, 65 $^{\circ}$ C (A) or 25 $^{\circ}$ C (B). (C) Fluorescence results and SEM image of lysozyme aggregate VI: generated from 120 μ M lysozyme at pH 7.0, 25 $^{\circ}$ C. (D) Fluorescence results and SEM image of lysozyme aggregate VII: generated from

120 μ M lysozyme at pH 12.0, 25 $^{\circ}$ C. (D) MTS assay of of SH-SY5Y cells incubated with 15 μ M lysozyme aggregates IV-VII. Error bars = \pm S.D. Scale bars in SEM images = 1 μ m.

Similar results have also been reported in studies of other proteins³⁵, such as α -synuclein³⁷, amyloid β peptide^{38,39}, and Hyp-F peptide⁴⁰. Many of these on-/off-pathway aggregates share similar morphologies or overlapping properties, but different toxic effects³⁶. It has been proposed that the increase toxicity of certain protein assemblies is due to their “biologically active conformation”³⁸, which exposes the “toxic surface”¹ on the molecules. However, the nature of either the “biologically active conformation” or the “toxic surface” remains elusive. Many previous studies suggest that the hydrophobic structures are potentially able to disrupt cell membrane, resulting in substantial cellular dysfunctions^{7, 41}. Whether or not hydrophobicity is directly related to toxicity is still a matter of debate. In the present study, toxicity observed in four out of five toxic lysozyme aggregates (lysozyme_I, II, III, IV, VII) showed a positive correlation to hydrophobicity (Figure 5.2, 5.4). However, the most hydrophobic species in lysozyme_VII and all the BSA samples were not the most toxic ones (Figure 5.3 and 5.4). Evidence can also be found in Hyp-F oligomers, where the structure with lower degree of hydrophobic packing were able to interact strongly with cell membranes, penetrate into cells, and resulted in high toxicity⁴⁰. The authors suggest that the toxicity may arise due to the structural flexibility^{40, 42}. This hypothesis is actually in line with our finding in lysozyme aggregates, that all the toxic structures showed high bis-ANS fluorescence compared with native monomers. From that point, toxicity could possibly resulted from the increased flexibility of the protein/peptide aggregates³⁶.

Among the results discussed above, we noticed that under many conditions, both the intermediates and mature aggregate structures caused low cell viability in MTS assay. To further understand the difference between these structures, the toxic structure selected by MTS assay were then tested using LDH and DCF assays, which determine cytotoxicity and the respiratory burst activity in cells, respectively. Release of the cytosolic enzyme lactate dehydrogenase (LDH) is known as an indicator of membrane leaking, a consequence of cell death. It is noticeable that only in BSA_III and IV, the mature structures are more toxic (Figure 5.5). In most of the tested samples, the intermediates showed higher toxicity than the mature structure, although they exhibited similar effect on cell viability (MTS) assay (Figure 5.5). This suggests that the intermediates exhibit higher cytotoxicity. The non-polar compound 2',7'-dichlorofluorescein diacetate (DCFH-DA) can penetrate the cell membrane, and be hydrolyzed by the intracellular esterase to 2',7'-dichlorofluorescein (DCFH). In the presence of reactive oxygen species (ROS), DCFH can be oxidized into the highly fluorescent 2',7'-dichlorofluorescein (DCF)³². Therefore, the DCF assay is widely used to measure the amount of intracellular ROS level^{32, 33, 43}. Increases in the ROS species indicates increased cellular stress. In general, DCF results of the selected toxic structures followed similar trend to LDH measurements (Figure 5.5), suggesting that the cytotoxicity may arise as a result of increased oxidative stress inside the cell. Overall, the parallel comparison of these different assays suggest that both intermediates and mature aggregates in protein aggregation process can affect cell proliferation, but the intermediates generally exhibit higher cytotoxicity, probably due to increased ROS in the cell. This also has the implication that different pathways for cytotoxicity may be activated depending on the nature of aggregates.

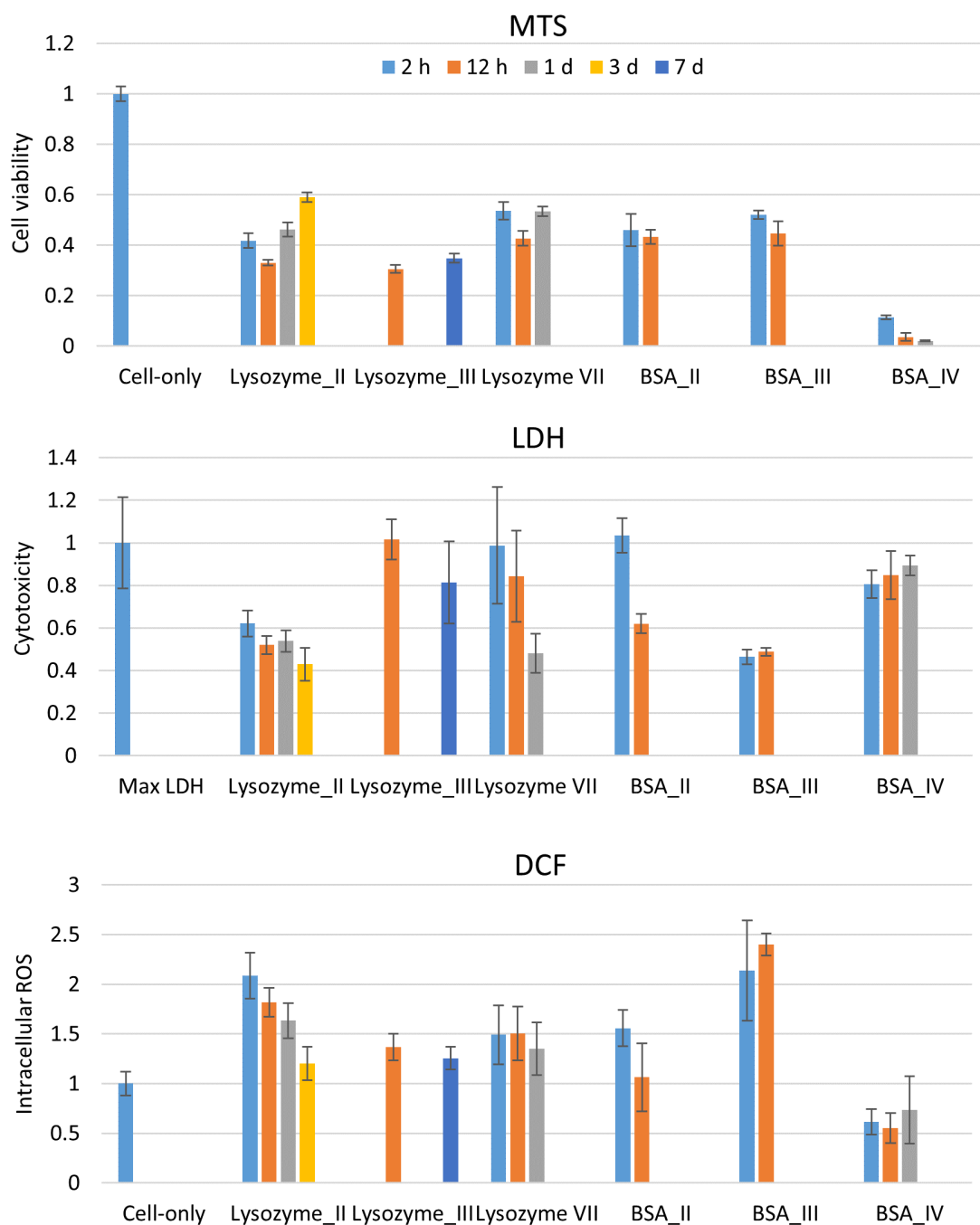


Figure 5.5. The toxicity of different protein aggregates were compared by MTS assay, LDH assay, and DCF assay. In each assay, SH-SY5Y cells were incubated with 15 μ M of selected aggregate samples. In MTS assay and DCF assay, data was normalized

based on cell-only control. In LDH assay, max LDH release was set as 1, and all other data was normalized accordingly. Error bars = \pm S.D.

Here in this study, the most toxic species were found at 2 h or 12 h incubations, which are flexible intermediate structures. This observation of toxic intermediates is in agreement with the hypothesis that toxicity is related to protein's flexibility as mentioned above. Alternatively, toxicity is also proposed as a consequence of the dynamics of protein aggregation process^{1, 20, 44, 45}. Studies of amyloid β peptide have shown strong correlations between toxicity and the free monomers or aggregation seeds, rather than mature amyloid fibrils¹. Considering the toxic intermediates observed in the present study and reported in the literature, the toxicity may also relate to the ongoing aggregation process and heterogeneous character of natural aggregates³⁷. Although this hypothesis of aggregation dynamics associated toxicity is able to explain many of the available observation in the field, its mechanism is even more difficult to understand. Future work on identifications of the diverse structures during aggregation process would be necessary. Comparing and contrasting the toxic structures observed *in vitro* and *in vivo* may also provide important insights for the actual toxic mechanism of protein aggregation.

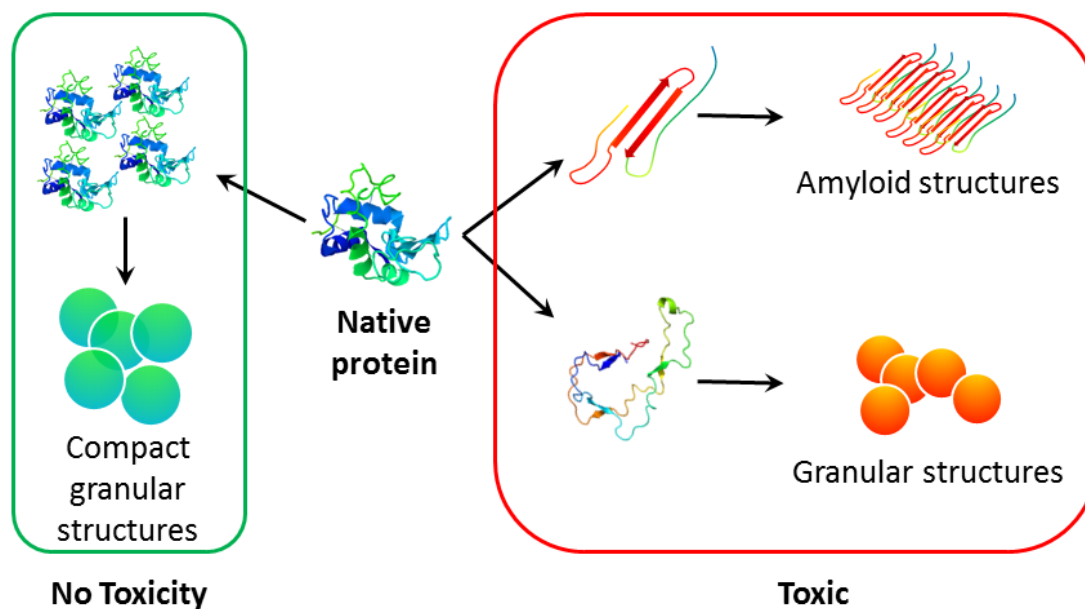


Figure 5.6. The initial conformational change during aggregation is a common key factor to different protein aggregates observed in this study. However, toxicity was observed in both types of intermediates that form amyloid and granular aggregates. Further precisely structure analysis is needed to full distinguish different aggregation intermediates in terms of toxicity.

5.4 Conclusion

In this study, different aggregate structures of lysozyme and BSA were generated, and compared for hydrophobicity, structural flexibility, and cytotoxicity. Results showed that aggregates in similar morphology could be differentiated on the biophysical properties and related cellular effects, which provide evidence of heterogeneous population of protein aggregates. In both lysozyme and BSA, cytotoxicity could arise as a consequence of structural flexibility. The aggregates that formed rapidly and had no significant conformational change from the protein native structure are essentially harmless to the cells. To further precisely define the toxic conformation of proteins, future work with high resolution structural identification would be needed.

5.5 References

1. Ross, C. A.; Poirier, M. A., What is the role of protein aggregation in neurodegeneration? *Nature Reviews Molecular Cell Biology* **2005**, *6*, 891-8.
2. Dobson, C. M., Protein aggregation and its consequences for human disease. *Protein Pept. Lett.* **2006**, *13*, 219-27.
3. Stefani, M.; Dobson, C. M., Protein aggregation and aggregate toxicity: new insights into protein folding, misfolding diseases and biological evolution. *Journal of Molecular Medicine-Jmm* **2003**, *81*, 678-99.
4. Eisenberg, D.; Jucker, M., The Amyloid State of Proteins in Human Diseases. *Cell* **2012**, *148*, 1188-203.
5. Ross, C. A.; Poirier, M. A., Protein aggregation and neurodegenerative disease. *Nat. Med.* **2004**, *10*, S10-S7.
6. Dobson, C. M., Protein folding and misfolding. *Nature* **2003**, *426*, 884-90.
7. Cheon, M.; Chang, I.; Mohanty, S.; Luheshi, L. M.; Dobson, C. M., et al., Structural reorganisation and potential toxicity of oligomeric species formed during the assembly of amyloid fibrils. *Plos Computational Biology* **2007**, *3*, 1727-38.
8. Glabe, C. G., Structural classification of toxic amyloid oligomers. *Journal of Biological Chemistry* **2008**, *283*, 29639-43.
9. Kaden, D.; Harmeier, A.; Weise, C.; Munter, L. M.; Althoff, V., et al., Novel APP/Abeta mutation K16N produces highly toxic heteromeric Abeta oligomers. *Embo Molecular Medicine* **2012**, *4*, 647-59.
10. Kumar, S.; Rezaei-Ghaleh, N.; Terwel, D.; Thal, D. R.; Richard, M., et al., Extracellular phosphorylation of the amyloid beta-peptide promotes formation of toxic aggregates during the pathogenesis of Alzheimer's disease. *Embo Journal* **2011**, *30*, 2255-65.

11. Yang, M.; Dutta, C.; Tiwari, A., Disulfide-Bond Scrambling Promotes Amorphous Aggregates in Lysozyme and Bovine Serum Albumin. *Journal of Physical Chemistry B* **2015**, *119*, 3969-81.
12. Olzscha, H.; Schermann, S. M.; Woerner, A. C.; Pinkert, S.; Hecht, M. H., et al., Amyloid-like Aggregates Sequester Numerous Metastable Proteins with Essential Cellular Functions. *Cell* **2011**, *144*, 67-78.
13. Westermark, P., Aspects on human amyloid forms and their fibril polypeptides. *Febs Journal* **2005**, *272*, 5942-9.
14. Terry, R. D.; Masliah, E.; Salmon, D. P.; Butters, N.; Deteresa, R., et al., Physical basis of cognitive alterations in Alzheimers-disease - synapse loss is the major correlate of cognitive impairment. *Annals of Neurology* **1991**, *30*, 572-80.
15. Tompkins, M. M.; Hill, W. D., Contribution of somal Lewy bodies to neuronal death. *Brain Research* **1997**, *775*, 24-9.
16. Gutekunst, C. A.; Li, S. H.; Yi, H.; Mulroy, J. S.; Kuemmerle, S., et al., Nuclear and neuropil aggregates in Huntington's disease: Relationship to neuropathology. *Journal of Neuroscience* **1999**, *19*, 2522-34.
17. Chapman, M. R.; Robinson, L. S.; Pinkner, J. S.; Roth, R.; Heuser, J., et al., Role of Escherichia coli curli operons in directing amyloid fiber formation. *Science* **2002**, *295*, 851-5.
18. Fowler, D. M.; Koulov, A. V.; Alory-Jost, C.; Marks, M. S.; Balch, W. E., et al., Functional amyloid formation within mammalian tissue. *Plos Biology* **2006**, *4*, 100-7.
19. Hou, F.; Sun, L.; Zheng, H.; Skaug, B.; Jiang, Q.-X., et al., MAVS Forms Functional Prion-like Aggregates to Activate and Propagate Antiviral Innate Immune Response. *Cell* **2011**, *146*, 448-61.

20. Hubin, E.; van Nuland, N. A. J.; Broersen, K.; Pauwels, K., Transient dynamics of A beta contribute to toxicity in Alzheimer's disease. *Cellular and Molecular Life Sciences* **2014**, *71*, 3507-21.
21. Lesne, S.; Koh, M. T.; Kotilinek, L.; Kaye, R.; Glabe, C. G., et al., A specific amyloid-beta protein assembly in the brain impairs memory. *Nature* **2006**, *440*, 352-7.
22. Shankar, G. M.; Li, S.; Mehta, T. H.; Garcia-Munoz, A.; Shepardson, N. E., et al., Amyloid-beta protein dimers isolated directly from Alzheimer's brains impair synaptic plasticity and memory. *Nat. Med.* **2008**, *14*, 837-42.
23. Engelender, S.; Kaminsky, Z.; Guo, X.; Sharp, A. H.; Amaravi, R. K., et al., Synphilin-1 associates with alpha-synuclein and promotes the formation of cytosolic inclusions. *Nature Genetics* **1999**, *22*, 110-4.
24. Tanaka, Y.; Engelender, S.; Igarashi, S.; Rao, R. K.; Wanner, T., et al., Inducible expression of mutant alpha-synuclein decreases proteasome activity and increases sensitivity to mitochondria-dependent apoptosis. *Human Molecular Genetics* **2001**, *10*, 919-26.
25. Krebs, M. R. H.; Wilkins, D. K.; Chung, E. W.; Pitkeathly, M. C.; Chamberlain, A. K., et al., Formation and seeding of amyloid fibrils from wild-type hen lysozyme and a peptide fragment from the beta-domain. *Journal of Molecular Biology* **2000**, *300*, 541-9.
26. Wang, S. S. S.; Liu, K.-N.; Wang, B.-W., Effects of dithiothreitol on the amyloid fibrillogenesis of hen egg-white lysozyme. *European Biophysics Journal with Biophysics Letters* **2010**, *39*, 1229-42.
27. Navarra, G.; Troia, F.; Militello, V.; Leone, M., Characterization of the nucleation process of lysozyme at physiological pH: Primary but not sole process. *Biophysical chemistry* **2013**, *177-178*, 24-33.

28. Kumar, S.; Ravi, V. K.; Swaminathan, R., How do surfactants and DTT affect the size, dynamics, activity and growth of soluble lysozyme aggregates? *Biochem. J.* **2008**, *415*, 275-88.
29. Bhattacharya, M.; Jain, N.; Mukhopadhyay, S., Insights into the mechanism of aggregation and fibril formation from bovine serum albumin. *Journal of Physical Chemistry B* **2011**, *115*, 4195-205.
30. Holm, N. K.; Jespersen, S. K.; Thomassen, L. V.; Wolff, T. Y.; Sehgal, P., et al., Aggregation and fibrillation of bovine serum albumin. *Biochimica Et Biophysica Acta-Proteins and Proteomics* **2007**, *1774*, 1128-38.
31. Vetri, V.; D'Amico, M.; Fodera, V.; Leone, M.; Ponzoni, A., et al., Bovine Serum Albumin protofibril-like aggregates formation: Solo but not simple mechanism. *Archives of Biochemistry and Biophysics* **2011**, *508*, 13-24.
32. Rosenkranz, A. R.; Schmaldienst, S.; Stuhlmeier, K. M.; Chen, W. J.; Knapp, W., et al., A microplate assay for the detection of oxidative productions using 2',7'-dichlorofluorescein-diacetate. *Journal of Immunological Methods* **1992**, *156*, 39-45.
33. Karlsson, H. L.; Cronholm, P.; Gustafsson, J.; Moller, L., Copper oxide nanoparticles are highly toxic: A comparison between metal oxide nanoparticles and carbon nanotubes. *Chemical Research in Toxicology* **2008**, *21*, 1726-32.
34. Holmes, C.; Boche, D.; Wilkinson, D.; Yadegarfar, G.; Hopkins, V., et al., Long-term effects of A beta(42) immunisation in Alzheimer's disease: follow-up of a randomised, placebo-controlled phase I trial. *Lancet* **2008**, *372*, 216-23.
35. Bucciantini, M.; Giannoni, E.; Chiti, F.; Baroni, F.; Formigli, L., et al., Inherent toxicity of aggregates implies a common mechanism for protein misfolding diseases. *Nature* **2002**, *416*, 507-11.

36. Benilova, I.; Karran, E.; De Strooper, B., The toxic A beta oligomer and Alzheimer's disease: an emperor in need of clothes. *Nature Neuroscience* **2012**, *15*, 349-57.
37. Danzer, K. M.; Haasen, D.; Karow, A. R.; Moussaud, S.; Habeck, M., et al., Different species of alpha-synuclein oligomers induce calcium influx and seeding. *Journal of Neuroscience* **2007**, *27*, 9220-32.
38. Townsend, M.; Shankar, G. M.; Mehta, T.; Walsh, D. M.; Selkoe, D. J., Effects of secreted oligomers of amyloid beta-protein on hippocampal synaptic plasticity: a potent role for trimers. *Journal of Physiology-London* **2006**, *572*, 477-92.
39. Kaye, R.; Head, E.; Thompson, J. L.; McIntire, T. M.; Milton, S. C., et al., Common structure of soluble amyloid oligomers implies common mechanism of pathogenesis. *Science* **2003**, *300*, 486-9.
40. Campioni, S.; Mannini, B.; Zampagni, M.; Pensalfini, A.; Parrini, C., et al., A causative link between the structure of aberrant protein oligomers and their toxicity. *Nature Chemical Biology* **2010**, *6*, 140-7.
41. Huang, B.; He, J.; Ren, J.; Yan, X. Y.; Zeng, C. M., Cellular Membrane Disruption by Amyloid Fibrils Involved Intermolecular Disulfide Cross-Linking. *Biochemistry* **2009**, *48*, 5794-800.
42. Winner, B.; Jappelli, R.; Maji, S. K.; Desplats, P. A.; Boyer, L., et al., In vivo demonstration that alpha-synuclein oligomers are toxic. *Proceedings of the National Academy of Sciences of the United States of America* **2011**, *108*, 4194-9.
43. Puntel, R. L.; Roos, D. H.; Folmer, V.; Nogueira, C. W.; Galina, A., et al., Mitochondrial Dysfunction Induced by Different Organochalcogens Is Mediated by Thiol Oxidation and Is Not Dependent of the Classical Mitochondrial Permeability Transition Pore Opening. *Toxicological Sciences* **2010**, *117*, 133-43.

44. Wogulis, M.; Wright, S.; Cunningham, D.; Chilcote, T.; Powell, K., et al., Nucleation-dependent polymerization is an essential component of amyloid-mediated neuronal cell death. *Journal of Neuroscience* **2005**, *25*, 1071-80.
45. Pauwels, K.; Williams, T. L.; Morris, K. L.; Jonckheere, W.; Vandersteen, A., et al., Structural Basis for Increased Toxicity of Pathological A beta(42):A beta(40) Ratios in Alzheimer Disease. *Journal of Biological Chemistry* **2012**, *287*, 5650-60.

Chapter 6 Live cell fluorescence imaging of fluorescent probes for sensitive detection of intracellular pH¹ and lysosomal pH²

Jingtuo Zhang, Mu Yang, Nethaniah Dorh, Fei Xie, Ashutosh Tiwari^a, Fen-Tair Luo^b, and Haiying Liu^a

¹The material was previously published in the *ACS Sensors*.

DOI: 10.1021/acssensors.5b00065

Web published date: Nov. 27 2015 Copyright © 2015 American Chemical Society

<http://pubs.acs.org/doi/abs/10.1021/acssensors.5b00065>

²The material was previously published in the *J. Mater. Chem. B*, 2015, 3, 2173-2184. DOI: 10.1039/c4tb01878h

Publication date: Jan. 19 2015 Copyright © The Royal Society of Chemistry 2015

<http://pubs.rsc.org/en/Content/ArticleLanding/2015/TB/c4tb01878h#!divAbstract>

6.1 Introduction

Intracellular pH is essential to regulate many important behaviors of a cell such as cell volume, membrane polarity, proliferation and apoptosis, ion transport, enzyme activity, and protein degradation¹. The pH varies considerably among subcellular compartments, ranging from 4.7 in lysosome to 8.0 in mitochondria. Changes of pH in living cells affect cellular internalization pathways, as well as synaptic transmission and signal cascades in the nervous system. Disruptive pH variations in organelles associate with dysfunctions and are observed in pathophysiology of many diseases, such as triggering cancer, stroke, and Alzheimer's disease. For example, the organelle lysosome maintains an acidic environment (pH 4.5–5.5) that serves to denature proteins or to activate degradation enzymes. Abnormal lysosomal pH can cause lysosome malfunction, accumulation of cell trashes, and even lysosomal storage diseases that can affect every part of the human body². Therefore, it is very important to monitor pH changes inside living cells in order to investigate cellular functions that can provide insight into physiological and pathological processes.

Intracellular pH is normally detected using NMR, microelectrodes, absorbance spectroscopy, and fluorescence spectroscopy¹. Compared with other methods, fluorescence detection of intracellular pH is not only simple-to-operate and highly sensitive, but also has advantages of excellent spatial and temporal observations²⁻⁴. Fluorescence-based techniques such as fluorescence microscopy and flow cytometry can provide high-resolution and high-throughput analysis, thus, they have been widely used to investigate intact subcellular pH. However, among the large numbers of pH fluorescent

probes, only a few have been applied inside living cells⁵⁻⁷. Most intracellular fluorescent probes have used morpholine residues for the selective accumulation in the acidic lysosomes, since the ionizable tertiary amine groups tend to be protonated in acidic environments⁴. As a consequence of tertiary amine protonation in acidic lysosomes, the photo-induced electron transfer (PET) from the tertiary amine to the probe fluorophores is prohibited, resulting in enhancement of the probe fluorescence⁸⁻¹⁰. The potential drawbacks of these fluorescent probes are that they have broad pH responses and relatively high fluorescent background issue at pH 7.4. Recently, fluorescein and rhodamine dyes were used in approaches to reduce the background fluorescent at pH 7.4¹¹⁻¹³. However, most fluorescent probes are still not soluble in aqueous solution, and some probes can cause severe photo-damage to cells due to their short absorption and emission wavelengths (< 600 nm)¹⁴⁻¹⁶. A series of rhodamine dye counterparts were recently reported to sensitively detect lysosomal pH in live cells. These fluorescent probes have near-infrared excitation and emission wavelengths with deep tissue light penetration, low cytotoxicity, excellent photostability, as well as low background fluorescence. However, they were still insoluble in aqueous solution¹⁷. Therefore, the readily accessible near-infrared fluorescent probes that have good water solubility, large dynamic range and high specificity are still a challenging task for near-infrared imaging, especially for sensitive detection of lysosomal pH in living cells.

In this chapter, one uncommon morpholine based fluorescent probe **1** with morpholine residues to BODIPY dyes will be introduced to sense abnormal, elevated intracellular pH. The fluorescent probe **1** selectively displays high fluorescence with great photostability in a basic condition, but exhibits very weak fluorescence in an acidic

condition. In addition, fluorescent probe **1** has a long emission wavelength and a high pKa near the physiological pH, which provide more advantages for live cell fluorescence imaging. To further sensitively detect lysosomal pH changes, another group of near-infrared BODIPY-based fluorescent probes, probes **2**, **3**, **4**, was synthesized for lysosomal pH detection. Piperazine moieties were attached to the fluorescent cores to manipulate the fluorescent responses of the probes at different pH values. Fluorescent probes display very weak fluorescence at basic and neutral pHs, while decreasing the pH significantly enhances fluorescence intensity. These fluorescent probes have advantages such as high photostability, sensitive and selective near-infrared imaging of lysosomal pH in living cells. They have potential for intact *in vivo* imaging and deep tissue penetration without auto-fluorescence and unintended cellular damage issues.

6.2 Materials and methods

Intracellular fluorescent probes **1** and lysosomal pH probes **2**, **3**, **4** were synthesized by Jingtuo Zhang from Dr. Haiying Liu's research group. Details of compound synthesis and characterization could be found in the original publication².

Optical measurements – All absorption and emission spectra were recorded as previously described in chapter 2. In brief, 20 mM and 50 mM of citrate-phosphate-borate buffers were used for pH dependency and photostability measurements of intracellular and lysosomal fluorescent probes, respectively. Stock solutions of all the probes are at 1.0 mM in DMSO (probes **2** and **3**) or aqueous solution (probe **1** and **4**). To avoid the interference caused by metal-phosphate and metal-citrate binding interactions (forming precipitates of divalent cation phosphate and forming complex of the metal-

citrate), 10 mM KHP buffer (pH 4.0) and 10 mM HEPES (pH 7.4) buffer were used for selectivity measurements of fluorescent probes. The UV-Vis absorption spectra of fluorescent probes **1**, **2**, **3**, and **4** for pH dependency, selectivity, photostability and solvent effect measurements were collected in the range from 300 to 800 nm with increments of 1 nm. Their corresponding fluorescence spectra were collected at the excitation wavelength of 580 nm for fluorescent probes **1**, and 620 nm for probes **2**, **3**, **4**. The excitation and emission slit widths were set up to 3 nm.

Determination of pKa by fluorometric titration – The constants Ka of fluorescent probes were determined in buffer solutions by fluorometric titration as a function of pH using the fluorescence spectra. The expression of the steady-state fluorescence intensity F as a function of the proton concentration has been extended for the case of an n: 1 complex between H⁺ and a fluorescent probe, which is expressed by the equation as below:

$$F = \frac{F_{min}[H^+]^n + F_{max}K_a}{K_a + [H^+]^n}$$

Fmin and Fmax stand for the fluorescence intensities at maximal and minimal H⁺ concentrations, respectively, and n is apparent stoichiometry of H⁺ binding to the probe which affects the fluorescent change. Nonlinear fitting of the above equation to the fluorescence titration data recoded as a function of H⁺ concentration with Ka and n as free adjustable parameters yields the estimated apparent constant of Ka.

Live cell fluorescence imaging – Breast cancer cells MDA-MB-231 and normal endothelial cells HUVEC-C (from ATCC) were cultured as previously described in chapter 2. In brief, cells were plated on 12-well culture plates at 1×10^5 cells per well and

incubated at 37 °C in a 5% CO₂ incubator overnight. The next day, the medium was removed and cells were rinsed twice with 1X PBS, after which fresh serum-free medium was added and cells were incubated for 2 h at 37 °C in a CO₂ incubator. Following 2 h serum starvation, fresh serum free media with/without indicated concentrations of probes and co-stains were added and incubated further with cells for 2 h. Cells were washed with fresh serum free media without any fluorescence dyes to remove background fluorescence. To adjust the intracellular pH, cells were treated with nigericin (5 mg mL⁻¹) in 2 mL potassium rich PBS at different pH values and incubated further for 15 min. Live cell images were acquired using an inverted fluorescence microscope (AMF-4306, EVOS_{fl}, AMG) with DAPI filter for Hoechst 33342 (Sigma-Aldrich), GFP filter for LysoSensor Green DND-189 (Invitrogen), and CY5 filter for fluorescent probes **1**, **2**, **3**, and **4**. The fluorescence images were obtained at 40X and 60X magnification for HUVEC-C and at 60X magnification for MDA-MB-231 cells. The exposure times for each filter were kept constant. Co-localization analysis based on Pearson's coefficient was done using JACoP plugin from ImageJ.³⁵

Determination of cellular uptake efficiency – HUVEC-C cells were plated at a density of 1×10^4 cells per well on a 96-well cell culture plate and incubated at 37 °C in a 5% CO₂ incubator overnight. The next day, the culture media was removed and cells were rinsed twice with PBS (pH 7.4). Fresh 100 mL media with indicated concentrations of probes were added to the wells in triplicate and incubated for 2 h. Controls and blanks were also set in triplicate at the same time. Controls had culture media and dyes but no cells. Blanks used for background subtraction had cells and media but no dyes. After 2 h incubation, the media (100 mL) was pipetted out from the plate and put in a fresh 96-well

plate. Each well was rinsed with 100 mL of fresh PBS (pH 7.4), and the solution was added to the respective wells in the fresh 96-well plate. Then the absorbance of the wells was measured by an ELISA plate reader (BioTek Instruments, Inc.) at 712 nm, 710 nm, and 687 nm (absorbance peaks of fluorescent probes **2**, **3**, or **4**, respectively). The values of the respective blanks were subtracted from samples (Adye) and controls (Actrl). Cellular uptake efficiency was calculated as $[1 - (\text{Adye}/\text{Actrl})] \times 100\%$.

Cell viability (MTS) assay – MTS assay was performed with MDA-MB-231 cells and HUVEC-C cells (ATCC), as previously described in chapter 2. Briefly, the cells were plated at a density of 5,000 cells per well on a 96-well cell culture plate and incubated at 37 °C in a 5% CO₂ incubator overnight. The next day, media were removed and the cells were washed with 1X PBS. Fresh media with 0-50 μM of fluorescent probes in DMSO (with <0.5% DMSO final concentration in media) were added to the wells and measured in 6 replicates for each dye concentration. Blanks that had everything else except the cells were prepared at the same time. The plates were incubated at 37 °C in a 5% CO₂ incubator for 72 h. After incubation, 20 μL of MTS reagent (CellTiter 96 Aqueous Non-Radioactive Cell proliferation Assay (MTS) kit, Promega) was added to each well. The absorbance at 490 nm was acquired after a 4 h incubation at 37 °C, using an ELISA plate reader (BioTek Instruments, Inc.). Plots were normalized to control wells containing media and cells only.

6.3 Results and discussion

6.3.1 Intracellular pH probe

The intracellular pH probe **1** (Figure 6.1) was synthesized by Dr. Haiying Liu's group. The tri-(ethylene glycol) methyl ether groups were introduced to the meso-phenyl rings and 1,7-positions of BODIPY dye, which enhances the solubility of probe **1** in polar solvents. The functionalizing groups, morpholine moieties, were attached to the BODIPY core at 4,4'-positions. The probe displays negligible change in absorption at different pHs (data not shown). However, a fluorescence turn-on behavior was observed at basic pH, with 14.3-fold enhancement of fluorescence intensity from pH 3.02 to 9.49 (Figure 6.1). Theoretical modeling results showed that the fluorescent probe responded to pH via a modulation of d-PET (photo-induced electron transfer) mechanism (Figure 6.2). At high pH, the calculated HOMO and LUMO energies of morpholine moieties are lower and higher than those of probe **1**, respectively. This suggests that the electrons cannot transfer from morpholine moieties to the probe core, leading to a prohibited a-PET mechanism and high fluorescence of probe **1**. Whereas at low pH, the protonation of morpholine moiety results in a dramatic decrease of HOMO and LUMO energies, where the LUMO energy of protonated morpholine moieties lies between the HOMO and LUMO energies of probe **1** (Figure 6.2). In this case, morpholine residues serve as electron acceptors, which quenched the fluorescence of the BODIPY dye via d-PET mechanism. In addition, probe **1** has a pKa value of 6.15, with maxima fluorescence increase lies in pH range 4.5-7.4, showing great potential to sensitively detect changes near physiological pH. Moreover, the deep-red emission prevents photo-damage to the cells, and the large Stokes shift

(from 550 nm excitation to 665 nm emission at pH 7.4, figure 6.1) minimizes the potential interference from excitation signals.

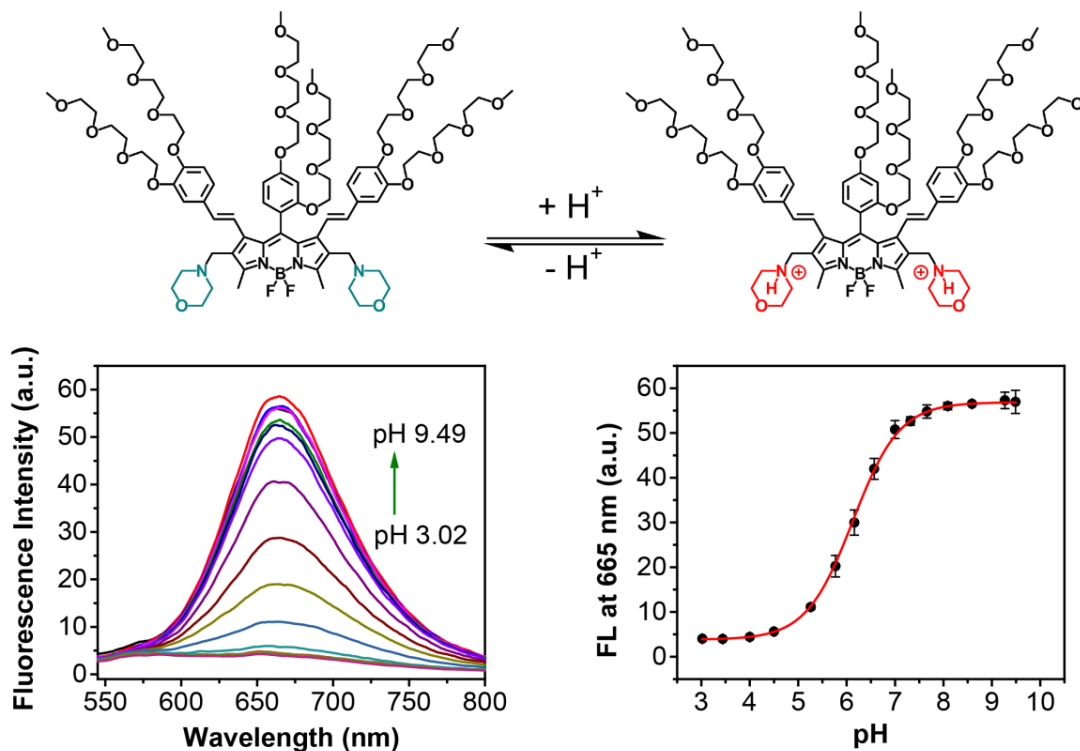


Figure 6.1. Chemical structure and fluorescence spectra of fluorescent probe **1** (5 μ M) in buffer solution at different pH (with 1% DMSO). The corresponding curve shows the increase of fluorescence intensity when pH increases.

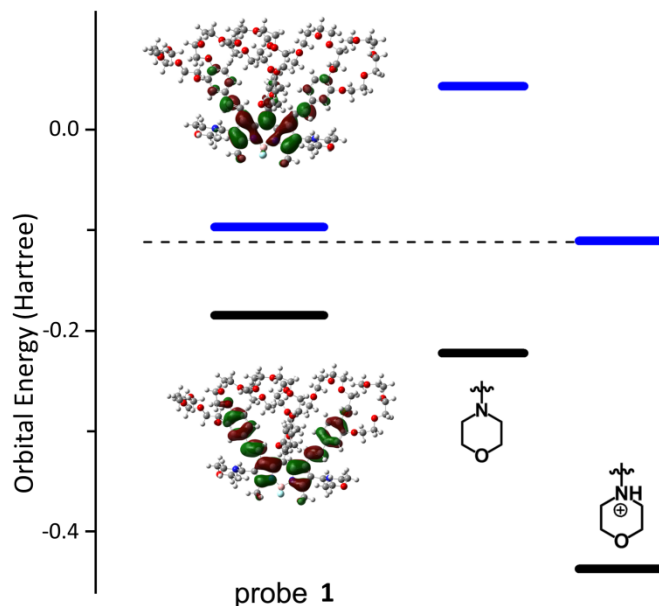
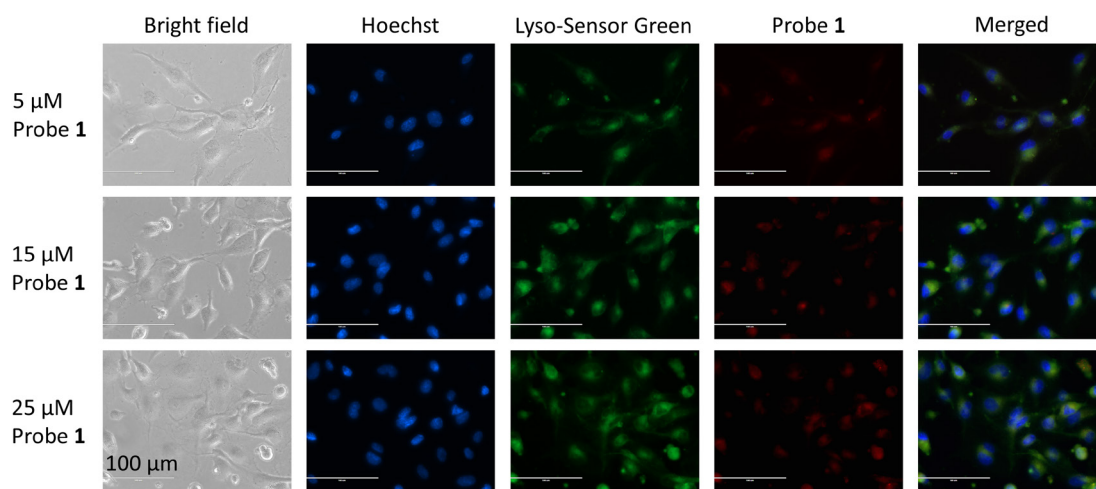


Figure 6.2. The HOMO and LUMO energies of fluorescent probe **1** and morpholine moiety (N-methylmorpholine, before and after protonation) were calculated.

Live cell fluorescence imaging of probe **1** was performed using HUVEC-C cells at different intracellular pH values (Figure 6.3, 6.4). Since the tertiary amines of the morpholine moieties tend to accumulate in acidic environments, we hypothesize that the fluorescent probe **1** may label lysosomes in the cell. Therefore, a well-known commercial lysosome probe, LysoSensor Green DND-189, was selected as a co-stain. Figure 6.3 shows that probe **1** exhibited very weak fluorescence signals at 5-25 μM . Slight fluorescence enhancements could be observed with increased probe concentrations. The merged fluorescence images show more green areas around the nucleus and only a few green-yellowish dot structures can be observed by a careful examination (Figure 6.3). However, the calculated Pearson's coefficients of red (fluorescent probe **1**) and green (LysoSensor Green) channels are 0.92, 0.85 and 0.88 for 5 μM , 15 μM and 25 μM probe **1**, respectively (Figure 6.3 cytofluorograms), indicating that the area stained by probe **1** matches those stained by LysoSensor Green in cells. This confirmed our hypothesis that

fluorescent probe **1** mainly stained lysosomes or other acidic organelles in cells. Therefore, the weak fluorescence of fluorescent probe **1** observed in the cells is a consequence of fluorescence quenching by the protonated morpholine moieties via a d-PET effect at lysosomal pH (4.5-5.5). In order to examine the fluorescence responses of fluorescent probe **1** to different pHs inside of cells, we further adjusted the intracellular pH of HUVEC-C cells using a widely used H^+/K^+ ionophore, nigericin, in K^+ rich PBS buffer solutions at pH 5.5, 6.5, 7.5, or 8.5 by equilibrating the intracellular and extracellular pHs. At all three concentrations, fluorescent probe **1** displayed very weak fluorescence at acidic pH (pH 5.5), whereas its fluorescence intensity showed gradual enhancement as intracellular pH increased from 5.5 to 8.5 (Figure 6.4). In addition, at each intracellular pH, higher probe concentration resulted in stronger fluorescence signals (Figure 6.4). These responses of fluorescent probe **1** to increased intracellular pH are in line with its optical responses to pH in buffer solutions (Figure 6.1), which further proved the d-PET mechanism of fluorescent probe **1** at different pHs in live cells. However, the commercial lysosome probe LysoSensor Green DND-189 did not exhibit any change in fluorescence upon change of intracellular pH (Figure 6.4).



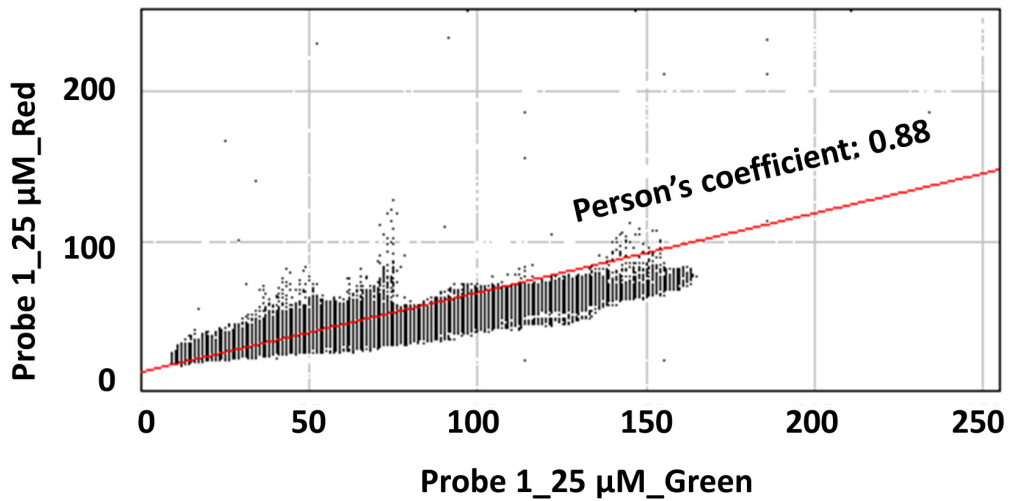
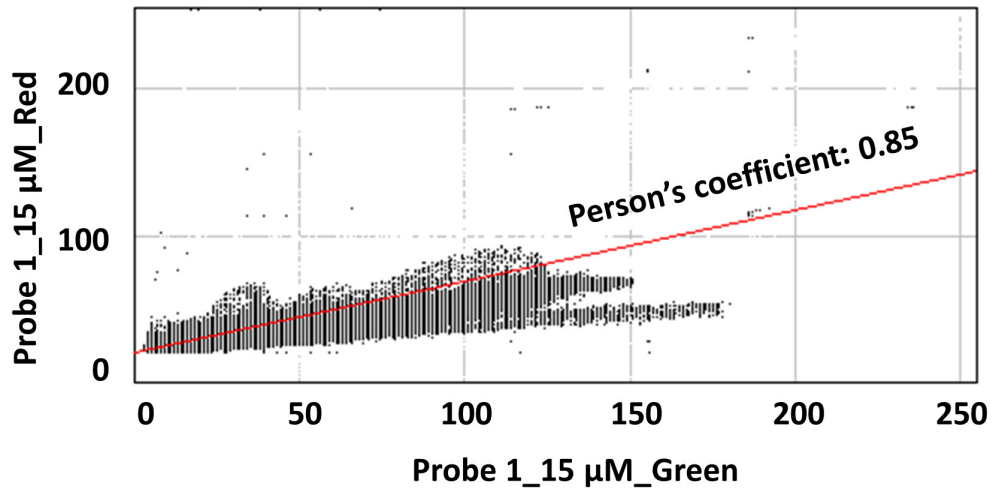
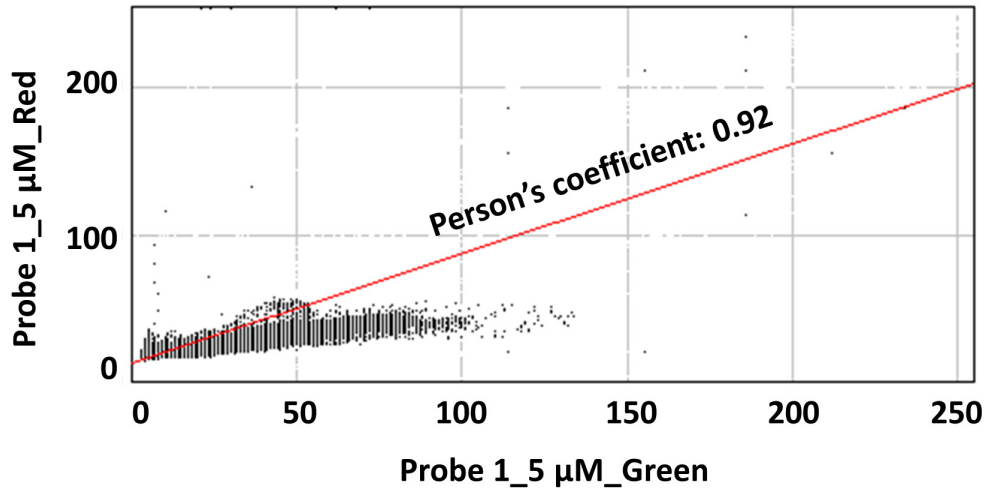


Figure 6.3. Fluorescence images of HUVEC-C cells incubated with 5 μM, 15 μM, or 25 μM fluorescent probe 1. HUVEC-C cells were incubated with fluorescent probe 1 for

2 h, post serum starvation (2 h) and imaged for co-localization with 1 μM LysoSensor Green and (1 $\mu\text{g}\cdot\text{mL}^{-1}$) Hoechst 33342 stains. Images were acquired using the inverted fluorescence microscope (AMF-4306, EVOSfl, AMG) at 40 \times magnification, scale bars = 100 μm . Cytofluorograms of green and red channel co-localization was carried out by JACoP plugin of ImageJ.

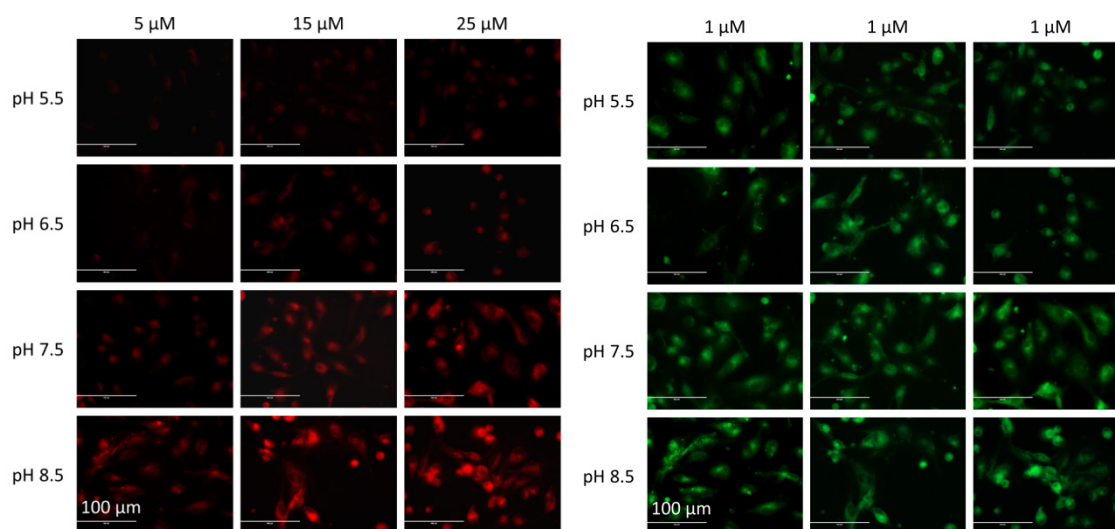


Figure 6.4. Fluorescence images of HUVEC-C cells incubated with 5 μM , 15 μM , or 25 μM fluorescent probe **1** (red channel) and LysoSensor Green (green channel) in buffers at different pH values of 5.5, 6.5, 7.5, or 8.5 having nigericin. Images were acquired using the inverted fluorescence microscope (AMF-4306, EVOSfl, AMG) at 40 \times magnification, scale bars = 100 μm .

We also investigated the toxicity of fluorescent probe **1** to HUVEC-C cells using MTS assay (Figure 6.5). At a low concentration, 5 μM , the fluorescent probe **1** provided more than 80% cell viability, when the concentration increased to 15 μM , the cell viability dropped to 60-70%, indicating the low to moderate toxicity of fluorescent probe **1** to the cells in this concentration range. However, fluorescent probe **1** at higher concentrations like 25 μM and 50 μM were very toxic to the cells as less than 10% cell viabilities were observed.

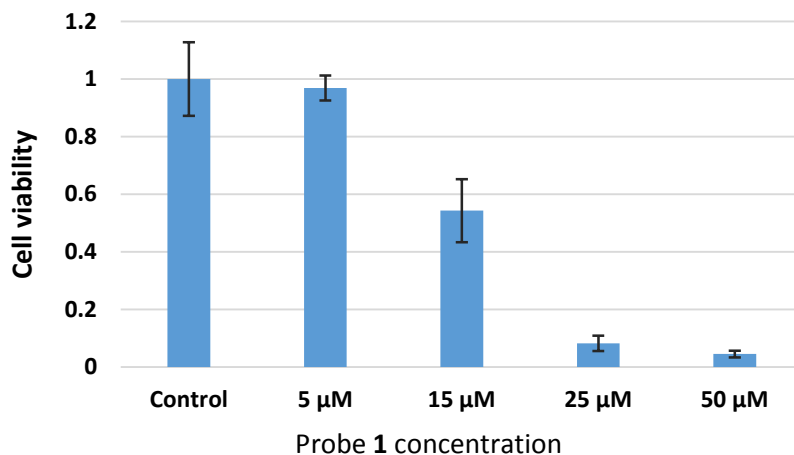


Figure 6.5. Effects of fluorescent probe 1 on cell proliferation measured by MTS assay. HUVEC-C cells were incubated with 5 μM , 15 μM , 25 μM , or 50 μM of fluorescent probe 1 for 48 h. To this 20 μL of MTS reagent was added per well and absorbance at 490 nm was measured to determine cell viability. Error bars indicate \pm SD.

6.3.2 Lysosomal pH probe

To further specifically target lysosome in the cells, piperazine moieties were conjugated at 3,5-positions of BODIPY core to prepare the BODIY-based near-infrared fluorescent probe 2 (Figure 6.6). However, the fluorescent probe 2 is hydrophobic and displays less than 0.1 mg/mL solubility in water. In order to facilitate the interactions of the probe with water molecules, the hydrophilic oligo(ethylene glycol)methyl ether residues were attached to meso- and 3,5-positions, resulting in probes 3 and 4 (Figure 6.6).

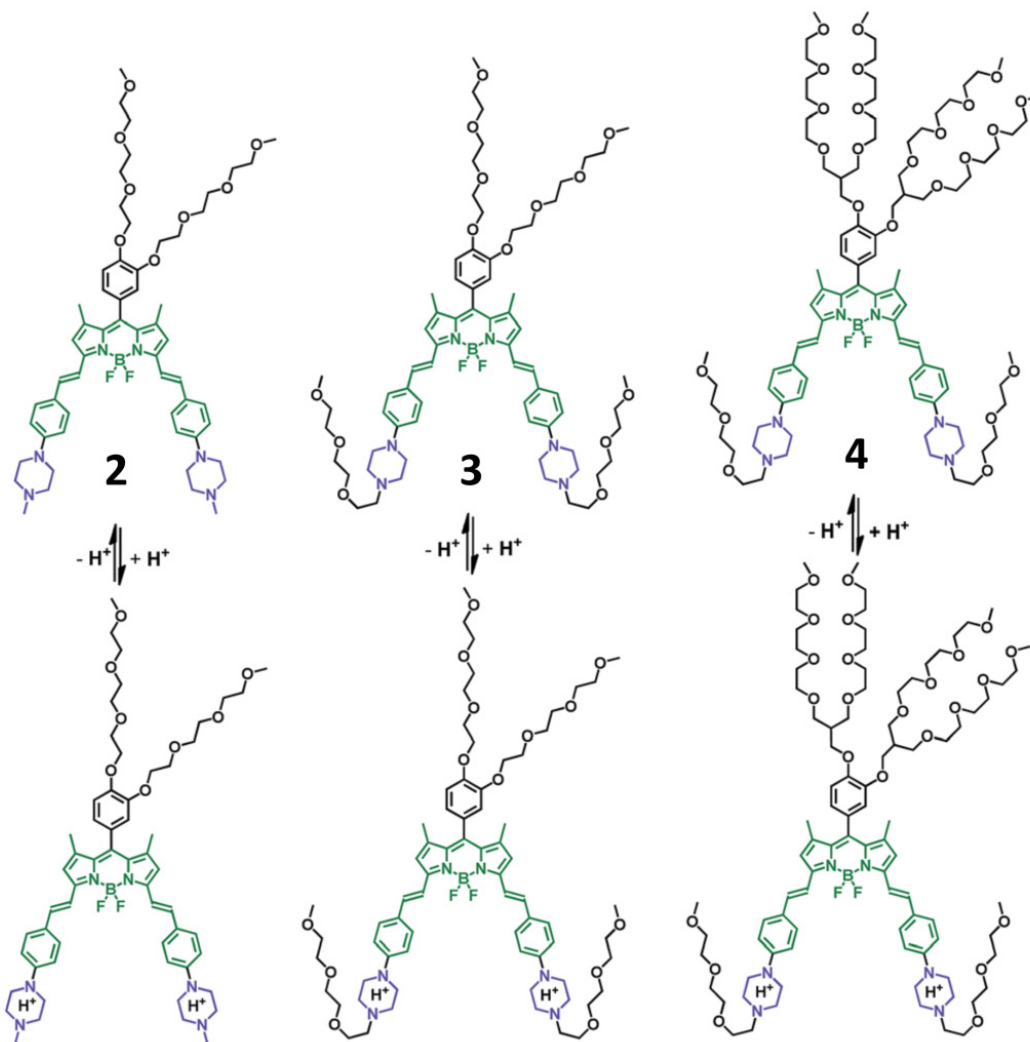


Figure 6.6. Chemical structures of fluorescent probes **2**, **3**, **4**.

In organic solvents such as ethanol, dichloromethane, and DMSO, fluorescent probe **2** displays absorption and emission peaks at 668 nm and 715 nm, respectively, due to the enhanced π -conjugation and intramolecular charge transfer (ICT) effect from piperazine moieties at 3,5-positions to the BODIPY core. However, in pH 7.4 buffer, probe **2** showed increased tendency of self-assembly, decreased fluorescence, and shifted absorption and emission peaks at 712 nm and 770 nm, caused by its hydrophobicity and the ICT effect in polar solution. Compared with fluorescence of probe **2**, probe **3** exhibits

similar optical properties in organic solvents, but blue-shifted absorption peak (710 nm) and emission peak (755 nm) in buffer solution (pH 7.4), which may be attributed to the reduced aggregation in aqueous solution with hydrophilic oligo(ethylene glycol)methyl ether residues. Fluorescent probe **4** has the highest water solubility, significant extended π -conjugation, and ICT effect from piperazine moieties to the BODIPY core, which shows absorption peaks at 669 nm and 687 nm, and emission peaks at 720 nm and 750 nm in ethanol and buffer solution (pH 7.4), respectively. In addition, the highly water-soluble character of probe **4** further reduced its self-aggregation effect in buffer solution.

On the other hand, all three fluorescent probes display very sensitive fluorescence responses to pH changes (Fig. 6.7). From pH 9.98 to 2.20, fluorescence enhancements of 75-, 88- and 102-fold were observed at 715 nm of fluorescent for probes **2**, **3** and **4**, respectively (Fig. 6.7). In addition, there are significant blue shifts of 55 nm, 41 nm and 35 nm in emission spectra of the probes **2**, **3** and **4**, respectively. This is because in acidic conditions, probe aggregation was reduced, and the nitrogen atoms in piperazine moieties were protonated, which reduced the ICT effect from piperazine moieties to BODIPY cores (Figure 6.6). Besides the ICT effect, potential PET effect from the lower nitrogen atoms of the piperazine moieties may also contribute to the extremely low fluorescence of all three probes in neutral/basic conditions. While at low pH, this potential PET quenching effect could be reduced via the protonation of piperazine moieties. Therefore, in basic to neutral pH range, all probes showed very weak fluorescence without any evident changes, whereas fluorescence intensities gradually increased from pH 7.0 to 2.2(Figure 6.7). However, highly acidic pHs from 2.20 to 1.01 significantly quenched fluorescence of the probes (Figure 6.7). More evidences are needed to fully understand

the fluorescence quenching mechanism of these probes at extremely low pH. The pKa values of probes **2**, **3** and **4** are 2.91, 3.19 and 3.57, respectively. It is very clear that probe **4** exhibits the highest fluorescence responses with the highest pKa value among all three probes, since this highly water-soluble probe has less aggregation, and is protonated considerably more easily in aqueous solution. As a consequence, probe **4** showed higher sensitivity to pH than probes **2** and **3**. Linear fluorescence responses to pH were shown between physiological pH (~7.4) and lysosomal pH (~4.2), where probe **4** displayed the highest sensitivity (Figure 6.7). The linear, high dynamic range, and sensitive responses of the probes to pH indicate the feasibility of intracellular pH detection.

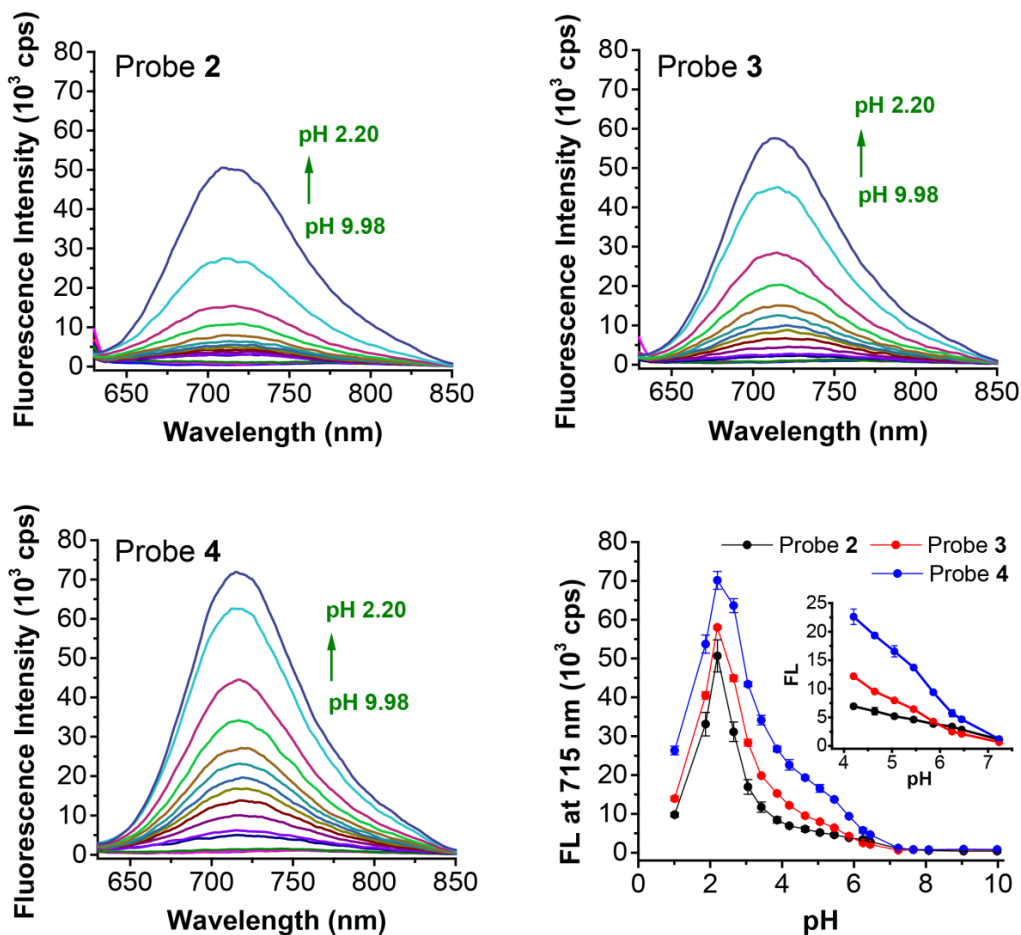


Figure 6.7. Emission spectra of fluorescent probes **2**, **3** and **4** (5 mM) were collected in buffer solution at pH 2.20-9.98.

Live cell imaging in various concentrations of all three probes were conducted using MDA-MB-231 cells and HUVEC-C cells (Figure 6.8, 6.9). In both cancer and normal cells, probes **2**, **3**, and **4** showed fluorescent signals, and the area in the cell that stained by probe **2**, **3**, or **4** (red channels in Figure 6.8, 6.9) matched those stained by LysoSensor Green (green channels in Figure 6.8, 6.9). The co-localization Pearson's coefficients are 8.5-9.4. Therefore, these probes are able to target lysosomes or other acidic cellular compartments in cells. Interestingly, the highly water soluble probe **4**, which fluorescent the strongest in buffers, displayed the weakest fluorescent signals inside cells. Whereas the most hydrophobic one, probe **2**, showed the highest fluorescent intensity among all three probes and displayed good signal even at 2 μ M concentration (data not shown). A possible reason could be that probes **2** and **3** are more hydrophobic and less sterically hindered than probe **4**, which could interact with the hydrophobic lipophilic membrane structures, thus, the fluorescence was activated by depressing ICT effect of the fluorophores¹⁸. On the other hand, probe **4** showed the lowest cytotoxicity after 72 h incubation with cells (Figure 6.10 A). While probe **2** is the most harmful to the cells, resulting in only ~50% viability at 5 μ M and less than 10% viability at 15 μ M and higher concentration (Figure 6.10 A). Probes **3** and **4** showed very mild toxicity with greater than 70% cell viability even at 50 μ M concentration (Figure 6.10 A).

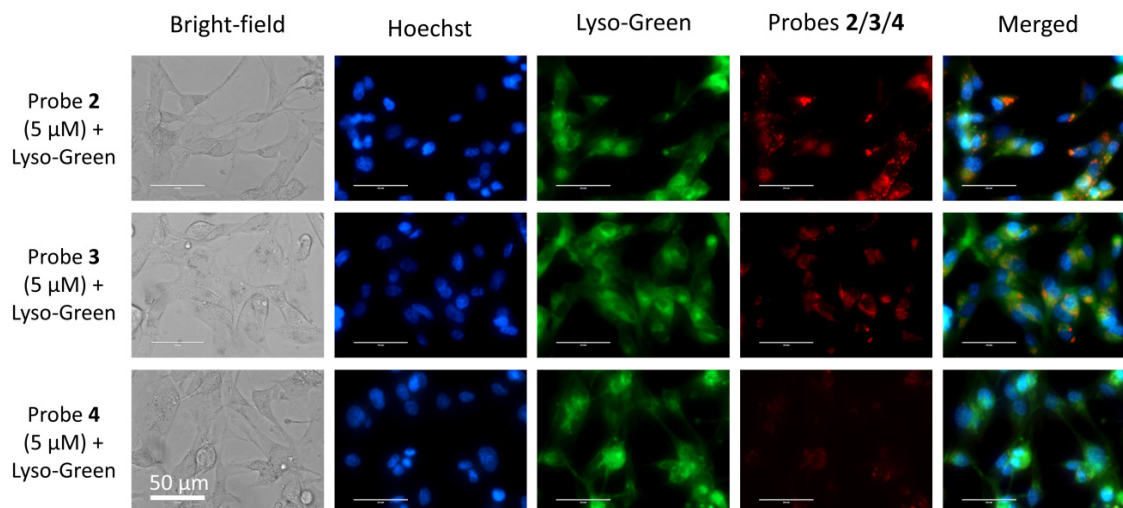


Figure 6.8. Live cell fluorescence images of probes **2**, **3**, and **4** in MDA-MB-231 cells. Cells incubated with 5 μ M of respective probes for 2 h, post serum starvation (2 h) and imaged for co-localization with 1 μ M LysoSensor Green and (1 μ g/mL) Hoechst 33342 stains. All images were acquired at 60X magnification using inverted fluorescence microscope (AMF-4306, EVOSfl, AMG).

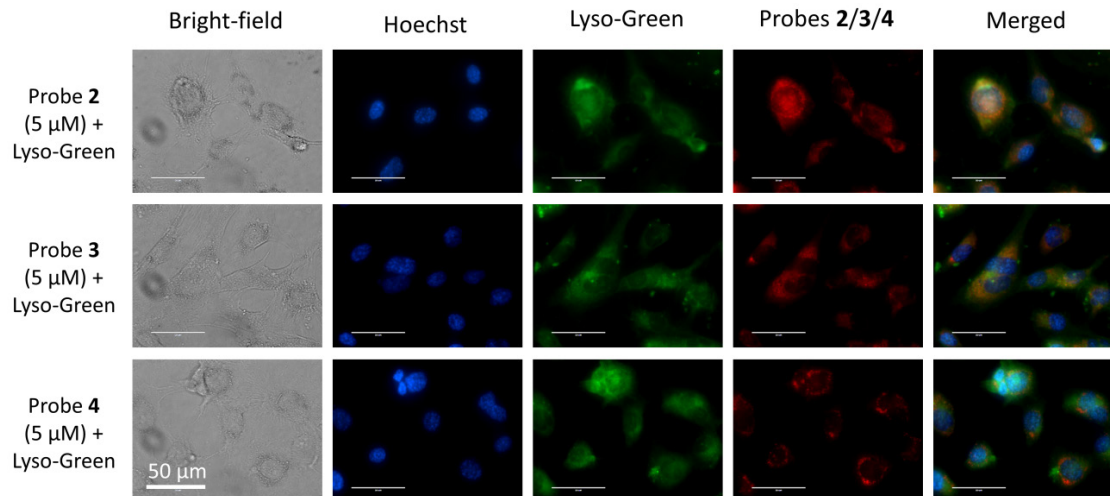


Figure 6.9. Live cell fluorescence images of probes **2**, **3**, and **4** in HUVEC-C cells. Cells were incubated with 5 μ M of respective probes for 2 h, post serum starvation (2 h) and imaged for co-localization with 1 μ M LysoSensor Green and (1 μ g/mL) Hoechst 33342 stains. Images were acquired using the using inverted fluorescence microscope (AMF-4306, EVOSfl, AMG) at 60X magnification.

To understand the differences of fluorescence responses in buffers and in cells, cellular uptake efficiency of the three probes was measured using HUVEC-C cells (Figure 6.10 B). We found that probe 2 has much higher cellular uptake efficiency (more than 30%) at all three concentrations compared with probes 3 and 4. Probe 3 has moderate cellular uptake efficiency (18%) at 5 μM , but there are only 8% and 4% of probe 3 were taken by the cells at 15 μM and 25 μM , respectively. In case of probe 4, the cellular uptake efficiencies were only 10%, 3% and 3% for incubation concentration of 5 μM , 15 μM and 25 μM , respectively. This low cellular uptake of probe 4 could be concluded as the main reason for its relatively weak intracellular fluorescence signals.

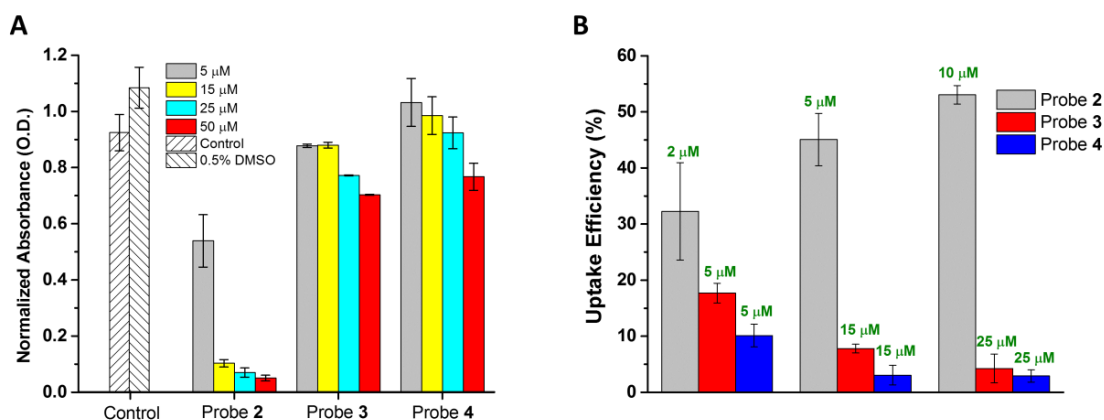


Figure 6.10. The cytotoxicity (A) and cellular uptake efficiency (B) of probes 2, 3 and 4 at different concentrations. (A) Cytotoxicity and cell proliferation effect of were tested by MTS assay. The MDA-MB-231 cells were incubated with 5-50 μM of probes 2, 3 and 4 for 72 h and cell viability was measured by adding MTS reagent and measuring the formation of formazon at 490 nm. Error bars indicate \pm S.D. (B) The cellular uptake efficiency was calculated as the percentage of probe taken up by cells out of total amount of probe in initial incubation solution.

We have further examined the pH dependency of the probes inside the living cells. The intracellular pH of HUVEC-C cells were adjusted using nigericin (5 $\mu\text{g mL}^{-1}$) in pH

5.0, 5.5, 6.0, and 7.5 buffer solutions¹⁸⁻²⁰. Even though probe **4** exhibited very weak fluorescence in cells near physiological pH (pH 7.5), its fluorescence intensity was significantly enhanced as the intracellular pH decreased to 5.0 (Figure 6.11). This turn-on response of probe **4** to acidic intracellular pH indicates that it is sensitive to pH inside the living cells, following the same ICT and potential PET mechanisms as previously described. In addition, commercial probe LysoSensor Green did not display any obvious change of fluorescence to pH changes. Probes **2** and **3** displayed similar but less fluorescence enhancements when the intracellular pH decreased from 7.5 to 5.0 (data not shown). This difference may be due to the fact that probe **4** has higher pKa value and better water solubility than probes **2** and **3**.

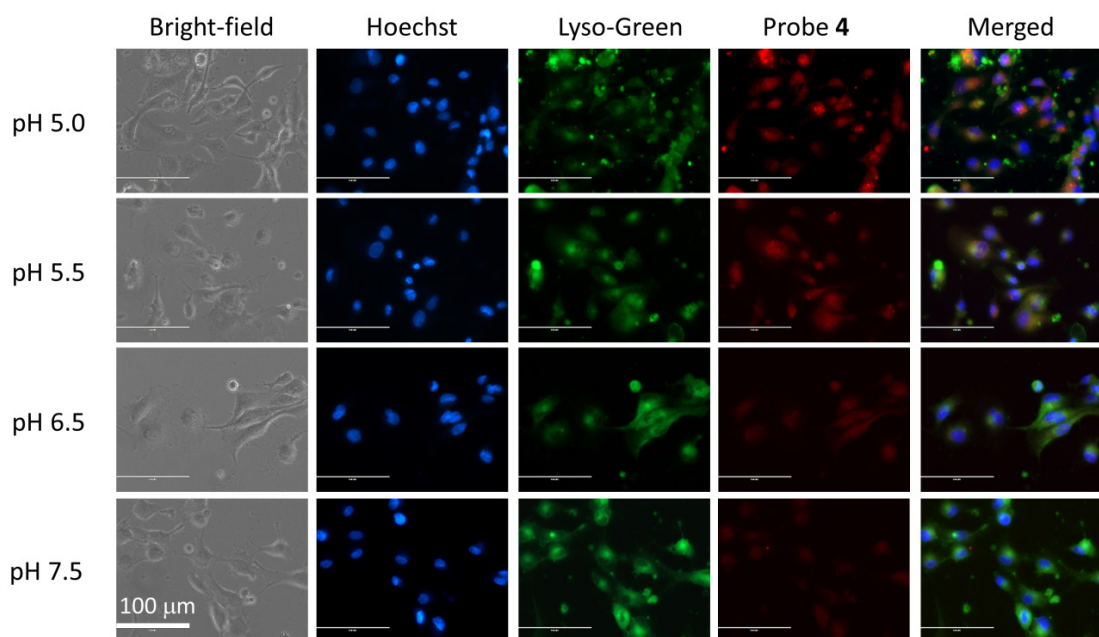


Figure 6.11. Fluorescence images of HUVEC-C cells incubated with 15 μ M probe **4** at different pH values. 1 μ M LysoSensor Green and 1 μ g/mL Hoechst 33342 were used

as co-stains. Images were acquired using the using inverted fluorescence microscope (AMF-4306, EVOSfl, AMG) at 40X magnification.

6.4 Conclusion

Based on modulation of ICT and/or PET mechanisms of the functionalizing groups to the fluorescent BODIPY core, four intracellular fluorescent probes were prepared, showing distinct responses to pH changes. The pH sensitive morpholine-functionalized fluorescent probe **1** displays unusual fluorescence turn-on response at basic pH in aqueous solutions, and quenched fluorescence in acidic condition via the d-PET effect from protonated morpholine moieties to the BODIPY cores. Whereas the lysosomal pH probes **2**, **3**, and **4** display extremely low fluorescent at neutral pH due to ICT and potential PET effects from the piperazine moieties to BODIPY cores, and become highly fluorescent at low pHs. All four probes are photostable, cell-permeable, and showed a potential non-invasive method with deep-red fluorescence and low background for monitoring intracellular/lysosomal pH changes inside of living cells.

6.5 Reference

1. Han, J.; Burgess, K., Fluorescent Indicators for Intracellular pH. *Chemical Reviews* **2010**, *110*, 2709-28.
2. Zhang, J.; Yang, M.; Li, C.; Dorh, N.; Xie, F., et al., Near-infrared fluorescent probes based on piperazine-functionalized BODIPY dyes for sensitive detection of lysosomal pH. *Journal of Materials Chemistry B* **2015**, *3*, 2173-84.
3. Wang, L.; Xiao, Y.; Tian, W.; Deng, L., Activatable Rotor for Quantifying Lysosomal Viscosity in Living Cells. *Journal of the American Chemical Society* **2013**, *135*, 2903-6.

4. Galindo, F.; Burguete, M. I.; Vigarra, L.; Luis, S. V.; Kabir, N., et al., Synthetic macrocyclic peptidomimetics as tunable pH probes for the fluorescence imaging of acidic organelles in live cells. *Angewandte Chemie-International Edition* **2005**, *44*, 6504-8.
5. Becke, A. D., A new mixing of hartree-fock and local density-functional theories. *Journal of Chemical Physics* **1993**, *98*, 1372-7.
6. Bolte, S.; Cordelieres, F. P., A guided tour into subcellular colocalization analysis in light microscopy. *Journal of Microscopy-Oxford* **2006**, *224*, 213-32.
7. Zhu, S.; Zhang, J.; Vegesna, G. K.; Pandey, R.; Luo, F.-T., et al., One-pot efficient synthesis of dimeric, trimeric, and tetrameric BODIPY dyes for panchromatic absorption. *Chemical Communications* **2011**, *47*, 3508-10.
8. Ying, L.-Q.; Branchaud, B. P., Selective labeling and monitoring pH changes of lysosomes in living cells with fluorogenic pH sensors. *Bioorganic & Medicinal Chemistry Letters* **2011**, *21*, 3546-9.
9. Li, G.; Zhu, D.; Xue, L.; Jiang, H., Quinoline-Based Fluorescent Probe for Ratiometric Detection of Lysosomal pH. *Organic Letters* **2013**, *15*, 5020-3.
10. Wang, X.; Ma, X.; Yang, Z.; Zhang, Z.; Wen, J., et al., An NBD-armed tetraaza macrocyclic lysosomal-targeted fluorescent probe for imaging copper(II) ions. *Chemical Communications* **2013**, *49*, 11263-5.
11. Zhu, H.; Fan, J.; Xu, Q.; Li, H.; Wang, J., et al., Imaging of lysosomal pH changes with a fluorescent sensor containing a novel lysosome-locating group. *Chemical Communications* **2012**, *48*, 11766-8.
12. Hasegawa, T.; Kondo, Y.; Koizumi, Y.; Sugiyama, T.; Takeda, A., et al., A highly sensitive probe detecting low pH area of HeLa cells based on rhodamine B modified beta-cyclodextrins. *Bioorganic & Medicinal Chemistry* **2009**, *17*, 6015-9.

13. Hu, Z.-Q.; Li, M.; Liu, M.-D.; Zhuang, W.-M.; Li, G.-K., A highly sensitive fluorescent acidic pH probe based on rhodamine B diethyl-2-aminobutenedioate conjugate and its application in living cells. *Dyes and Pigments* **2013**, *96*, 71-5.
14. Lee, H.; Akers, W.; Bhushan, K.; Bloch, S.; Sudlow, G., et al., Near-Infrared pH-Activatable Fluorescent Probes for Imaging Primary and Metastatic Breast Tumors. *Bioconjugate Chemistry* **2011**, *22*, 777-84.
15. Li, C.; Greenwood, T. R.; Glunde, K., Glucosamine-bound near-infrared fluorescent probes with lysosomal specificity for breast tumor imaging. *Neoplasia* **2008**, *10*, 389-98.
16. Wang, X.; Nguyen, D. M.; Yanez, C. O.; Rodriguez, L.; Ahn, H.-Y., et al., High-Fidelity Hydrophilic Probe for Two-Photon Fluorescence Lysosomal Imaging. *Journal of the American Chemical Society* **2010**, *132*, 12237-9.
17. Vegesna, G. K.; Janjanam, J.; Bi, J.; Luo, F.-T.; Zhang, J., et al., pH-activatable near-infrared fluorescent probes for detection of lysosomal pH inside living cells. *Journal of Materials Chemistry B* **2014**, *2*, 4500-8.
18. Thomas, J. A.; Buchsbaum, R. N.; Zimniak, A.; Racker, E., Intracellular pH measurements in ehrlich ascites tumor-cells utilizing spectroscopic probes generated insitu. *Biochemistry* **1979**, *18*, 2210-8.
19. Llopis, J.; McCaffery, J. M.; Miyawaki, A.; Farquhar, M. G.; Tsien, R. Y., Measurement of cytosolic, mitochondrial, and Golgi pH in single living cells with green fluorescent proteins. *Proceedings of the National Academy of Sciences of the United States of America* **1998**, *95*, 6803-8.
20. Han, J.; Loudet, A.; Barhoumi, R.; Burghardt, R. C.; Burgess, K., A ratiometric pH reporter for imaging protein-dye conjugates in living cells. *Journal of the American Chemical Society* **2009**, *131*, 1642-3.

Chapter 7 Summary and perspectives

In the field of protein folding and aggregation, considerable process has been made in characterization of the native proteins and the amyloid fibrils. However, our knowledge of amorphous aggregates is still very limit, although they have been constantly observed in protein aggregation and disease processes. In this dissertation, we have focused on characterizing the amorphous aggregates formed from two globular proteins (lysozyme and BSA) and one intrinsically disordered peptide (A β). Among these lysozyme and A β have been linked to human amyloid diseases. Two types of posttranslational modifications, disulfide bonding and side-chain acetylation, were demonstrated to alter the morphologies of protein aggregates. In addition, diverse amorphous aggregates using literature reported conditions were also prepared to investigate the relationship between aggregate structure and cytotoxicity.

In chapter 3, the scrambling of disulfide bonds in lysozyme and BSA were observed in aggregation of these proteins at condition close to physiological. Even though both protein aggregates were amorphous in morphology, the two structures are very distinct in terms of size, shape, flexibility and surface hydrophobicity as reflected by spectral characteristics. The differences between the two types of structures may be a consequence of protein size, reduction level, and the structure properties of the local environment near disulfide bonds. Since lysozyme is an amyloidogenic protein while BSA is not, observations of aggregates from these two different types of proteins could give insight into the aggregation pathways that may be relevant for several other globular proteins.

In chapter 4, we blocked the positive charge on the two lysine residues of A β peptide, K16 and K28 by acetylation. Interestingly, only acetylation on K16 was able to affect molecular property and amyloid formation of A β . Acetylation on K16 position can significantly increase the hydrophobicity of residues 16-21, which consequently disrupts the amyloid fibril formation. Whereas, the peptides with single acetylation on K28 can still assemble into typical amyloid fibrils and were confirmed by ThT fluorescence and SEM images. Furthermore, the amorphous aggregates formed from heterogeneous mixtures of WT and acetylated peptides exhibit severe cytotoxicity to SH-SY5Y cells, indicating the heterogeneity of aggregates may be central to cellular toxicity.

After generating diverse amorphous aggregates as per reported literature that are different in size, morphology, and cytotoxicity, we noticed that many amorphous structures were subtly different. We have generated eleven different aggregates from two proteins, lysozyme and BSA. These aggregates varied in morphology, size, flexibility, and hydrophobicity. The aggregates were then compared for surface hydrophobicity, structural flexibility, and cytotoxicity, which provide evidence of heterogeneous population of protein aggregates being critical for cytotoxicity. We observed that the conformational changes of native monomer that occur in the early stage of aggregation process is essential for toxicity. Most toxic species are structurally flexible, however, no clear correlation was found between cytotoxicity and extent of hydrophobicity. Therefore, the observed cytotoxicity of different structures may result from the heterogeneous dynamics of the aggregation process.

We are also facing problems similar to many research groups focusing on protein aggregation: overlapping biochemical/biophysical properties of the protein aggregates

generated under different conditions were observed with no clear correlations to cytotoxicity. To have a better understanding of protein aggregation and its relationship to cellular toxicity, we need to first, develop high resolution structure analysis techniques of protein aggregates. Recently, the aggregation intermediates or oligomers are recognized as the major toxic species. But these structures are usually highly unstable, which cannot be analyzed using traditional X-Ray crystallography or NMR methods. Fluorescent probes used in our research are sensitive to certain properties, but still not able to provide precise description of the structure. Some conformation specific antibodies that have been developed from *in vivo* samples are applied in detection of amyloid structure, but these antibodies were not suitable in detection of smaller oligomers or other species. Another problem in the field is the disconnection between *in vitro* and *in vivo* studies. Although with the help of modern technology, people can prepare almost all kinds of protein aggregates in the laboratory, the ultimate goal is to understand the *in vivo* disease process. *In vivo* proteins have higher level of heterogeneousness and posttranslational modifications that are absent *in vitro*. This is also why we have performed acetylation study of A β peptide in chapter 4. In addition, the nature of many naturally derived protein assemblies still remains unclear. Although more work is needed, this dissertation research is a step in the direction to correlate different structural aggregates generated from same protein to cellular toxicities.

Appendix A Supporting Information for Chapter 4

Table A1. The top 10 most stable ANS-WT A β 42 complexes analyzed by AutoDock Vina and DSX (scores in kcal/mol).

Vina Ranking	Main Interacting Residues	Vina Score	Z_{vina}	DSX Score	Z_{dsx}
1	10 and 14	-6.1	-2.48	-12.386	-1.120
2	10 and 14	-5.5	-0.91	-8.264	-0.301
3	40-42	-5.2	-0.13	-1.975	0.950
4	10 and 14	-5.1	0.13	-6.066	0.137
5	40-42	-5.0	0.39	-1.402	1.064
6	40-42	-5.0	0.39	-8.916	-0.430
7	40-42	-4.9	0.65	-7.941	-0.236
8	40-42	-4.9	0.65	1.946	1.730
9	40-42	-4.9	0.65	-8.171	-0.282
10	17 and 18	-4.9	0.65	-14.353	-1.512

Table A2. The top 10 most stable ANS-K16Ac A β 42 complexes analyzed by AutoDock Vina and DSX (scores in kcal/mol).

Vina Ranking	Main Interacting Residues	Vina Score	Z_{vina}	DSX Score	Z_{dsx}
1	10 and 14	-6.1	-1.958	-12.311	-1.740
2	10 and 14	-5.5	-0.636	-8.049	-0.519
3	10	-5.5	-0.636	-9.119	-0.826
4	10	-5.2	0.024	-5.428	0.231
5	31	-5.2	0.024	-3.362	0.822
6	10 and 14	-5.1	0.245	-6.244	-0.003
7	15 and 19	-5.0	0.465	-3.56	0.766
8	15 and 19	-4.7	1.126	-7.425	-0.341
9	19	-4.6	1.346	-0.612	1.610

Table A3. The top 10 most stable ANS-K28Ac A β 42 complexes analyzed by AutoDock Vina and DSX (scores in kcal/mol).

Vina Ranking	Main Interacting Residues	Vina Score	Z_{vina}	DSX Score	Z_{dsx}
1	10 and 14	-6.1	-2.041	-12.312	-1.390
2	10	-5.5	-0.816	-8.888	-0.777
3	10 and 14	-5.3	-0.408	-2.478	0.371
4	40-42	-5.2	-0.204	-2.234	0.415
5	40-42	-5.0	0.204	-0.274	0.766
6	17 and 18	-4.9	0.408	-13.65	-1.629
7	40-42	-4.7	0.816	-1.474	0.551
8	15	-4.6	1.021	-1.478	0.550
9	40-42	-4.6	1.021	1.838	1.144

Table A4. The top 10 most stable ANS-KKAc A β 42 complexes analyzed by AutoDock Vina and DSX (scores in kcal/mol).

Vina Ranking	Main Interacting Residues	Vina Score	Z_{vina}	DSX Score	Z_{dsx}
1	10 and 14	-6.1	-2.179	-12.339	-1.468
2	10 and 14	-5.5	-0.567	-8.092	-0.446
3	10	-5.5	-0.567	-9.018	-0.669
4	10 and 14	-5.3	-0.030	-5.683	0.133
5	40-42	-5.2	0.239	-2.514	0.896
6	40-42	-5.1	0.507	-9.67	-0.826
7	40-42	-5	0.776	-0.645	1.345
8	40-42	-5	0.776	-7.496	-0.303
9	19	-4.9	1.045	-0.672	1.339

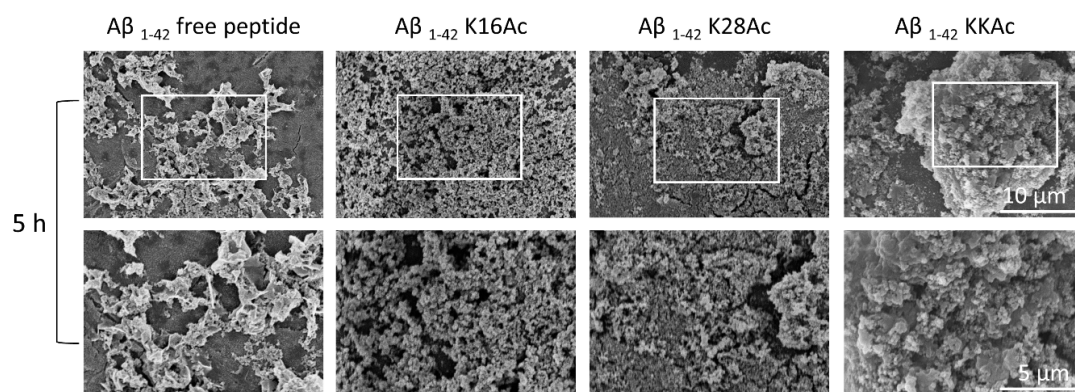
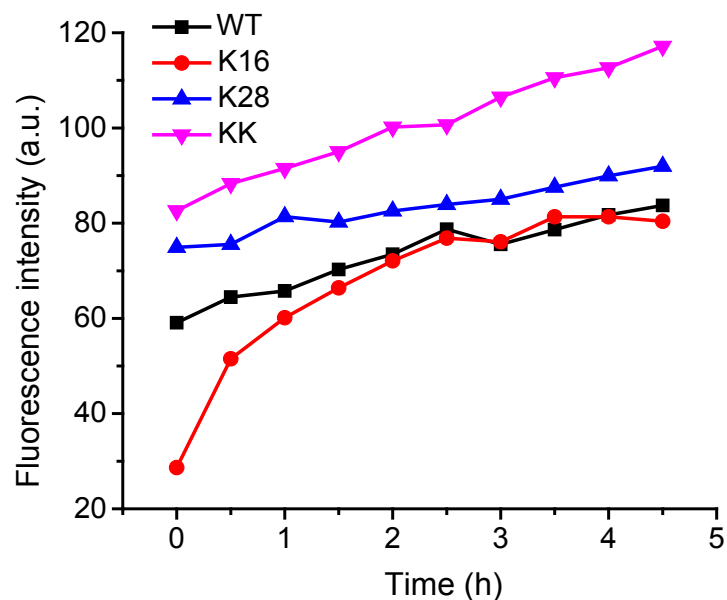


Figure A1. Fibrillation/aggregation of WT and acetylation modified peptides in the first 5 hours was monitored by ThT. Ten μM of peptide samples were incubates with 10 μM of ThT. Fluorescence emission spectra was collected at 460-700 nm with excitation at 450 nm. Peak intensities at 487 nm were plotted in function of time. SEM images of samples after 5 hours of incubation. Scale bars are 10 μm and 5 μm for top panel and bottom panel, respectively.

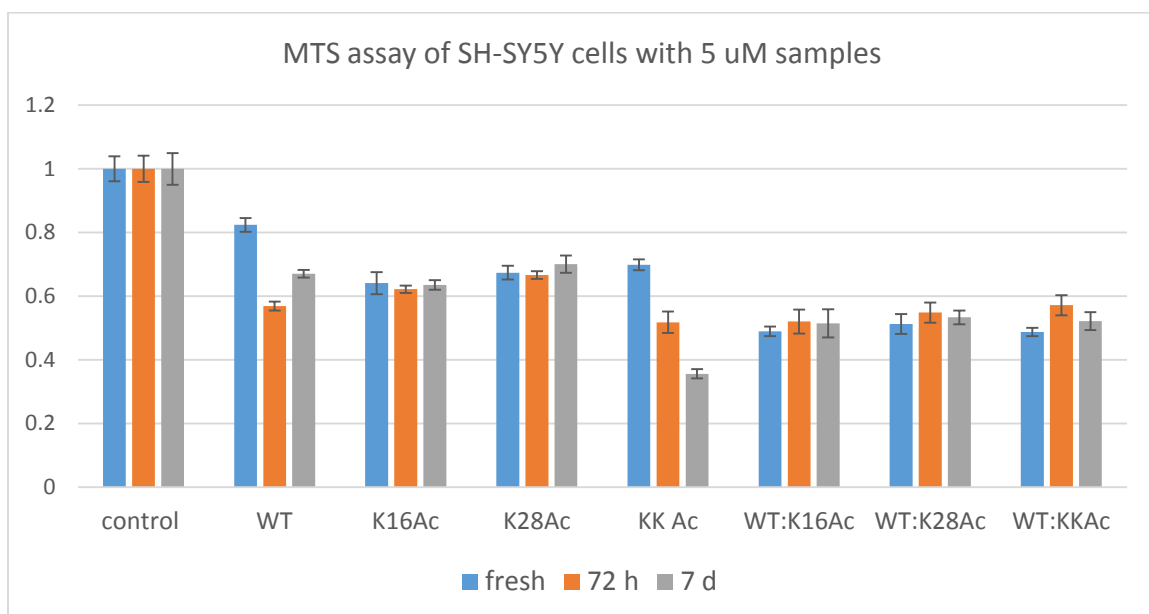
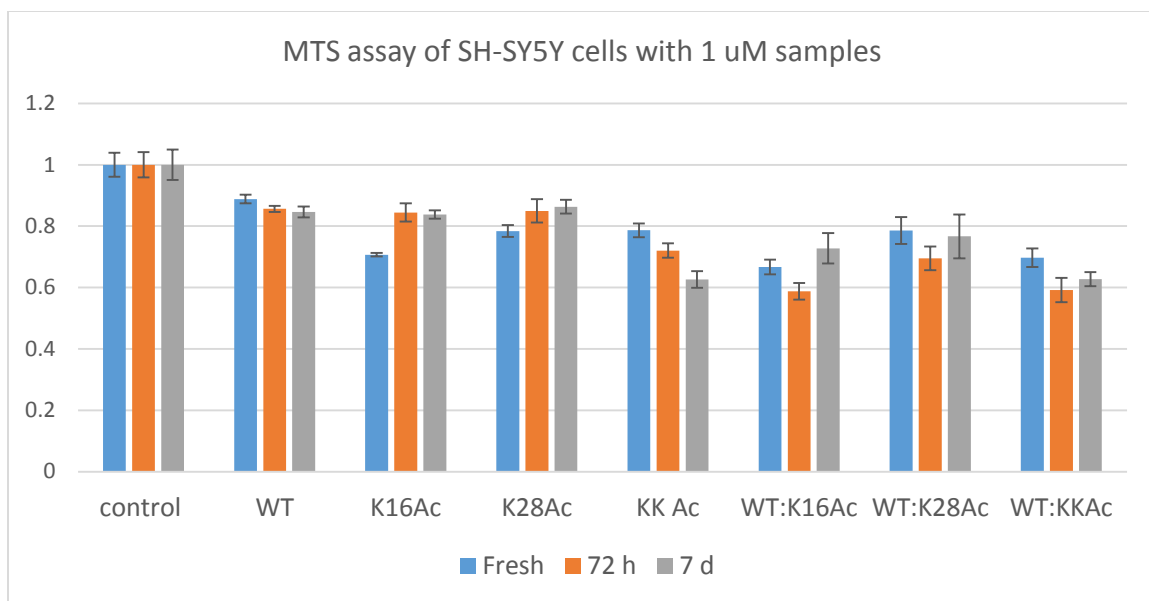


Figure A2. Cell viability of SH-SY5Y cells with $A\beta_{42}$ fibrils or aggregates. The free $A\beta_{42}$ or acetylation modified $A\beta_{42}$ peptides were incubated at pH 7.4 and 37 °C for 0 h, 72 h, or 7 d, and then added to SH-SY5Y cells to a final concentration of 1 or 5 μ M. Cell proliferation were measured after 48 h incubation with samples by taking absorbance at 490 nm. Error bars = \pm S.D.

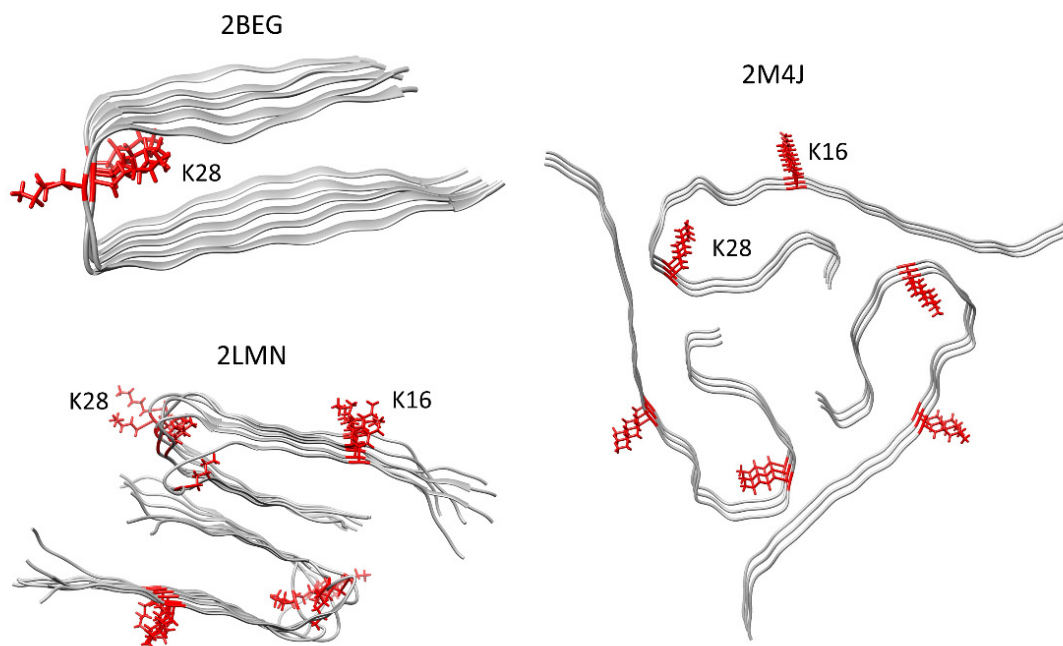


Figure A3. Atomic models of U-shape $A\beta_{42}$ fibrils (2BEG) and $A\beta_{40}$ fibrils (2LMN and 2M4J). The two lysine residues K16 and K28 are shown in red stick structures. In fibril model 2BEG, the disordered first 16 N-terminal residues are omitted. The structures were generated using USCF Chimera.

Appendix B Supporting Information for Chapter 5

Table B1. Sample preparation conditions of all the 17 lysozyme and BSA samples

Sample #	structure	condition
1	Amyloid	Samples contain 1 mM lysozyme in HCl solution (pH 2.0) were incubated at 65 °C for 7 days ¹
2 & 12	Amorphous aggregates	Samples contain 40 µM lysozyme (#2) or BSA (#12) in phosphate buffer (pH 7.2, 20 mM, with 150 mM NaCl) were incubated at 37 °C for 7 days ²
3 & 4	Amorphous aggregates	Samples contain 699 µM lysozyme in Phosphate buffer (pH 7.4, 100 mM) were incubated at 56 °C (#3) and 25 °C (#4) ³
5-6	Amorphous aggregates	Samples contain 80 µM (#5) and 120 µM (#6) lysozyme in Phosphate buffer (pH 7.0, 50 mM) were incubated at 25 °C ⁴
7-9 15-17	Amorphous aggregates	Samples contain 40 µM (#7, #15), 80 µM (#8, #16) and 120 µM (#9, #17) lysozyme in Phosphate-NaOH buffer (pH 12.0, 50 mM) with 0M (#7-9) or 14 mM (#15-17) of SDS were incubated at 25 °C ⁴
10	Amyloid	Samples contain 100 µM BSA in glycine-HCl buffer (pH 3.0, 50 mM , with 50 mM NaCl) were incubated at 65 °C for 4 h then followed by room temperature incubation for 30 days ⁵
11	Amorphous aggregates	Samples contain 140 uM lysozyme in HCl solution (pH 2.0, with 136.7 mM NaCl, 2.68 mM KCl, and 4 mM

DTT). Samples were first mixed via vortex and then incubated were incubated at 55 °C for 30 days⁶

13	protofibrils	Samples contain 37.6 μM BSA in Tris-HCl buffer (pH 7.4, 20 mM) were incubated at 70 °C for 4 days ⁷
14	Amorphous aggregates	Samples contain 7.5 uM BSA in phosphate buffer (pH 8.9, 0.1 M) were incubated at 62 °C over 10 h ⁸

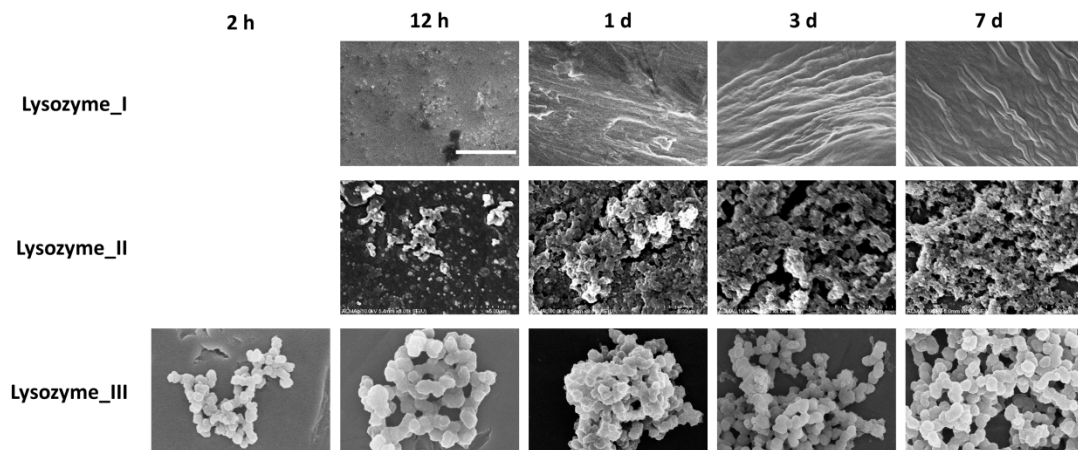


Figure B1. SEM images of lysozyme_I, II, and III. Scale bars = 5 μm .

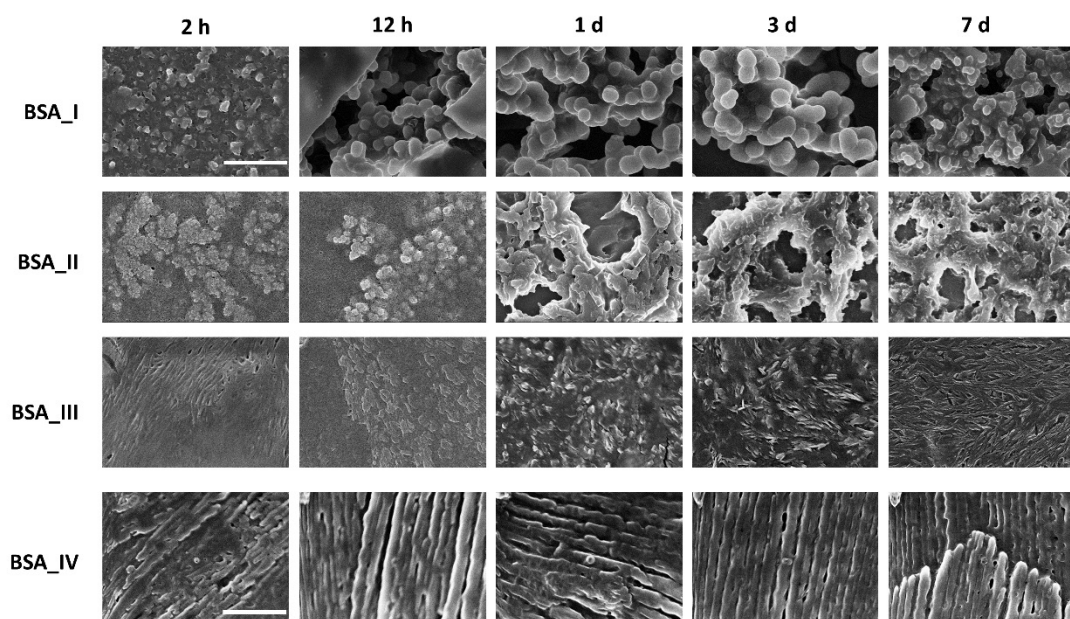


Figure B2. SEM images of BSA_I, II, III, and IV. Scale bars = 5 μm (for BSA_I, II, and III) or 10 μm (for BSA_IV).

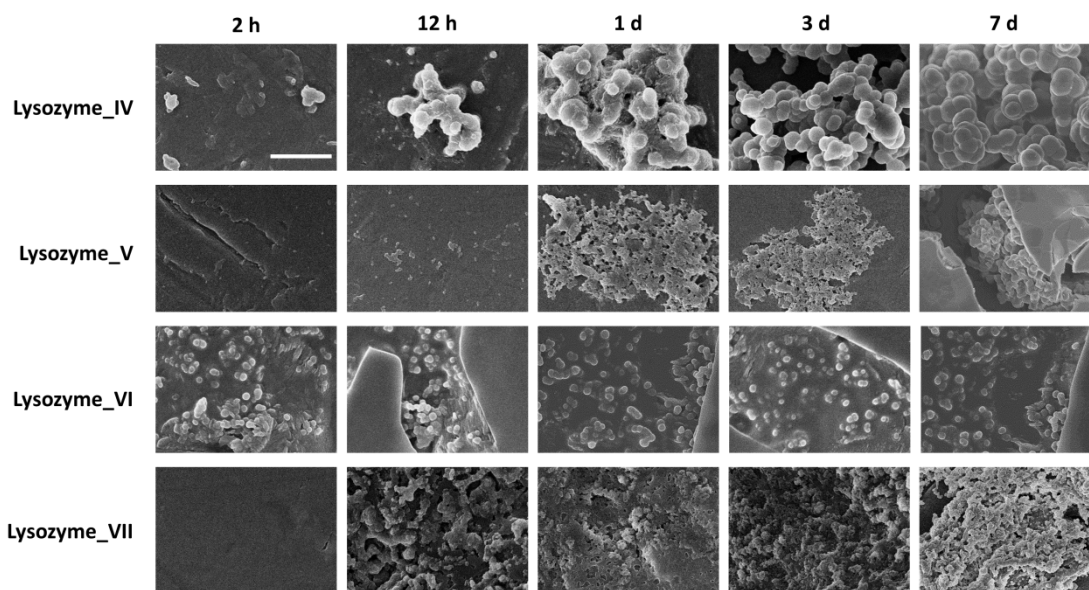


Figure B3. SEM images of lysozyme_IV, V, IV and VII. Scale bars = 5 μ m.

1. Krebs, M. R. H.; Wilkins, D. K.; Chung, E. W.; Pitkeathly, M. C.; Chamberlain, A. K., et al., Formation and seeding of amyloid fibrils from wild-type hen lysozyme and a peptide fragment from the beta-domain. *Journal of Molecular Biology* **2000**, *300*, 541-9.
2. Yang, M.; Dutta, C.; Tiwari, A., Disulfide-Bond Scrambling Promotes Amorphous Aggregates in Lysozyme and Bovine Serum Albumin. *Journal of Physical Chemistry B* **2015**, *119*, 3969-81.
3. Navarra, G.; Troia, F.; Militello, V.; Leone, M., Characterization of the nucleation process of lysozyme at physiological pH: Primary but not sole process. *Biophysical chemistry* **2013**, *177-178*, 24-33.
4. Kumar, S.; Ravi, V. K.; Swaminathan, R., How do surfactants and DTT affect the size, dynamics, activity and growth of soluble lysozyme aggregates? *Biochem. J.* **2008**, *415*, 275-88.

5. Bhattacharya, M.; Jain, N.; Mukhopadhyay, S., Insights into the mechanism of aggregation and fibril formation from bovine serum albumin. *Journal of Physical Chemistry B* **2011**, *115*, 4195-205.
6. Wang, S. S. S.; Liu, K.-N.; Wang, B.-W., Effects of dithiothreitol on the amyloid fibrillogenesis of hen egg-white lysozyme. *European Biophysics Journal with Biophysics Letters* **2010**, *39*, 1229-42.
7. Holm, N. K.; Jespersen, S. K.; Thomassen, L. V.; Wolff, T. Y.; Sehgal, P., et al., Aggregation and fibrillation of bovine serum albumin. *Biochimica Et Biophysica Acta-Proteins and Proteomics* **2007**, *1774*, 1128-38.
8. Vetri, V.; D'Amico, M.; Fodera, V.; Leone, M.; Ponzoni, A., et al., Bovine Serum Albumin protofibril-like aggregates formation: Solo but not simple mechanism. *Archives of Biochemistry and Biophysics* **2011**, *508*, 13-24.

Copyright permissions

This letter is for Figure 1.2.

Publication contents reuse permission from Annual Reviews



RightsLink®

Home

Create Account

Help



Title: THEORY OF PROTEIN FOLDING:
The Energy Landscape
Perspective

Author: José Nelson Onuchic, Zaida
Luthey-Schulten, Peter G.
Wolynes

Publication: Annual Review of Physical
Chemistry

Publisher: Annual Reviews

Date: Oct 1, 1997

Copyright © 1997, Annual Reviews

LOGIN
If you're a copyright.com user, you can login to RightsLink using your copyright.com credentials. Already a RightsLink user or want to [learn more?](#)

Permission Not Required

Material may be republished in a thesis / dissertation without obtaining additional permission from Annual Reviews, providing that the author and the original source of publication are fully acknowledged.

BACK

CLOSE WINDOW

Copyright © 2016 [Copyright Clearance Center, Inc.](#) All Rights Reserved. [Privacy statement.](#) [Terms and Conditions.](#) Comments? We would like to hear from you. E-mail us at customercare@copyright.com

This letter is for Figure 1.3.

Publication contents reuse permission from Nature Publication Group (NPG)

1/19/2016

RightsLink Printable License

**NATURE PUBLISHING GROUP LICENSE
TERMS AND CONDITIONS**

Jan 19, 2016

This is a License Agreement between Mu Yang ("You") and Nature Publishing Group ("Nature Publishing Group") provided by Copyright Clearance Center ("CCC"). The license consists of your order details, the terms and conditions provided by Nature Publishing Group, and the payment terms and conditions.

All payments must be made in full to CCC. For payment instructions, please see information listed at the bottom of this form.

License Number	3792600582099
License date	Jan 19, 2016
Licensed content publisher	Nature Publishing Group
Licensed content publication	Nature Structural and Molecular Biology
Licensed content title	Converging concepts of protein folding : in vitro: and : in vivo
Licensed content author	F Ulrich Hartl and Manajit Hayer-Hartl
Licensed content date	Jun 3, 2009
Volume number	16
Issue number	6
Type of Use	reuse in a dissertation / thesis
Requestor type	academic/educational
Format	print and electronic
Portion	figures/tables/illustrations
Number of figures/tables/illustrations	1
High-res required	no
Figures	Figure 1 - Energy landscape scheme of protein folding and aggregation.
Author of this NPG article	no
Your reference number	None
Title of your thesis / dissertation	THE EFFECT OF POSTTRANSLATIONAL MODIFICATIONS ON PROTEIN AGGREGATION, MORPHOLOGY, AND TOXICITY
Expected completion date	Jan 2016
Estimated size (number of pages)	180
Total	0,00 USD
Terms and Conditions	

Terms and Conditions for Permissions

Nature Publishing Group hereby grants you a non-exclusive license to reproduce this material for this purpose, and for no other use, subject to the conditions below:

<https://s100.copyright.com/AppDispatchServlet>

This letter is for Figure 1.4.

Publication contents reuse permission from American Chemical Society (ACS)

9/24/2015 Rightslink® by Copyright Clearance Center

 **Copyright Clearance Center**  **RightsLink®** [Home](#) [Create Account](#) [Help](#)  **Live Chat**

 **ACS Publications** Most Trusted. Most Cited. Most Read. **Title:** Molecular Structures of Amyloid and Prion Fibrils: Consensus versus Controversy

Author: Robert Tycko, Reed B. Wickner

Publication: Accounts of Chemical Research

Publisher: American Chemical Society

Date: Jul 1, 2013

Copyright © 2013, American Chemical Society

[LOGIN](#)

If you're a **copyright.com** user, you can login to RightsLink using your copyright.com credentials. Already a **RightsLink** user or want to [learn more?](#)

PERMISSION/LICENSE IS GRANTED FOR YOUR ORDER AT NO CHARGE

This type of permission/license, instead of the standard Terms & Conditions, is sent to you because no fee is being charged for your order. Please note the following:

- Permission is granted for your request in both print and electronic formats, and translations.
- If figures and/or tables were requested, they may be adapted or used in part.
- Please print this page for your records and send a copy of it to your publisher/graduate school.
- Appropriate credit for the requested material should be given as follows: "Reprinted (adapted) with permission from (COMPLETE REFERENCE CITATION). Copyright (YEAR) American Chemical Society." Insert appropriate information in place of the capitalized words.
- One-time permission is granted only for the use specified in your request. No additional uses are granted (such as derivative works or other editions). For any other uses, please submit a new request.

If credit is given to another source for the material you requested, permission must be obtained from that source.

[BACK](#) [CLOSE WINDOW](#)

Copyright © 2015 [Copyright Clearance Center, Inc.](#) All Rights Reserved. [Privacy statement](#). [Terms and Conditions](#). Comments? We would like to hear from you. E-mail us at customercare@copyright.com

This letter is for Table 1.1 and Figure 1.6.

Publication contents reuse permission from John Wiley and Sons

1/19/2016

RightsLink Printable License

**JOHN WILEY AND SONS LICENSE
TERMS AND CONDITIONS**

Jan 19, 2016

This Agreement between Mu Yang ("You") and John Wiley and Sons ("John Wiley and Sons") consists of your license details and the terms and conditions provided by John Wiley and Sons and Copyright Clearance Center.

License Number	3792601263979
License date	Jan 19, 2016
Licensed Content Publisher	John Wiley and Sons
Licensed Content Publication	Proteins: Structure, Function and Bioinformatics
Licensed Content Title	Disulfide bonds in amyloidogenesis diseases related proteins
Licensed Content Author	Yang Li,Juan Yan,Xin Zhang,Kun Huang
Licensed Content Date	Aug 18, 2013
Pages	12
Type of use	Dissertation/Thesis
Requestor type	University/Academic
Format	Print and electronic
Portion	Figure/table
Number of figures/tables	1
Original Wiley figure/table number(s)	Table 1. Disulfide Bonds in Amyloidogenesis Diseases Related Proteins Figure 1. The transformation of non-toxic PrPc (blue) into toxic PrPsc (red),
Will you be translating?	No
Title of your thesis / dissertation	THE EFFECT OF POSTTRANSLATIONAL MODIFICATIONS ON PROTEIN AGGREGATION, MORPHOLOGY, AND TOXICITY
Expected completion date	Jan 2016
Expected size (number of pages)	180
Requestor Location	Mu Yang 1908 Woodmar Dr APT E HOUGHTON, MI 49931 United States Attn: Mu Yang
Billing Type	Invoice
Billing Address	Mu Yang 1908 Woodmar Dr APT E HOUGHTON, MI 49931 United States Attn: Mu Yang

<https://s100.copyright.com/AppDispatchServlet>

1/5

This letter is for Figure 1.5, Figure 2.7, and Chapter 3.

Publication contents reuse permission from American Chemical Society (ACS)

9/24/2015

Rightslink® by Copyright Clearance Center



RightsLink®

Home

Create Account

Help



Title: Disulfide-Bond Scrambling Promotes Amorphous Aggregates in Lysozyme and Bovine Serum Albumin

Author: Mu Yang, Colina Dutta, Ashutosh Tiwari

Publication: The Journal of Physical Chemistry B

Publisher: American Chemical Society

Date: Mar 1, 2015

Copyright © 2015, American Chemical Society

LOGIN

If you're a [copyright.com](#) user, you can login to RightsLink using your [copyright.com](#) credentials. Already a [RightsLink user](#) or want to [learn more?](#)

PERMISSION/LICENSE IS GRANTED FOR YOUR ORDER AT NO CHARGE

This type of permission/license, instead of the standard Terms & Conditions, is sent to you because no fee is being charged for your order. Please note the following:

- Permission is granted for your request in both print and electronic formats, and translations.
- If figures and/or tables were requested, they may be adapted or used in part.
- Please print this page for your records and send a copy of it to your publisher/graduate school.
- Appropriate credit for the requested material should be given as follows: "Reprinted (adapted) with permission from (COMPLETE REFERENCE CITATION). Copyright (YEAR) American Chemical Society." Insert appropriate information in place of the capitalized words.
- One-time permission is granted only for the use specified in your request. No additional uses are granted (such as derivative works or other editions). For any other uses, please submit a new request.

BACK

CLOSE WINDOW

Copyright © 2015 [Copyright Clearance Center, Inc.](#) All Rights Reserved. [Privacy statement](#). [Terms and Conditions](#). Comments? We would like to hear from you. E-mail us at customer care@copyright.com

This letter is for Table 1.2.

Publication contents reuse permission from John Wiley and Sons

1/19/2016

RightsLink Printable License

**JOHN WILEY AND SONS LICENSE
TERMS AND CONDITIONS**

Jan 19, 2016

This Agreement between Mu Yang ("You") and John Wiley and Sons ("John Wiley and Sons") consists of your license details and the terms and conditions provided by John Wiley and Sons and Copyright Clearance Center.

License Number	3792610188801
License date	Jan 19, 2016
Licensed Content Publisher	John Wiley and Sons
Licensed Content Publication	Angewandte Chemie International Edition
Licensed Content Title	Protein Posttranslational Modifications: The Chemistry of Proteome Diversifications
Licensed Content Author	Christopher T. Walsh,Sylvie Garneau-Tsodikova,Gregory J. Gatto
Licensed Content Date	Nov 3, 2005
Pages	31
Type of use	Dissertation/Thesis
Requestor type	University/Academic
Format	Print and electronic
Portion	Figure/table
Number of figures/tables	1
Original Wiley figure/table number(s)	Table 1: Posttranslational protein modifications at the side chains
Will you be translating?	No
Title of your thesis / dissertation	THE EFFECT OF POSTTRANSLATIONAL MODIFICATIONS ON PROTEIN AGGREGATION, MORPHOLOGY, AND TOXICITY
Expected completion date	Jan 2016
Expected size (number of pages)	180
Requestor Location	Mu Yang 1908 Woodmar Dr APT E HOUGHTON, MI 49931 United States Attn: Mu Yang
Billing Type	Invoice
Billing Address	Mu Yang 1908 Woodmar Dr APT E HOUGHTON, MI 49931 United States Attn: Mu Yang

<https://s100.copyright.com/AppDispatchServlet>

1/5

This letter is for Table 2.1

Publication contents reuse permission from John Wiley and Sons

1/19/2016

RightsLink Printable License

**JOHN WILEY AND SONS LICENSE
TERMS AND CONDITIONS**

Jan 19, 2016

This Agreement between Mu Yang ("You") and John Wiley and Sons ("John Wiley and Sons") consists of your license details and the terms and conditions provided by John Wiley and Sons and Copyright Clearance Center.

License Number	3792610555249
License date	Jan 19, 2016
Licensed Content Publisher	John Wiley and Sons
Licensed Content Publication	FEBS Journal
Licensed Content Title	The Yin and Yang of protein folding
Licensed Content Author	Thomas R. Jahn,Sheena E. Radford
Licensed Content Date	Nov 10, 2005
Pages	9
Type of use	Dissertation/Thesis
Requestor type	University/Academic
Format	Print and electronic
Portion	Figure/table
Number of figures/tables	1
Original Wiley figure/table number(s)	Table 1
Will you be translating?	No
Title of your thesis / dissertation	THE EFFECT OF POSTTRANSLATIONAL MODIFICATIONS ON PROTEIN AGGREGATION, MORPHOLOGY, AND TOXICITY
Expected completion date	Jan 2016
Expected size (number of pages)	180
Requestor Location	Mu Yang 1908 Woodmar Dr APT E HOUGHTON, MI 49931 United States Attn: Mu Yang
Billing Type	Invoice
Billing Address	Mu Yang 1908 Woodmar Dr APT E HOUGHTON, MI 49931 United States Attn: Mu Yang

<https://s100.copyright.com/AppDispatchServlet>

1/5

This letter is for Table 2.1

Publication contents reuse permission from Elsevier

1/19/2016

RightsLink Printable License

**ELSEVIER LICENSE
TERMS AND CONDITIONS**

Jan 19, 2016

This is a License Agreement between Mu Yang ("You") and Elsevier ("Elsevier") provided by Copyright Clearance Center ("CCC"). The license consists of your order details, the terms and conditions provided by Elsevier, and the payment terms and conditions.

All payments must be made in full to CCC. For payment instructions, please see information listed at the bottom of this form.

Supplier	Elsevier Limited The Boulevard, Langford Lane Kidlington, Oxford, OX5 1GB, UK
Registered Company Number	1982084
Customer name	Mu Yang
Customer address	1908 Woodmar Dr HOUGHTON, MI 49931
License number	3792610819983
License date	Jan 19, 2016
Licensed content publisher	Elsevier
Licensed content publication	Methods
Licensed content title	Experimental investigation of protein folding and misfolding
Licensed content author	Christopher M Dobson
Licensed content date	September 2004
Licensed content volume number	34
Licensed content issue number	1
Number of pages	11
Start Page	4
End Page	14
Type of Use	reuse in a thesis/dissertation
Intended publisher of new work	other
Portion	figures/tables/illustrations
Number of figures/tables/illustrations	1
Format	both print and electronic
Are you the author of this Elsevier article?	No
Will you be translating?	No

<https://s100.copyright.com/AppDispatchServlet>

1/6

This letter is for Figure 2.6.

Publication contents reuse permission from W.H. Freeman and Company



Mu Yang <muy@mtu.edu>

Re: New Permissions Request

1 message

McCarty, Michael <Michael.McCarty@macmillan.com>
To: "muy@mtu.edu" <muy@mtu.edu>

Tue, Feb 2, 2016 at 11:53 AM

Hello,

Thank you for your interest. If you wish to use this figure in your dissertation, please include this credit line in close proximity to the figure:

From: BIOCHEMISTRY 8E, by Jeremy M. Berg, John L. Tymoczko, Gregory, J. Gatto, Lubert Stryer, Copyright 2015 by W,H, Freeman and Company, Used by Permission of the publisher.

Please note that the citation references the 8th edition, the most recent, rather than the 7th, which was in your request. We are only able to grant permission for figures from the current edition.

Best Regards,
Michael

Michael McCarty
Permissions Assistant
Higher Education

T 212-375-7198

Michael.McCarty@macmillan.com

<mailto:Felice.Pilchik@macmillan.com>>www.macmillanhighered.com

<<http://www.macmillanhighered.com/>>

<<http://www.macmillanlearning.com/>>

| Bedford/St Martin's | Freeman | Hayden-McNeil | Late Nite Labs | Sapling
Learning | Worth Publishers

One New York Plaza
New York, NY 10004-1562

This letter is for Figure 2.9 and Chapter 6.

Publication contents reuse permission from Royal Society of Chemistry (RSC)

Near-infrared fluorescent probes based on piperazine-functionalized BODIPY dyes for sensitive detection of lysosomal pH

J. Zhang, M. Yang, C. Li, N. Dorh, F. Xie, F. Luo, A. Tiwari and H. Liu, *J. Mater. Chem. B*, 2015, **3**, 2173

DOI: 10.1039/C4TB01878H

Authors contributing to RSC publications (journal articles, books or book chapters) do not need to formally request permission to reproduce material contained in this article provided that the correct acknowledgement is given with the reproduced material.

Reproduced material should be attributed as follows:

- > For reproduction of material from NJC:
Reproduced from Ref. XX with permission from the Centre National de la Recherche Scientifique (CNRS) and The Royal Society of Chemistry.
- > For reproduction of material from PCCP:
Reproduced from Ref. XX with permission from the PCCP Owner Societies.
- > For reproduction of material from PPS:
Reproduced from Ref. XX with permission from the European Society for Photobiology, the European Photochemistry Association, and The Royal Society of Chemistry.
- > For reproduction of material from all other RSC journals and books:
Reproduced from Ref. XX with permission from The Royal Society of Chemistry.

If the material has been adapted instead of reproduced from the original RSC publication "Reproduced from" can be substituted with "Adapted from".

This letter is for Chapter 6.

Publication contents reuse permission from American Chemical Society (ACS)

1/19/2016

Rightslink® by Copyright Clearance Center



RightsLink®

Home

Account Info

Help



ACS Publications
Most Trusted. Most Cited. Most Read.

Title:

Unusual Fluorescent Responses of Morpholine-Functionalized Fluorescent Probes to pH via Manipulation of BODIPY's HOMO and LUMO Energy Orbitals for Intracellular pH Detection

Logged in as:

Mu Yang

Account #: 3000961053

LOGOUT

Author:

Jingtuo Zhang, Mu Yang, Wafa Mazi, et al

Publication: ACS Sensors

Publisher: American Chemical Society

Date: Dec 1, 2015

Copyright © 2015, American Chemical Society

PERMISSION/LICENSE IS GRANTED FOR YOUR ORDER AT NO CHARGE

This type of permission/license, instead of the standard Terms & Conditions, is sent to you because no fee is being charged for your order. Please note the following:

- Permission is granted for your request in both print and electronic formats, and translations.
- If figures and/or tables were requested, they may be adapted or used in part.
- Please print this page for your records and send a copy of it to your publisher/graduate school.
- Appropriate credit for the requested material should be given as follows: "Reprinted (adapted) with permission from (COMPLETE REFERENCE CITATION). Copyright (YEAR) American Chemical Society." Insert appropriate information in place of the capitalized words.
- One-time permission is granted only for the use specified in your request. No additional uses are granted (such as derivative works or other editions). For any other uses, please submit a new request.

If credit is given to another source for the material you requested, permission must be obtained from that source.

BACK

CLOSE WINDOW

Copyright © 2016 Copyright Clearance Center, Inc. All Rights Reserved. [Privacy statement](#), [Terms and Conditions](#). Comments? We would like to hear from you, E-mail us at customer care@copyright.com